SYNTHESIS AND CHARACTERIZATION OF NANO NSAIDS, BIOMEDICAL APPLICATION AND POTENTIAL TOXIC EFFECTS

BY

AYESHA RAZZAQ

DEPARTMENT OF ZOOLOGY

FACULTY OF BIOLOGICAL SCIENCES

QUAID-I-AZAM UNIVERSITY

ISLAMABAD

2023

SYNTHESIS AND CHARACTERIZATION OF NANO NSAIDS, BIOMEDICAL APPLICATION AND POTENTIAL TOXIC EFFECTS

QUAID-I-AZAM UNIVERSITY

ISLAMABAD

A thesis submitted in the partial fulfillment of the requirement for the degree of

Doctor of Philosophy

In

Physiology

By

AYESHA RAZZAQ

DEPARTMENT OF ZOOLOGY

FACULTY OF BIOLOGICAL SCIENCES

QUAID-I-AZAM UNIVERSITY

ISLAMABAD

2023

IN THE NAME OF ALLAH, THE MOST GRACIOUS THE MOST MERCIFUL

Author's Declaration

I **Ms. Ayesha Razzaq** hereby state that my PhD thesis titled "Synthesis and Characterization of nano NSAIDs, Biomedical Application and Potential Toxic Effects" is my own work and has not been submitted previously by me for taking any degree from Quaid-i-Azam University, Islamabad, Pakistan.

At any time if my statement is found to be incorrect even after my Graduate the University has the right to withdraw my Ph.D. degree.

Ayesha.

Ms. Ayesha Razzaq

Certificate of Approval

This is to certify that the research work presented in this thesis, entitled "Synthesis and Characterization of nano NSAIDs, Biomedical Application and Potential Toxic Effects" was conducted by **Ms. Ayesha Razzaq** under the supervision of **Prof. Dr. Irfan Zia Qureshi**. No part of this thesis has been submitted anywhere else for any other degree. This thesis is submitted to the Department of Zoology of Quaid-i-Azam University, Islamabad in partial fulfillment of the requirements for the degree of Doctor of Philosophy in Field of Physiology.

Student Name: **Ms. Ayesha Razzaq**   Signature: _____
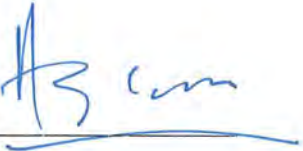
Examination Committee:

a) External Examiner 1:   Signature: _____

   Dr. Akram Shah
   Professor
   Department of Zoology
   University of Peshawar,
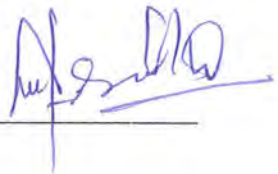   Peshawar
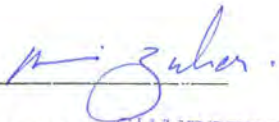
b) External Examiner 2:   Signature: _____

   Maj. Gen. (Retd.) Dr. Muhammad Aslam
   Professor
   House No. 169, Street 6 Race Course Road,
   Rawalpindi

Supervisor Name: **Prof. Dr. Irfan Zia Qureshi**   Signature: _____

Name of HOD: **Prof. Dr. Amina Zuberi**   Signature: _____

Date: 30.10.2023

CHAIRPERSON
Department of Zoology
Quaid-i-Azam University
Islamabad.

Plagiarism Undertaking

I solemnly declare that research work presented in the thesis "Synthesis and Characterization of nano NSAIDs, Biomedical Application and Potential Toxic Effects" is solely my research work with no significant contribution from any other person. Small contribution/ help wherever taken has been duly acknowledged and that complete thesis has been written by me.

I understand the zero tolerance policy of the HEC and Quaid-i-Azam University towards plagiarism. Therefore I as an Author of the above titled thesis declare that no portion of my thesis has been plagiarized and any material used as reference is properly referred/ cited.

I undertake that if I am found guilty of any formal plagiarism in the above titled thesis even after award of Ph.D degree, HEC and the University has the right to publish my name on the HEC/University Website on which names of students are placed who submitted plagiarized thesis.

Student / Author Signature: _Ayesha_ .

Name: **Ms. Ayesha Razzaq**

Oh, my lord!

Open for my chest (Grant me self-confidence, contentment and boldness) And ease my task for me,

And loose the knot of my tongue that they understand my speech (words)

Surah 20, Ta-Ha (Al Quran)

THIS THESIS IS DEDICATED TO MY ABBU AND AMMI

You let go of your dreams and sacrificed a ton so that I can achieve mine. I cannot say enough thanks to you in this lifetime for your contribution to my life.

TABLE OF CONTENT

ACKNOWLEDGMENTS

Praise is to **Allah**, the Cherisher and Sustainer of the worlds, who showed His countless blessings upon us. Almighty Allah enabled me to compile my humble endeavors in the shape of this thesis. All respect goes to the **Holy Prophet Hazrat Muhammad (PBUH)** whose teachings strengthened our faith in Allah, who is the source of knowledge and wisdom for the entire humanity, and who clarified that the pursuit of knowledge is a divine commandment.

This work would not have been accomplished without the support and encouragement of a whole team of people. The magnitude of gratitude towards them cannot be possibly expressed in the limited space available here.

I wish to express my sincere appreciation and thanks to my supervisor and my mentor, **Professor Irfan Zia Qureshi**, who has the substance of a genius: he convincingly guided and encouraged me to be professional and do the right thing even when the road got tough. Without his persistent help, the goal of this project would not have been realized. Your insightful feedback pushed me to sharpen my thinking and brought my work to a higher level. I am very thankful for the patient guidance, encouragement, and advice he has provided throughout my time as his student. I have been extremely lucky to have a supervisor who cared so much about my work, and who responded to my questions and queries so promptly.

I am most grateful to **Dr. Sohaila Naz** for the introduction to the world of nanoscience and technology. Her vast knowledge of the field has been my aid, and her nonstop guidance, my support system, whenever I was bewildered. I also want to thank her for having enough faith in me to learn the synthesis of nanoparticles and to set it up in our laboratory, and for allowing me to develop this method further once I got started.

I would also like to extend my thanks to the technicians of the synthesis and characterization laboratory at the National Center of Physics for their help in offering me the resources in running the program. I am deeply grateful for their unwavering patience, constant availability, and willingness to go the extra mile to ensure that I had all the necessary resources and technical support.

My fellow members of The Physiology Lab, **Nageena** and **Tariq Aziz** deserve my sincerest thanks for their support and willingness to allow me to practice my supervision

skills on them. My juniors, **Momina Nazir** and **Shafqat** thank you for being my helping hand during thesis finalization.

I would also like to acknowledge my dear fellows **Suleiman** and **Fiza ur Rehman** who I work with, in the synthesis and characterization lab at National Center for Physics (NCP), for their generosity with advice, materials, and other support.

The lively company of my best friend and lab mates **Iffat Fatima and Haleema Sadia** relieved my moods in times of tension and stress. I appreciate your compassion and understanding during my hard times. Words alone cannot express the thanks I owe to my buddy, **Nilofer**, this thesis would not have been possible without your unrelenting support, care, love, and prayers. Thank you for being there for me during these years!

Nothing would be possible without my family. They are, like every family, the most dysfunctional, lovely, caring, and sometimes over baring people ever. But they are my people. Without my parents, I would not be where I am now or who I am. They have provided me with the best opportunities one could have or want. They have spoiled me beyond comprehension; push me to always achieve my goals but most of all they have loved me beyond words. All along they stood by me and for that, I will never be able to thank you enough. Therefore, I dedicate this work to them, because without them this would have never been possible.

Special thanks to my lovely sister **khoula Razzaq**, you have been a blessing to my kids when I was away doing research and thesis writing and you took care of them really well. Without you being with my kids I wouldn't have completed my work. **Ahmad**, my beloved husband, I would not be the person I am today without you in my life. Thank you for your love, care, and attention, for putting up with my crankiness and horrible mood, and most of all...my lack of skills as a homemaker. You are both my rock and my soft place to fall, my source of daily laughter and my shoulder to cry on. Lastly, thanks to **Zainu** and **Muhammad Ali** my precious, my little stars, for making, and studying as a mum "normal". You truly are my motivation and my greatest fondness in the world.

Ayesha Razzaq

LIST OF TABLES

LIST OF FIGURES

LIST OF ABBREVIATIONS

ALP	Alkaline phosphatase
ALT	Alanine aminotransferase
AST	Aspartate aminotransferase
CAT	Catalase assay
COX	Cyclooxygenase
DDS	Drug delivery system
DEPPD	N.N-diethylpara phenyl diamine sulfate
FDA	Food and drug administration
GIT	Gastro-intestinal tract
LD	Lethal Dose
GSH	Reduced glutathione
LDH	Lactate dehydrogenase
MDA	Malondialdehyde
MgO NPs	Magnesium oxide nanoparticles
NBT	Nitro blue tetrazolium
NOAEL	No-observed-adverse-effect level
NOELs	No effects are observed
NSAIDs	Nonsteroidal anti-inflammatory drugs
OECD	Organization for Economic Co-operation and Development
PDC	Polymer Drug Conjugates
PEG	Polyethylene glycol
PLA	Poly (lactic acid)
PLGA	Poly(D,L-lactic-co-glycolic acid)
PNPs	Polymeric nanoparticles
POD	Peroxidase Enzyme Assay
PVA	Polyvinyl-alcohol
RES	Reticuloendothelial system
ROS	Reactive oxygen Species
SOD	Superoxide Dismutase Assay
TBA	Thiobarbituric acid
TBARS	Thiobarbituric acid reactive substance assay
TCA	Trichloroacetic acid

ABSTRACT

The therapeutic use of non-steroidal anti-inflammatory agents is associated with several tissue toxicities or organ failure. While these agents offer excellent anti-inflammatory, analgesic, and antipyretic effects, their therapeutic use is linked to tissue toxicities and organ failure. Reducing drug doses or discontinuing their use entirely is not practical, as alternate effective medications are lacking, and low dosages may not achieve the required therapeutic plasma concentration. Nano-drug delivery offers rational solutions to the challenges associated with high-dose drug formulations by decreasing the effective drug doses through conjugation to nanocarrier without compromising its therapeutic efficacy. Among nanocarriers, magnesium oxide nanoparticles can be used as an excellent drug delivery tool due to their mechanical strength, small particle size, wide surface area, and superior drug adsorption capabilities.

In this investigation, we synthesized MgO nanoparticles (NPs) as carriers for naproxen sodium, creating two nanoformulations: "coated nanoformulation" (CNF) with naproxen sodium conjugated to MgO NPs and polyvinyl alcohol (PVA) as a capping agent, and "uncoated nanoformulation" (UNF) without PVA coating. Various analytical techniques, including UV-visible spectroscopy, Fourier-transform infrared spectroscopy (FTIR), X-ray diffraction (XRD), thermogravimetric analysis (TGA), differential scanning calorimetry (DSC), and laser-induced breakdown spectroscopy (LIBS), were used to analyze and compare all compounds. *In vitro, the* drug loading efficiency of MgO NPs and the drug release profile of CNF were also studied.

Thorough acute and sub-acute toxicity experiments were conducted on male and female mice to assess the potential adverse effects and determine the lethal dose and no-observed-adverse-effect level (NOAEL) of the CNF. Ultimately, a comprehensive investigation aimed to gain an understanding of any potential differences in organ-specific responses between the conventional naproxen and its nanoformulations (CNF, UNF) at human therapeutic doses was conducted on target organs, specifically the heart, liver, stomach, and kidneys. To ensure unbiased results, bare MgO nanoparticles underwent separate and thorough evaluations to mitigate potential biases and provide a reliable assessment of the safety profile.

At present, CNF with a hydrodynamic size of 161 nm and surface charge of -8.85 mV, showed maximal and sustained release of naproxen (>95%) at pH 6.8 within 24 h.

Investigation of thermal attributes showed that the CNF was more stable at a higher temperature than free NPRS and UNF. *In vivo* anti-inflammatory, analgesic, and antipyretic activities revealed that in all cases, the potency and efficacy of CNF were found to be higher ($p < 0.05$- $p < 0.001$) than conventional NPRS and UNF. The ratio between the minimum effective dose (1 mg/kg) and LD_{50} indicated a broader therapeutic window. Since the concentration of NPRS in CNF was only $43.2 \pm 2\%$, our results indicated that conjugation to MgO nanocarrier boosts the biological activity of NPRS by approximately 2.3 times. In addition, CNF is found to be biocompatible and hemocompatible.

Data from the acute toxicity study of CNF indicated that it was well tolerated up to 2000 mg/kg b.w with an LD_{50} of 2574.77 mg/kg. While a 14-day subacute toxicity testing revealed that low dose (30 mg/kg) administration of CNF for 14 days did not produce any adverse effect on male and female Balb/c mice blood profile, serum ALT, AST, ALP, creatinine, bilirubin (total and direct), triglyceride, cholesterol, and LDH. Additionally, tissue oxidative stress markers (ROS and MDA) and antioxidant enzymes (CAT, SOD POD, and GSH) were found near normal levels. Histological assessment of brain, heart, stomach, spleen, liver, kidney, seminal vesicles, and testicular tissue obtained from male and female mice showed no evidence of toxicity. Mice when administrated a medium dose of naproxen nanoformulation (300 mg/kg) showed mild to moderated toxic effects ($p < 0.05$) specifically on the brain, stomach, and heart in male and female mice. while, in the liver, kidney, spleen, testis, and seminal vehicles, the levels of ROS, LPO, CAT, SOD, POD, and GSH remained unaffected. Histological assessment revealed that administration of medium-dose has caused mild toxicity to brain, kidneys, and stomach tissues in male and female mice. Serum biochemical parameters, however, remained unaffected. At present some aspects of the toxicity were observed associated with the minimum dose (300 mg/kg) and in comparison, with the existing detecting indexes to determine the no-observed-adverse-effect level (NOAEL), the NOAEL of CNF was regarded as higher than 300 mg/kg in this study. The administration of a high dose (1000 mg/kg) altered all hematological, serum, and tissue biochemical and morphological parameters in both male and female mice significantly, therefore regarded as toxic.

 In the comparative study, compared to NPRS-treated mice data revealed that

administration of the therapeutic dose of CNF and UNF to the experimental mice at a human therapeutic dose succeeded in preventing tissue damage through the restoration of all hematological, serum, and tissue biochemical, histological, and immunohistochemical alterations to near control levels. However this effect was more pronounced in CNF treated mice as compared to UNF treated mice. on the other, the administration of NPRS alone had elevated MDA and ROS levels, and deceased CAT, POD, SOD, and GSH levels, significantly increased expression of IL-1β, IL-6, and TNF-α mRNA, COX-2, i-NOS, and caspase-3 expression in mice heart, liver, kidney, and stomach tissues. The present study demonstrates that CNF has a tissue-protective action and in the clinical setup can be a better alternative to conventional naproxen.

In conclusion, the nanosizing of a drug offer much promise as a better alternative to standard anti-inflammatory drugs for the treatment of various diseases. In addition, synthesized nanoformulation "CNF" has potent anti-inflammatory activity, low toxicity, and a better safety profile than naproxen sodium alone, so it is recommended that the potential of this drug delivery system should be explored for the treatment of other inflammatory diseases for example chronic peptic ulcer, asthma, arthritis, tuberculosis, sinusitis, and active hepatitis.

GENERAL INTRODUCTION

Non-steroidal anti-inflammatory drugs commonly knowns as NSAIDs are the most popularly used medications with analgesic, anti-inflammatory, and antipyretic properties (Schultz, 2011). These medications are often used to treat acute and chronic inflammatory disorders. Hoffmann created the very first nonsteroidal anti-inflammatory agent (NSAID) in 1897, acetylsalicylic acid (Kolbe, 1860; Brune and Hinz, 2004). It was the first medicine to be tested for safety in an industrial facility on animals and was commercialized as aspirin in 1899, after human trials. There are currently more than 50 distinct NSAIDs available, worldwide (Singh, 2000). NSAIDs are renowned for their preventive benefits against cancer and heart disease, in addition to their immediate analgesic, anti-inflammatory, and antipyretic properties (Wong, 2019; Ma and Chen, 2021).

Despite NSAIDs' preventive and therapeutic properties have now been widely documented, their dosage and duration-dependent adverse effects on gastrointestinal, cardiovascular, hepatic, renal, cerebral, and pulmonary systems have also been reported in several placebo-controlled studies and meta-analyses (Vonkeman and van de Laar, 2010; Bessone, 2010; Bindu et al., 2020). To reduce dosage or duration-dependent NSAID toxicities, several approaches have been explored, including sustained-release drug formulation, particle size reduction, and low-dose administration over a brief period. However, neither of these techniques was able to demonstrate a significant improvement in organ toxicity among NSAID users (Kawada et al., 2012; Guo and Leung, 2020).

Nanotechnology-based enhanced medication delivery systems had already gained significant prominence as a viable alternative to traditional/conventional treatments. This method allows the use of engineered nanomaterials with desired properties to create nano-sized drug formulations for controlled drug distribution in target areas to reduce dose-dependent side effects (Yih and Al-Fandi, 2006; Kim et al., 2010; Kopeckova et al., 2019; Peng et al., 2021). The fundamental purpose of low dosage nanoformulation is to lower the amount of therapeutic dose without compromising the therapeutic effectiveness of a drug to preserve organ homeostasis (Alavi and Nokhodchi 2022; Qiao et al., 2022).

1.1 Inflammation

Inflammation is the reaction of the body to damage and involves a dynamic chain of events such as intracellular signaling, mediator release, increased fluid permeability, cell migration, tissue disintegration, and repair (Gopalan and Kirk, 2022). Proinflammatory molecules are produced as a result of the initial onset of inflammation, which therefore promotes and increases the inflammatory processes (Fig 1.1) (Ratan et al., 2022). The most significant biochemical responses to inflammatory signals are given below (Table 1.1).
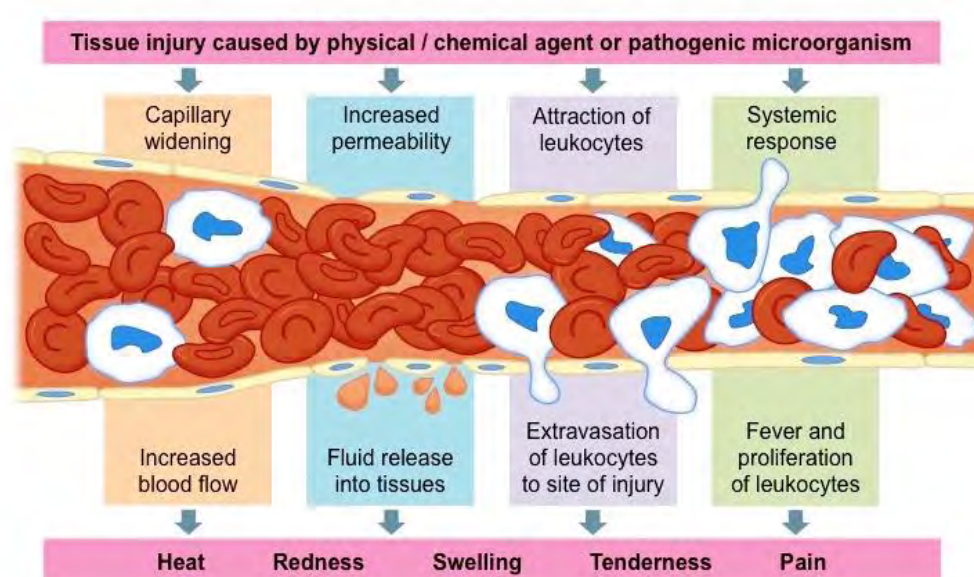
Fig. 1.1 A simple illustration is showing the significant steps involved in the onset of the acute inflammatory response (https://ib.bioninja.com.au/standard).

The complex and regulated production of several components, including cytokines, chemokines, proteases, lipids, and growth factors, is required for the induction and to resolve the inflammatory response (Varela et al., 2018). The generation of proinflammatory mediators such as inflammatory cytokines family, tumor necrosis factor- α (TNF), interferon-gamma (IFN), lipid inflammatory mediators such as eicosanoids, and platelet-activating factors working together to advance the inflammatory process is balanced by the release of another cytokine work to resolve inflammation such as interleukin-10 (Lordan et al., 2019). Chronic production and instability of these local chemical mediators can result in chronic illnesses (Fig 1.2)

(Rankin, 2004; Moore et al., 2001).

Table 1.1 Inflammatory signals that trigger biological reactions (Monastero and Pentyala, 2017)

Response	Results
Increased blood flow, enhanced vascular permeability, and increasing cellular infiltration	Macrophages and dendritic cells are stimulated; circulating neutrophils and monocytes are recruited, and endothelial cells are engaged.
Platelets activation	Coagulation factors are stimulated, fibroblasts are attracted, and inflammatory mediators and adhesive molecules are released.
Production of growth factors	Enhanced cell proliferation and biosynthesis of cellular components.
Stimulation of immune response	metabolic and catabolic characteristics have changed

Chronic inflammation leads to chronic conditions like unusual weight gain, metabolic disorders, cancers, atherosclerosis, hypertension, and cardiovascular events. Chronic inflammation is becoming a severe healthcare concern, and it has been termed a "silent killer" because of its covert and quiet progression, with no clinical symptoms visible until late in the pathological process (Garcia et al., 2010; Fullerton et al., 2013). Chronic inflammation disrupts homeostasis in all circumstances, escalating physiological and immunological states toward a proinflammatory damaging milieu involving cells and released substances (Pahwa et al., 2021).
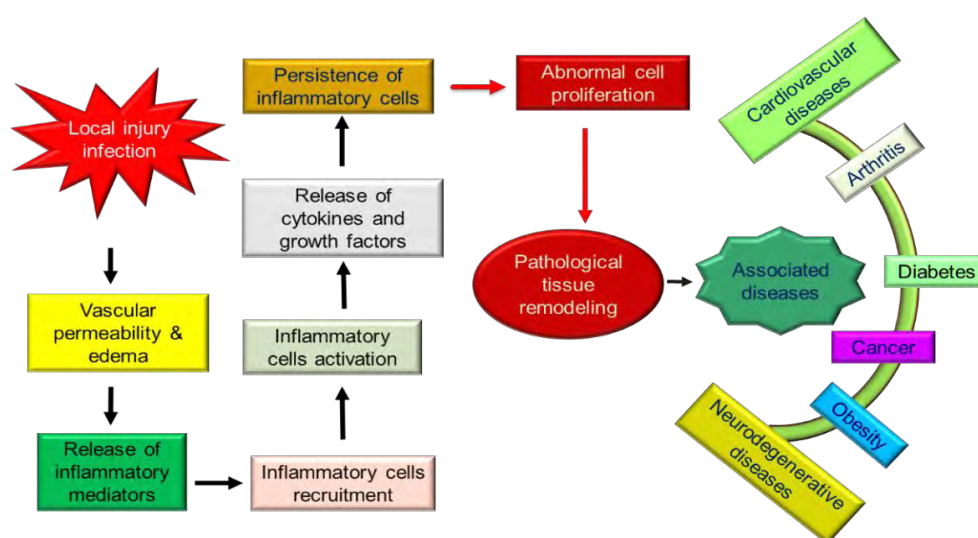
Fig. 1.2 Steps involved in the onset of chronic inflammatory diseases.

1.2 Standard Therapies for the Treatment of Inflammatory Disorders

Anti-inflammatory drugs are used extensively to suppress pain, erythema, edema, and tissue destruction during acute and chronic inflammatory conditions. At clinical doses, provides therapeutic benefits by suppressing the components of the inflammatory reaction, therefore, resolving inflammations. Broadly, anti-inflammatory agents are classified into nonsteroidal anti-inflammatory drugs (NSAIDs) and corticosteroids (Green, 2001; Barnes, 2006).

Corticosteroids (steroids) are synthesized steroid treatments that decrease all components of the inflammatory response when administered. However, long-term usage results in various side effects, including slowed wound healing, minor hirsutism, cushingoid habitus, candidiasis, fractures, muscle rigidity, osteopenia, peptic ulcers, linear growth inhibition, and pancreatitis (Saag et al., 1994). As a result, corticosteroids and/or immunosuppressive medicines are used only to decrease inflammatory responses in autoimmune illnesses such as systemic lupus, rheumatoid or osteo arthritis, and erythematosus, as well as in transplanted organs showing immunoreactivity (Schäcke et al., 2002). Because of the risks associated with corticosteroids, NSAIDs are the preferred choice to treat pain and inflammatory diseases (Marjoribanks et al., 2015; Wong, 2019).

1.3 Nonsteroidal Anti-inflammatory Drugs: Therapeutic Actions and Adverse Reactions

Nonsteroidal anti-inflammatory medicines (NSAIDs) are among the most frequently prescribed drug classes, with global sales of $6 to $7 billion (Simmons et al., 2000). Edward Stone employed willow, myrtle, and another medicinal plant extract (containing salicylic acid) to cure fever in 1763, which was the first time NSAIDs were discovered. Following that, in 1829, Henri Leroux in France acquired a crystalline form of salicylic acid (known as sailfin) and separated it to obtain salicylic acid in its crystalline state (Gorodetsky, 2014). Professor Hermann Kolbe later determined the molecular structure of salicylic acid and succeeded in its chemical synthesis in 1859 in Germany. In 1875, sodium salicylate was used for the first time to treat rheumatic fever (Rao and Knaus, 2008). Shortly after aspirin was introduced to the market, other medicines with comparable therapeutic properties were discovered and classed together

as NSAIDs (Rainsford, 2007).

1.3.1 Pharmacologic Mode of Action

These compounds exhibit their therapeutic actions by suppressing the biosynthesis of prostaglandins and proteinoids produced from arachidonic acid, which are important in the pathogenesis of inflammatory responses following tissue damage, to varying degrees (Zarghi and Arfaei, 2011). There are currently two enzymes are known to date involved in the transformation of arachidonic acid (AA) to eicosanoids: cyclooxygenase (COX) COX-1 and COX-2. These eicosanoids are autocrine since they are produced inside the tissue they impact (Gandotra, 2020).

COX-1 is a fundamental enzyme involved in basic cellular events such as GI tract defense from stomach acids through the production of bicarbonate ions, kidney perfusion, vasoconstriction, and platelet activation. Therefore, the COX-1 enzyme is found in the gut, intestines, kidneys, blood vessels, and platelets (Hinz and Pahl, 2007). On the other, the cyclooxygenase isoenzyme (COX-2) has specific sequences 60 % identical to COX-1 and is produced and expressed during inflammation by inflammatory cells such as macrophages, leukocytes, and fibroblasts. The enzyme has been termed 'inducible' as it is readily found in response to inflammatory mediators, tumor promoters, and growth factors (Simon, 1999).

These two enzymes work together to make prostaglandin G_2 (PGG_2) and prostaglandin H_2 (PGH_2), although both are intermediates for a variety of additional prostaglandins (PGs) and thromboxanes, including prostaglandin E_2 (PGE_2), prostaglandin F2a (PGF2a), thromboxane A_2 (TxA_2), and prostacyclin (PG_{I2}). The manufacture of these prostaglandins (PGs) is greatly elevated in inflamed tissue, and they play a critical role in the establishment of the inflammatory response (Gad, 2014). The development of the cardinal symptoms of acute inflammation, such as redness, elevated microcirculation, vascular permeability, edema formation, and heightened sensitivity to painful stimuli, is aided by these PGs (hyperalgesia). Prostaglandins appear to have a role in the transition to and sustaining of an inflammatory process, according to the studies on experimental animals (Fig 1. 3) (Ricciotti and FitzGerald, 2011).
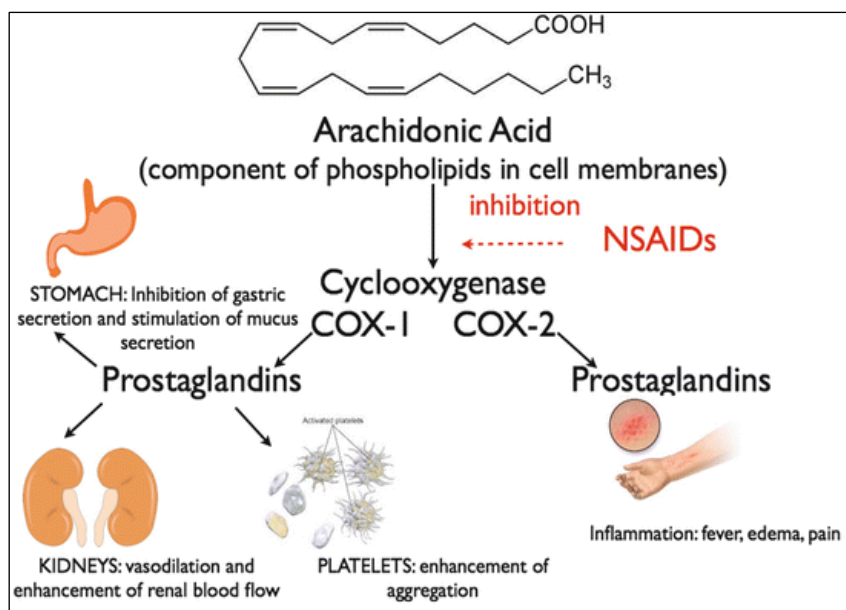
Fig. 1.3 A schematic presentation of the basic mode of action shown by
         NSAIDs (Zarghi and Arfaei, 2011).

The categorization of nonsteroidal anti-inflammatory drugs (NSAIDs) into conventional and COX-2-selective groups based on their selectivity for either of the COX isoforms is shown in Fig 1.4. NSAIDs such as naproxen, ketoprofen, ibuprofen, indomethacin, piroxicam, ketorolac, paracetamol, and aspirin are nonselective COX inhibitors, whereas meloxicam etodolac, celecoxib, diclofenac, nimesulide, valdecoxib, parecoxib, rofecoxib, and etoricoxib are more selective towards COX-2 and are also known as coxibs (Frölich, 1997).
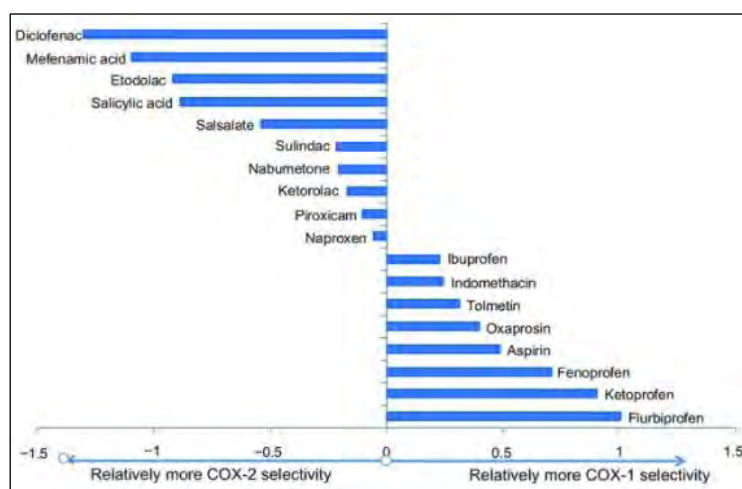
Fig. 1.4   Relative COX-1/COX-2 selectivity of various nonselective NSAIDs (Park
          and Bavry, 2014).

1.4 Adverse Effects of NSAIDs on Organ Systems

NSAIDs, despite their chemical variety, are exceptionally well tolerated when compared to all other non-opioid medications. In particular, Conventional nonsteroidal anti-inflammatory drugs (NSAIDs; relatively nonselective in their inhibition of cyclo-oxygenase (COX-1 and COX-2) are widely used for the treatment of pain and inflammation (Rhen and Cidlowski, 2005).

However, the deleterious gastrointestinal effects potentially associated with their use, accounting for approximately 21% of adverse drug reactions reported in the USA have shown concerning evidence about the usage of NSAIDs (Bindu et al., 2020). On the other, studies of the COX-2 selective agents (COX-2 inhibitors) have demonstrated that they are associated with a significantly reduced risk for upper and lower gastrointestinal complications compared with conventional NSAIDs, whereas their use has been caused cardiovascular adverse effects among users and resulted in their ultimate elimination from the market (Saad and Mathew, 2022). Currently, some of NSAID-induced organ toxicities are discussed below in detail:

1.4.1 Cardiovascular Effects

The use of non-selective NSAIDs and cyclooxygenase-2 inhibitors has been associated with several cardiovascular complications including ischemic stroke, myocardial infarction, increase in blood pressure, the structural and functional response of blood vessels to stress, and the onset and early development of atherosclerosis (Fanelli et al., 2013; Varga et al., 2017). These drugs have shown the risk of cardiovascular incidents in over 3 million individuals worldwide. In terms of percent cardiovascular risk, COX-2 usages showed a 45% increase in cardiovascular events, while the users of non-selective COX inhibitors are reported to show a 20-40 % increased risk. Among all NSAIDs, ibuprofen showed cardiovascular events at higher doses while naproxen was reported to be relatively less cardiotoxic (Simmons et al., 2000).

1.4.2 Gastrointestinal Adverse Effects

The first indication that NSAIDs might cause gastric injury dates back to 1938 and was based on an examination of an ulcerated stomach obtained from the aspirin-treated specimen. This idea was further confirmed by additional case-control studies in the

1950s and 1960s, which indicated that gastric ulcers were associated with NSAID use (Green, 2001). NSAID-related fatalities have been documented at a rate of 0.22 percent each year, with an annual rise in the mortality rate of 4.21 percent predicted (Laine, 2002). The tendency of NSAIDs to produce gastric ulcers and bleeding depends upon their ability to inhibit prostaglandin production and corresponds to the dose and duration for which NSAIDs are administered. Reduction in prostaglandin production affects the normal physiological functioning of gastric mucosa by inhibiting mucus production, reduced blood flow, and reduction in bicarbonate secretions (Kimmey, 1992). All of these factors contribute together to GIT toxicity (Mizushima, 2010).

The 'trapping' theory is another mechanism by which NSAIDs induce their toxic effect through their accumulation in the gastric mucosa. According to this theory, the majority of NSAIDs are weak acids and remain non-ionized in an acidic environment. These NSAIDs when moving across the gastrointestinal mucosal membranes into the cytoplasm, they encounter a basic pH. In basic pH, NSAIDs are re-ionized and form aggregates within cells, resulting in cellular damage (Brand et al., 2004; Nagano et al., 2005).

Moreover, NSAIDs are known to cause gastrointestinal toxicity through "topical" effects. In topical effect, NSAIDs act as chemical irritants to gastric or intestinal cells and cause damage by disrupting cellular membrane integration through the production of free radicles (Matsui et al., 2011). Besides, the uncoupling of mitochondria due to NSAID action results in decreased production of cellular ATP, Ca^{+2} ions release, osmotic imbalance, and a lack of control over intracellular junctions, which resulted in enhanced cellular permeability and subsequent mucosal injury (Somasundaram et al., 1995). Older age, a history of ulcers, concurrent use of corticosteroids, and higher NSAID dosages have all been recognized as risk factors that potentially worsen NSAID-induced ulcers (Drini, 2017).

1.4.3 Hepatotoxicity

The liver injury appears to be an uncommon side effect of most NSAIDs. NSAIDs have been linked to hepatic side effects in 3% of patients. Almost all NSAIDs cause hepatoxicity through an immunologic or metabolic mechanism, with dose-related toxicity reported in aspirin and acetaminophen (Manov et al., 2006). NSAIDs can cause

hepatotoxicity in two ways: the first is acute hepatitis which is marked by fever, nausea, and as well as raised serum transaminases, whereas the other kind is chronic active hepatitis characterized by the study of seroma markers and liver lesions (O'Connor et al., 2003).

Depending on the type of drug, hepatotoxic mode of action of NSAIDs may vary greatly (Sriuttha et al., 2018). Hypersensitivity and metabolic abnormalities have been regarded as the two most common causes. Individuals who have experience hepatotoxicity with one NSAID are prone to the same reaction when the medication is resumed or a drug with the same chemical composition is administered (Bessone et al., 2016). Metabolic problems, on the other hand, might be caused by genetic polymorphisms and varying sensitivity to a variety of medicines, as evidenced by *in vitro* studies that revealed phenotypic diversity in aceclofenac metabolism among donor liver cells (Kwon et al., 2019).

Paracetamol is the most prominent with known hepatotoxic potential among all NSAIDs and accounts for about 42% of all acute liver failure cases reported to date in the United States (US). Paracetamol-induced liver failure is now becoming the most prevalent cause of acute liver failure in the US. The majority of these instances were caused by deliberate or inadvertent overdose, with 79 % of those who took the painkiller primarily for pain and 38% were those using two distinct medicinal formulations at the same time (Donati et al., 2016).

1.4.4. Renal Complications

NSAIDs have been demonstrated to affect renal function, with acute renal failure occurring in roughly 6% of NSAID users. Peripheral edemas, transitory acute renal failure, acute interstitial nephropathy, electrolyte imbalances, and papillary atrophy have all been reported as side effects of these medicines (Lucas et al., 2018). Acute renal failure can occur with the use of any anti-inflammatory drug irrespective of its mode of action. Piroxicam, tolmetin, and, in particular, sulindac are thought to be less likely to induce renal adversities (Zhang et al., 2017). Whereas indomethacin, ibuprofen, fenoprofen, mefenamic acid, naproxen, and diclofenac have a greater rate of deleterious effects on renal function. The postulated mechanism is that NSAID usage may result in decreased prostaglandin synthesis, resulting in decreased renal blood flow

and consequent medullary ischemia in vulnerable people (Bensman, 2019).

1.5 Food and Drug Administration (FDA) Warning

The US food and drug administration (FDA) passed a rule in 2015, according to which a warning label accompanying NSAID prescriptions is a legal necessity to inform consumers of the drug's side effects. "FDA warnings" states that (FDA, 2015),

1.   "NSAIDs are associated with an increased risk of adverse cardiovascular thrombotic events, including myocardial infarction and stroke".

2.   "NSAIDs may increase the risk of GI irritation, inflammation, ulceration, bleeding, and perforation. These events may occur at any time during therapy and without warning".

With these cautions on the prescription box, the frequency of NSAID usage could not be reduced since they give considerable relief in pain states associated with inflammation. More significantly, when compared to the major alternatives, corticosteroids, NSAIDs are more efficient and nonaddictive, which is a significant benefit considering the physical, social, and economic devastation caused by chronic opioid users. Second, the absence of potential innovative, efficient, and viable alternatives has also led to the continued use of NSAIDs across the world (Schjerning et al., 2020).

1.6 Strategies to Minimize NSAIDs Induce Side Effects: Target Specific Pharmacotherapy

Due to their well-documented adversities, several strategies, therefore, have been investigated to minimize dose or duration-dependent NSAID toxicities, including sustained released formulations, reduction in particle size, or low-dose administrations for a short period (Goldstein and Cryer, 2015; Drini, 2017). However, these formulations suffered various disadvantages as low dosage administrations or high and frequent medication administrations resulted in unreachable therapeutic effects due to instability of drug in biological systems which results in insufficient bioavailability, off-targeted local and systemic adverse effects, or both. As a result, treating inflammatory illnesses remains a significant challenge (Smolinske et al., 1990). As a

result, the development of innovative nano-formulations has become a major priority (Al-Lawati et al., 2019).

1.6.1 Nano-Based Drug Delivery Systems

With major advancements in nanotechnology in recent years, research has focused on optimizing therapeutic dosages by employing nano-drug delivery systems to reduce drug-induced adverse effects (Abadi et al., 2016). This technique allows the encapsulation or attachment of therapeutic medications to nanosized particles as delivery agents, allowing them to be delivered to target tissues more accurately and with a continuous release (Weissig et al., 2014). These nanoscale particles remain in the blood circulation for an extended period, allowing the sustained release of loaded drugs. As a result, they lead to reduced plasma fluctuation and fewer side effects (Subramanian et al., 2004; McDonald et al., 2015).

Furthermore, these nanosized structures may permeate the tissue system, allowing for simple drug absorption by cells, effective drug transport, and activity in the intended area (Fig. 1.5) (Mennini et al., 2014).
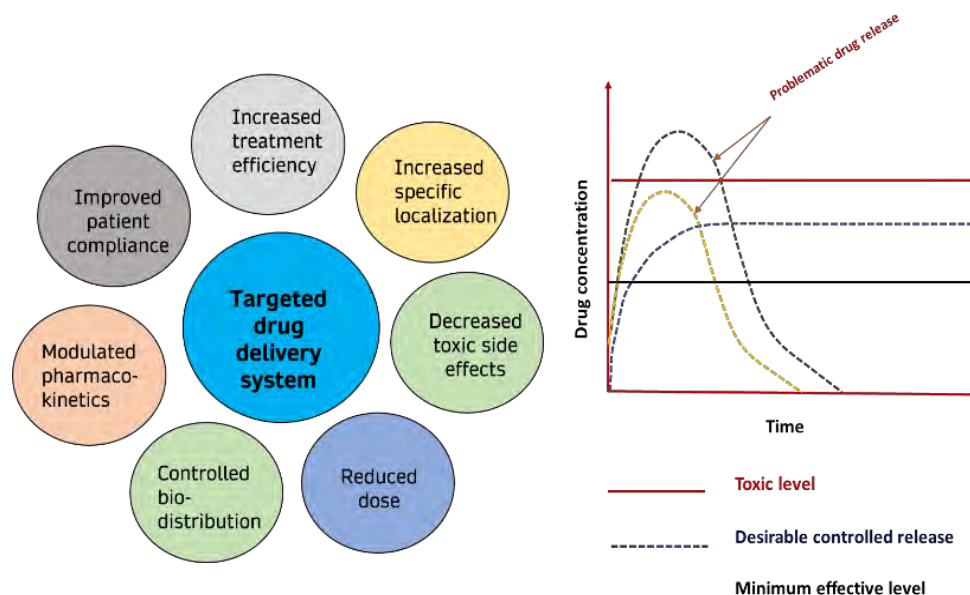
Fig.1.5 A presentation of drug release behavior in targeted drug delivery system. (Chandrakala et al., 2022).

Nanostructures of various kinds such as organic, inorganic, metallic, and polymeric nanostructures, including dendrimers, micelles, and liposomes are considered frequently drug delivery systems as drug carriers (Fig 1.6) (Mirza and Siddiqui, 2014). Medications with solubility issues and low absorption are attached to these nanostructures in form of chemical or physical bonding and transported to the targeted areas within the body, resulting in improved accessibility of drug at the target site (Parveen et al., 2012). With desired attributes, these delivery methods have been proven to be non-toxic, physiologically specific, non-hemolytic, cell, and tissue compatible, and safe at high doses (Patra et al., 2018).
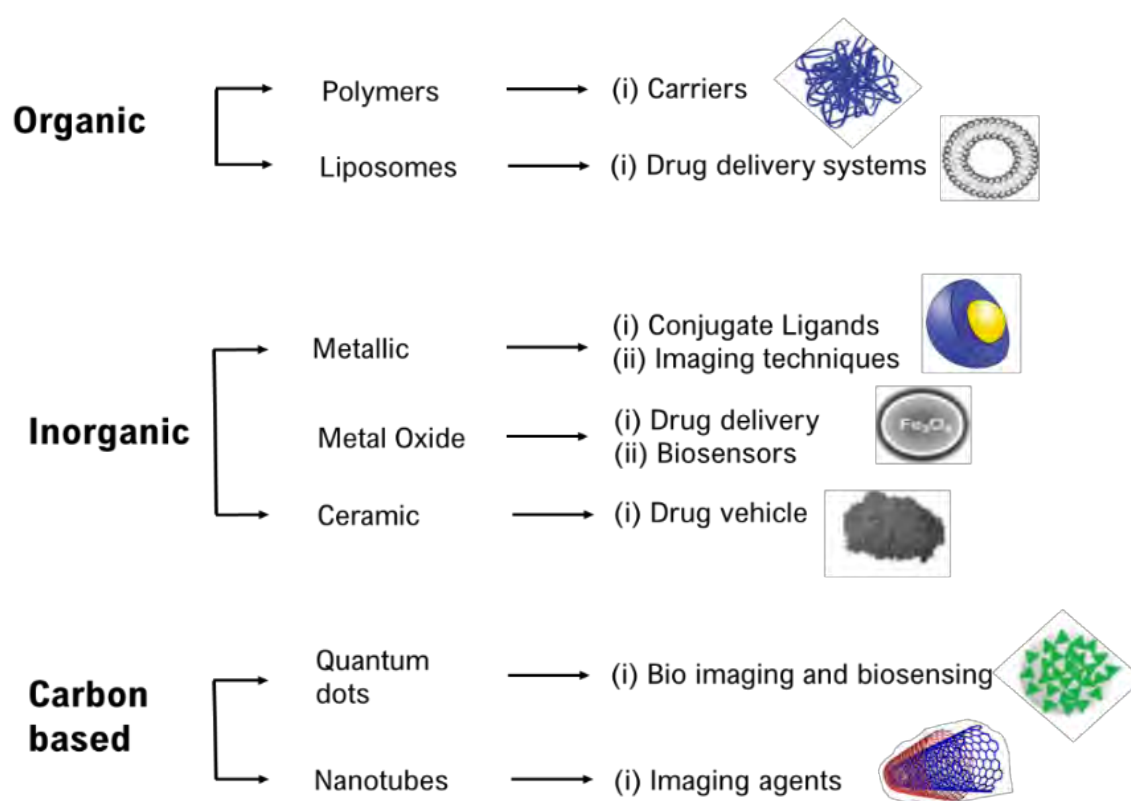
Fig. 1.6 Types of nanoparticles used in various applications of nanotechnology including drug delivery and bioimaging (Wang, 2014).

The efficiency of these nanoparticles as nanocarriers, however, differs each depending on their size, shape, and other biophysical and chemical attributes (Ramezanpour et al., 2016).

1.6.2 Advantages of Nano-Based Drug Delivery Systems

Nano delivery technologies can improve the therapeutic efficacy of NSAIDs in a

variety of ways.

1. Reduction in Organ Toxicity

Nano delivery systems employ several types of nanoparticles as drug delivery vehicles, based on the type of drug used and the preferred route of administration. This technology not only improves medication absorption across various biological barriers but also allows for long-term drug delivery via local or systemic dosing (Kermanizadeh et al., 2018). In addition to lowering systemic toxicity, this drug-carrying system modifies NSAID pharmacokinetic profile in such a manner that it would not impact their COX-1/COX-2 specificity while keeping them away from drug-prone organs such as the liver, kidneys, and the heart (Prasad et al., 2015). For instance, NSAIDs in encapsulated form show a minimum effect on the mucus membrane of the stomach following oral administration, thus causing minimal irritating effects which leads to a substantial reduction in GI ulcerations or damage (Sarfraz et al., 2019; Noreen et al., 2021).

2. Enhancing the Solubility of NSAIDs

Most NSAIDs are weak acids with poor solubility at low pH and are categorized as Biopharmaceutics Classification System (BCS) class II medications (Tsume et al., 2014). Since the therapeutic activity of an orally administered NSAID is largely dependent on drug solubility from the dosage form and subsequent absorption at the target site (Lawati and Jamali, 2016), solubility issues associated with NSAIDs may limit their therapeutic potential (Mazaleuskaya et al., 2021). Whereas the increased solubility and absorption leading to prolonged systemic circulation can enhance the efficacy and safety of these agents. Thus, nanosizing, through encapsulation of drugs with nanoparticles offers a solution to solubility issues of drugs through its increased bioavailability and plays an important role in overall formulation efficacy and sustainability (Cao et al., 2021).

3. Localized Administration of NSAIDs

Systemic nano delivery systems provide alternate drug administration methods such as dermal application, subcutaneous injections near inflammatory joints, or intraarticular application. This mode of delivery has various advantages over the parenteral route,

including the prevention of first-pass metabolism, increased bioavailability, and consistent dose administration, which optimizes the efficacy of NSAIDs by limiting their systemic exposure (Nikolić et al., 2019).

Additionally, the preparations can enable improved skin permeation of NSAIDs to attain a high plasma concentration while extending drug release. Such preparations have the potential to minimize NSAID GI adverse effects and/or frequency of NSAID administrations (Irvine et al., 2018; Sarfraz et al., 2019). Nanoscale delivery methods also allow the use of high dose concentrations in the form of encapsulated medications, paving the way for investigation into their off-label usage in various disease situations (Barani et al., 2021).

4. Sustained Release of Drug from Nanoparticles

Sustained release of drugs from nanoparticles refers to a controlled and gradual release of therapeutic agents (such as drugs or other bioactive compounds) over an extended period of time. This mechanism is achieved by encapsulating the drug within nanoscale particles, which are extremely small structures typically ranging from 1 to 100 nanometers in size. The process involves designing and formulating nanoparticles in a way that allows for the gradual diffusion or controlled degradation of the nanoparticle matrix, leading to the gradual release of the enclosed drug (Bai et al., 2022).

This controlled release is advantageous in various medical and pharmaceutical applications because it offers several benefits including, steady therapeutic levels, reduced frequency of administration, minimized side effects, enhanced efficacy, and tailored release profiles. Methods to achieve sustained drug release from nanoparticles include adjusting the particle size, composition, surface properties, and the use of various encapsulation techniques. These nanoparticles can be fabricated from a variety of materials, including polymers, lipids, metals, and inorganic materials (Jacobson et al., 2008).

1.7 Nano Particles Used in NSAIDs Delivery Systems (Pre-Clinical Studies)

Numerous nano-delivery strategies have been researched in preclinical investigations for various NSAIDs for numerous clinical disorders.

1.7.1   Polymeric Micelles

"Polymeric micelles are nano-sized colloidal particles made up of self-assembled amphiphilic copolymers with hydrophobic and hydrophilic block domains with a core-shell" (Croy and Kwon, 2006). Micellar nanoparticles are known for their well-adjustable features such as desired nanoparticles size, particle dispersion index, and customized physicochemical properties, making them ideal for medicine delivery to inflamed tissues (Kim et al., 2018).

Celecoxib, a selective COX-2 inhibitor with potent anti-inflammatory activity is generally less soluble in water with a solubility of just 4-7μg/mL, when nanosized, showed a significant increase in solubility along with an enhanced pharmacokinetics and pharmacodynamics profile (McCormack, 2011). In a similar study, chitosan nanoparticle-based celecoxib nanoformulation with an average particle size < 200 nm exhibited a 57-fold improvement in celecoxib water solubility than free form. The same nanoformulation when tested for its analgesic effects against acetic acid-induced writhing demonstrated a quicker (30 min vs. 120 min) and more severe analgesia compared to conventional celecoxib formulation (Mennini et al., 2014). Despite a 57-fold increase in celecoxib solubility was observed in the solubility study of micellar formulation, an increase in solubility is still needed to enhance the therapeutic efficacy of water-insoluble drugs.

Another study reported the increase in the therapeutic efficacy of lornoxicam when conjugated with micelle-based nanoparticles. When tested against the carrageenan indued edema model, the nanoformulation with a mean particle size of 170 nm showed better anti-inflammatory activity compared to a free lornoxicam. Moreover, the therapeutic efficacy of lornoxicam was compared to diclofenac sodium and found that the lornoxicam nanoformulation has comparable therapeutic effects (Helmy et al., 2017). Yoshitomi et al. (2014) showed that the indomethacin conjugated with polymeric nanoparticles exhibited increased bioavailability, and suppressed inflammation in the GI tract (Yoshitomi et al., 2014). Diclofenac sodium, another drug with significant anti-inflammatory effects, showed organ toxicity when administered for a 3- and 7- day period. However, conjugation of diclofenac with polymer demonstrated no adverse effects on tissue architecture at the same dose administered (Al-Lawati et al., 2016).

1.7.2   Polymeric Microspheres

One of the most effective drug delivery systems (DDS) in the field of nanomedicine having a clinical application is poly(D, L-lactic-co-glycolic acid) (PLGA)/poly (lactic acid) (PLA) microspheres or nanoparticles. They can be employed in a variety of drug delivery applications due to their characteristic features like the sustained release of conjugated drugs, biocompatibility, and biodegradability (Loureiro and Pereira, 2020).

Ibuprofen is a potent anti-inflammatory drug but suffers from its rapid elimination from system circulation. To address this issue, a nanoformulation based on polyethylene glycol (PEG) with a mean size of ~ 200 nm was prepared and evaluated. Histopathological analysis of rats administered with ibuprofen formulation revealed its safety. Moreover, ibuprofen loaded on PEG nanoparticles indicated a 4- 5-fold better plasma concentration than free ibuprofen in a pharmacokinetic profile testing in healthy rats. The presence of a desired concentration of ibuprofen in plasma for 5 days after injection also suggested that it has the potential to minimize frequent administration, implying that it might be used in clinical trials in the future, particularly when IV dosing is required (Narayanan et al., 2013).

Harirforoosh et al. (2016) compared the renal and GI safety of diclofenac nanoformulation prepared through encapsulation of diclofenac in poly(lactic-co-glycolic) (PLGA) nanoparticles to free diclofenac. The nanoformulation and free drug were administered at a dosage of 10 mg/kg through gavage. Analysis of tissue histology revealed that nanoparticles did not affect the integrity of kidney structures while free diclofenac caused significant lesions and necrosis of kidney tissues. Similarly, encapsulation of a COX-2 inhibitor, celecoxib in PLGA nanoparticles, provided significant GI protection by regulating the PGE_2 production needed for mucosal protection, as compared to free celecoxib (Harirforoosh et al., 2016).

1.7.3   Dendrimers

Dendrimers are three-dimensional macromolecules that possess unique characteristics such as monodispersing molecular structure, branch-like shape, and elevated drug entrapment efficiency, all attributes considered suitable in drug delivery applications (Abbasi et al., 2014). Although the use of dendrimers in drug delivery applications is knowns for decades, however, another advantage associated with dendrimer use was its

anti-inflammatory potential discovered recently (Fruchon and Poupot, 2017). Dendrimers show their anti-inflammatory effect through the inhibition of proinflammatory cytokines. This additional property of dendrimers has made them a suitable nanocarrier for antiarthritic drug delivery (Qi et al., 2015).

1.7.4 Polymer Drug Conjugates (PDC)

Polymer drug conjugates are the nanodrug delivery system in which a polymeric carrier is chemically bonded to drugs with low molecular weights (Duncan, 2003). Polymer drug conjugate is considered a toxicity-free drug delivery system due to its increased circulation time, controlled particle size that surpasses renal filtration, tendency to accumulate in inflamed joints, and biodegradable (De Souza et al., 2010; Sun et al., 2011).

Human serum albumin conjugated with methotrexate when tested for anti-inflammatory activity showed a high accumulation of methotrexate in the inflamed paw and resulted in significant anti-inflammatory activity. Moreover, albumin which was used as a drug carrier was taken up by blood cells indicating its potential for use in drug delivery applications (Fiehn et al., 2004). Similarly, indomethacin encapsulated polymeric capsules (mean size = 240 nm) prepared with the aim to treat rheumatoid arthritis, demonstrated excellent anti-inflammatory potential in various experimental models. The anti-inflammatory activity was found comparable to free indomethacin. While, the nanoformulation showed a significant reduction in mucosal and intestinal damage as compared to the conventional drug (Bernardi et al., 2009).

1.7.5 Liposomes

Liposomes as the name indicate phospholipid bilayer containing vesicles with the ability to entrap hydrophobic and hydrophilic drugs inside the internal aqueous structure (Daraee et al., 2016). As a result, it is one of the most effective ways to get medicine to the inflamed parts of the body (Williams et al., 1987; Kapoor et al., 2014). The accumulation of the drug in the targeted site such as inflamed joints thus helped in the reduction of its systemic toxicity (Dingle et al., 1978).

In a comparative study diclofenac sodium encapsulated liposome nanoparticles with a mean size of 260 nm showed a better analgesic effect as compared to free form. The

analgesic effect of liposomal diclofenac and free diclofenac was assayed using an acetic acid-induced writhing model. Results indicated that liposomal diclofenac formulation caused 70 % inhibition in writhing response as compared to free diclofenac which showed only 56 % inhibition in writhing response. Moreover, compared to 61% for free diclofenac in the formalin test, the liposomal diclofenac caused 79 % inhibition in pain perception. It was suggested that the higher analgesic activity showed by the encapsulated drug was likely due to enhancement in diclofenac bioavailability and its active transport to the inflamed tissues (Goh, 2015).

Indomethacin, a drug with excellent analgesic effect is no longer used or prescribed due to its ulcerative activity in gastric mucosa. However, its conjugation with liposomes provided a 75% protection against ulceration in rats in comparison to free indomethacin. Furthermore, as compared to free indomethacin, liposomes provided over 99 % protection against intestinal ulcers in a 2-week chronic ulceration model in rats (Soehngen et al., 1988).

1.7.6 Solid Lipid Nanoparticles

Solid lipid nanoparticles (SLN) are spherical nanoparticles consisting of a solid lipid core and an amphiphilic outer shell. Characteristics, such as control release of the drug, stability of nanoformulation, protection against degradation, and biocompatibility make them suitable in several drug delivery applications (Salminen and Weiss, 2021). Using the bead mill technique, Nagai and Ito (2014) created a solid nanoparticle-based preparation of indomethacin for oral administration with a mean size of 80 nm. This nanoformulation was tested for its bioavailability, anti-inflammatory, and anti-ulcer activity in comparison to free indomethacin. Two different doses of indomethacin nanoformulations were selected, a high dose (2 mg/kg) therapeutic and a low dose (0.4 mg/kg) and compared with the high dose (4 mg/kg) of free indomethacin. The indomethacin lipid nanoparticles showed 5.3-fold higher bioavailability at both doses as compared to its conventional form in adjuvant arthritic (AA) rats. The low dose nanoformulation showed a better anti-inflammatory activity compared to high dose free indomethacin.

Moreover, administration of high-dose nanoformulation showed a less GI lesions compared to higher doses of free indomethacin (Nagai and Ito, 2014).

1.7.7   Self- Nano Emulsifying Granules

Self-emulsifying drug delivery systems are unique kind of nano formulations prepared by using homogeneous compositions of synthetic oils, solid or liquid surfactants, and co-surfactants. When subjected to an aqueous medium i.e., gastric fluids, they self-emulsify to produce nanoemulsion with droplet sizes ranging from 20 to 200 nm. (Aboul-Fotouh, 2019). In a study, meloxicam, an NSAID with a specific COX-2 inhibitory action, was studied to investigate the effect of self-nano emulsifying granules on its solubility and therapeutic efficacy. *In vivo* analysis showed that in a carrageenan-induced rat paw edema model, the nanoformulation exhibited a faster and more strong anti-inflammatory effect, with a 26 % reduction of paw edema one h after the carrageenan dosage, this inhibitory effect was sustained throughout the experimental period i.e., 5 h. The free drug, on the other hand, had a slow and less strong impact, with no discernible suppression of paw edema in the first hour after the carrageenan dosage (Parekh et al., 2017).

A nanoemulsion containing aspirin was prepared and tested against carrageenan-induced paw edema. Results showed that nanoemulsion administered 4 h before testing at an oral dose of 60 mg/kg, had a significant inhibitory effect on a carrageenan-induced paw edema model of inflammation in rats. This effect was nearly double the inhibitory effect displayed by free aspirin suspension at the same dose. Furthermore, as compared to free aspirin, the same formulation resulted in a stronger suppression of abdominal writing (91 % versus 81 %) in acetic acid-induced writhing. The investigators attributed these effects to quick dissolution, improved drug solubility, and high bioavailability following oral administration (Tang et al., 2012).

1.8 Clinical Research on the Nano-Delivery of NSAIDs

It's concerning that, despite the huge preclinical success, the translation of established nano delivery formulations from preclinical to clinical application has been slow and does not equate to the advances seen with other medications like anti-cancer therapies (Wicki et al., 2015; Al-Lawati et al., 2018). With recent advancements in the field of nano delivery systems, such barriers may be addressed soon, allowing nano-NSAIDs to be translated from preclinical research to clinical application (Soares et al., 2018; Desai, 2012).

During a clinical study, nanosized liquid crystalline particles were prepared and loaded with etodolac, a selective COX-2 inhibitor, and the nanoformulation was therapeutically examined as part of the clinical trial on transdermal nano delivery of NSAID. Data from transdermal delivery of nanoformulation in six human volunteers revealed sustained absorption of nanoformulation with a droplet size of 136–288 nm with a 3.8-fold increase in half-life. Moreover, compared to oral capsules available commercially, the relative bioavailability was 266.11% after 48 hours (Salah et al., 2017).

An indomethacin-based liposomal hydrogel with an average size = of 200 nm was tested for its anti-inflammatory effects on twelve human subjects as a part of a clinical study of the drug. The individuals were exposed to UVB to induce skin erythema inflammation and then were applied with nanoformulation. The formulation maintained its anti-inflammatory activity up to 6 hours after gel removal, exhibiting considerably better inhibition at 3 and 6 hours after gel removal as compared to free indomethacin formulation. This advantage is attributed to the continuous release of indomethacin due to an apparent interaction between the lipids in the nanoformulation and stratum corneum (Puglia et al., 2010).

1.9 Nanosizing of Drug Particles

In addition to nano delivery methods, particle nanosizing technologies such as SoluMatrix Fine Particle Technology TM (iCeutica Inc., Philadelphia, PA) have been researched for NSAIDs as a means of reducing dosages and, as a result, lowering toxicities (Desjardins et al., 2015; Hussaini et al., 2016). As a result, several drugs with nanosize particles are approved and available for therapeutic use.

1.10 Deficiencies in NSAIDs Nano-Delivery Systems

Polymeric nanoparticles (PNPs) have probably been the most investigated of the many nanocarriers as drug delivery agents for NSAIDs, to achieve higher therapeutic performances in the oral delivery area as well as other administration routes (Syed and Devi, 2019). Despite the preclinical success, the translation of the established nano delivery formulations for NSAIDs to clinical research has been extremely restricted (Martinho et al., 2011; Soares et al., 2018).

This might be due to concerns of drug manufacturers about using comparatively expensive innovative delivery methods for NSAIDs that are used by patients on a long-term basis (Pandey and Jain, 2020). Massive production issues, as well as safety concerns and strict regulations, may have led to the minimal clinical usage of NSAIDs-based nanodrug delivery systems (Sainz et al., 2015). Second, polymeric nanoparticles as NSAID carriers have significant drawbacks, including high cost, precipitation, drug permeability, buildup in human tissues, cytotoxicity, and difficulty clearing from the circulatory system (Smet et al., 2013; Ghasemiyeh and Mohammadi-Samani, 2018; Vega et al., 2020). Thus, as an alternative, the use of metal oxides as drug carriers shows potential in drug delivery applications.

1.11   Metal oxide Nanoparticle as Drug carriers

Metal oxides have been researched vigorously in a variety of drug delivery applications throughout recent years (Yaqoob et al., 2020) due to their specific physicochemical characteristics, cost-effective production, and easy preparation procedures (Nikolova and Chavali, 2020). Metal oxide nanoparticles are highly stable and can be constructed according to the desired size, structure, and porosity. Metal oxide nanoparticles can incorporate hydrophilic and hydrophobic drugs efficiently which results in the effective delivery of drugs to target sites. Moreover, metal oxide can be used in implant, theranostic, wound healing, cancer therapy, antimicrobial, and drug delivery applications (García et al., 2022).

Unlike polymeric nanoparticles, metal oxides are available in a wide range of shapes and sizes. These qualities are proportionate to the synthesis process used. Metal oxide nanoparticles (MPs) can be anywhere from 1 and 100 nanometers in size (Murthy et al., 2020). Ideally, the metal oxide NPs should have the following features for their biomedical applications: (1) it should be chemically stable, (2) resistance to wear and scratch, (3) biocompatible, and (4) nontoxic (Din et al., 2017).

1.11.1 Magnesium Oxide Nanoparticles; An Emerging Candidate in Drug Delivery Applications

Magnesium is the second most frequent cation among trace elements and required for the normal functioning of a variety of human body systems and activities (Jahnen-Dechent and Ketteler, 2012). Magnesium plays an important role in the regulation of

glucose through insulin secretion, enzymatic activity, and cell signaling activities. Whereas its deficiency leads to cardiovascular problems and metabolic disorders (Paolisso et al., 1990; Ryan, 1991). The National Academy of Sciences' Institute of Medicine has advised a daily magnesium intake of 400–420 mg for men and 320 mg for women, which is adequate to fulfill the requirements (Dwyer, 2004).

Due to their mechanical strength, small particle size, wide surface area, and superior drug adsorption capabilities, magnesium oxide nanoparticles (MgO NPs) have suddenly acquired prominence as drug carriers, in the field of nanotechnology (Gajengi et al., 2017). Several anticancer medicines, including doxorubicin (Ranathunge et al., 2019), and 2-Methoxyestradiol (Alfaro et al., 2019), have been successfully delivered using MgO NPs and nanoflakes, indicating their effectiveness in controlled drug delivery systems (Sun et al., 2011). MgO NPs are effectively converted into Mg^{2+} and OH^- ions, which are eliminated from biological systems, reducing tissue buildup and toxicities seen with other nanoparticle forms (NPs) (Nguyen et al., 2018).

MgO NPs may be easily made utilizing bulk synthesis and tailored particle design, as well as simple and affordable techniques like chemical co-precipitation procedures. (Fernandes et al., 2020). Several studies have reported that prepared MgO NPs possess promising anti-inflammatory (Shahid et al., 2022), analgesic (Jahangiri et al., 2013), antibacterial (He et al., 2016), anti-viral (Rafiei et al., 2015), anti-convulsive (Jahangiri et al., 2014) and anti-diabetic (Shehata et al., 2020) properties superior to copper, silver, TiO_2 nanoparticles (Karimiyan et al., 2015; Imani and Safaei, 2019).

Together with the customizable particle design in the bulk synthesis using easy and affordable procedures, MgO NPs are an excellent drug delivery tool (Noori and Kareem, 2019; Imani and Safaei, 2019). In the current work, MgO NPs were chosen as drug carriers, whereas naproxen sodium (NPRS) was chosen as an anti-inflammatory model due to its extensive usage in the management of pain and therapy of numerous inflammatory disorders such as arthritis, ankylosing spondylitis, and tendinitis (Mello and Ricci-Júnior, 2011).

Once within the biological system, plasma proteins detect nanoparticles and create a protein corona around them, a process known as opsonization. Because hydrophobic NPs are more prone to opsonization, the reticuloendothelial system (RES) gets

stimulated, allowing for the fast removal of opsonized NPs from circulation (Wani et al., 2020). However, coating with a non-toxic, biocompatible, biodegradable, and hydrophilic polymer such as polyvinyl alcohol (PVA) prevents opsonization and hence ensures *in vivo* stability. Apart from that, uncoated NPs tend to form aggregates (Soddu et al., 2020), whereas polymer-coated NPs show highly dispersed NPs (Quarta et al., 2012). Moreover, coating with PVA improves the size, surface charge, and physicochemical dynamics of NPs (Park et al., 2019).

Developing novel tailored nanocarriers which may influence the pharmacokinetic profile, biodistribution, and bioactivity of drug molecules without affecting healthy organs and tissues demands to be examined. This is the motivation of the thesis.

Aim and Objectives

This thesis aimed to investigate the efficacy of a nano-drug delivery system in terms of the therapeutic potential and organ toxicities in comparison to the conventional anti-inflammatory drug through various sets of *in vitro* and *in vivo* experimental models.

Objectives

- To prepare and characterize a cost-effective, efficient, multifunctional metal oxide nano particle (MgO NPs), capable of efficiently carrying naproxen sodium (NSAID) into the body; a drug formulation coated with PVA, produced at a nano scale level with the aim of improved therapeutic index and less toxicity compared to its free form (Chapter II).

- To examine the therapeutic potential of naproxen nanoformulations (uncoated and PVA coated) through various sets of standard *in vitro* and *in vivo* physiological activity models (Chapter III).

- To thoroughly investigate the *in vivo* toxicity of uncoated and coated naproxen nanoformulation on male and female mice to reveal the organ- and dose-specific toxic effects according to The US Food and Drug Administration (FDA) and Organization for Economic Co-operation and Development (OECD) guidelines (Chapter IV).

- To investigate the systemic effects of naproxen nanoformulations at human therapeutic dose by converting human therapeutic dose to animal equivalent dose (AED) in comparison with free form naproxen sodium using standard procedures (Chapter V).

Chapter 2

Synthesis And Characterization of MgO NPs and Naproxen Nanoformulations

Summary

MgO nanoparticles (NPs) were synthesized through the chemical coprecipitation method using magnesium nitrate hexahydrate as a precursor. Naproxen sodium (NPRS) was post-loaded on MgO NPs, and the nano-drug complex was capped with polyvinyl alcohol. The percent encapsulation efficiency EE (%) and loading capacity LC (%) of naproxen nanoformulation were found to be $50.4 \pm 3.2\%$ and $43.2 \pm 2\%$ respectively. Changes in UV-Visible and FTIR spectral patterns through each step during the preparation of MgO NPs and naproxen nanoformulations (UNF and CNF) verified the successful formation of nanomaterials. Hydrodynamic size and surface charge of coated nanoformulation were found to be 161 nm and -8 mV respectively, which indicated the formation of a particle size suitable for nanotherapeutic applications.

Introduction

Nanoscience and nano-delivery systems are a pretty recent but fast-evolving field of science, where nano-sized materials are employed as targeted therapies or to deliver drugs in a controlled manner (Soares et al., 2018; Patra et al., 2018). The nanoparticle is the most basic component of nanotechnology. Nanoparticles are materials with at least one dimension of 1 to 100 nanometers and are formed of carbon, metal, metal oxides, or organic substances (Nagarajan, 2008). Because of their size, nanoparticles have distinct physical, chemical, and biological features as compared to their molecular and bulk analogs. Nanoparticles have piqued interest in a variety of applications because of their enormous surface area to volume ratio, greater reactivity (or stability in a chemical process), and increased mechanical strength (Asha and Narain, 2020).

In target-specific drug delivery systems, organic, inorganic, metallic, and polymeric nanostructures, including dendrimers, micelles, and liposomes, are widely utilized (Ahmad et al., 2010; Abasian et al., 2020). These nanoparticles are used to tag drugs that have low solubility and are difficult to metabolize (Kalepu and Nekkanti, 2016). Metal oxide nanoparticles have several advantages over their metal counterparts, including biocompatibility, flexibility, and surface plasmon resonance (SPR) (Mitra, 2022). Genomic research, bioimaging, biosensors, clinical chemistry, immune response augmentation, target/sustained drug delivery, hyperthermia, and photoablation treatment have all benefited from these features (Gao et al., 2019; Malik et al., 2021).

2.1 Synthesis of Metal Oxide Nanoparticles

Controlled synthesis of metal oxide nanoparticles is essential for their successful application in drug delivery applications (Nguyen and Do, 2011). Drugs can be attached to the surfaces of metal oxide nanoparticles by ionic or covalent bonding as well as physical absorption, and they can be delivered and controlled via biological stimuli. (Patra et al., 2018). Furthermore, these nanoparticles can attach to antibodies, medicines, and other ligands due to their modification and functionalization with certain functional groups (Gupta and Gupta, 2005; Rasmussen et al., 2010), increasing the potential of these systems in biological applications. Although gold, silver, iron, and copper are the most thoroughly researched metallic nanoparticles, there has been a surge in interest in other types of metal-based nanoparticles, such as zinc oxide,

magnesium oxide, titanium oxide, selenium, platinum, and cerium dioxide, among others (Falcaro et al., 2016; McNamara and Tofail, 2017).

Several synthesis procedures are now well-established according to the need and requirement of each drug delivery system. These systems offer customized development to improve the characteristics of nanoparticles and also aim at lowering the manufacturing costs. To improve the optical, mechanical, physical, and chemical characteristics of nanoparticles, several procedures are adjusted to produce process-specific nanoparticles (Baig et al., 2021). Instrumentation advancements have resulted in enhanced nanoparticle characterization and application (Lin et al., 2014).

2.2 Methods for Preparation of Nanoparticles

Coprecipitation, sol-gel, inert gas condensation, microemulsion, microwave, hydrothermal synthesis pulse laser ablation, sono-chemical, spark discharge, template synthesis, ion sputtering scattering and biological synthesis are some of the common approaches used to construct nanoparticles of varied sizes (Rane et al., 2018). Bottom-up and top-down techniques are two basic techniques to produce nanoparticles (Wang and Xia, 2004). A simplified representation of the process is presented in Fig 2.1.

The top-down or destructive strategy involves reducing bulk material to nanometer-sized particles. Some of the most extensively utilized nanoparticle production technologies include nanolithography, laser ablation, sputtering, mechanical milling, and thermal breakdown. Because the physical characteristics and surface chemistry of NPs are excessively dependent on the surface structure, this strategy generates imperfections in the product's surface structure, which becomes a major limitation (Vollath, 2008). To maintain specific characteristics such as pressure, temperature, and environment during the process of reducing bulk materials requires a sophisticated, expensive, high-energy-intensive, and specialized setup (inert and non-flammable). Therefore, the top-down technique creates nanomaterial with surface flaws and non-uniform forms, which inhibits usability, even utilizing high-cost setup/instrumentation (Jamkhande et al., 2019).

The bottom-up approach, also known as the constructive technique, is the process of building up a nanomaterial from the bottom up resulting in a material build-up from atoms to clusters to nanoparticles. The most common bottom-up processes for

nanoparticle generation include sol-gel, chemical co-precipitation, spinning, chemical vapor deposition (CVD), pyrolysis, and biosynthesis (Ashik et al., 2018). The nanoparticles (NPs) are made from smaller starting materials using oxidation and reduction methods in the bottom-up approach (Fig 2.1). At the nanoscale, atoms aggregate to form nuclei, so the NPs produced have very few flaws (Gerberich et al., 2003).
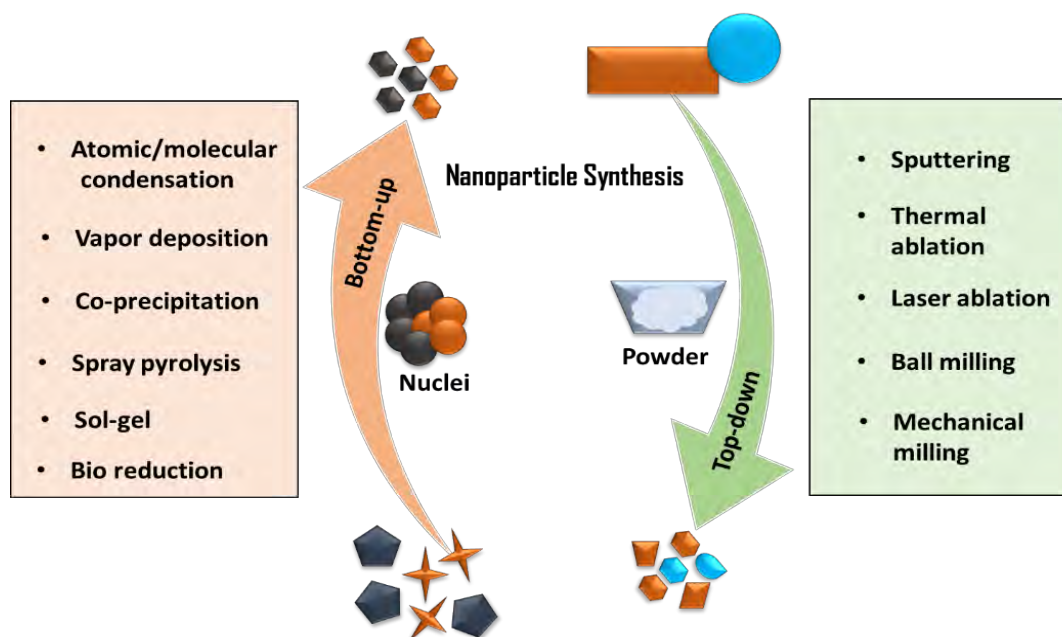
Fig. 2.1 Method for creating nanoparticles of various sizes (Ramanathan et al., 2021).

2.2.1 Coprecipitation Method of Nanoparticles Synthesis

Among bottom-up approaches to creating metal oxide nanoparticles, the co-precipitation method is one of the easiest and most efficient methods (Kandpal et al., 2014; Janjua, 2019). Using this approach uniformed-sized nanoparticles with high purity and size distribution can be produced effectively. The inorganic metal salt precursors, such as chloride and nitride, are dissolved in distilled water in the reaction process during the co-precipitation technique of nanoparticle production. Then a basic solution, such as NaOH or NH_4OH, is then gently added to it, causing the metal species to hydrolyze. The metal oxide nanoparticles are then cleaned, filtered, dried, and calcined to produce the final product. In the co-precipitation process, four important phases must be followed to generate a successful product (Fig. 2.2), which are the "simultaneous occurrence of nucleation, growth, coarsening, and/or agglomeration"

(Stankic et al., 2016). A typical reaction involving co-precipitation method of nanoparticle synthesis demonstrate the following attributes:

1. "The products are generally insoluble species formed under conditions of high supersaturation.

2. Nucleation is a key step; many small particles will be formed.

3. Secondary processes, such as Ostwald ripening and aggregation, dramatically affect the size, morphology, and properties of the products.

4. The supersaturation conditions necessary to induce precipitation are usually the result of a chemical reaction (Athar, 2015).

$$X\,Ay^{+}(aq)\ +\ Y\,Bx^{-}\,(aq)\ \rightarrow\ AxBy\,(s) \qquad (1)"$$
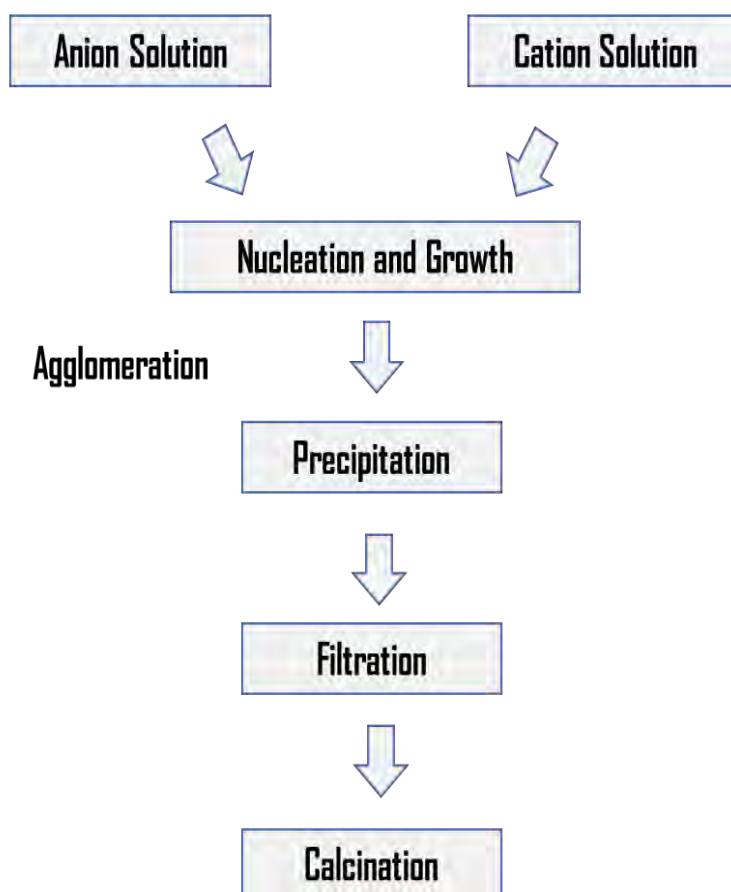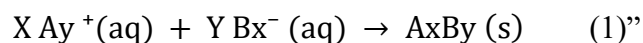
Fig.   2.2   Several   steps   involve   in   the   co-precipitation   technique (https://en.wikipedia.org/wiki/Coprecipitation#/media/File:Co-precipitation.png)

2.3 Strategies for Synthesis of Drug-Loaded Nanoparticles

Nanomedicine grants medications with novel qualities such as better availability and improved pharmacokinetics, fewer harmful adverse effects, sustained release, and the capacity to increase the therapeutic dosage, among other things. Many effective therapeutic medicines, for example, are insoluble in water, restricting their clinical usefulness. The formation of hydrophilic drug-loaded nanomedicines increases not only their solubility but also their bioavailability (Duncan et al., 2010), improves stability, biodistribution, pharmacokinetics, and pharmacodynamics (Tran et al., 2010; Van Ngo et al., 2016).

It is possible to achieve a constant and uniform presence of medications in plasma for a certain amount of time with the help of this technology, and variations in drug concentration above and below the therapeutic levels may be avoided (Lee and Yeo, 2015). As a result, the therapeutic concentration of the medicine will achieve its maximal level in the tissues, resulting in fewer adverse side effects and increased pharmacological efficacy (ur Rehman et al., 2021). An optimum drug delivery system should be biodegradable, biocompatible, and convenient for patients both during and after drug administration (Tiwari et al., 2012). A high drug loading capacity can be achieved through simple, cost-effective, and efficient methods (Shen et al., 2017).

For synthesizing high drug-loading nanoparticles, three key approaches have been established: post-loading, co-loading, and pre-loading (Fig. 2.3) (Liu et al., 2020). In the post-loading technique, porous nanocarriers based on silica and carbon, are synthesized first, and the drug is then loaded onto these nanoparticles by different processes such as electrostatic interactions, entrapment, chemisorption or physisorption, noncovalent hydrophobic interactions hydrogen bonding, or π–π^* stacking (Fig. 2.3a) (Liu et al., 2020).

Co-loading is the process of conjugating a drug to a polymer or macromolecule, then allowing the drug conjugates to self-assemble to produce drug-loaded nanoparticles (Fig. 2.3b). On the other hand, in the pre-loading approach drug nanoparticles are prepared first, then coated with a layer of desired materials, resulting in nanoparticles that have a drug core and a protective shell (Zhao et al., 2010; Wang et al., 2016) (Fig. 3.3c).
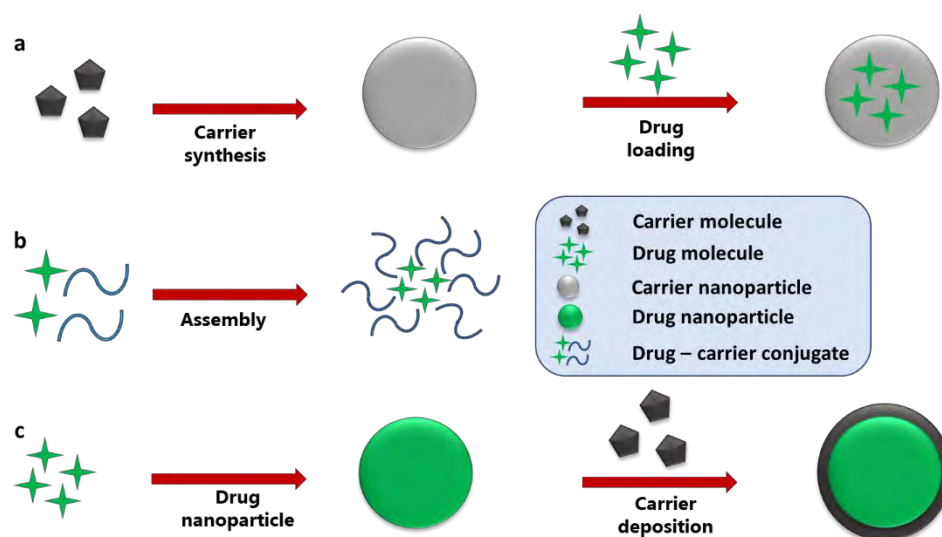
Fig. 2.3 Strategies used for the synthesis of drug-loaded nanoparticles (a) post-loading of the drug on nanocarrier. (b) co-loading of drug and nanocarrier. (c) formation of drug nanoparticles and deposition of nanocarrier on drug nanoparticles (Liu et al., 2020).

2.4 Coating of Drug Loaded Nanoparticles

Because post-loading is simple and ubiquitous, it may be used to load a variety of medications, particularly for those using mesoporous materials. However, due to the adsorption of drugs on particle surfaces, these drug-loaded nanoparticles may confront problems *in vivo*, such as limited loading efficiency and unwanted burst release (Rizvi and Saleh, 2018). Furthermore, nanoparticles in the blood circulation might form aggregates shortly after administration. Other than that, the absorption of plasma proteins on the surface of the nanoparticle may stimulate the immune system and causes macrophage cells to initiate the clearance process, causing nanoparticles to be promptly removed from circulation (Issa et al., 2011; Liu et al., 2011). This, as a result, compromises the effectiveness of nanoparticle-based therapies. A typical and successful way to minimize the burst release and prevent opsonization is to coat the nanoparticle-drug complex with a small layer of additional material, such as a biocompatible polymer (Kayal and Ramanujan, 2010).

Several biodegradable and biocompatible polymers have been thoroughly investigated as nanoparticle coating agents (Wang et al., 2004) such as chitosan, polyvinyl alcohol (PVA), poly- (acrylic acid), polyethylene glycol (PEG), dextran, poly (lactide-co-

glycolide) (PLGA), and poly (ethyleneimine) (PEI) (Lee and Yeo, 2015; ur Rehman et al., 2021). Among them, polyvinyl alcohol (PVA) has outstanding film-forming, emulsifying, and adhesive characteristics (Riva'i et al., 2018). The coating of nanoparticle surfaces with PVA seems to reduce nanoparticle agglomeration and the creation of monodisperse nanoparticles while also preventing drug burst release (ur Rehman et al., 2021).

2.5 Physico-Chemical Characterization of Nanomaterials

The most important factors characterizing the nanoparticles or nanoparticle-drug complexes are their morphology and particle size distribution (Ridolfo et al., 2021, Mourdikoudis et al., 2018). These characteristics highly affect the drug targeting, release kinetics, *in vivo* distribution of the drug, and tissue toxicity (Caster et al., 2017, Sukhanova et al., 2018). Thus, microparticles with greater particle sizes are less successful in drug delivery applications than nanoparticles with lower sizes (Banerjee et al., 2016; Shojaee et al., 2020) providing a large surface area for drug interaction (Çalış et al., 2019).

An array of characterization techniques is available today to analyze the characteristic features of synthesized nanoformulations, a few of them are discussed here.

2.5.1 Determination of Optical Properties of Nanoparticles

Since the optical characteristics of metallic nanoparticles are highly dependent on size, shape, aggregation state, and refractive index near the nanoparticle surface, UV/Visible spectroscopy is a useful method for detecting, characterizing, and investigating nanoparticles (Amendola and Meneghetti, 2009; Grand et al., 2019; Neupane et al., 2019). In a particular procedure, the light that is absorbed and scattered by the sample is detected using the photodetector to assess the sample (Schmid, 2001) Fig. 2.4.

Numerical models can be used to compare the measured spectrum to the expected spectrum. The wavelength ranges from 300 to 800 nanometers are used in spectroscopic analysis of compounds. This approach is also used to determine the production and stability of nanoparticles in an aqueous solution (Rizwan and Gwenin, 2021).
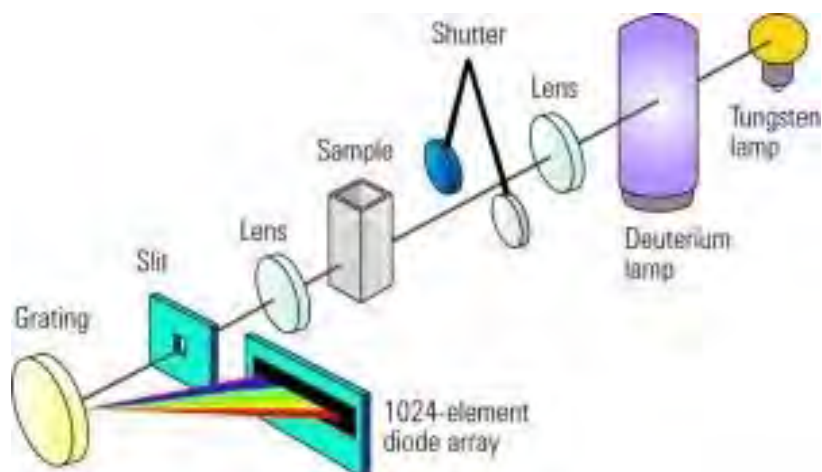
Fig.2.4.　　Schematic　diagram　of　UV-Visible　spectrophotometer (https://nanocomposix.com/pages/nanoparticle-characterization-techniques).

2.5.2 Fourier Transform Infrared Spectroscopy (FTIR)

Every compound possesses specific kind of atomic arrangements which give a fingerprint to that compound. This fingerprint region of compound or nanoformulations is detected through Fourier transform infrared spectroscopy (Titus et al., 2019). During a spectroscopic analysis infrared light in the range of 10,000 to 100 cm^{-1} is allowed to pass through the material of interest. Sample absorbs some light while reflect the rest. The absorbed light is converted into rotational and/or vibrational energy by the sample and detected.

The resultant signal at the detector appears as a spectrum, ranging from 4000 cm^{-1} to 400 cm^{-1}, and represents the sample's chemical fingerprint. FTIR analysis is a powerful technique for chemical identification since each molecule or chemical structure produces a unique spectral fingerprint (Singh and Singh, 2022) Fig. 2.5. FTIR analysis may be utilized for quantitative (quantity) analysis as well as qualitative (identification) examination of materials when appropriate standards are applied (Tinoco et al., 2022).

Based on the FTIR spectra, one may identify functional groups of nanoparticles inside the nanoparticles and detect effective capping of the nanoparticles since each type of nanoparticle has a unique mix of atoms (Raj and Prabha, 2016; Yu et al., 2019; Vigato

et al., 2022).
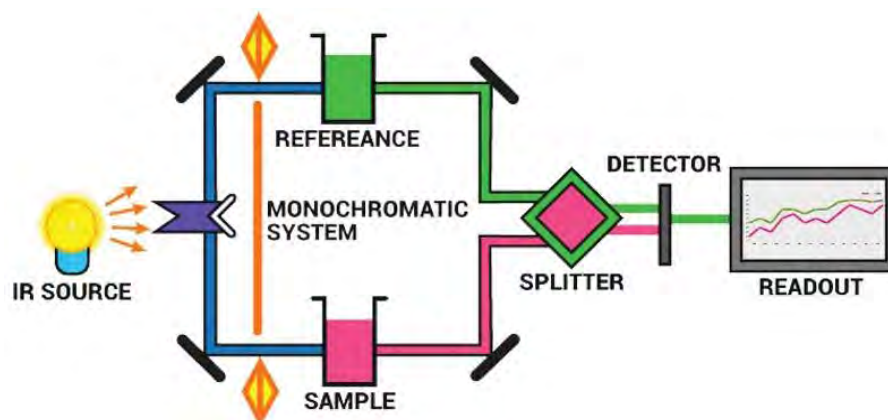
Fig. 2.5 Working principle of Fourier transform infrared spectroscopy
(https://byjus.com/chemistry/infrared-spectroscopy/).

2.5.3 Crystallinity Analysis

The X-ray powder diffraction (XRD) is a flexible, non-destructive characterization technique that typically yields information on crystalline structure, phase nature, (Giannini et al., 2016) lattice parameters, and crystalline grain size (Ananda et al., 2022). This indicates that the XRD method may be used to monitor structural changes in crystalline materials caused by mixing with other materials (Zhang et al., 2016). The Scherrer formula is used to calculate particle size based on the width of the X-ray peaks (Bishnoi et al., 2017). A particle composition may be established by comparing the magnitude and position of the peaks with reference patterns from the International Centre for Diffraction Data (ICDD) database (Saleh, 2021) Fig. 2.6.
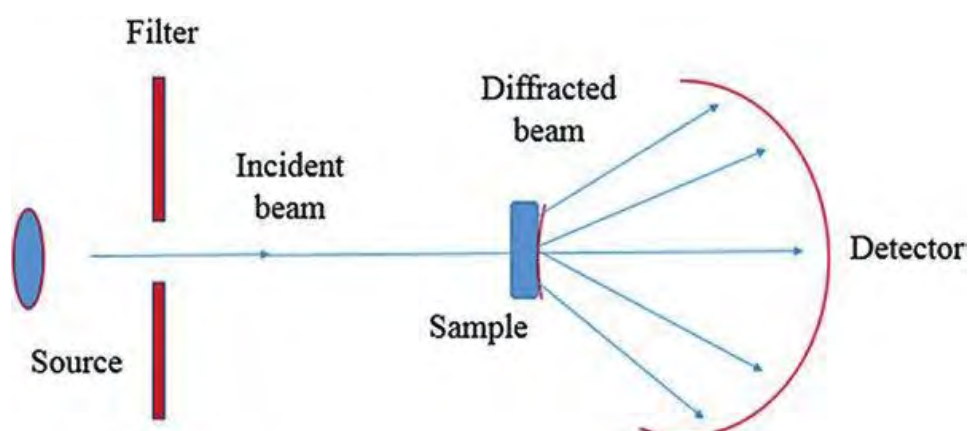
Fig. 2.6 A schematic representation of X-ray crystallography (Hitkari et al., 2019).

2.5.4 Elemental Analysis

Laser-Induced Breakdown Spectroscopy (LIBS) is an atomic spectroscopy technique that is used to assess the elemental composition of a sample. LIBS can detect major and trace elements present in any kind of material like solid, liquid, or gases (Ahmed and Baig, 2009). Each LIBS spectrum offers information on not only the quantities of its element but also isotopic ratios and the atomic structure of the compound (Moros and Laserna, 2019) Fig. 2.7.

In a typical procedure, a high-intensity laser beam is projected on the sample surface to ablate atoms from its top layer which results in the production of a short-lived, high-temperature plasma (Anabitarte et al., 2012). This plasma contains enough energy with a temperature higher than 10,000 K to excite electron presents in the outer orbitals. The plasma when cools, electrons present in the outermost orbitals drop to lower-energy orbitals and release photons. The photons in the form of wavelengths are inversely proportional to the energy difference between the excited and base orbitals detected to assess material composition (Cremers et al., 2016).

Since LIBS is a technique based on spot analysis, it may be used to assess spatial changes in material composition as well as to average photos gathered from a variety of sites on the materials to get a bulk composition. Furthermore, LIBS spectra offer extensive material compositional information, making the method perfect for determining the metal composition and purity of nanoparticles (Gaudiuso et al., 2010).
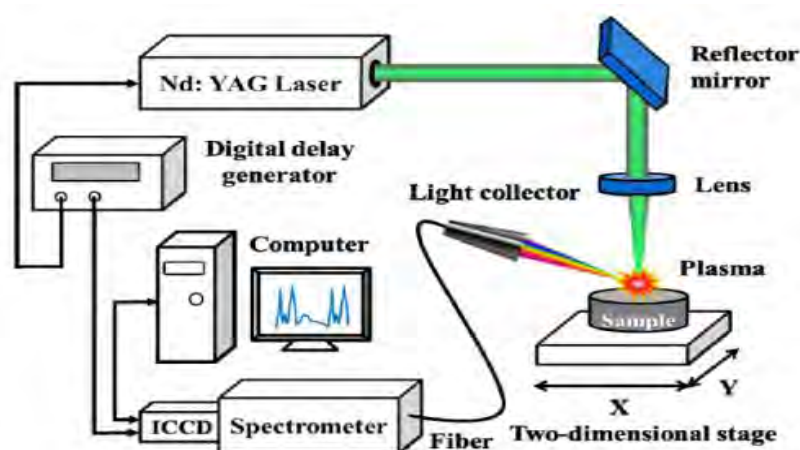
Fig. 2.7 Schematic diagram of laser-induced breakdown spectroscopy (Zou et al., 2014).

2.5.5 Investigation of Thermal Behavior

"Thermogravimetric Analysis is a technique in which the mass of a substance is monitored as a function of temperature or time as the sample specimen is subjected to a controlled temperature program in a controlled atmosphere" (Rajisha et al., 2011). During thermal stability assessment, the sample is kept in a furnace and subjected to gradually increasing temperature and the mass loss shown by the sample is monitored on an analytical scale outside the furnace (Loganathan et al., 2017). TGA provides useful information about the thermal properties of nanostructures, such as fingerprint materials for identification and quality assurance, oxidative stability of materials, an approximate lifetime of a product, and decomposition kinetics, which includes reaction rate and activation energy (Pagar et al., 2022) Fig. 2.8.
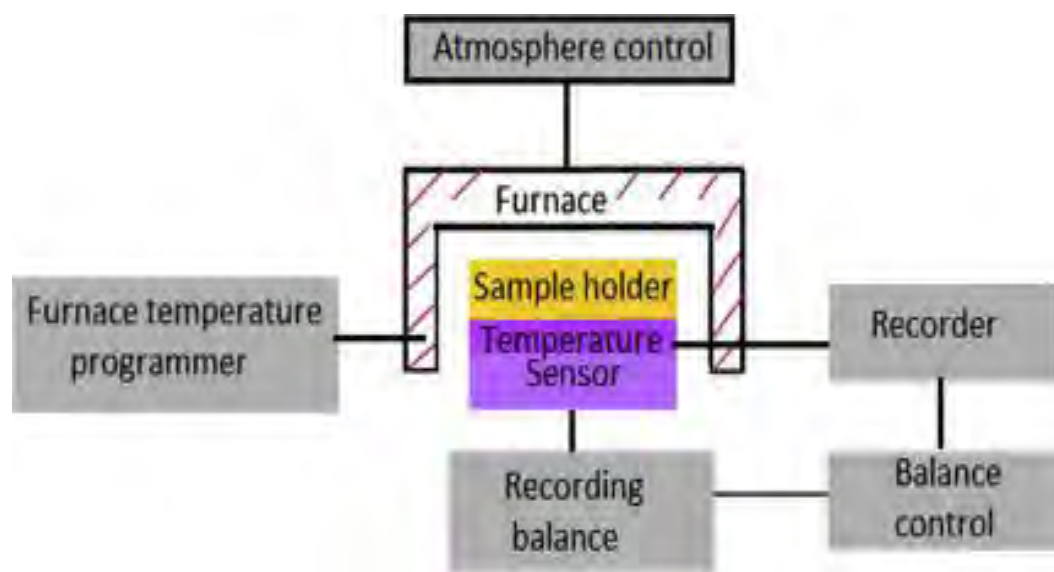
Fig. 2.8 A standard setup for thermogravimetric analysis (Loganathan et al., 2017)

2.5.6   Particle Size and Surface Charge Measurement

Dynamic light scattering (DLS) – also known as photon correlation spectroscopy and zeta potential are two different and advanced table-top techniques for investigating the hydrodynamic size and surface charge of nanoparticles or nanoformulations, respectively (Falke and Betzel, 2019). The interaction of nanoparticles with biological systems is complex. It includes cellular absorption (Fröhlich, 2012), dissolution rate, and the extent to which it can cause toxicity (Bhattacharjee et al., 2013). All of these

attributes are highly dependent on the size and surface charge of nanoparticles or nanoformulation. In addition, proteins present in blood circulation tend to accumulate on nano-based drugs based on their surface charge, hence forming a corona-like structure modifying the unique characteristics of nanoparticles. Therefore, it is critical to study and optimize these two parameters during the formation of nanoparticulate drug delivery systems (DDS) for their normal functioning (Lima et al., 2020).

Particle size assessment through DLS is based on the random motion of particles in a solution, known as Brownian motion, where particles with larger sizes move slowly and scatter more light as compared to smaller particles that move fast and scattered less light. The temporal dependence of scattering intensity data may be used to compute the hydrodynamic diameter (Soares et al., 2018) Fig. 2.9.

The zeta potential (also known as the electrokinetic potential) assesses the charge stability of colloidal nanoparticles by measuring the "effective" electric charge on the nanoparticle surface (Shnoudeh et al., 2019). When a nanoparticle possesses a net surface charge, a greater concentration of ions with opposite charges accumulates near the nanoparticle surface (Kumal et al., 2015). This layer of electrostatic forces travels with the nanoparticle and is made up of the layer of surface charge and opposite charges ions. The magnitude of charge present in his layer defines the particle durability, with greater magnitude indicating stronger electrostatic repulsion, therefore, increased stability and vice versa (Shnoudeh et al., 2019).
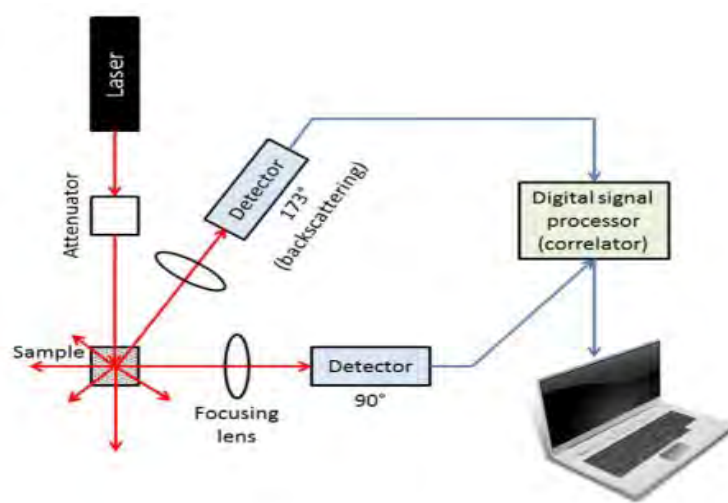
Fig. 2.9 Dynamic light scattering (DLS) particle size analysis (Bhattacharjee, 2016)

2.6 Drug Loading and Encapsulation Efficiency

Drug-loading capacity and drug-loading efficiency are two key features that should be determined during the nanomedicine development process (Shen et al., 2017). In this way, the quantity of drugs entrapped within nanoparticles is assessed. Drug-loading refers to the mass ratio of drugs to nanomedicines, whereas drug-encapsulation efficiency refers to the quantity of the drug being encapsulated by nanoparticles (Sun et al., 2015). Since drug-loading capacity demonstrates the physical and chemical features of carrier material these characteristics have a significant impact on drug metabolism, side effects, additional load, and therapeutic efficacy *in vivo* (Zhang et al., 2017). Drug loading efficiency is calculated as follows (Bao et al., 2021).

$$DL\% = (\text{mass of the drug}\,/\text{total mass of the drug} - \text{loaded nanoparticles}) \times 100\%\ (2)$$

Encapsulation is defined as "the coating or entrapping of an active ingredient inside a solid shell or within a liquid or solid matrix of another material," i.e., in a nano-drug carrier system, the drug's adsorption on the nanoparticle's surfaces is the drug's encapsulation on nanoparticle's surfaces (Kumari et al., 2014).

The encapsulation efficiency (EE%) is defined by "the concentration of the incorporated material (such as active ingredients, drugs, fragrances, proteins, pesticides, antimicrobial agents, etc.) in the formulation over the initial concentration used to make the formulation" (Gaikwad et al., 2019). Encapsulation efficiency (EE %) is calculated using the formula given below (Bao et al., 2021):

$$EE\% = (Wt/Wi) \times 100\%\quad (3)$$

2.7 *In vitro* Drug Release Profile

In vitro drug release analysis is an analytical tool used to investigate the product's pharmacokinetic behavior at various stages of drug development and provide key information about drug half-life. When properly studied, *in vitro* drug release profile, may provide essential information regards its expected behavior in biological systems (D'Souza, 2014). In complicated nanoformulations, *in vitro* drug release testing is critically important to determine therapeutic efficacy, bioavailability, and adverse

effects of the loaded drug. Furthermore, the drug release profile gives structural information, such as porosity and molecular interactions between the drug and the matrix material, and acts as a quality control criterion to ensure the system's integrity, validity, and dependability (Rawal and Patel, 2018).

Among many methods used for *in vitro* drug release testing, the dialysis membrane method is a very simple, reproducible, and commonly used method (Shen and Burgess, 2013). Dialysis membrane testing can be performed in two ways: direct dialysis method and reverse dialysis method. In the direct dialysis method, nanoformulation is loaded in a dialysis membrane filled with the inner media and sealed carefully. This sealed membrane is then placed in a container carrying release media (outer media/compartment). The whole system is gently agitated using an automatic shaker. The quantity of drug release from nanoformulation over time is quantified by taking a sample from outer media and assayed through a UV-visible spectrophotometer (D'Souza, 2014). On the other, in the reverse dialysis method, the nanoformulation containing media is placed in the outer compartment or container having media, and the inner compartment is sampled for the drug release and quantitative assessment (Fig. 2.10 a, b) (Levy and Benita,1990; Gao et al., 2013).
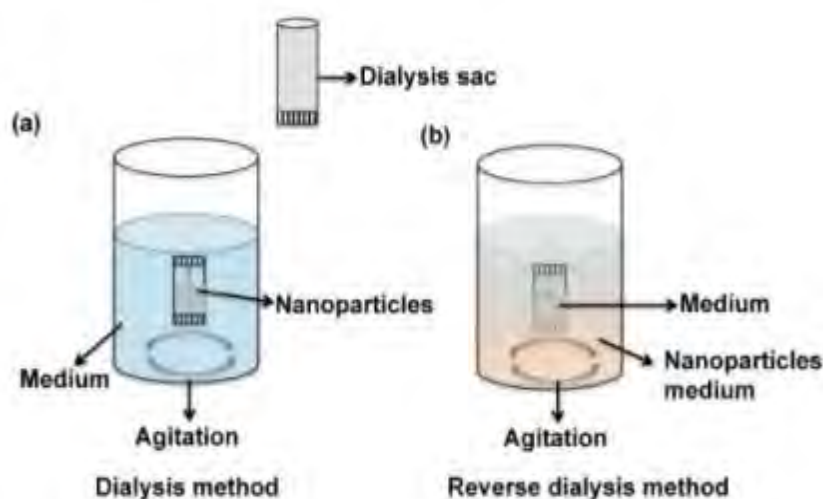
Fig. 2.10 Schematic presentation of *in vitro* drug release (a) Nanoformulation is loaded into dialysis sacs in the simple dialysis method (b) reverse dialysis sac method (Shen and Burgess, 2013).

With the help of nanotechnology, the present study aims to construct a cost-effective low-dose, nanoformulation of naproxen, with improved biological activity and low toxicity compared to conventional naproxen. For this, MgO NPs were synthesized using the chemical co-precipitation method and used as drug carriers, while naproxen sodium (NPRS) was selected as an anti-inflammatory model drug that has widespread use in the management of pain and inflammatory conditions. As a final step, the nano-formulation (NPRS–MgO NPs) was coated with PVA. To confirm the formation of nanoparticles and naproxen nanoformulations, physicochemical characterization was performed using various analytical techniques including UV-visible, FTIR, XRD, TGA, DSC, and LIBS. While the *in vitro* drug loading efficiency of MgO NPs and drug release profiles were also studied.

Materials and Methods

2.8 Synthesis and Characterization of MgO NPs and Naproxen Nanoformulation

2.8.1 Chemicals and Drugs

Magnesium nitrate hexahydrate (Mg $(NO_3)_2.6H_2O$), polyvinyl alcohol (Mw = 89000-98000) (PVA), polyethylene glycol (PEG-600), sodium hydroxide (NaOH), Tween-80, ethanol, and other reagents were procured from Sigma-Aldrich (St Louis, Missouri, USA). Naproxen sodium (NPRS) (99.9 %), diclofenac sodium, and paracetamol were obtained locally (Venus Pharma, Lahore, Pakistan). All solutions were prepared with deionized distilled water.

2.8.2 Characterization

Synthesis and physio-chemical characterization of pure drug naproxen sodium, drug carrier magnesium oxide nanoparticles (MgO NPs), and nano-formulated naproxen sodium were evaluated through various techniques. Spectrophotometry of all compounds was achieved using a UV-Visible spectrophotometer (Perkin Elmer, Lambda 25). Meanwhile, IR spectra of compounds were obtained on a JASCO FTIR-6600 spectrometer in 400-4000 cm^{-1} using the ATR mode. The crystallographic structure of all compounds was determined through an X-Ray diffractometer (D8 ADVANCE, BRUKER) at 2θ ranges from 10 to 80° using a Cu Kα type radiation wavelength adjusted at 1.54 A°. The Zetasizer Nano ZS was adjusted at 635 nm and a 90˚ scattering angle (Malvern Instruments, UK) was used to assess the test materials' ionization and stability. A water-ethanol mixture was used for the dissolution of test samples. Elemental composition and qualification of the drug, MgO NPs, and nanoformulations were detected using Laser-induced breakdown spectroscopy (LIBS). For this, the plasma produced by highly energized (300 mJ) laser beams with 523 nm wavelength and pulse repetition /duration rate was adjusted at 10 Hz and 6 s, respectively, and fixed on the target material's surface to obtain respective spectra.

The pulse repetition and duration rate were adjusted at 118 Hz and 6 s, respectively. A simultaneous thermal analyzer was used to measure 119 thermogravimetric analyses (TGA) in a temperature range of 50-800 ºC at the rate of 10 ºC/min under 120 N_2 environments with a flow rate of 30 mL/min.

2.9 Preparation of MgO NPs

Nanostructured magnesium oxide or MgO NPs were prepared using the standard chemical co-precipitation method (Rao and Chakra, 2014) with necessary modifications. Briefly, a 0.05 M solution of magnesium nitrate was prepared in distilled water (200 mL). A predetermined quantity of polyethylene glycol (PEG-600) was added to this solution and allowed to dissolve completely. To this mixture, 0.05 M solution of NaOH (200 mL) was added slowly, under constant stirring at the rate of 300 rpm until the pH approached 10.4. The obtained mixture was stirred for an additional 30 min at 60 °C. The precipitated particles of magnesium hydroxide (Mg (OH)$_2$) were collected through filtration. The precipitate was then washed with deionized water and ethanol several times and air-dried thoroughly. The dried powder was heated at 100 °C for 1 h and subjected to calcination (muffle furnace) thereafter, for 4 h at 500 °C to obtain the final product MgO NPs. A series of characterization analyses were conducted to confirm the formation of the MgO NPs.

2.10 Preparation of Naproxen loaded MgO NPs (UNF)

To synthesize NPRS-loaded MgO NPs, an ethanolic solution of NPRS was prepared by the addition of 200 mg of NPRS in 20 mL ethanol. This solution was dripped slowly to the ethanolic dispersion of MgO NPs (300 mg in 20 mL ethanol) under constant stirring. Following the completion of this step, the reaction mixture was then stirred for another 2 h. The mixture was then sonicated in a bath sonicator for 1 h at 37 °C (PG43301, MSE Instruments, UK) and centrifuged for 30 min at 3500 rpm. The precipitate obtained was then dried, analyzed, and termed as uncoated nanoformulation UNF (NPRS–MgO NPs). A series of drug loading efficiency experiments were conducted to optimize the drug to MgO NPs ratio in the final product (data not shown). The drug to NPs weight ratio was finalized at NPRS: MgO NPs = 2: 3.

2.11 Coating of Naproxen conjugated MgO NPs

Following successful conjugation of NPRS and MgO NPs, the nanoparticle and drug conjugate (UCF) were subjected to coating with PVA. In this step, a predetermined quantity (97 mg) of UNF was added into a freshly prepared 0.5 % aqueous solution of tween-80 (5 mL ethanolic solution), under constant stirring for 25- 30 min. The prepared mixture was then added to the polymeric solution (2.5% PVA in distilled

water) and constantly stirred for 3 h at room temperature. The final mixture was dried in petri plates, collected, and stored for further experimentation , and characterizations. The weight percent (wt. %) of bare NPRS–MgO NPs, PVA, and tween–80 in the final product was 97%, 2.5%, and 0.5%, respectively. The final coated product was termed coated nanoformulation (CNF) in the current study.

2.12 Drug Encapsulation and Loading Efficiency Studies

The NPRS content adsorbed on MgO NPs was calculated through the Beer-Lambert law (Vincent et al., 2020). For this, a standard calibration curve representing serial dilutions of NPRS in ethanol was obtained with a correlation coefficient of 0.99 or more. Following this, 1 mL of supernatant containing unbound NPRS from the freshly prepared UNF solution was taken and diluted quantitatively to take UV absorbance at λ = 232 nm (wavelength for the detection of NPRS) with the help of a spectrophotometer. The absorbance values were subjected to the standard calibration curve to quantify NPRS content using the Beer-Lambert law, and the obtained values were added to the following equations to determine the percent encapsulation efficiency (EE) and drug loading efficiency (LE).

$$\text{Percent encapsulation efficiency} = \frac{\text{NPRS total (mg)} - \text{unadsorbed NPRS (mg)}}{\text{NPRS total (mg)}} \times 100 \quad (4)$$

$$\text{Loading efficiency (\%)} = \frac{\text{NPRS total (mg)} - \text{unadsorbed NPRS (mg)}}{\text{mass of nanoformulation (mg)}} \times 100 \quad (5)$$

The whole experiment was repeated three times, and values were averaged before final calculations.

2.13 Drug Release Study and Kinetics

Drug release from the coated nanoformulation was investigated *in vitro* at various physiologic pH levels, including 7.4, 6.8, 4.5, and 1.2. At the same time, the temperature was kept constant at 37 ± 0.1 °C. Two different buffers, the phosphate-buffered saline (PBS) and acetate buffer were used as media. Briefly, dialysis bags were prepared using a dialysis membrane of molecular weight cut-off at 1 KDa and diameter = 11.5 mm (CelluSep®). Coated nanoformulation (CNF, 10 mg) was dispersed in the dialysis bag and held tightly. The dialysis bags were placed in 50 mL of release media

(acceptor compartment) and constantly stirred (100 rpm) in an incubator shaker (SV 1422, WNB 14, memmert, Germany) until the completion of the experiment. At specific time intervals, 3 mL of samples were taken and refilled immediately with a fresh medium to retain the sink condition. The dissolute drug content in each sample was quantified spectrophotometrically. The whole experiment was performed three times. Samples were taken out initially at an hourly interval from 0 to 9 h and then after 6 h interval, i.e., 12 h, 18 h, and 24 h. The percentage release of NPRS was calculated using the formula below.

$$\text{Drug release (\%)} = {}^{Dt}/_{Do} \times 100 \qquad (6)$$

The amount of drug released from nanoparticles at a given time is denoted by D_t, while the total amount of drug loaded on the MgO nanoparticles is denoted by D_o.

The drug release study results were fitted to various mathematical drug release kinetic models, including i.e., zero and first orders, Higuchi and Korsmeyer-Peppas (Somanathan et al., 2016). Moreover, the graphs with the highest R^2 value were considered to estimate the drug release pattern.

Results

2.14 Preparation of MgO NPs, and Naproxen Nanoformulations

In the current study, a co-preparticipation method was adapted to synthesize magnesium oxide nanoparticles (MgO NPs). The synthesis step to prepare naproxen nanoformulation included the preparation of MgO NPs and loading of naproxen sodium (NPRS) onto MgO NPs which was termed uncoated nanoformulation (UNF), and finally, the surface modification of MgO NPs–NPRS complex using a biocompatible and biodegradable polymer, PVA. The final product in the process was termed coated nanoformulation (CNF). The formation of the product in each step was verified by the characterization analyses of the resultant compounds. Fig. 2.11 shows the various steps involved in preparing naproxen nanoformulation.

2.15 Characterization of NPRS, MgO NPs, UNF and CNF

2.15.1 UV-visible Spectroscopic Investigations

The UV-visible absorption for coated and uncoated nanoformulation (NPRS–MgO NPs) in the range of 200–800 nm was performed and the change in spectra was compared with NPRS and MgO NPs spectra Fig. 2.12.

The absorption spectrum of NPRS showed two characteristic peaks at 261 nm and 273 nm. A low intensity broader hump present between 260-330 nm in the MgO NPs spectrum indicated the formation of amorphous natured MgO NPs. Furthermore, analyzing the spectrum of NPRS–MgO NPs, showed the peak shift of MgO NPs toward smaller wavelengths and the loss of NPRS plasmon peak at 260-275 nm. Lastly, the absorption spectrum of PVA-coated NPRS–MgO NPs remained unchanged and appeared at 231 nm with a slight increase in peak intensity due to the addition of PVA to nanoformulation.

2.15.2 FTIR Spectroscopic Analysis of Functional Groups

The functional groups of MgO NPs (a), pure NPRS (b), and chemical modification of uncoated NPRS–MgO NPs (c) and PVA coated NPRS–MgO NPs (d) were determined through FTIR spectroscopy. Fig. 2.13 illustrates the IR- spectra of the test compounds mentioned earlier.

For MgO NPs, four characteristic bands were observed at 3446 cm^{-1}, 1425 cm^{-1}, 862 cm^{-1}, and 630 cm^{-1}. A wideband at 3446 cm^{-1} corresponds to hydroxyl group -OH stretching, while a medium-wide band at 1425 cm^{-1} and a strong peak at 630 cm^{-1} is attributed to Mg-O stretching. The band at 862 cm^{-1} depicts the formation of MgO NPs.

The FTIR spectrum for the pure NPRS showed a characteristic broad peak at 3337 cm^{-1} and less intense bands at 2960 cm^{-1}, and 2903 cm^{-1}. A set of medium to intense absorption bands was found at 1600 cm^{-1},1584 cm^{-1},1491 cm^{-1},1389 cm^{-1}, 1360 cm^{-1},1254 cm^{-1}, and 1210 cm^{-1}, while a few peaks with weak intensity were observed between 1197-1010 cm^{-1}. The peak observed at 1491 cm^{-1} is asymmetrical COO- stretching, while the band at 1,584 cm^{-1} corresponds to symmetrical stretching of COO. FTIR Peak at 1,394 cm^{-1} to 1,365 cm^{-1} is attributed to CH$_3$ bending. The peak at 1,210 cm^{-1} represents C-O- stretching (ether), whereas the peak at 1,254 cm^{-1} corresponds to C-O- bond stretching. Furthermore, bands at 3,057 cm^{-1} and 2,838 cm^{-1} show an aliphatic stretch of the C-H bond.

In the FTIR spectrum of NPRS-loaded MgO NPs, several changes regarding characteristic bands of MgO and NPRS were identified. Distinct bands at 3368 cm^{-1}, 2325 cm^{-1}, 2323 cm^{-1}, 1603 cm^{-1}, 1392 cm^{-1}, 850 cm^{-1} and 637 cm^{-1} were detected. Interestingly, the broadband associated with -OH stretching was modified and wider than NPRS and MgO NPs alone and shifted at 3368 cm^{-1}. Moreover, characteristic bands representing functional groups of NPRS at 1584 cm^{-1},1491 cm^{-1}, 1389 cm^{-1}, 1360 cm^{-1}, 1254 cm^{-1}, and 1210 cm^{-1} were diminished and replaced with a medium-wide band at 1394 cm^{-1}. Also, absorption bands of NPRS at 1603 cm^{-1} and 1630 cm^{-1} improved in NPRS-MgO NPs complex and shifted to 1600 cm^{-1} and appeared as a single moderate peak. Furthermore, the bands associated with MgO NPs at 630 cm^{-1} and 862 cm^{-1} were shifted to 637 cm^{-1} and 850 cm^{-1}, respectively. FTIR results suggested, therefore, chemisorption of NPRS onto the surface of MgO NPs.

Interestingly, when PVA was added to uncoated NPRS – MgO NPs, compared to uncoated NPRS-MgO NPs at 3384 cm^{-1} (-OH stretching), a spectral peak shift to a higher frequency was observed. Moreover, characteristic FTIR bands of uncoated NPRS-MgO NPs at 3368 cm^{-1}, 2325 cm^{-1}, 2323 cm^{-1}, 1600 cm^{-1}, 1392 cm^{-1}, 850 cm^{-1}, and 637 cm^{-1} disappeared, and an IR spectrum corresponds to PVA was observed. The bands between 3000 cm^{-1} to 2,800 cm^{-1} (2915 cm^{-1}, 2859 cm^{-1}) are attributed to

the C–H stretching vibration of the alkyl group of PVA. In contrast, peaks at 1420 cm^{-1} and 1092 cm^{-1} depict the C–O group.

2.15.3 XRD Characterization

Initially, a series of experiments were conducted and optimized to obtain MgO NPs of desired characteristics. Magnesium hydroxide (Mg-OH) obtained by the co-precipitation method was subjected to calcination at 500 °C, 600 °C, and 700 °C and characterized for crystallite structure using the XRD. The XRD patterns of MgO NPs calcinated at 500 °C, 600 °C, and 700 °C for 5 hours are shown in Fig. 2.14. Results showed significant reflection angles at 42.94° and 62.09° corresponding to (200) and (220) planes of MgO, indicative of the cubic phase of MgO NPs with no impurities. It was observed that with the increase in calcination temperature, the width of the diffraction peaks narrowed, indicating improved crystallinity. While at a low temperature, of 500 °C, the diffraction peaks were broadened, which signified the amorphousness of MgO NPs. Eubank (Eubank, 1951) concluded in his study that MgO NPs obtained after calcination at lower temperatures (500 °C) show a higher surface area and more vital adsorptive ability. Therefore, we chose 500 °C as calcination temperature to synthesize amorphous natured MgO NPs.

To obtain and compare structural information of bare MgO NPs, NPRS alone, uncoated NPRS–MgO NPs, and coated nanoformulation, X-ray diffraction analysis was performed. Data are shown in Fig. 2.15

Fig. 2.15a. shows the XRD pattern obtained for MgO NPs. The XRD pattern of free drug NPRS displayed the diffraction peak at 18.85° 2θ range associated with as shown in Fig. 2.15b. In the uncoated nanoformulation, as shown in Fig. 2.15c, the broad peaks in 18.85° and 38°, 58° at 2θ regions indicate contributions from both MgO NPs and NPRS, upon adsorption of NPRS on the surface of MgO NPs On the other, CNF did not show any well-defined crystalline peaks. However, a broad hump at 19.87° (halo diffraction peak) is indicative of the amorphous state of PVA Fig. 2.15 d. Additionally, in a CNF diffractogram, low-intensity broad peaks at 40° and 50° predominantly indicate partial crystallinity of MgO NPs. However, the disappearance of characteristic diffraction peaks associated with NPRS confirms the amorphous state of PVA-coated NPRS–MgO NPs. In brief, the diffraction pattern of CNF shows a loss of crystallinity.

2.15.4 Elemental Analysis

In the present study also, the purity and quality of the test samples were investigated through LIBS. Fig. 2.16 illustrates the elemental spectra obtained for free drugs, MgO NPs, and uncoated and coated nanoformulations. The sodium salt of naproxen is frequently prescribed to increase its oral solubility. Since NPRS was used to synthesize NF in this study, sodium in the given sample accounts for drug presence in that sample. Likewise, distinctive signals associated with the magnesium metal indicated MgO NPs in the given sample. Therefore, as shown in Fig. 2.16, sodium was detected in the drug, coated, and uncoated NF samples, which demonstrated the drug-carrying ability of MgO NPs.

On the other hand, magnesium was detected in the MgO NPs, and uncoated, and coated nanoformulations ascribed to the presence of MgO NPs in the samples. As the peak height indicates the elemental intensity in the analyzed sample, less intense magnesium and sodium peaks were observed in CNF, suggesting PVA coating on nanoformulation. On the contrary, elemental peaks were found more intense in the uncoated formulation.

2.15.5 Investigation of Thermal Behavior

Thermogravimetric curves of (a) MgO NPs, (b) NPRS, (c) UNF, and (d) CNF are shown in Fig. 2.17. All samples showed a weight loss of about 3-7 % below 107 °C due to physical retained water. MgO NPs showed decomposition in the interval of 330-420 °C with an endothermic peak appearing at 412 °C and weight loss of 52 %. In the TGA curve of NPRS, two decomposition points were identified. The 1st decomposition point was noted at 122-219 °C having an endothermic peak commencing near 154 °C, which is the melting point of naproxen. After 219 °C, it was found to be stable up to 304 °C. The 2nd decomposition point started at 295 °C and continues up to 450 °C with an endothermic peak falling at 420 °C. UNF showed three degradation steps. During 1st degradation step, there was a gradual weight loss of 20 % within a temperature range of 102-196 °C. An endothermic peak was observed at 146 °C. Further, stability was observed in the range of 196-275 °C. In the 2nd degradation stage, sudden weight loss of 62 % was observed in the range of 275-422 °C with an endothermic peak of 376 °C. Stability was observed in the range of 422-653 °C. The last step of decomposition started at 653 °C and ends up at 800 °C, showing a 15 % mass reduction with an

endothermic peak appearing at 716 °C. In UNF, the melting of naproxen was observed at 146 °C which is 8 °C less than the traditional naproxen. While decomposition of MgO was noted at 376 °C. CNF also showed 3 stages of degradation. In 1st stage of degradation, 16 % mass loss was calculated in an interval of 95-268 °C with an endodermic signal commencing at 250 °C. It was found to be stable between 268-308 °C. A maximum weight loss of about 54 % was observed in the 2nd stage of decomposition which occurred between 308-427 °C with an endothermic peak appearing at 340 °C. No change in mass was observed in the range of 427-622 °C. During the final step of decomposition, a 28 % reduction in mass was noted within a temperature range of 622-750 °C having an endothermic peak at 725 °C. In CNF the melting of naproxen was increased and identified at 250 °C which is about 100 °C more than the traditional naproxen. This showed the stability of nano-formulated naproxen (CNF) than the traditional naproxen. The stability of PVA and MgO was also increased in CNF as they showed decomposition at 340 and 725 °C, respectively.

2.15.6 Particle Size and Surface Charge Assessment

Figure 2.18 shows the size distribution and surface charge on MgO NPs, NPRS, and uncoated and coated nanoformulation. Results demonstrated that the particle size of MgO NPs varied between 140 nm - 484 nm. The agglomeration of MgO NPs could be one of the reasons for this variation. The adsorption of NPRS on the surfaces of MgO NPs resulted in an improved hydrodynamic size with a more pronounced peak in the 152 nm region indicating the presence of nano-sized (152 nm) uncoated NPs (66%), but, due to aggregated particles, the second less intense peak appeared simultaneously at 399 nm region. The PVA coating on NPRS-MgO NPs reduced the aggregation between the NPs, resulting in an ideal particle size of 161 nm suitable for nanotherapeutic applications.

The cumulative ionic charge on MgO NPs, synthesized using the co-precipitation method, was found to be -28.8, which was reduced to -11.7 after NPRS adsorption. Following PVA coating, the surface charge of nanoformulation showed a further decrease in zeta potential to -8.85.

2.16 Drug Loading and Encapsulation Studies

In the present study, the drug to nanoparticles ratio by weight was 3: 2 during the

Synthesis of NPRS-loaded MgO NPs. EE (%) and LC (%) were to be $50.4 \pm 3.2\%$ and $43.2 \pm 2\%$, respectively.

2.17 *In vitro* Drug Release Study

The data obtained in the drug release profile demonstrated the expected phenomena shown by the CNF, the controlled release of drug in the media, where the R^2 value of NF is attributed to the first-order release kinetics Fig. 2.19.

An *in vitro* drug release study was performed for CNF at various physiological pH levels ranging from highly acidic to neutral, i.e., 1.2, 4.5, 6.8, and 7.4. As indicated in Fig. 2.19. CNF showed a prolonged release of NPRS in all test media with no immediate release effect. While a maximum drug release was observed at pH 6.8, with $> 95\%$ drug release in 24 h, minimum drug release was observed at 1.2 (acidic pH) over time.
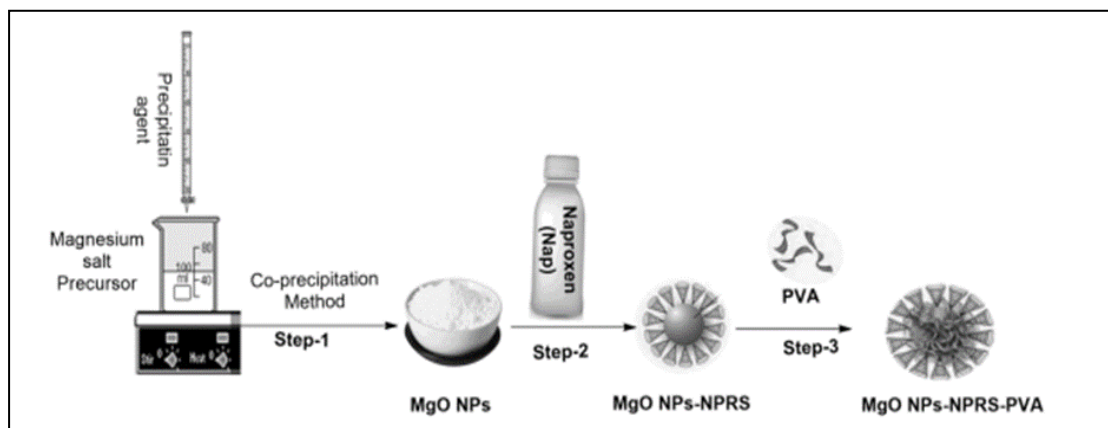
Fig. 2.11 Systematic representation of synthesis step involved in the formation of coated nanoformulation (CNF).
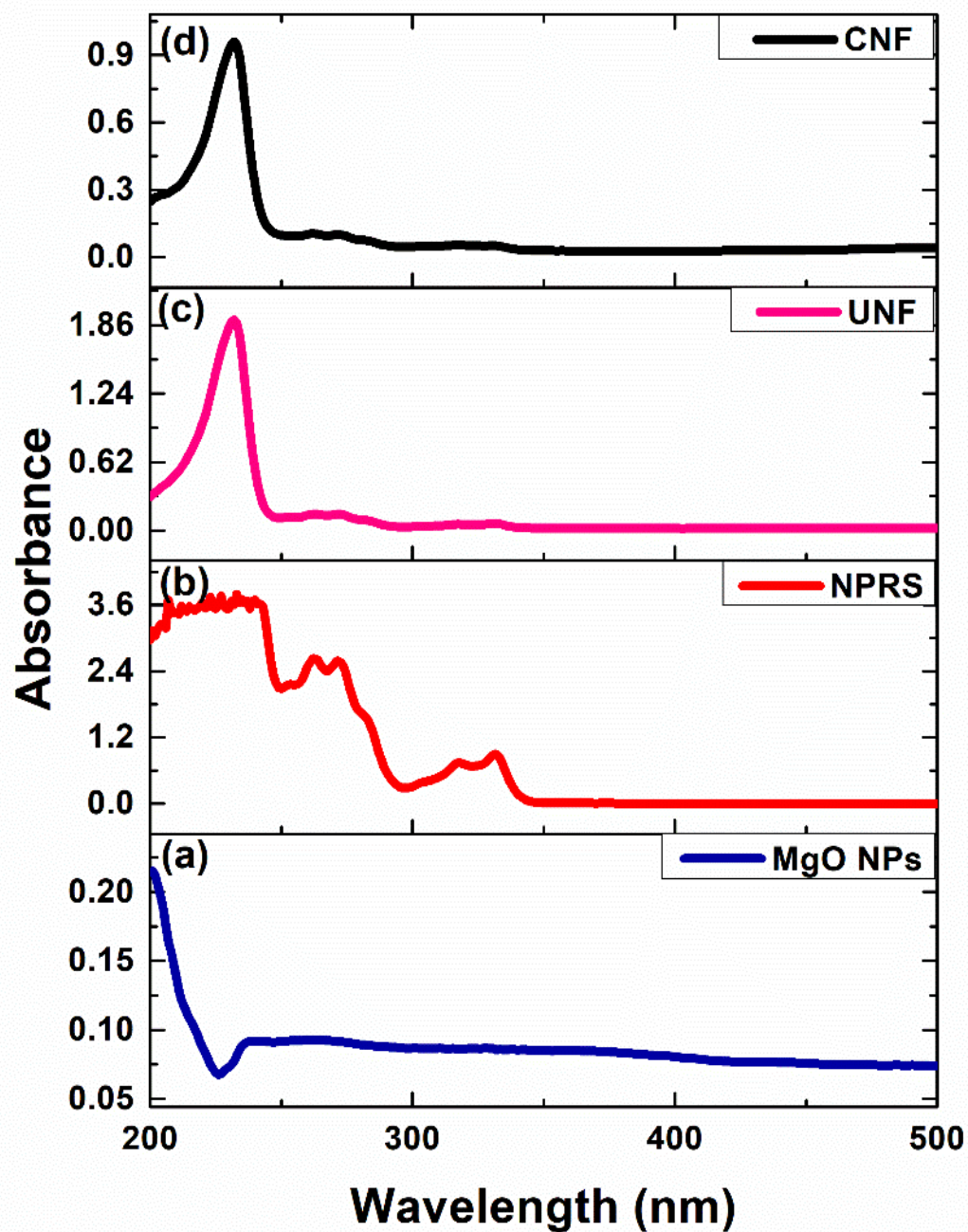
Fig. 2.12 UV-Visible spectra. (a) Magnesium oxide nanoparticles (MgO NPs), (b) Pure
        naproxen sodium (NPRS), (c) Uncoated nanoformulation (UNF, NPRS–MgO
        NPs, and (d) coated nanoformulation (CNF, polyvinyl alcohol coated NPRS–
        MgO NPs).
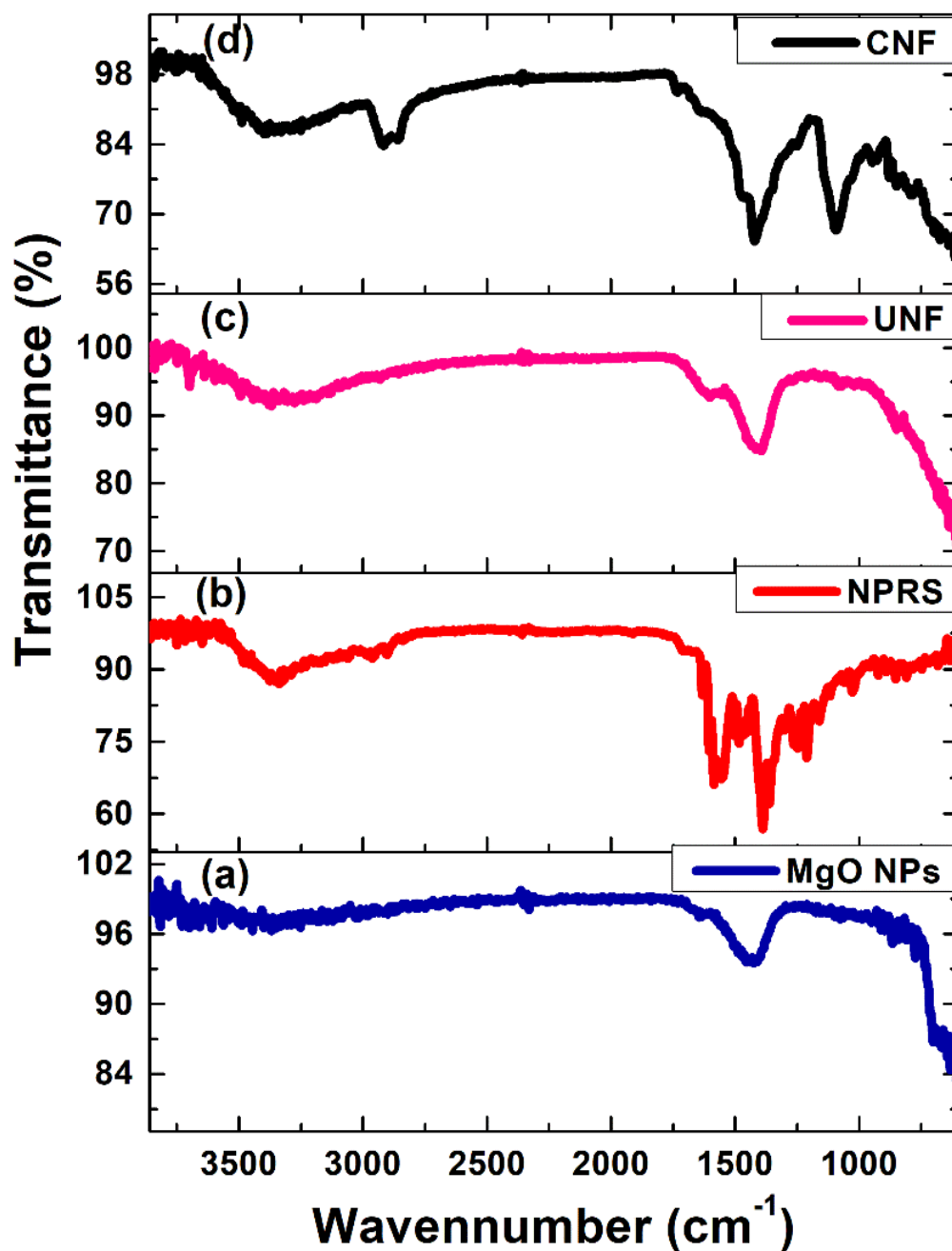
Fig. 2.13 FTIR spectra. (a) Magnesium oxide nanoparticles (MgO NPs), (b) Pure naproxen sodium (NPRS), (c) Uncoated nanoformulation (UNF, NPRS–MgO NPs, and (d) coated nanoformulation (CNF, polyvinyl alcohol coated NPRS– MgO NPs).
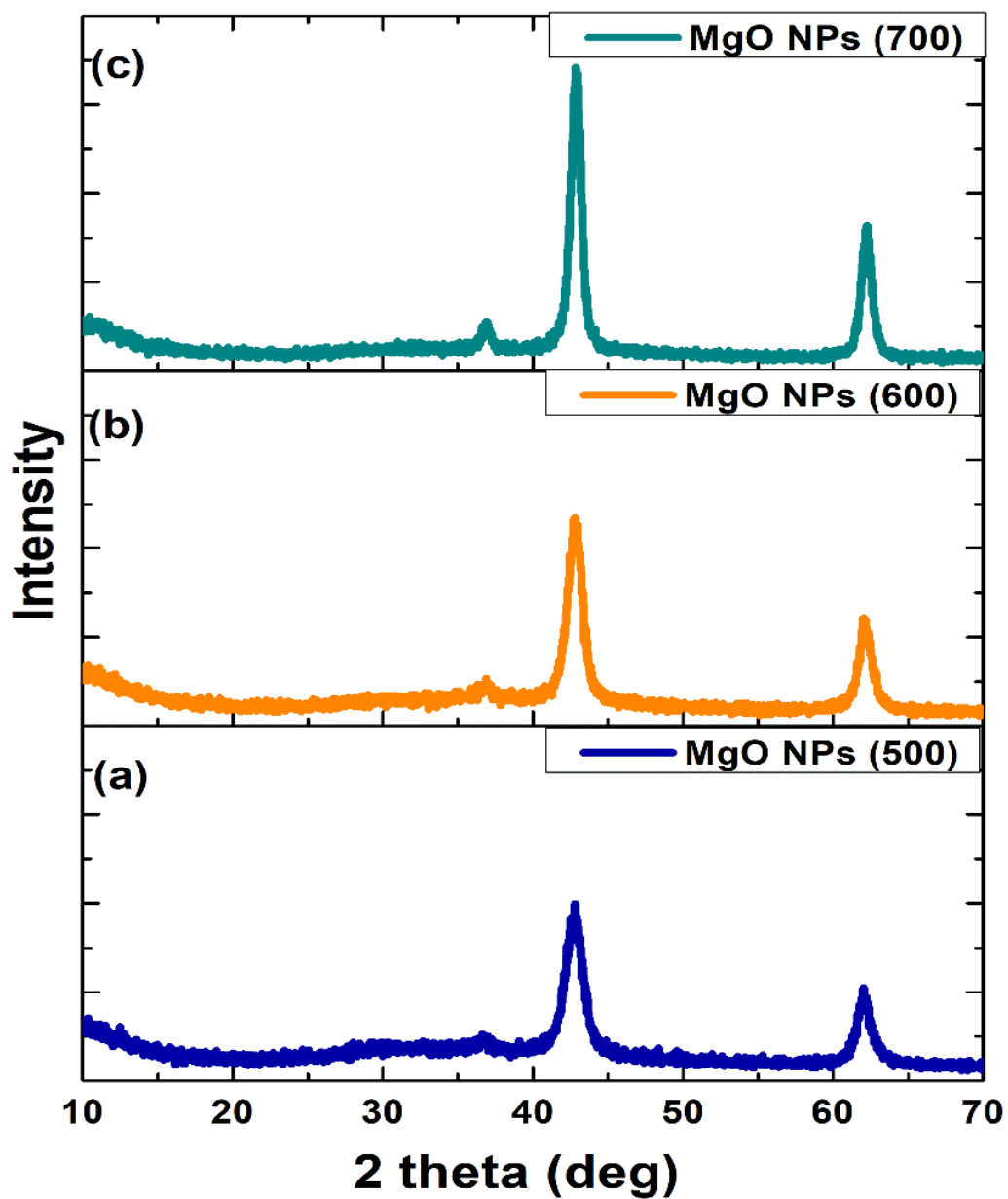
Fig. 2.14 XRD diffractogram. Diffraction patterns are shown by Magnesium oxide nano particles (MgO NPs) at various temperatures.
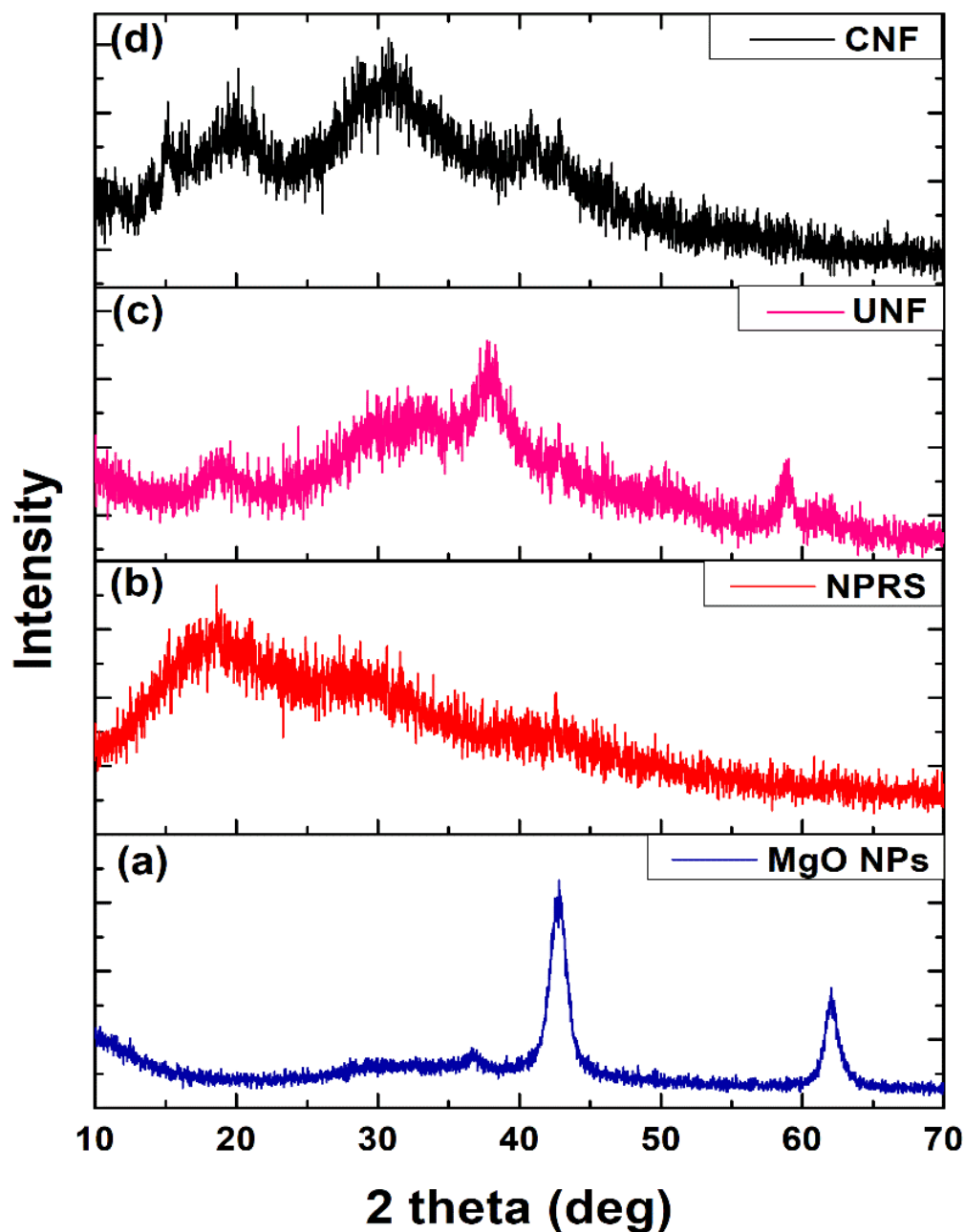
Fig. 2.15 X-ray diffraction patterns. (a) Magnesium oxide nanoparticles (MgO NPs), (b) Pure naproxen sodium (NPRS), (c) Uncoated nanoformulation (UNF, NPRS–MgO NPs, and (d) coated nanoformulation (CNF, polyvinyl alcohol coated NPRS–MgO NPs).
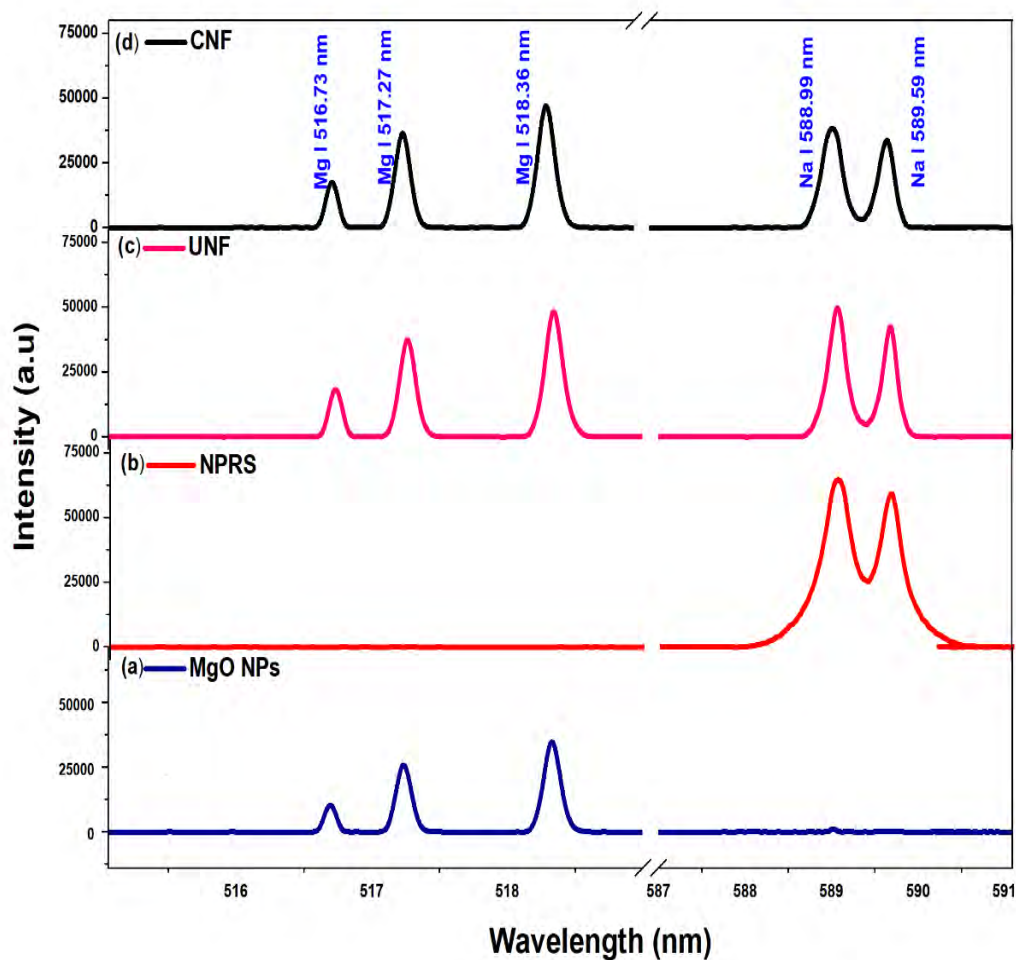
Fig. 2.16 LIBS spectra between 400-600 nm. (a) Magnesium oxide nanoparticles (MgO NPs), (b) Pure naproxen sodium (NPRS), (c) Uncoated nanoformulation (UNF, NPRS–MgO NPs, and (d) coated nanoformulation (CNF, polyvinyl alcohol coated NPRS–MgO NPs).
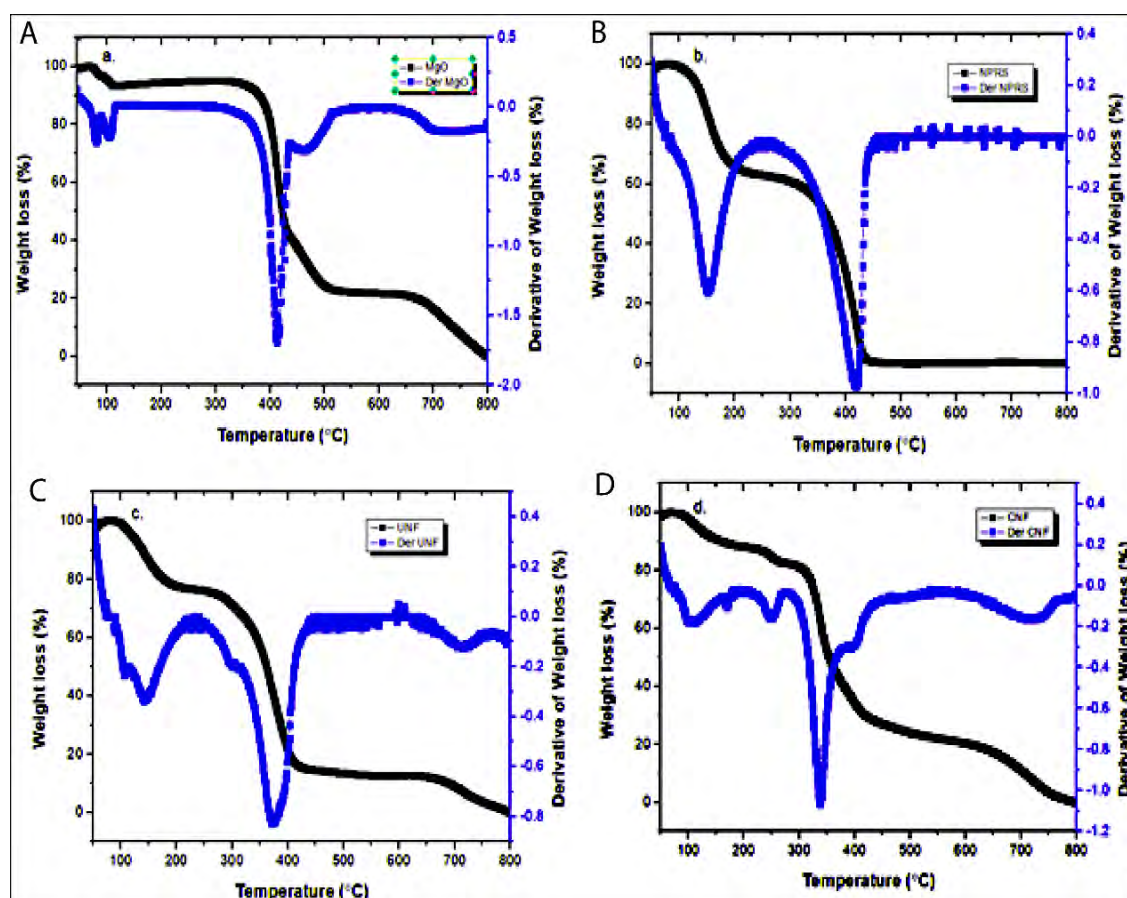
Fig. 2.17 Thermogravimetric curves of (A) MgO NPs, (B) NPRS, (C) UNF and (D) CNF(a) Magnesium oxide nanoparticles (MgO NPs), (b) Pure naproxen sodium (NPRS), (c) Uncoated nanoformulation (UNF, NPRS–MgO NPs, and (d) coated nanoformulation (CNF, polyvinyl alcohol coated NPRS–MgO NPs).
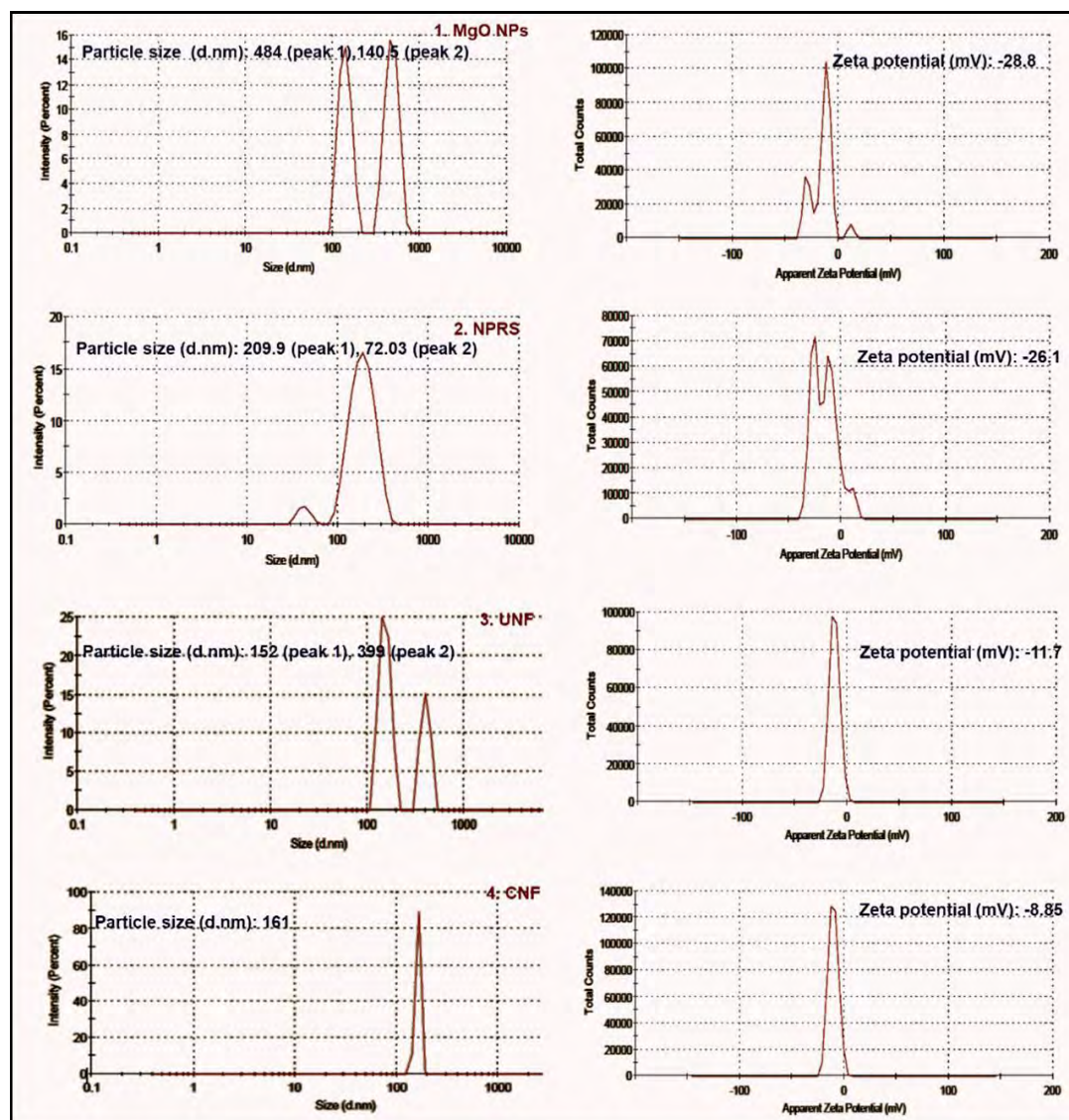
Fig. 2.18 Particle size and zeta potential. (a) Magnesium oxide nanoparticles (MgO NPs), (b) Pure naproxen sodium (NPRS), (c) Uncoated nanoformulation (UNF, NPRS–MgO NPs, and (d) coated nanoformulation (CNF, polyvinyl alcohol coated NPRS–MgO NPs).

	Zero order	First order	Hixson—Crowell	Higuchi	Korsmeyer—Peppas
A	$C=K_o t$	$\ln C = \ln C_0 - K_t$	$Q_0^{1/3} - Q_t^{1/3} = K_{HC}t$	$Q=K_H t^{1/2}$	$M_t/M_\infty = K_p t^n$
	R^2	R^2	R^2	R^2	R^2
	0.95	0.98	0.96	0.94	0.92
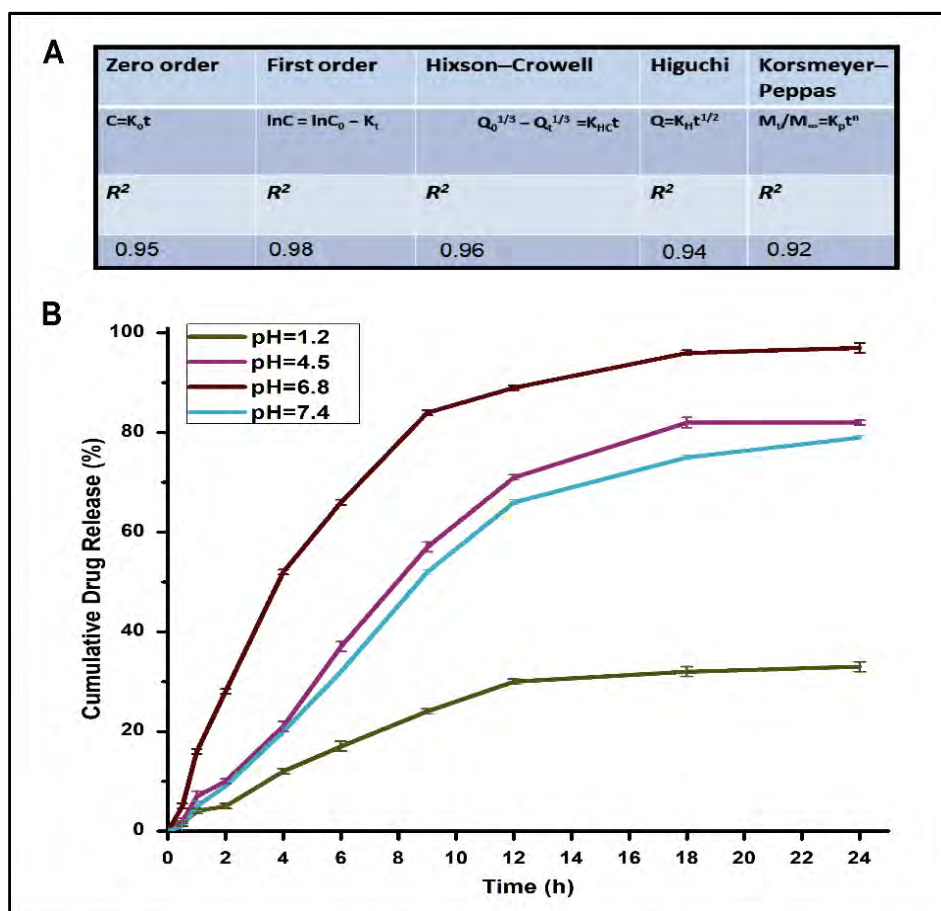
Fig. 2.19 *In vitro* drug release kinetic models (A). Controlled release of NPRS from coated nanoformulation in a pH-responsive manner (B).

Discussion

Given the long-term use of anti-inflammatory drugs causing organ damage (Singh, 2000, Bindu et al., 2020), enormous research has been focused to explore the potential of nanoparticles as drug carriers to formulate novel nanoformulation. The main idea behind these formulations is to reduce drug toxicity by effectively carrying and releasing the loaded drug into biological systems at the lowest possible quantity while maintaining the plasma concentration needed for therapeutic efficacy (Prasad et al., 2015). Therefore, based on their physio-chemical characteristics, drug-carrying and release capability, behavior, and compatibility with biological systems, there has always been a growing need to develop better nanocarriers used for drug delivery (Din et al., 2017; Shen et al., 2017).

Presently, one such nanodrug delivery system was designed to enhance therapeutic potential while lowering the quantity of active/effective therapeutic doses with the help of nanotechnology and investigating its therapeutic index, biological compatibility, and toxicity. Presently, naproxen sodium (NPRS) was selected as a model anti-inflammatory drug due to its excellent therapeutic properties (Hsueh et al., 2020), but the use of NPRS has been limited due to certain gastrointestinal and other physiological complications reported widely at doses, indicated for the treatment of certain inflammatory diseases (500 mg to 1200 mg/day for an adult human) for long durations (from month to years) (Maniar et al., 2018).

Reported as one of the most convenient, economical, and efficient methods to prepare nanoparticles, the co-precipitation method is employed to prepare MgO NPs in the present study (Pudovkin et al., 2018).

Initially, the magnesium hydroxide (the product obtained before the final step of calcination was performed) was subjected to calcination at three different temperatures 500, 600, and 700 °C for 5 h, and their XRD pattern was recorded. The selection of calcination temperature is one of the important steps during the preparation of nanoparticles as it greatly impacts the form and structure of the nanoparticle (Eubank, 1951). Results indicated that all the three spectra showed significant reflections at 42.94° and 62.09° corresponding to (200) and (220) planes of MgO, which are very similar to the "standard JCPDS card (No: 78-0430)" and indicative of the cubic phase

of MgO NPs with no impurities. It was observed that with an increase in calcination temperature, the width of the diffraction peaks narrowed, indicating improved crystallinity. While at 500 °C, the diffraction peaks were broadened, signifying the formation of amorphous natured MgO NPs. Eubank (Eubank, 1951) concluded in his study that MgO NPs obtained after calcination at lower temperatures (500 °C) show a higher surface area and more vital adsorptive ability. Crystallite sizes of 500, 600, and 700 °C were found to be 12.6, 13, and 20 nm, respectively. Finally, 500 °C was selected as the calcination temperature due to its resultant product, amorphous natured MgO NPs.

The XRD data obtained on the free drug form NPRS was in good agreement with the previous finding and displayed the characteristics diffraction peak at 18.85° (Nokhodchi and Maghsoodi, 2008), which upon adsorption on the surface of MgO NPs, in the uncoated nanoformulation, appeared as a broader peak indicating contribution from both MgO NPs and NPRS. On the other, after the addition of PVA coating on the surface of MgO NPs conjugated NPRS (UNF), the formulation showed a broad hump at 19.87° (halo diffraction peak) indicative of the amorphous state due to PVA coating (Kayal and Ramanujan, 2010).

In brief, the diffraction pattern of CNF shows a loss of crystallinity and the overall amorphous state of the final naproxen formulation. A particular and most important problem associated with the emerging molecules from the drug discovery pipeline in recent years was found to be their low solubility and bioavailability due to their nanocrystalline materials (Jog and Burgess, 2017). On the other, amorphous nanoparticles have the advantage of synergistic mechanisms of enhancing dissolution rates (due to their nano size range and amorphous nature) as well as increasing saturation levels (due to their amorphous nature) (Van Eerdenbrugh et al., 2010). Our results indicate that the addition of PVA as a coating material helped in the loss of crystallinity and formation of an amorphous nanoformulation.

UV–Vis spectrophotometric studies enable researchers to determine the transition of electrons within conjugating compounds by analyzing discrete changes in their respective absorption spectra (Passos et al., 2019). Hence, assisting in the identification and quantification of organic compounds. Results from UV-Visible spectroscopy showed a broad peak indicating the formation of amorphous natured MgO NPs different

sized nanoparticles (Almontasser et al., 2019). Furthermore, a comparison of NPRS–MgO NPs spectrum with that of MgO NPs and NPRS showed a modification in peak patterns (a shift towards lower wavelengths (blue shift), which can be attributed to hydrogen bond formation as the hydrogen bonds lower the energy of 'n' orbitals of the compounds and results in a hypochromic peak shift (Banik et al., 2012). Thus, backing up the idea that NPRS is entrapped on the MgO NPs, these results were further confirmed through FTIR. Lastly, the addition of PVA to the NPRS–MgO NPs resulted in a slight increase in peak intensity indicating the successful coating of PVA on nanoformulation.

Interpreting and comparing FTIR spectra of naproxen nanoformulations revealed a few interesting results. IR spectroscopy is a proven tool to identify the characteristic group in a compound (Vigato et al., 2022) hence used in the current study to identify any chemical or physical bonding that happens between MgO NPs, NPRS, and PVA. Firstly, the IR data obtained from the synthesized MgO NPs is consistent with the finding of Alfaro et al. (2019) who specifies that during the formation of MgO NPs any band in the region from 3660 cm^{-1} to 3440 cm^{-1} represent the presence of O–H group due to moisture adsorbed by MgO NPs (Alfaro et al., 2019). Jeevanandam et al. (2017) on the other, suggested that magnesium nitrate used as the precursor for the synthesis of MgO NPs results in peaks at the region from 897 cm^{-1} to 820 cm^{-1} ascribed to the presence of MgO along with δ (O-C=O) (Jeevanandam et al., 2017). Sutapa et al. (2018) associated the FTIR transmission peak at 862.18 cm^{-1} with the Mg-O stretching vibrations (Sutapa et al., 2018). All findings regarding MgO NPs in the present study corroborated well with these earlier mentioned studies. As expected NPRS, the drug showed characteristic peaks associated with the pure naproxen sodium. It was reported by Bhise et al. (2008) that the peak at 3337 cm^{-1} is assigned to the hydroxyl (O-H) moiety of the carboxylic group (Bhise et al., 2008), whereas the band at 1600 cm^{-1} depicts the C=C stretching of the aromatic benzene ring in NPRS. FTIR Peak at $1,394$ cm^{-1} to $1,365$ cm^{-1} is attributed to CH$_3$ bending. According to Reddy et al., (2012) the peak at $1,210$ cm^{-1} represents C-O- stretching (ether), whereas the peak at $1,254$ cm^{-1} corresponds to C-O- bond stretching (Reddy et al., 2012). Furthermore, bands at $3,057$ cm^{-1} and $2,838$ cm^{-1} show an aliphatic stretch of the C-H bond.

Interestingly, the IR data obtained for an uncoated formulation that contained both MgO

NPs and NPRS showed chemisorption of NPRS onto the surface of MgO NPs. The distinct peak patterns associated with the MgO NPs and NPRS were modified and were wider than NPRS and MgO NPs alone and shifted at 3368 cm^{-1}. Moreover, characteristic bands representing functional groups of NPRS were diminished and replaced with a single medium-wide band. Furthermore, the bands associated with MgO NPs were shifted toward higher frequencies indicating the change in the chemical structure of compounds after chemisorption. Likely, the addition/ coating of PVA brought some interesting changes in peak patterns. Compared to the uncoated form, a spectral peak shift to a higher frequency was observed. Moreover, characteristic FTIR bands of uncoated NPRS-MgO NPs disappeared, and an IR spectrum corresponding to PVA was observed. According to Sabirneeza and Subhashini (2014), such peaks are ascribed to the C–H stretching vibration of the alkyl group of PVA (Sabirneeza and Subhashini, 2014). Currently, we concluded from our FTIR results that MgO NPs were synthesized successfully, and NPRS was adsorbed onto the surface of MgO NPs through chemisorption, while diminished bands of uncoated NPRS–MgO NPs along with characteristic PVA absorption bands proved that MgO NPs-NPRS complex was entirely coated with PVA.

The comparison of thermal behavior of the free drug naproxen sodium and MgO NPs before and after conjugation revealed that both NPRS and MgO NPs were more thermostable at higher temperatures when conjugated together. The increase in the melting point of naproxen sodium from 154 to 250 °C in CNF which is about 100 °C more than the NPRS can be attributed to the coating and stabilizing effect of an amorphous polymer, PVA (ur Rehman et al., 2021), indicating the formation of a stable nanoformulation.

Laser-induced breakdown spectroscopy (LIBS) is a highly effective laser-based single-step technique that utilizes a high-energy laser beam to excite and detect various elements in the given sample in a single step (Wong et al., 2010). In the present study, magnesium was detected in MgO NPs, UNF, and CNF while sodium was found in NPRS, UNF, and CNF indicating the presence of MgO NPs and NPRS in their respective nanoformulations.

Moreover, the peak height indicates the elemental intensity in the analyzed sample. In CNF the less intense peaks of magnesium and sodium compared to that in UNF is

suggestive of successful coating of PVA on the surface of UNF. In brief, the LIBS data showed the presence of specific elements in their respective products devoid of any contamination.

Two of the most critical parameters while the preparation of any particle at the nanoscale level are the particle size and surface charge (Falke and Betzel, 2019), both of them play a critical role in a particle's biocompatibility and functionality *in vivo*. Considering both parameters, we analyzed the change in particle size and surface charge during the development of naproxen nanoformulation.

As expected, the charge and size of the particle greatly changed when the NPRS-loaded MgO NPs were coated with PVA. Results demonstrated that the particle size of MgO NPs varied between 140-484 nm. A possible reason behind the variation in sizes of MgO NPs is the agglomeration of MgO NPs. This is consistent with the finding of Hamimed et al. (2020), who suggests that MgO NPs tend to agglomerate because of Vander Waals forces and high energy interactions that exist among MgO NPs (Hamimed et al., 2020). Hence, the variation in MgO NPs size could be ascribed to the agglomeration of MgO NPs during production. The UNF showed an improvement in hydrodynamic size ranging between 152 and 399 nm. Most likely, this variation in size may be due to the agglomeration of drug conjugated NPs. However, following PVA coating, a significant improvement and uniformity in the particle size were observed and particle size was found to be 161 nm. These findings suggested that polymeric coating over NP aggregates helped in particle segregation and uniformity in particle size (Ventola, 2017). The particle size obtained in the current study, for CNF (161 nm), is considered a suitable particle size for most nanotherapeutic applications.

Toxic studies based on the size of nanoparticles performed on the murine model have revealed that smaller sizes (60 and 100 nm) have shown significant cytotoxicity in all treatment groups. However, exposure to nanoparticles larger than 100 nm did not encourage the release of cytokines (Xiong et al., 2013). It is indicated that particles with a size >100 nm are non-toxic, therefore, indicative of the safety of CNF *in vivo* in clinical applications. A change in surface charge from -11.7 in NPRS loaded MgO NPs to -8.85 mV following PVA coating was observed, in the present study. There can be many reasons behind a drop in surface charge of CNF, for instance, the involvement of the charges on the solution layer from acetate groups in PVA or adsorption of the

polymeric layer may have caused a shift of the slipping planes of solid or the polymeric binding of PVA with oxides may have displaced the counter-ions from the slipping plane layer (Wiśniewska et al., 2016). Reportedly, the nanoparticles with a zeta potential < -25mV are known as stable particles (Thilagam and Gnanamani, 2020). A study by Shao et al. (2015) examining the effect of NP charge on cell viability revealed that positively charged nanoparticles were more cytotoxic than negatively charged particles (Shao et al., 2015). Also, particles with similar high charges were found to be more toxic than low-charged particles. Considering these findings, the final nanoformulation (CNF) possesses a suitable surface charge and size essential in pharmaceutical applications.

Drug encapsulation and loading studies were performed to analyze the drug-carrying potential of MgO NPs, for that, various ratios of MgO NPs to NPRS were added in the reaction process (drug loading process) and finalized at 2:3 as for MgO NPs to NPRS, resulting in the EE (%) and LC (%) of $50.4 \pm 3.2\%$ and $43.2 \pm 2\%$, respectively. Though the encapsulation and loading efficiency of NPRS in MgO NPs can be altered through a change in the concentration of encapsulated drugs and nanoparticles. However, our results suggest that MgO NP is capable of adsorbing NPRS on its surface almost equal to its quantity added.

In vitro drug release profile of CNF in acidic and basic media is shown in Fig. 2.19 R^2 value is attributed to the 1st order release kinetics. This study was performed at various physiological pH levels ranging from highly acidic to neutral, i.e., 1.2, 4.5, 6.8, and 7.4. As indicated in Fig. 2.19 CNF showed a prolonged release of NPRS in all test media with no immediate release effect. Maximum drug release was observed at pH 6.8 (> 95%) in 24 h. Minimum drug release was observed at acidic pH (1.2) over time.

Though the gastric damaging effect of the acidic NSAIDs is primarily attributed to the inhibition of prostaglandins synthesis, however, there have been many studies suggesting that NSAIDs induced stomach injury may not only be due to inhibition of prostaglandin production but their topical irritating effects on the stomach lining (Somasundaram et al., 1997; Lichtenberger, 2001; Whittle, 2003). For example, acidic NSAIDs, which can concentrate inside stomach cells due to the phenomena of ion trapping, are the most common source of direct irritating effects. Ionic fluxes across the stomach mucosa are disrupted by the internalized buildup of NSAIDs, with potassium

and sodium ions being the most affected and discharged into the luminal fluid, whilst hydrogen ions flow back from the lumen to the mucosa, exacerbating the gastric injury (Salvatella et al., 2004).

Used as a model drug in the current study, naproxen is among the acidic NSAIDs that tend to accumulate in the gastric cells at low pH, causing damage to the gastric lumen (Rodriguez-Stanley et al., 2006). The maximum release of NPRS at intestinal pH (6.8) and minimal release at stomach pH (1.2– 4.0) in the present study may be attributed to the conjugation of NPRS with MgO nanocarrier (Sarfraz et al., 2020). Such type pH-dependent pattern of drug release of this drug delivery system made it a suitable candidate for gastroprotective delivery of naproxen sodium as less drug was released at stomach pH and the maximum drug was released at intestinal pH. Similar pH-dependent drug release was reported in studies performed by Sarfraz et al. (2019) where they reported the gastro-protective delivery of naproxen sodium by using a polymeric nano hydrogel carrier system where pH-dependent swelling and release of drug was observed in basic pH (Sarfraz et al., 2019).

Taken together, all the encouraging outcomes in the current study suggest that MgO NPs can be conveniently and efficiently used as a nano-drug carrier. Characteristic features such as high drug-carrying capability and effectively releasing it in a controlled manner, are the ones always looked for in an ideal drug delivery system.

Chapter 3

Evaluation of Therapeutic Effects of Naproxen Nanoformulations in Comparison to Naproxen Alone

Summary

Biological activity assays for evaluating the therapeutic efficacy of newly created compounds are regarded as the foundation of drug research. Constructed, based on pharmacological principles, these models provide physiologically and clinically relevant data to predict treatment outcomes in humans. Therefore, in this specific study, using these standard pharmacological models, the therapeutic efficiency of UNF and CNF was tested. Presently, *in vitro* anti-inflammatory activity of naproxen nanoformulation revealed that CNF and UNF are potent protein denaturation inhibitors. Also, both nanoformulations significantly protected the RBC membranes from hemolysis. When tested *in vivo* for anti-inflammatory, analgesic, and antipyretic effects, both nanoformulations showed a considerable therapeutic activity comparable to diclofenac sodium and superior to NPRS and paracetamol. Though the exact mechanism underlying these effects is unknown and needs an in-depth mechanistic study, adsorption of naproxen on MgO NPs, and coating with PVA may have contributed to the stability and controlled release of the drug.

Introduction

Inflammation is a frequent event in the majority of acute and chronic illnesses, and it is a leading source of morbidity in today's modern era (Ptaschinski and Lukacs, 2020). Inflammation causes Alzheimer's disease, diabetes, cancer, atherosclerosis, rheumatoid arthritis, as well as respiratory, autoimmune, and cardiovascular disorders if left unchecked (Lordan et al., 2019). It entails a complicated network of various mediators, a wide range of cells, and the execution of several pathways (Rankin, 2004).

Anti-inflammatory drugs, both steroidal and non-steroidal, are being used to treat inflammatory illnesses (Del Grossi Moura et al., 2018; Wongrakpanich et al., 2018). Chronic usage of NSAIDs has been linked to serious side effects such as gastrointestinal, cardiovascular, and renal problems (Bindu et al., 2020). On the other hand, increased corticosteroid use is linked to mood fluctuations, increased hunger, weight gain, muscular weakness, psychological issues, and easy bruising, among other things (Stanbury and Graham, 1998). As a result, novel anti-inflammatory drugs with specific activity and lower toxicity are greatly needed.

Multifunctional nanoparticle development and design provide a new possibility for interdisciplinary researchers to target, diagnose, and treat acute and chronic inflammatory disorders (Çalış et al., 2019). Nanotechnology focuses on improving drug delivery systems to provide advanced therapy within the realm of nanomaterial research and development (Kumari et al., 2014; Daraee et al., 2016).

The concept of drug production using nanotechnology has placed a huge responsibility on the scientific community in terms of physical, chemical, and biological aspects of nanoscale material (Çalış et al., 2019), so that better drugs with fewer side effects may be utilized to help people live healthier lives (Foulkes et al., 2020).

In this context, where nanotherapeutic drug characterization is critical for understanding the mutual interaction of nanoparticles and cells that influences biological responses, equally important is the assessment of those compounds for biological activities *in vivo* and *in vitro* before clinical translation (Tomé et al., 2021; Sreeharsha et al., 2021). The biological activity of any compound is defined as "The capacity of a certain molecular entity to accomplish a defined biological effect on a target" (Jackson et al., 2007). It is assessed by a biological experiment and evaluated

in terms of potency, or the concentration of the molecular entity required to generate the effect (Batista-Navarro, 2013). The pharmacological concepts are employed to create the experimental models used in the preclinical biological activity assessments (Dougall and Unitt, 2015). In the clinical setup, these models give physiologically and clinically appropriate data to expect treatment outcomes (Gupta et al., 2015).

The careful selection of a pharmacological activity model has always been necessary, as it offers a basic study design for drug discovery and development. The improper animal model selection might result in misleading positive or negative results, limiting the discovery of potential therapeutic compounds from a screening program. As a result, it is extremely beneficial to use a systematic technique for the anti-inflammatory screening of newly formulated drug formulations (Patil et al., 2019). Vogel et al. (2002) identify several *in vivo* and *in vitro* strategies for anti-inflammatory medication pre-clinical testing. Before doing the actual test, it is strongly advised that each experiment should be designed well in terms of sample size, methodologies used to analyze data statistics, mode of drug administration, and usage of positive control (Vogel, 2002).

3.1 Animal Model Selection and *In vivo* Biological Activities Assessment

Laboratory animals such as Mus musculus mice (average weight: 30±5 g) and Rattus norvegicus rats (average weight: 150±20 g) are extensively employed as a model for *in vivo* testing of biological assays across the world. The choice of animal model used in the biological activity evaluation is dependent on the expected outcome of the study. It is also recommended to acclimatize the animal for a week, under standard laboratory conditions with a temperature set at 25±3 °C and a light/dark (12h) cycle with plenty of food and water before conduction of the experiment (Almeida, 2019).

Carrageenan, a seaweed extract is non-antigenic and has no known systemic effects. It is used as a stimulator to initiate an inflammatory cascade in the model animal. The early phase of inflammation is initiated by stimulation of phospholipase A_2, causing several pro-inflammatory mediators, inflammatory fluid, and cells to leak through dilation of postcapillary venules. These events represent the early exudative inflammatory phase, and its inhibition terminates the inflammatory process (Nantel et al., 1999). Whereas the second phase takes place after cytotoxicity induced by carrageenan (Morris, 2003) and begins three hours after carrageenan injection, through

activation of prostaglandins (Mansouri et al., 2015).

Due to its unique characteristics, the carrageenan-induced paw edema model is commonly used to investigate the anti-inflammatory properties of natural and synthesized compounds (Gao et al., 2019; Rachmawati et al., 2016). Inhibition of carrageenan-induced inflammation by test compounds has been demonstrated to be a strong predictor of anti-inflammatory medication efficacy in human inflammatory illness, and NSAID dosages tested in this model are similar to therapeutic levels in humans (Morris, 2003).

Pain, as defined by the International Association for the Study of Pain (IASP), is "an unpleasant sensory and emotional experience associated with actual or potential tissue damage or described in terms of such damage" (Deuis et al., 2017). The pain process involves numerous routes, including the transduction and propagation of nociceptive signals, as well as the detection and regulation of nociceptive stimuli (Van Rensburg and Reuter, 2019). Analgesic effects of nonsteroidal anti-inflammatory medicines (NSAIDs) are largely achieved by inhibiting cyclooxygenase (COX) enzymes, which reduces the generation of prostaglandins and reduces nociceptive signal transmission (Walker, 1995). Therefore, to test the analgesic potential of any compound several approaches have been developed in pharmacological investigations.

Pain in rodents cannot be directly assessed, therefore numerous approaches for quantifying "pain-like" behaviors or nociception have been devised and effectively employed in the field of pharmacological research (Deuis et al., 2017). To make the test more obvious for the analgesic effect of the newly created synthetic compounds, both peripheral and central pain models are included.

The acetic acid writhing test in mice is a standard method for researching the pharmacological action of peripheral analgesics. In this test, acetic acid (AA) in a (100µL/10g of the animal) is administered to test the animal intraperitoneally (i.p), which causes lesions on the abdomen enough to produce contractions known as writhing (Gawade, 2012). The production and release of pro-inflammatory cytokines from resident peritoneal macrophages and mast cells have been demonstrated to have a role in the abdominal spasm caused by acetic acid (Ribeiro et al., 2000).

The tail-flick test, first reported in 1941, includes subjecting the tails of mice and rats

to heat stimuli and recording the time it takes for the tail to "flick" or twitch. (D'Armour, 1941). The antinociceptive activity produced by the central nervous system is evaluated using either radiant heat or hot water, in which the end of the rodent tail is immersed in a hot water bath set at a temperature up to 52 °C (Carter and Shieh, 2015). The time taken to show a reflex reaction by tail withdrawal is noted and compared.

Almost all of the research on the pathophysiology of pyrexia has focused on humoral mediatory mechanisms. According to these theories, external pyrogens first persuade the production of pyrogenic cytokines, which then induce endogenous pyrogens to stimulate prostaglandin E synthesis near the hypothalamic area and thereby trigger the hypothalamus to elevate the body temperature. The changes in CNS activities are reflected in changes in peripheral thermoregulatory effector functions, which raise body temperature at the onset of fever and sustain it throughout the illness (Walter et al., 2016). Brewer's yeast, which is used to generate fever for antipyretic purposes, causes the production of both TNF and prostaglandins (Dangarembizi et al., 2018). As a result, the test chemicals' prevention of greater levels of prostaglandin E_2 production decreases the raised body temperature and keeps it at a steady level.

3.2 *In vitro* Assays to Investigate the Anti-inflammatory Activity

In vitro tests serve as a starting point for drug discovery methods. To screen the early anti-inflammatory effectiveness of novel medicinal drugs, a variety of *in vitro* assays/techniques have been established, and the choice of an *in vitro* assay or technique is largely dependent on the specific research issue to be investigated (Singh et al., 2018; Truong et al., 2019). For example, *in vitro* albumin denaturation assay, bovine serum albumin (BSA) is used to examine the anti-denaturation capability of anti-inflammatory medications (Phukan et al., 2021). When heated, BSA denatures and produces antigens connected to hypersensitivity and associated with various kinds of illnesses such as systemic sickness, glomerulonephritis, rheumatoid arthritis, and lupus erythematosus (Elisha et al., 2016), and the anti-inflammatory drugs work by inhibiting the denaturation of albumin proteins. Protein denaturation has been linked to the onset of inflammatory diseases such as rheumatoid arthritis and osteoarthritis. Hyaline articular cartilage loss, increased thickness and hardness of the subchondral bony plate, development of osteophytes at the joint edge, stretching of the articular capsule, and moderate synovitis in joints and muscle bridging are pathological changes that occur

during inflammatory illnesses (Saso et al., 2001)

Another assay known as hemolytic activity of the compound is used to test the potential of test compounds to protect biological cell membranes or lysosomal membranes from any damage. During inflammation, the membranous structure of lysosomes tends to disintegrate resulting in the release of all content outside the cells. Therefore, stability of this membrane is of critical importance for controlling the inflammatory response (Wang et al., 2018). Anti-inflammatory drugs either inhibit the COX enzyme or protect the lysosomal membrane from breakdown, preventing autocoid production (Lewis, 1970). Because the composition of red blood cell membranes is comparable to lysosomal membranes, human erythrocytes are being used for the membrane-stabilizing action of anti-inflammatory drugs or compounds (Evans et al., 2013).

In this particular study, newly synthesized coated naproxen nanoformulation (CNF) was investigated for its pharmacological potential through *in vitro* anti-inflammatory methods such as membrane stabilization assay and protein denaturation assay. Whereas various sets of *in vivo* anti-inflammatories, analgesic, and antipyretic activities were also performed to assess its therapeutic effect at various dose levels. The results obtained were compared with negative control, positive control such as diclofenac sodium and paracetamol, reference drug naproxen sodium, and UNF. Moreover, the carrier used in the current drug delivery system; the magnesium oxide nanoparticles (MgO NPs) were also studied for each activity to avoid any potential biases.

Materials and Methods

3.3 Evaluation of *In vitro* Biological Potential of Naproxen Nanoformulation

Before the commencement of the therapeutic efficacy experiments on mice, the nanomaterials were tested *in vitro* for anti-inflammatory and antihemolytic properties.

3.4 Ethics Statement

The "Bioethical Committee (BEC)" at Quaid-i-Azam University approved (BEC-FBS-QAU2021-298) the design and experimental procedures used to carry out test compounds' hemolytic activity against human red blood cells. Blood was obtained from a healthy volunteer following informed consent.

3.4.1 Hemocompatibility Assay

In the current study, synthesized nanomaterials hemocompatibility was studied as described by Rehman et al. (2021) (Rehman et al., 2021). Briefly, a 5 mL blood sample from a healthy volunteer was collected in a tube containing EDTA (anticoagulant). A ratio of 1: 9 blood and PBS were used to dilute the blood sample. 100 μL of various concentrations of nanoformulations and NPRS (50, 100, and 250 μg/mL) were added to 1 mL of a diluted blood sample to prepare the reaction mixtures. Likewise, positive, and negative controls corresponding to 100 % and 0 % hemolysis of RBCs were prepared by adding 0.1 % Triton X-100 and PBS to 1 mL of diluted blood. These mixtures were then incubated overnight at 37 ± 0.1 ºC. The next day, samples were centrifuged (10 min, 4000 rpm) for serum collection. The supernatant's hemoglobin content was evaluated using a UV-spectrophotometer at 540 nm. The percent hemolysis was calculated using the formula below.

$$\text{Hemolysis } (\%) = 100 - \frac{S\,(absorbance) - N(absorbance)}{P\,(absorbance) - N(absorbance)} \times 100 \text{ (1)}$$

S = Absorbance of samples. P = Absorbance of Triton X-100 at 540 nm and N = Absorbance of PBS. The whole experiment was conducted three times.

3.4.2 Evaluation of *In vitro* Anti-Inflammatory Activity (BSA Method)

Synthesized nanomaterial and standard anti-inflammatory drugs were tested for protein

anti-denaturation activity using the bovine serum albumin (BSA) protein denaturation inhibition assay (Kiranmayi, 2018). The test compounds exhibiting > 80% inhibitory activity against heat-induced protein denaturation were categorized as most potent.

Briefly, 50 µL of prepared solutions of 50, 100, and 250 µg/mL concentration of MgO NPs, NPRS, UNF, CNF, and diclofenac sodium (positive control) were mixed with 450 µL of BSA (5 % w/v aqueous solution) in separate tubes to make a reaction mixture of 500 µL. The control mixture contains 50 µL of deionized water in 450 µL of BSA. Samples were incubated for 25 min at room temperature and heated for 3 min at 57 °C and then cooled. Phosphate buffer (2.5 mL, pH 6.3) was added to the cooled samples and the measurements were carried out at 255 nm. The assay was repeated three times. The control represented the complete denaturation of BSA. The anti-denaturation activity of all compounds was determined with the following formula:

$$\text{Percent inhibition of BSA denaturation} = 100 - \frac{\text{OD test} - \text{OD control}}{\text{OD test}} \times 100 \qquad (2)$$

3.5 *In vivo* Biological Testing of Naproxen Nanoformulations

The therapeutic potential of synthesized nanoformulations was studied following standard laboratory models for various physiologic conditions. The results were compared with the vehicle control or conventional anti-inflammatory and antipyretic drugs. Diclofenac sodium and paracetamol were used as positive controls. Naproxen sodium was used as a reference drug.

3.5.1 Animals

7–8-week-old BALB/c mice of either sex, procured from the National Institute of Health (NIH), Islamabad were used in the current study. These mice were kept under pathogen-free standard laboratory conditions. Animals were offered standard rodent feed and clean water *ad libitum*. The "Bioethical Committee (BEC)" at Quaid-i-Azam University approved the current study's animal handling and experimental procedures (BEC-FBS-QAU2021-298).

The related guidelines for the use and treatment of laboratory animals were strictly followed.

3.6 Anti-inflammatory Activity

A mouse model for assessing the anti-inflammatory potential of nanoformulations was prepared by inducing pedal inflammation acceding to the reported protocol (Gupta et al., 2015). Briefly, experimental mice were grouped into fourteen treatment groups (n=6). The positive control group received per oral (p.o.) treatment of diclofenac sodium (15 mg/kg) while mice in the treatment groups received oral doses of naproxen sodium (NPRS; reference drug), UNF, CNF, and MgO NPs at varying dose concentrations (1, 5 and 10 mg/kg). Samples were prepared in deionized water, whereas dimethyl sulfoxide (0.1 % DMSO) was used as a suspending agent. An equivalent quantity of the vehicle was given to the control group. All doses were administered orally 1 h before carrageenan injection. Paw edema was induced by injecting 50 μL of carrageenan suspension (1 % w/v) into the intra-planter region of the mice's hind paw. The paw width change was observed by measuring the paw thickness before (basal level) and at subsequent hours (1-5 h) after carrageenan injection using a digital caliper. Percent inhibition in edema formation was calculated using the following equation.

$$\text{Inhibition in edema formation (\%)} = \frac{\text{Ncontrol} - \text{Ntreated}}{\text{Ncontrol}} \times 100 \ (3)$$

Where *N* indicates the change in paw thickness (mm) at the time indicated from the basal level.

3.7 Analgesic Activity

3.7.1 Assessment of Central Analgesic Activity

The tail withdrawal response (Ge et al., 2005) was determined by immersing the distal 3 cm of mice tails in 52 °C ± 0.5 water, with a 15 s "cut-off" time for non-responsive animals. Initially, mice were tested for the baseline reaction time and randomly assigned to different treatment groups (n = 6) and administered with NPRS, MgO NPs, UNF, CNF, diclofenac sodium, or vehicle. Analgesic activity was measured at 30, 60-, 90-, 120- and 180-min following dose administration. The percentage latency was calculated according to the following equation.

$$\text{Percent latency (\%)} = \frac{\text{Latency post drug} - \text{Latency predrug}}{\text{cutoff time} - \text{latency predrug}} \times 100 \ (4)$$

3.7.2 Assessment of Peripheral Analgesic Activity

The pain response (constrictions across the abdominal region) in mice caused by the intraperitoneal (i.p) dose of acetic acid was used to assess the peripheral analgesic potential of UNF and CNF (Zhang et al., 2016). In this experiment, mice in treatment groups (n =6) were orally administered 1, 5, and 10 mg/kg of each sample. Control groups were administered with either diclofenac sodium (positive control) at a 15 mg/kg dose or vehicle. After 1 h, the writhing was induced with (i.p) acetic acid (1% v/v prepared in deionized water, 1 mL/100 g) and the number of writhes (distinctive abdominal constrictions along with hind limb stretching) was counted over 10 min, starting at 5 min after injection. The antinociceptive activity of test compounds was attributed to decreased writhing response compared to the control group. Percent inhibition in writhes was calculated as follows.

$$\text{Inhibition (\%)} = \frac{\text{Ncontrol} - \text{Ntest}}{\text{Ncontrol}} \times 100 \ (5)$$

Where N = Mean number of writhes

3.8 Antipyretic Activity

3.8.1 Yeast-induced Hyperpyrexia in Mice

Induction of pyrexia was carried out as described by Hegazi et al (Hegazi et al., 2019). Before initiating the experiment, the body temperature of mice was determined by inserting a well-lubricated bulb of the digital thermometer into the mice's rectum. Mice that showed a body temperature within a normal physiological range were selected and hyperpyrexia was induced by s.c injection of (1 mL/100 g) aqueous suspension (20 %) of brewer's yeast in the nape. Pre-drug rectal temperatures were recorded after 18 h and mice with a rectal temperature increase of 0.3 °C or more were classified as pyretic and randomly assigned to one of fourteen groups (n = 6). A single oral dose of test compounds (1, 5, and 10 mg/kg), paracetamol (positive control; administered at 100 mg/kg), or vehicle was given, and rectal temperatures were retaken 1 to 3 h later.

3.9 Statistical Analysis

The *in vitro* experiments were repeated three times while the number of animals in the

in vivo experiments was kept sufficient to derive the statistical analysis of the data obtained from the treatment groups. The data are reported as mean ± s.e. Statistical difference between groups was determined using one way-ANOVA, followed by Dunnett and Bonferroni tests (Sigma Plot, Version 12.0, Microsoft Inc, California USA). A p-value *<0.05, **<0.01 or ***<0.001 denoted statistically significant difference.

Results

3.10 *In vitro* biological potential of Naproxen Nanoformulations

3.10.1 Hemocompatibility Assay

Currently, we assessed the hemocompatibility of free form NPRS, MgO NPs, uncoated, and PVA-coated nanoformulation. PBS and Triton X-100 were used as negative and positive controls representing 0% and 100% hemolysis of erythrocytes in the given sample. To evaluate the dose-dependent effect, three concentrations for each test group were prepared. Results indicated (Fig. 3.1) that Triton X-100 caused complete hemolysis of erythrocytes. Data from treatment groups, when compared at the low dose, showed that the CNF was the safest among all and protect cell membranes from lysis by 99.98 % (0.11% hemolytic activity), compared to that of UNF (0.42%), NPRS (0.63%) and MgO NPs (0.51%). Hemolysis of RBC when observed at the highest concentration tested (250 µL/mL) revealed that uncoated and PVA coated nanoformulation and MgO NPs, exhibited excellent hemocompatibility with only 0.72%, 0.78%, and 0.77% hemolytic activity, respectively. Whereas, reference drug naproxen sodium, displayed the highest hemolytic activity among all, 1.35 percent at the same dose (250 µL/mL).

3.10.2 *In vitro* Anti-inflammatory Activity

The results shown in Fig. 3.2 revealed that the positive control diclofenac sodium showed 82 ± 1.12, 83 ± 1.50, and 84 ± 2.33 % of protein anti-denaturation activity. CNF on the other, demonstrated 87 ± 2, 88 ± 3.10, and 90 ± 4.87 % inhibition activity at 50, 100, and 250 µg/mL concentrations which are 4 – 6 % greater than standard drug diclofenac sodium at the same doses. Similarly, UNF displayed 86 ± 2.10, 88 ± 1.87 and 89 ± 3.44 % at 50, 100 and 250 µg/mL activity. This activity was significantly higher than diclofenac sodium but lower than that of shown by CNF. Magnesium oxide nanoparticles (MgO NPs) protected BSA from denaturation with 84 ± 2.40, 85 ± 3.41 and 86 ± 2.19 % in a dose-dependent manner. The inhibitory effect of MgO NPs was comparable to that observed in diclofenac-treated test samples. NPRS exhibited the lowest inhibitory activity with 71 ± 2.10, 72 ± 2.30, and 73 ± 2.94 % at all doses, and this effect was almost 17% lesser than demonstrated by our synthesized CNF. Hence, the synthesized nanomaterials in the current study presented the most potent protein

anti-denaturation inhibitor than the parent drug (NPRS) and standard drug (diclofenac sodium) in a dose-dependent manner.

3.11 *In vivo* Investigation of Anti-Inflammatory Action

Currently, we employed the paw edema model following the carrageenan (chemical irritant) administration to assess the inflammation inhibition effect of naproxen nanoformulation. Results were compared to control (carrageenan only), reference drug, and positive control (diclofenac sodium). Table 3.1 summarizes the change in paw thickness (mm) and percent inhibition of inflammation by the test compounds at a specific time interval after carrageenan injection. Whereas Fig. 3.3 a, b illustrates the degree of inflammation in experimental mice at 2 h (Ist phase of inflammation) and 5 h (2nd phase of inflammation).

As evident in Table 3.1, mice in the carrageenan-only group showed a significant increase in paw thickness when measured at subsequent hours after carrageenan injection. The highest thickness was observed at 5 h. UNF and CNF displayed a significant anti-inflammatory effect ($p<0.001$) at 10 mg/kg during the initial phase (2 h) of inflammation. This effect was comparable to diclofenac sodium and better than that shown by NPRS.

During the second phase of inflammation, in terms of percent inhibition in edema formation, CNF showed 69, 81, and 97 % inhibition at 1, 5, and 10 mg/kg doses, respectively at 5 h. It should be noted that CNF (10 mg/kg dose) strongly inhibited edema formation (70 %) within 1 h after carrageenan administration and this effect persisted throughout the experiment. UNF significantly prevented inflammatory edema by 59, 63, and 77.8 % at 1, 5, and 10 mg/kg oral doses, respectively after 5h. NPRS inhibited paw swelling by 59.5, 66.4, and 75.5 % at 1, 5, and 10 mg/kg doses, respectively at 5 h. Mice treated with diclofenac sodium (15 mg/kg p.o.) showed 53.8 % inhibition in paw edema after 5 h. Thus, the activity of CNF was found to be greater than UNF, NPRS, and diclofenac sodium.

3.12 Analgesic Activity of Naproxen Nanoformulations

The central and peripheral analgesic effects of naproxen nanoformulations were studied using two experimental models, and data obtained were compared to vehicle control

and standard drug diclofenac sodium. Any compound that showed a positive antinociceptive effect in both activities was considered a potent analgesic.

3.12.1 Tail Immersion Test

The central nociceptive capacity of naproxen nanoformulations and other test compounds was assessed through the tail-immersion assay. Data are shown in Fig. 3.4 and Table 3.2. After dose administration, CNF showed highest analgesic effect (10 mg/kg, $p<0.001$) at 30-120 (100 % at 120 min) followed by UNF (10 mg/kg, 95 % at 120 min, $p<0.001$). The effect of CNF was interestingly superior to the standard analgesic drugs (diclofenac sodium and naproxen sodium). Likewise, compared to control, MgO NPs (10 mg/kg) produced a significant analgesic effect at all intervals. In this experiment, mice treated with NPRS (10 mg/kg) showed a minimum analgesic effect after 60 min; contrary to CNF, which showed a significant analgesic effect after 30 min.

Interestingly, the CNF showed a prominent analgesic effect at the lowest doses administered (1 mg/kg) to mice in comparison to the vehicle control (Table 3.2). These findings suggested that CNF is a better analgesic than conventional NPRS and diclofenac sodium.

3.12.2 Acetic Acid-Induced Abdominal Writhing

Results of peripheral analgesic activity are shown in Fig. 3.5 a, b. Mice that received no treatment, have shown the maximum number of writhes i.e., 37, following acetic acid intraperitoneal injections (i.p) over 10 min. Although all the tested compounds showed a significant reduction in writhes compared to the control, the highest activity was demonstrated by UNF and CNF ($p<0.001$) at a 10 mg/kg dose. These effects were comparable to those of NPRS but superior to the standard drug diclofenac sodium. The lowest inhibitory action was shown by MgO NPs with only 27 and 49 % inhibition at a dose of 5 and 10 mg/kg, respectively.

3.13 Antipyretic Activity of Naproxen Nanoformulation

In this study, apart from testing synthesized compounds for anti-inflammatory and analgesic activity, we tested the antipyretic potency of naproxen nanoformulations

against pyrogenic fever. For this, mice were injected subcutaneously (s.c) with brewer's yeast suspension, and the mice showed a marked elevation in rectal temperature of 1°C from baseline rectal temperature after 18 h, were selected to test the antipyretic efficacy of the test compounds.

As illustrated in Fig. 3.6 and Table 3.3, a striking decrease in rectal temperature was observed following administration of the CNF at a 10 mg/kg dose, compared to the control group, starting at 1 h (35.07 °C vs. 37.69 °C for control) and achieved the highest decrease in rectal temperature at 3 h (35.52 °C vs. 37.65 °C). Remarkably, this effect of CNF was found to be superior to the standard antipyretic drug (paracetamol) that induced an antipyretic effect (36.94 °C in 1 h and 36.82 °C in 3 h) at a ten times greater dose than CNF. In comparison to vehicle control and paracetamol, a significant antipyretic effect was displayed by MgO NPs at all doses (1, 5, and 10 mg/kg) starting at 2 h and continuing until the completion of the experiment. At a high dose, UNF displayed a significant antipyretic effect of 35.91 °C at 2 h and 35.28 °C at 3 h in comparison to vehicle control and standard drug paracetamol.

Paracetamol decreased rectal temperature by 1.5 °C compared to the pre-dose rectal temperature of treated animals. However, this difference was non-significant compared to vehicle control.
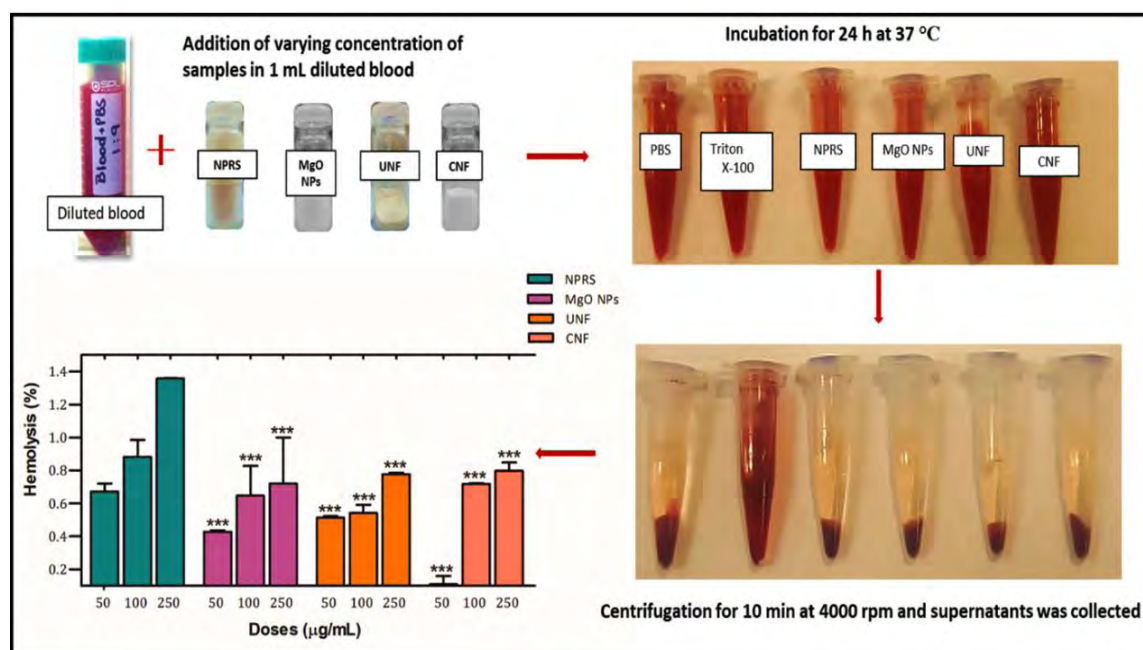
Fig. 3.1 Procedure and results of the antihemolytic activity. Data are shown as mean ±s.e. of three independent experiments. *$p<0.05$. **$p<0.01$. ***$p<0.001$ compared to NPRS.
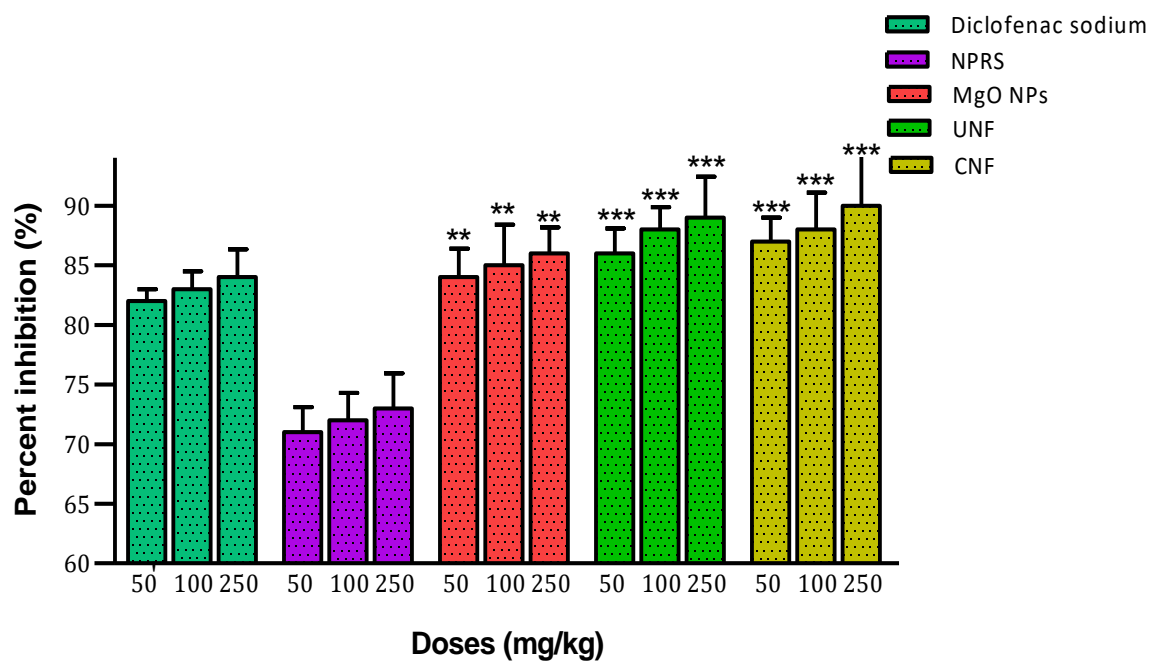
Fig. 3.2 Protein (BSA) denaturation activity. Data are shown as mean ± s.e. *p<0.05, **p<0.01, ***p<0.001 compared to NPRS.
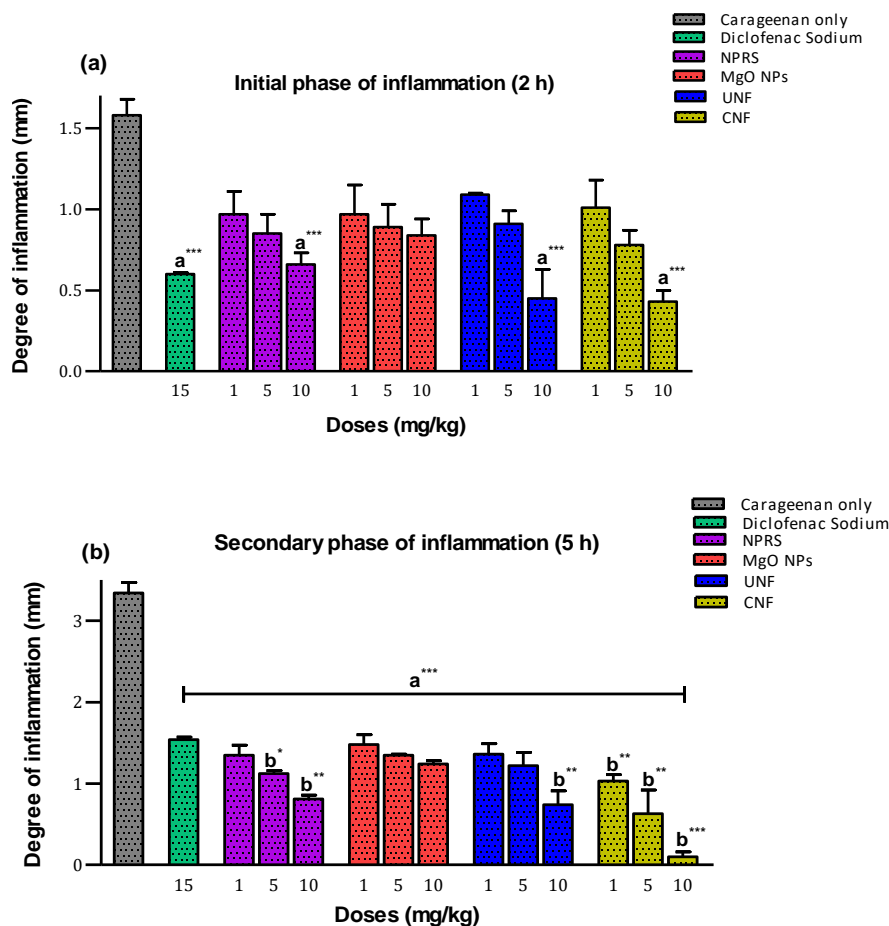
Fig.3.3 Inhibitory effect of test compounds against carrageenan-induced paw edema. Test compounds; NPRS, MgO NPs, UNF, and CNF at various doses (1, 5, and 10 mg/kg). Data are shown as mean ± s.e. at 2 h (a) the first phase of inflammatory onset and 5 h (b) the second phase of inflammation, compared to the negative control (carrageenan only) and positive control (diclofenac sodium). n = 6, *p<0.05. **p<0.01.***p<0.001 a = compared to carrageenan only, b = compared to diclofenac sodium.
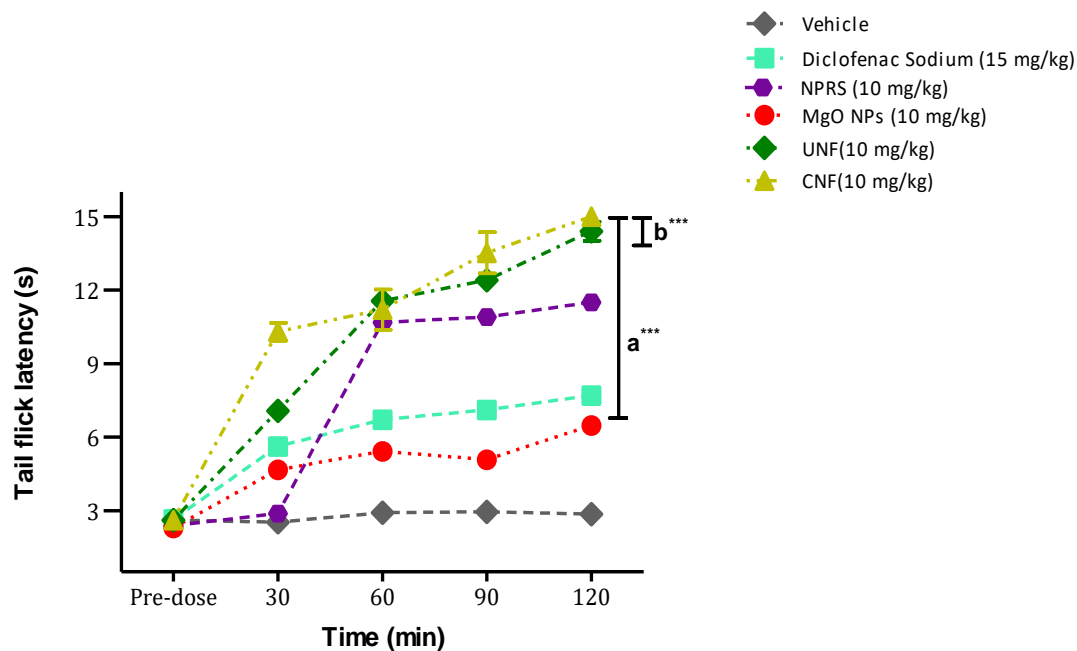
Fig. 3.4 Evaluation of central analgesic activity. NPRS, MgO NPs, UNF, CNF (10 mg/kg), and diclofenac sodium (15 mg/kg) were administered orally to respective groups. The time (s) to withdraw the tail from hot water (55 °C) was recorded and presented as latency response (s). The cut-off time was 15 s. Values are stated as mean ± s.e (n = 6). (ANOVA followed by Bonferroni posthoc). Statistical comparison between groups was made at 120 min following dose administration. a = compared to control, b = compared to the diclofenac sodium.
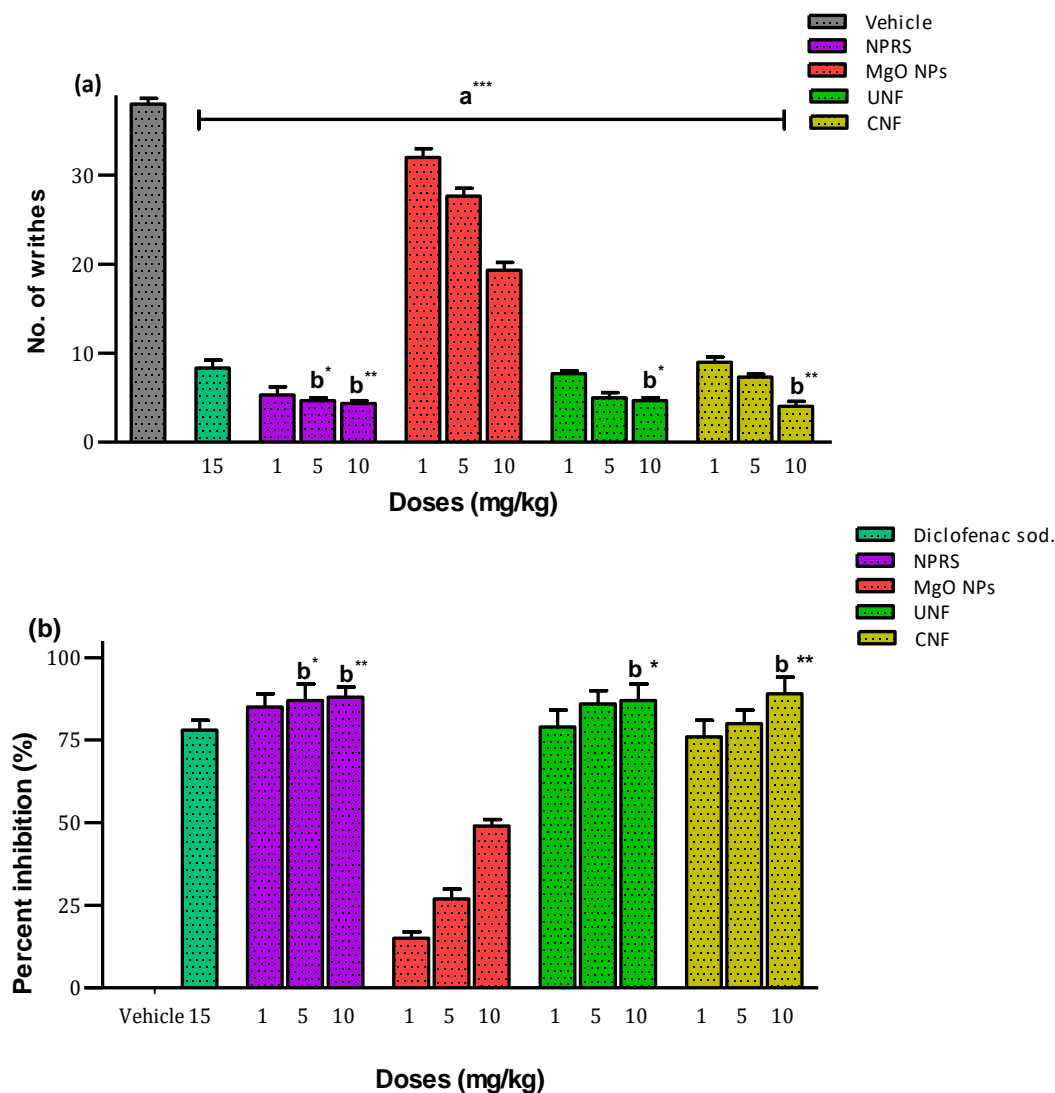
Fig. 3.5 Evaluation of peripheral analgesic activity. Effect of NPRS, MgO NPs, UNF, and CNF (1, 5, and 10 mg/kg, p.o.) diclofenac sodium (15 mg/kg, p.o.) on acetic acid-induced writhing in mice. Each data represents mean ± s.e (n = 6) (a). Inhibition of writhes by tested compounds in percentage. (b) Data are expressed as mean percent inhibition of writhes by tested compounds (ANOVA followed by Bonferroni posthoc) "a" indicated a significant difference from the control. "b" indicated statistical difference compared to the positive control diclofenac sodium.
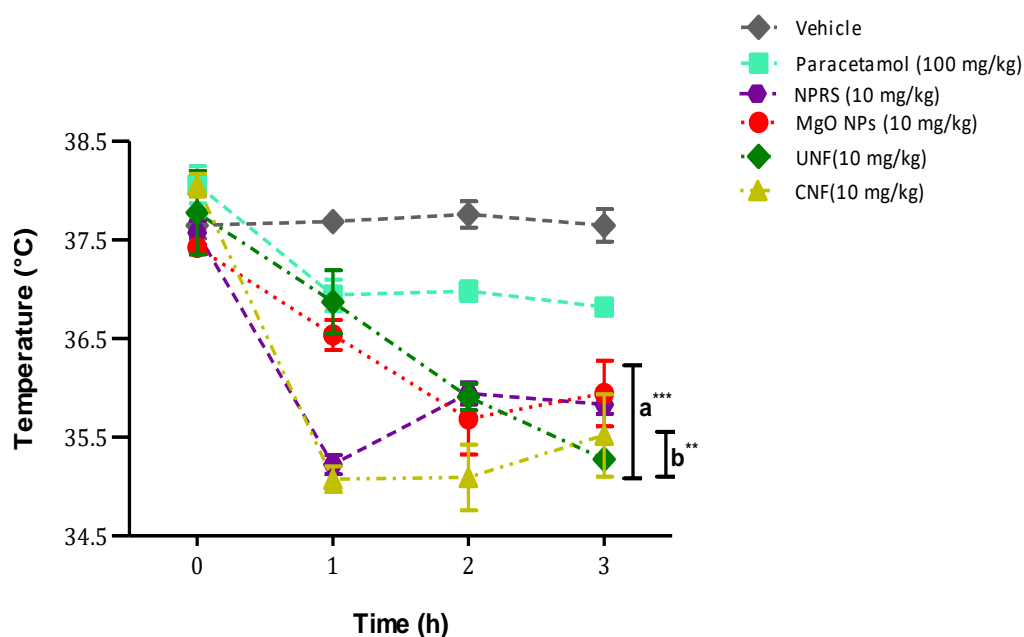
Fig. 3.6 Evaluation of antipyretic effect using yeast-induced pyrexia test in mice. NPRS (a), MgO NPs (b), UNF (c), CNF (d), or paracetamol (PCM), Statistical comparison was made at 3 h following test compounds administration. Values are stated as mean ± s.e (n = 6). Symbols indicate statistical difference compared to the vehicle control group and positive control, paracetamol. (a = vehicle control, b=positive control).

Table 3.1. Effect of naproxen nanoformulations and other test compounds on carrageenan-induce paw edema on mice

Treatment	Dose (mg/kg)	Δ change in edema thickness (mm), inhibition (%)					Inhibition (%) average
		1 h	2 h	3 h	4 h	5 h	
Control (carrageenan only)	–	1.12 ± 0.04	1.58 ± 0.10	1.77 ± 0.01	2.81 ± 0.14	3.34 ± 0.13	–
Positive control (Diclofenac Sod.)	15	0.58 ± 0.06 (48.2) [a]	0.60 ± 0.02 (60.0) [a]	0.70 ± 0.02 (60.4) [a]	0.83 ± 0.01(70.4) [a]	1.54 ± 0.03 (53.8) [a]	58.56
NPRS	1	0.68 ± 0.05 (39.2)	0.97 ± 0.14 (38.6)	1.14 ± 0.07 (35.5)	1.32 ± 0.12(53.0) [a]	1.35 ± 0.12 (59.5) [a]	45.16
	5	0.66 ± 0.07 (41.0)	0.85 ± 0.12 (46.2)	1.03 ± 0.18 (41.8)	1.10 ± 0.20(60.8) [a]	1.12 ± 0.04 (66.4) [a, z]	51.24
	10	0.60 ± 0.06 (46.4) [a]	0.66 ± 0.07 (58.2) [a]	0.74 ± 0.06 (58.1) [a]	0.74 ± 0.07(73.6) [a]	0.81 ± 0.05 (75.5) [a, y]	62.40
MgO NPs	1	0.88 ± 0.16 (21.4)	0.99 ± 0.17 (37.3)	1.29 ± 0.14 (27.1)	1.21 ± 0.14(56.9) [a]	1.48 ± 0.12 (55.6) [a]	39.66
	5	0.91 ± 0.12 (18.7)	0.95 ± 0.14 (39.8)	1.19 ± 0.10 (32.7)	1.28 ± 0.08(54.4) [a]	1.35 ± 0.01 (59.5) [a]	41.02
	10	0.81 ± 0.06 (27.6)	0.94 ± 0.11 (40.5)	0.98 ± 0.08 (44.6) [a]	1.25 ± 0.13(55.5) [a]	1.24 ± 0.04 (62.8) [a]	46.20
UNF	1	0.74 ± 0.05 (33.9)	1.09 ± 0.01 (31.0)	1.08 ± 0.02 (38.9)	1.06 ± 0.07(62.2) [a]	1.36 ± 0.13 (59.2) [a]	45.04
	5	0.62 ± 0.18 (44.6)	0.91 ± 0.08 (42.4)	0.79 ± 0.24 (55.3) [a]	0.84 ± 0.24(70.1) [a]	1.22 ± 0.16 (63.5) [a]	55.18
	10	0.53 ± 0.18 (52.6) [b]	0.45 ± 0.18 (71.5) [a]	0.47 ± 0.09 (73.4) [a, z]	0.66 ± 0.12(76.5) [a, z]	0.74 ± 0.17 (77.8) [a, y]	70.36
CNF	1	0.54 ± 0.17 (51.7)	1.01 ± 0.17 (36.0)	1.15 ± 0.18 (35.0)	1.29 ± 0.14(54.0) [a]	1.03 ± 0.08 (69.1) [a, y]	49.16
	5	0.40 ± 0.04 (64.3)	0.78 ± 0.09 (50.6)	0.97 ± 0.16 (45.1) [a]	1.17 ± 0.16(58.3) [a]	0.63 ± 0.29 (81.2) [a, y]	59.78
	10	0.34 ± 0.12 (70.0) [a]	0.43 ± 0.07 (72.7) [a]	0.50 ± 0.08 (71.7) [a, z]	0.52 ± 0.07(81.4) [a, y]	0.10 ± 0.06 (97.0) [a, x]	78.56

Data are shown as mean ± s.e, n = 6.

a, b, c symbols indicate statistical difference, p < 0.001, 0.01 and 0.05, Bonferroni post-hoc respectively, compared to control group while, x, y, z symbols indicate statistical difference (p < 0.001, 0.01 and 0.05) compared to positive control (diclofenac sodium).

Table 3.2. Analgesic effect of naproxen nanoformulation and other test compounds on tail withdrawal reflex induced by immersion of mice tail in hot water.

Treatment	Dose (mg/kg)	Mean reaction time (s), Percent inhibition (%)					Inhibition (%) average
		0 min	30 min	60 min	90 min	120 min	
Control	–	2.61 ± 0.12	2.53 ± 0.10	2.91 ± 0.13	2.95 ± 0.13	2.85 ± 0.14	–
Positive control (Diclofenac Sod.)	15	2.64 ± 0.13	5.61 ± 0.30 (24) [b]	6.71 ± 0.23 (33) [a]	7.11 ± 0.13 (36) [a]	7.69 ± 0.29 (41) [a]	33.50 [a]
NPRS	1	2.40 ± 0.11	2.49 ± 0.08 (6.4)	3.71 ± 0.31 (10)	4.57 ± 0.16 (17)	5.27 ± 0.10 (23)	14.10
	5	2.49 ± 0.03	3.38 ± 0.09 (7.1)	6.75 ± 0.23 (34) [a]	8.64 ± 0.45 (49) [a]	11.0 ± 0.18 (68) [a, x]	39.52 [a]
	10	2.38 ± 0.02	2.88 ± 0.27 (3.9)	10.6 ± 0.17 (66) [a, y]	10.9 ± 0.16 (68) [a, y]	11.5 ± 0.16 (72) [a, x]	52.47 [a, x]
MgO NPs	1	2.23 ± 0.06	2.80 ± 0.32 (4.4)	2.59 ± 0.14 (2.8)	2.60 ± 0.18 (2.9)	2.46 ± 0.27 (1.8)	02.97
	5	2.81 ± 0.05	5.28 ± 0.16 (20) [b]	5.42 ± 0.26 (21) [c]	5.81 ± 0.70 (25) [c]	6.25 ± 0.46 (28) [b]	23.50
	10	2.29 ± 0.08	4.66 ± 0.14 (19) [c]	5.41 ± 0.29 (25) [c]	5.07 ± 0.11 (22) [c]	6.47 ± 0.16 (33) [a]	24.75
UNF	1	2.60 ± 0.17	2.80 ± 0.07 (1.6)	2.76 ± 0.06 (1.3)	2.64 ± 0.12 (0.3)	2.73 ± 0.04 (1.1)	01.07
	5	2.84 ± 0.04	5.40 ± 0.62 (21) [b]	6.84 ± 1.06 (33) [a]	7.29 ± 1.12 (37) [a]	10.4 ± 1.18 (62) [a, x]	38.25
	10	2.61 ± 0.08	7.07 ± 0.14 (36) [a]	11.5 ± 0.26 (72) [a, x]	12.4 ± 0.29 (79) [a, x]	14.4 ± 0.39 (95) [a, x]	70.50 [a, x]
CNF	1	2.72 ± 0.04	3.64 ± 0.45 (7.5)	4.36 ± 0.94 (13)	5.14 ± 0.61 (19)	6.00 ± 0.11 (27) [b]	31.62
	5	2.62 ± 0.26	5.62 ± 1.18 (24) [b]	7.11 ± 0.46 (36) [a]	9.54 ± 0.25 (55) [a]	11.5 ± 0.28 (72) [a, x]	46.75
	10	2.61 ± 0.11	10.3 ± 0.30 (62) [a, x]	11.2 ± 0.82 (69) [a, x]	13.5 ± 0.84 (88) [a, x]	15.0 ± 0.00 (100) [a, x]	79.75 [a, x]

Data are shown as mean ± s.e, n = 6.

a, b, c symbols indicated statistical difference ($p < 0.001$, 0.01 and 0.05, Bonferroni post-hoc) and compared to the control group while, x, y, z symbols indicate statistical difference ($p < 0.001$, 0.01 and 0.05) compared to diclofenac sodium.

Table 3.3. Antipyretic activity of NPRS, MgO NPs, UNF, and CNF on brewer's yeast-induced pyrexia at successive time intervals (h).

Treatment groups	Dose (mg/kg)	Rectal temperature (°C)				
		Before treatment		After treatment		
		Initial	After 18 h	1 h	2 h	3 h
Vehicle control	–	36.85 ± 0.34	37.65 ± 0.13	37.69 ± 0.02	37.76 ± 0.13	37.65 ± 0.17
Positive control (paracetamol)	100	36.80 ± 0.12	38.06 ± 0.19	36.94 ± 0.16	36.98 ± 0.10	36.82 ± 0.07
NPRS	1	36.63 ± 0.26	37.24 ± 0.08	36.63 ± 0.18	36.37 ± 0.95	37.37 ± 0.60
	5	36.82 ± 0.38	37.59 ± 0.23	36.50 ± 0.56	36.54 ± 0.21	37.59 ± 0.42
	10	36.67 ± 0.06	37.57 ± 0.12	35.22 ± 0.10 [a, x]	35.94 ± 0.11 [c]	35.83 ± 0.10 [c]
MgO NPs	1	36.57 ± 0.02	37.43 ± 0.26	36.33 ± 0.13 [b]	35.63 ± 0.05 [b]	35.80 ± 0.54 [b]
	5	36.20 ± 0.18	37.28 ± 0.31	36.43 ± 0.15 [c]	35.87 ± 0.58 [b]	35.91 ± 0.46 [c]
	10	36.46 ± 0.29	37.43 ± 0.08	36.54 ± 0.15	35.69 ± 0.36 [c]	35.94 ± 0.33 [c]
UNF	1	36.63 ± 0.21	38.07 ± 0.08	37.30 ± 0.41	37.06 ± 0.29	37.83 ± 0.36
	5	36.78 ± 0.22	38.24 ± 0.49	37.35 ± 0.45	37.33 ± 0.50	37.63 ± 0.63
	10	36.72 ± 0.18	37.78 ± 0.42	36.87 ± 0.32	35.91 ± 0.13 [c]	35.28 ± 0.06 [b, y]
CNF	1	37.32 ± 0.21	38.19 ± 0.20	37.61 ± 0.03	37.57 ± 0.15	37.82 ± 0.17
	5	36.72 ± 0.37	37.54 ± 0.43	37.39 ± 0.08	37.61 ± 0.28	37.76 ± 0.08
	10	37.28 ± 0.13	38.06 ± 0.12	35.07 ± 0.13 [a, x]	35.09 ± 0.33 [a, z]	35.52 ± 0.42 [b, y]

Data are shown as mean ± s.e, n = 6/group.

a, b, c symbols indicate statistically significant difference ($p < 0.001$, 0.01 and 0.05, Bonferroni post-hoc) from vehicle control, while, x, y, z indicate statistical difference compared to positive control, paracetamol ($p < 0.001$, 0.01 and 0.05).

Discussion

Currently, anti-inflammation therapy is limited to steroidal and non-steroidal anti-inflammatory drugs both of which have been reported to have several adverse effects at therapeutic doses (Bindu et al., 2020). Due to which that has been a rising need to develop new therapeutic compounds or drug delivery systems (Peng et al., 2021; García et al., 2022). Nanotechnology has emerged as an innovative way to eliminate drug-related adverse effects, given the rapid advancement of nanoscience and the exceptional performance of nanomaterials (Daraee et al., 2016). Nanotechnology has various advantages in medication development, including improved drug solubility and water solubility, sustained release of drug from nanoformulations, and increased absorption rate of target cells or tissues all of which improve therapeutic safety and effectiveness, while keeping the therapeutic dose quantity to the minimum (Patra et al., 2018)

Considering this, we have successfully designed a drug delivery system using MgO NPs as drug carriers while naproxen sodium was used as a model anti-inflammatory drug. The entire complex was then, coated with polyvinyl alcohol. In this particular work, we have tested the therapeutic efficacy of synthesized naproxen nanoformulation using well-established *in vitro* and *in vivo* pharmacological models. The implication of current findings is discussed here.

In vitro hemolytic or membrane stability assay and protein denaturation inhibition assay, are two particular assays used worldwide, to analyze the anti-inflammatory effect of newly synthesized compounds (Wang et al., 2018). Since lysosomal membranes disrupt and release their content outside the cells during inflammation a phenomenon known as cellular infiltration, anti-inflammatory compounds work by inhibiting the disruption of lysosomal membranes (Lewis, 1970). Likewise, the erythrocyte membrane akin to lysosomal membranes, constitutes lipids, protein, carbohydrates, and water (Li and Lykotrafitis, 2014) and upon interaction with the non-compatible compound, it causes efflux of hemoglobin, resulting in hemolysis (Hurley, 2007). Thus, RBCs are used in this assay to test the anti-inflammatory potential of the test compounds.

It was observed that naproxen nanoformulations either coated or non-coated and MgO NPs acted as RBCs membrane stabilizers and protected the RBC membranes from

hemolysis, thus can be classified as potent anti-inflammatory agents and non-toxic (Nelsonjoseph et al., 2022). On the contrary, treatment with NPRS alone caused significant hemolysis of red blood cells. This result led to a similar conclusion where a study conducted by Orhan and Sahin. (2001) revealed that naproxen causes significant hemolysis at therapeutic and high concentrations, thus confirming the conventional free-form drug's hemotoxic nature (Orhan and Şahin, 2001).

Furthermore, naproxen nanoformulations when tested for protein denaturation inhibition revealed that naproxen nanoformulation coated with PVA exhibited the highest inhibition potential against heat-induced protein denaturation in a concentration-dependent manner (Hasan, 2019). The anti-inflammatory action of naproxen nanoformulation was superior to both conventional NSAIDs i.e., naproxen sodium and diclofenac sodium. Taken together, coated nanoformulation possessed an outstanding anti-inflammatory effect. This effect may be ascribed to the slow release of naproxen from MgO NPs which led to a constant protective effect.

In general, carrageenan-induced paw edema in mice is a very popular model used for investigating the anti-inflammatory and immunomodulatory effects of new compounds. Development of edema after carrageenan injection in paw indicates the progression of inflammatory response. This response comprises two phases with inflammatory mediators working in order (Gupta et al., 2015). The release of 5-hydroxytryptamine, histamine, cyclooxygenase, and bradykinin characterize the initial phase of inflammation (0–2 hours after carrageenan injection), whereas increased production of prostaglandins (PGs), free radicals production and neutrophil infiltration mark the subsequent second phase (2– 6 hours after carrageenan injection) (Vinegar et al., 1969). Again, naproxen nanoformulation significantly alleviated paw edema in a dose-dependent manner. This effect was observed right after dose (CNF) administration (early phase of inflammation) and continued toward a later phase of inflammation. In short, CNF possesses a potent anti-inflammatory effect and significantly ameliorated carrageenan-induced paw edema even at the lowest dose (1 mg/kg) compared to vehicle control. The results of *in vivo* anti-inflammatory activity were similar to those obtained from *in vitro* anti-inflammatory activity. At the lowest dose, CNF exhibited more potency than standard anti-inflammatory drugs (NPRS and diclofenac sodium).

Though the exact mechanism underlying this effect is unknown and needs an in-depth

mechanistic study, however, adsorption of naproxen on MgO NPs, and coating with PVA may have contributed to the stability of the formulation, controlled release of the drug, and constant anti-inflammatory effect. Secondly, it is also assumed that the use of MgO NPs as drug carriers may potentiate the anti-inflammatory effect of NPRS in nanoformulation of CNF, showing the improved performance (Jahangiri et al., 2013).

Pain and inflammation are two different responses yet physiologically same responses to noxious stimuli and NSAID show their effect against both through inhibition of prostaglandin synthesis. Immersion of mice tails in hot water initiate pain at the spinal level and the delay in response time for tail withdrawal is recorded to assess the test compounds' central analgesic effect (Hole and Tjølsen, 2007). Whereas intraperitoneal (i.p.) injection of acetic acid to experimental animals results in a writhing response characterized by constrictions of abdominal muscles with stretching of hindlimbs. This model is used to analyze the peripheral analgesic effect of the synthesized compounds. Proinflammatory mediators such as prostaglandins release in response to these noxious stimuli and activate the peripheral nociceptors on the sensory nerves, leading to acute pain and inflammation (Gawade, 2012).

Presently, we tested the analgesic effect of nanoformulation using both models, and the results were compared to those produced by conventional NSAIDs. Data obtained from both experiments indicated that CNF possessed a better analgesic activity than NPRS alone, UNF and diclofenac sodium. This effect is attributed to the slow release of NPRS in the GI environment which possibly regulated the release of endogenous inflammatory mediators namely prostaglandins, serotonin, and histamine (Gupta et al., 2015).

Currently, the distinct impacts of magnesium oxide nanoparticles (MgO NPs) on a mouse model, aiming to evaluate their analgesic properties, were investigated as well. The data indicates that MgO NPs have a noticeable central analgesic effect. Nevertheless, in comparison to traditional medications and naproxen nano formulations, MgO NPs do not exhibit a significant analgesic effect in peripheral areas. Numerous studies concur with these current findings, emphasizing that MgO NPs with average particle size ~ 50 nm possess robust pain-relieving properties in mouse models.

Magnesium functions as a noncompetitive inhibitor of the N-methyl D-aspartate

(NMDA) receptor, impeding the influx of calcium into cells. This relationship has been investigated by Begon et al and Hasanein et al, who have postulated an association linking magnesium, the NMDA receptor, and the regulation of pain. Additionally, magnesium serves as a natural antagonist to calcium in various voltage-gated channels, potentially contributing to mechanisms that alleviate pain. At present, the considerable analgesic effect at the central level and the relatively insignificant analgesic impact at the peripheral level can be attributed to the size of MgO nanoparticles (NPs) which was found to be approximately ~ 200 nm in the present study. The particle size may have been more effective in producing a central analgesic effect due to the presence of NMDA receptors, whereas its size may not be small enough to efficiently penetrate peripheral tissues and generate an analgesic response in those areas.

Besides being prescribed as potent anti-inflammatory and analgesic drugs, NSAIDs are also indicated to cure fever as antipyretics (Dangarembizi et al., 2018). Presently, the nanoformulation was analyzed for its antipyretic effect as well, using the brewer's yeast-induced pyrexia model. Remarkably, the antipyretic effect of CNF was found to be superior to the standard antipyretic drug paracetamol at doses ten times lower than paracetamol.   The rise in body temperature, known as fever, is a complex physiologic reaction to external stimuli or disturbance of internal homeostasis. It involves the activation and release of pro-inflammatory cytokines and the initiation of inflammatory cascades (Aronoff and Neilson, 2001). Various mechanisms are proposed through which NSAIDs show their antipyretic effect.

Most NSAIDs, such as naproxen, ibuprofen, aspirin, and acetaminophen, which have moderate to high antipyretic activity bind selectively or non-selectively to different COX variants (Tomić et al., 2017). Inhibition of COX enzyme expression prevents the activity of phospholipase A_2, an important enzyme that mediates the synthesis of prostaglandins, thus suppressing fever (Rainsford, 2007). Recently, a few studies have suggested that paracetamol showed its antipyretic effect by selectively inhibiting the COX-3 enzyme, a variant of COX-1 in the hypothalamus (Hilário et al., 2006). However, the exact mechanism by which NSAIDs suppress fever is still unknown. CNF contains NPRS and NPRS showed its antipyretic effect by inhibiting COX enzyme, therefore, it would be reasonable to assume that CNF demonstrated its potent antipyretic activity by inhibiting the COX enzyme. However, additional in-depth

biochemical and biomolecular studies are required to uncover the underlying mechanism by which synthesized nanoformulations promptly lowered the experimental mice's body temperature.

In conclusion, the data obtained in the current study revealed that the naproxen nanoformulation is a potent anti-inflammatory, analgesic, and antipyretic agent, with efficiency 10-times higher than conventional NSAIDs such as naproxen sodium, paracetamol, and diclofenac sodium at the same doses or even at low doses administered. Therefore reasonably, in connection with the overall positive findings regarding the *in vivo* and *in vitro* biological testing, the novel naproxen nanoformulations can represent a usable alternative to conventional anti-inflammatory drugs widely used to treat acute and chronic inflammatory diseases affecting humankind negatively. The enhanced therapeutic effects observed are attributed to the use of MgO NPs as a nanocarrier for NPRS. Therefore, it may also be used as a biocompatible drug carrier to enhance the therapeutic efficacy and reduce the toxicity of other therapeutic and anti-inflammatory drugs. In addition, synthesized nanoformulation "CNF" has potent anti-inflammatory activity, so it is recommended to explore its potential for the treatment of other inflammatory diseases for example chronic peptic ulcer, asthma, arthritis, tuberculosis, sinusitis, and active hepatitis.

Chapter 4

Acute and sub-acute toxicity study of naproxen nanoformulation (CNF) in Balb/c mice

Summary

Nanotoxicology is a subfield of toxicology that examines the toxicity of nanoparticles, particularly those employed in pharmaceuticals. In this specific work, we performed acute and sub-acute toxicity experiments of CNF mentioned as NpNF, using male and female mice. the oral LD_{50} value of coated naproxen nanoformulation (NpNF or CNF[1]) was found to be 2574 mg/kg in mice, therefore it could be categorized as safe (category 5; no warning on label) according to the Global Harmonized System for classifying hazardous chemicals (GSH). While the no-observed-adverse-effect level (NOAEL) of NpNF was considered lower than 300 mg/kg in this study. The reduced toxicity of naproxen nanoformulation is most likely due to the drug's altered biodistribution mediated by nanoparticles.

---

[1] The abbreviation NpNF is used in the present chapter only to mention the coated naproxen nanoformulation.

Introduction

The combination of pharmaceutics with nanotechnology has significantly improved human health and life expectancy. Remarkable growth has been observed in the field of nanomedicine in recent years which has opened new avenues of research for scientists all over the world (Mazayen et al., 2022). To create targeted drug delivery systems, several kinds of nanomaterials are used as drug carriers such as organic, inorganic, and polymeric including micelles, dendrimers, liposomes, and metallic nanoparticles (Trucillo, 2021).

The structure/function correlations of nanomaterials, as well as their composition, surface characteristics, and interaction with the biomolecules, are of fundamental significance (Rosado balmayor et al., 2011). Second, during preclinical research, it is critical to discover the possible acute and chronic adverse effects and toxicity that these new nanomaterials may induce (Parasuraman, 2011). Nanotoxicology is a subfield of toxicology that examines the toxicity of nanoparticles, particularly ones employed in pharmaceuticals. Nanotoxicological research primarily focuses on determining the hazardous effects of nanoparticles and nano-based drugs on both people and the environment (Fadeel, 2019).

Although there are no defined rules for assessing the systemic toxicity of nanopharmaceuticals available to date, essential toxicological research *in vitro* and *in vivo*, with basic toxicity testing procedures, can be utilized to evaluate their hazardous effects (Erkekoglu and Kocer-Gumusel, 2018). Since these investigations are performed on laboratory animals, authentic assessment of obtained results is critical and should be consistent with human body functioning (Farjadian et al., 2019). Briefly, the nonclinical safety evaluation aims at identifying the adverse effects of nanomaterials on living systems, dosage dependency, connection to exposures, and any possible reversibility of damaging effects on target organs (FDA, 2010).

These tests include an acute toxicity study which is used to identify a single dose causing major adverse effects/life-threatening toxicity. This test is normally conducted on rodents and consists of a single dosage up to a maximum of 2000 mg/kg, or the utmost technically possible. This research helps in establishing the median lethal dosage (LD_{50}) and effective dose (ED_{50}) of the test materials (Hayes et al., 2020). The

LD_{50} (median lethal dose) is defined as "a statistically derived single dose of a substance that can be expected to cause death in 50% of animals when administered by the oral route." While the ED_{50}, is an effective dosage that induces any effect other than fatality. The dose ratio of both is used to determine the therapeutic index of the therapeutic drug or material and is defined as "the ratio between the lethal dose and the pharmacologically effective dose (LD_{50}/ED_{50})". The greater the index, the lesser the substance's toxicity, and vice versa (Communication from the Commission to the European Parliament, 2012; Erhirhie et al., 2018).

On the other hand, the repeat-dose toxicity studies usually conducted for 14-28 days hold great significance in the preclinical investigation, during drug development. These investigations serve to establish the extent to which medications might cause toxicity and also the amount at which they are regarded safe. Collectively this data establishes the drug dose at which no effects are observed (NOELs) or no-observed adverse effect levels (NOAELs) are detected. Moreover, demonstrates drug-induced organ toxicity, an estimation of the dose for the initial human trials, and possible prodromal markers that could be used to monitor the onset of adverse responses in humans (Dorato and Engelhardt, 2005). Furthermore, repeat dose toxicity is described as any reported toxicities associated with multiple dosage-response and the dose at which the toxic symptoms initially arise (threshold dose). Repeat-dose studies can be brief (e.g., daily dosing for up to 14 days), sub-chronic (up to 3 months), or chronic in nature (longer than 3 months and usually up to 2 years) (Stark and Steger-Hartmann, 2016). (Fig. 4.1)
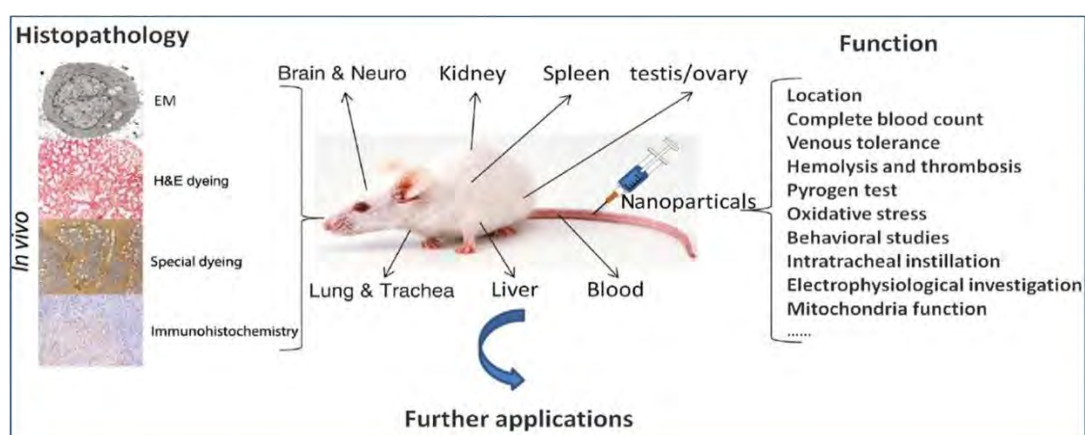
Fig. 4.1 A presentation of *in vitro* and *in vivo* toxicity testing methods that can be used to assess the safety of nanomaterials in mice models (Yang et al., 2020).

It is well known that no therapeutic compound is without risk, as a result, a thorough evaluation of the usage and suitability of new substances, test materials, and products in the research requires insight into potential consequences (Ventola, 2017). In the light of previous findings regarding naproxen nanoformulation (CNF now named naproxen nanoformulation NpNF for the current study), as a potential anti-inflammatory agent that holds great promise for clinical translation, the present study aimed at assessing the safety of NpNF by carrying out acute and subacute toxicity in male and female BALB/c mice.

Materials and Methods

4.1 Chemicals

All chemicals, potassium phosphate monobasic, potassium phosphate diabasic, sodium phosphate monobasic, sodium phosphate diabasic, trisodium citrate, ferrous sulfate ($FeSO_4$), guaiacol, 4-(2-hydroxyethyl)-1-piperazineethanesulfonic acid (HEPES), sodium azide, hydroxymethyl aminomethane (Tris), thiobarbituric acid (TBA), trichloroacetic acid (TCA), ascorbic acid, acetylsalicylic acid, n-Acetyl-L-cysteine, N.N-Diethylpara phenyl diamine sulfate (DEPPD), bovine serum albumin (BSA), sodium chloride, potassium chloride, sodium dodecyl sulfate (SDS), riboflavin, L-Methionine, 5.5′-dithiobis-(2-nitrobenzoic acid) (DTNB), nitroblue tetrazolium (NBT), hematoxylin and eosin, were purchased from Sigma Aldrich (St. Louis, Missouri, USA). Other reagents such as formaldehyde, chloroform phosphoric acid, methanol, hydrogen peroxide H_2O_2 (30 % w/w), xylene, and triton X-100 used in the current study were of analytical grade and purchased from Merck (Darmstadt, Germany) or Sigma Aldrich (St. Louis, Missouri, USA).

All solutions were prepared in deionized/distilled water. Serum biochemical analyses were performed using the commercially available kits (LAB KIT diagnostic kits, Spain).

4.2 Animals and Housing

Healthy male and female Balb/c mice, weighing 25 – 30 g were procured from the National Institute of Health (NIH), Islamabad. Animals were, tagged, and housed in polypropylene cages with a maximum of three animals per sex per cage, in the Animal House Facility of Quaid-i-Azam University Islamabad. Cages were layered with autoclaved paddy husk and the husk was replaced twice a week. Animals were offered a conventional rodent diet and drinking water *ad libitum*. Mice were maintained in well-ventilated pathogen-free rooms under standard laboratory conditions of temperature (22 °C ± 1.5 °C), relative humidity (60% ± 10%), and a 12-hour light/dark cycle.

The animals were allowed to acclimatize to the laboratory conditions for 5 days before the start of the study. All experimental procedures performed in the current study were carefully reviewed, revised, and approved by the "Bioethical Committee (BEC)" at

Quaid-i-Azam University (BEC FBS-QAU2021-298) and conducted under the National Institutes of Health guidelines for the care and use of laboratory animals.

As the current study aimed to assess the safety profile of the naproxen nanoformulation (NpNF) therefore, an acute toxicity experiment was conducted first, followed by a 14-day repeated dose oral toxicity study.

4.3 Acute Oral Toxicity Study and Determination of LD_{50}

Based on their body weights, nulliparous and non-pregnant healthy female BALB/c mice (n = 5) were randomly selected and divided into five treatments and a control group. The treatment groups were orally administered with successive doses (1000 – 3200 mg/kg) of NpNF, suspended in distilled water. The control group received distilled water only. The volume of orally given doses was calculated based on each animal's fasting body weight. Food was withheld for another 4 hours after the experimental dosages were given. According to the Organization for Economic Co-operation and Development (OECD) guidelines (OECD, 2001) for the selection of animal models in acute toxicity testing only female mice were used in this experiment.

All of the experimental animals were maintained under constant observation for the first 6 h after the dosage was administered and then monitored for any behavioral changes or death for up to 14 days. Any alterations in physical appearance and behavioral pattern, toxicity signs such as shivering, salivation, tiredness, diarrhea, sleep, coma, and/or mortality were observed and documented daily for the entire study period. Individual body weights of all mice were recorded on days 0 (day of dosing), 7, and 14. In addition, the daily food intake of each animal was recorded, and the mean daily food consumption was computed by subtracting the quantity of the remaining food from the weight of the supplied food. Animals were euthanized via cervical dislocation at the end of the experimental period and subjected to gross necropsy. In terms of percent mortality, dose-response data from treatment groups were subjected to the computerized Statistical Analysis System (SAS) for probit analysis to estimate an accurate lethal dose (LD_{50}) that would cause 50% mortality in female mice.

4.4 Subacute Toxicity Studies

The results obtained from the acute toxicity study (mentioned earlier) were used to

design a sub-acute toxicity study also known as, a range-finding study to assess the safety of the naproxen nanoformulation, following its 14-day oral administration at various dose levels.

4.5 Experimental Design

According to the international council for harmonization of technical requirements for pharmaceuticals for human use (ICH), a non-clinical safety assessment of any new/novel therapeutic compound on animals should contain an appropriate control group; a low dose group that may or may not induce any toxicity, a medium dose group sufficient to produce a result in systemic exposure comparable with that expected at the intended clinical use, such as the geometric mean between the high and the low dose and a high dose, chosen to allow for the detection of target organ damage or other non-specific toxicity, or until limited by the volume of dose (Persson et al., 2017). A limit dose of 1000 mg/kg/day is considered appropriate in sub-acute toxicity testing in rodents.

Therefore presently, a total of 48 mice were randomly assigned to three test groups and the control group (12 mice in each group, female: male = 1:1). The body weight at the beginning of treatment was 34.05±1.34 for males and 30.25±1.44 for females. During the administration period, the control group of mice was dosed with distilled water, while treatment groups were orally administered with 30, 300, and 1000 mg/kg naproxen nanoformulation daily for a continuous 14 days. Clinical observations were made at least twice a day at the same time each day and considered the peak period of anticipated effects after the daily dosing.

4.5.1 Clinical Observation, Body Weight, and Food Consumption

All animals were subjected to detailed clinical observation once before the initial dose exposure (to allow for within-subject comparisons) and at least once a week afterward. These observations were obtained employing a grading scale outside the home cage. During the second exposure week, both the control and test animals were subjected to a modified in-house functional observation battery of tests, which included home-cage observations, hand-held observations, sensory input, and other additional measures. Each animal's body weight was measured the day before dosing started, then once a week after that, and lastly on the day of dissection. Food consumption was also tracked

daily.

4.5.2 Hematology, Clinical Biochemistry, and Collection of Tissues

On the 14th day of the experiment, mice were kept fasted for 12 h. The next day, whole blood was collected in EDTA tubes, under ketamine (100 mg/mL)/xylazine (20 mg/mL) anesthesia given intraperitoneally. Blood samples were labeled and analyzed for white blood cell count (WBC), erythrocyte count (RBC), hemoglobin (Hb), mean corpuscular volume (MCV), hematocrit (HCT), mean corpuscular hemoglobin (MCH), mean corpuscular hemoglobin concentration (MCHC), platelets, neutrophils, lymphocytes, monocytes, eosinophils, and basophils. Besides, blood samples were collected in a gel tube and allowed to stand for 1 h at room temperature and then subjected to centrifugation (3000 rpm for 10 min). Sera were collected, labeled carefully, and stored at − 20 °C for the serum biochemical assays.

Vital organs *viz*, brain, heart, liver, spleen, stomach, kidneys, testes, epididymis, and seminal vesicles of all animals (apart from those found moribund and/or euthanized before the termination of the study) were appropriately trimmed of any adherent tissue, and their wet weight was taken immediately after dissection to avoid drying. Approximately 0.1 g of each tissue was then cut, rinsed with ice-cold saline solution, and kept at −20 °C for preparation of tissue homogenates for tissue biochemical assessment. Whereas remaining tissues were fixed in 10 % neutral buffered formalin solution for histopathological studies.

4.6 Serum Biochemical Assays

Serum biochemical assays were performed on an automatic chemistry analyzer (Agilent-8453, California, U.S.A.) using commercially available kits (LAB KIT diagnostic kits Spain). Assays included alanine aminotransferase (ALT), aspartate aminotransferase (AST), alkaline phosphatase (ALP), total bilirubin, bilirubin direct, creatinine, lactate dehydrogenase (LDH), total cholesterol, and triglyceride.

4.6.1 Alanine-Aminotransferase (ALT-GPT)

Reagent Composition

Reagent R1: R1 contained L-alanine 750 mmol/L, Tris buffer 150 mmol/L of pH 7, and

Lactate dehydrogenase >1.350 U/L. Reagent R2: R2 contained 2-oxoglutarate 75 mmol/L, NADH 1.3 mmol/L

Principle

The transfer of amino group is catalyzed by the enzyme Alanine aminotransferase (ALT) to oxoglutarate thus forming glutamate and pyruvate. Another enzyme Lactate dehydrogenase (LDH) then reduces pyruvate to lactate in the presence of nicotinamide-adenine-dinucleotide (NADH) and also NADH is oxidized to NAD^+.

Procedure

Initially, a working reagent solution (WR) was prepared by carefully adding 1 part of R2 and 4 parts of R1 in a glass beaker. Following this 50 μl and 1000 μl of WR were mixed in a glass cuvette and incubated at 37 °C for 1 min and an initial absorbance was recorded at 340 nm. Absorbance was repeated after 1 min interval for 3 min and averaged. An equal quantity of distilled water was added to the blank sample. The final quantity of ALT was calculated by using the following formula:

$$\Delta A/min \times 3333 = ALT/GPT \text{ activity [U/L] at 37 °C}$$

4.6.2 Aspartate Amino Transferase (AST/GOT)

Reagent Composition

Reagent 1 (R1): R1 contained L-Aspartate 200 mmol/L, Tris 80 mmol/L of pH 7.8, Lactate dehydrogenase (LDH) 800U/L, and Malate dehydrogenase (MDH) 600 U/L

Reagent 2 (R2): R2 contained NADH 0.18 mmol/L and alpha-Ketoglutarate.

Principle

The enzyme aspartate-aminotransferase (AST) catalyzes the reversible transamination of aspartate to form alpha-ketoglutarate giving rise to oxaloacetate and glutamate. In the presence of malate dehydrogenase (MDH) and NADH, oxaloacetate is reduced to malate.

The quantity of NADH is relational to the activity of AST catalytic concentration in the sample.

Procedure

Working reagent (WR) was prepared by mixing R1 and R2 at a ratio of 4:1. For blank and sample, 100 µl of distilled water or serum sample was mixed with 1000 µl of WR. Contents were incubated at 37°C for 1 min. Change in absorbance was detected at 340 nm wavelength at 1 min interval thereafter for 3 min. The difference in absorbances was calculated and averaged.

Final calculations for the test were done as followed:

$$AST/GOT\ U/L = \Delta A/min \times 1750$$

4.6.3 Alkaline Phosphatase (ALP/DEA)

Reagent Composition

Reagent 1 (R1): R1 contained DEA buffer Magnesium Chloride 0.6mmol/L, 1.25 mol/L of pH 10.2; Reagent 2 (R2): R2 contained 4-Nitrophenylephosphate 50 mmol/L.

Principle

The enzyme alkaline phosphatase (ALP) catalyzes the hydrolysis of 4-nitrophenyl phosphate (4-NPP) producing free inorganic phosphate and 4-nitrophenol. The alkaline buffer acts as an acceptor of the phosphate group. Absorbance is read at 405 nm. The formation of 4-nitrophenol is equivalent to ALP activity in the sample.

Procedure

To prepare the working reagent, R1 and R2 were mixed at a proportion of 4:1. After that, 1000 µl of working reagent and 20 µl of samples were gently mixed. Absorbance was noted at 405 nm after 1 min incubation at 37 °C. Readings were taken in triplicate after 1 min interval to take the average value. The final concentration of ALP was calculated by using the following formula:

$$\Delta A/min \times 2764 = ALP\ activity\ (U/L)$$

The blank sample contained an equal quantity of distilled water instead of serum.

4.6.4 Serum Creatinine

Reagent's Composition

Reagent 1 (R1): Picric reagent contained 17.5 mmol/L of Picric Acid

Reagent 2 (R2): Alkaline reagent contained 0.29 mol/L of Sodium Hydroxide

Creatinine calibrator: Creatinine aqueous primary calibrator, 2 mg/dl

Principle

This test depends on the reaction of creatinine with sodium picrate (Alkaline picrate) that forms a red-colored complex. The color intensity is related to creatinine concentration in the sample.

Procedure

An equal volume of R1 (Picric reagent) and R2 (Alkaline reagent) were carefully mixed. A 100 μl of creatinine calibrator or 100 μl of serum was then mixed with 1000 μl of working reagent to measure the absorbance for standard, and samples. Blank contained WR (1000 μl) without any sample. All samples were incubated at 37 °C for 1 min. Absorbances were taken after 30 sec (A1) and after 90 sec (A2) at 492 nm. Change in ΔA (A2-A1) was determined for the calibrator and samples and the final concentration was determined using the given formula:

$$\text{Creatinine (mg/dL)} = (\Delta A \text{ Sample}) / (\Delta A) \text{ Calibrator x 2(Calibrator conc.)}$$

4.6.5 Serum Bilirubin (total and direct)

Reactive Ingredients Concentration

Reagent 1 (R1) contained sulfamic acid 9.7 g/L, while reagent 2 (R2) contained 2, 4-dichloroaniline 0.081 g/L, sodium nitrite 0.035 g/L and HCL 1.68 g/L

Principle

The reaction of bilirubin with a diazotized sulfanilic acid is used to determine bilirubin levels. In the presence of sulfamic acid, direct (conjugated fractions) bilirubin interacts with a diazonium salt to generate the colorful complex azobilirubin. The increase in absorbance at 548 nm due to azobilirubin is proportional to the direct bilirubin concentration.

4.6.6 Total Cholesterol

Working solution: It contained phosphate buffer 30.0 mmol/l of pH 7, 4-aminoantipyrie 0.25 mmol/l, 25.0 mmol/l of phenol, > 5.0 of KU/l peroxide, > 150.0 U/l of cholesterolesterase, > 100.0 U/L of cholesteroloxydase, < 0.01 % of sodium azide and standard 200 mg/dL.

Principle

Oxidation and enzymatic hydrolysis processes determine cholesterol concentration. The reaction of hydrogen peroxide with 4-amino antipyrine produced red dyestuff in the presence of phenol and peroxidase. The concentration of the color formed is related directly to the concentration of cholesterol.

Procedure

From each sample, 10 µl of serum was mixed with 1000 µl of reagent, while for standard 10 µl of the standard was mixed with 1000 µl of reagent. The contents were then incubated for 5 min at 37°C in an incubator. The absorbance of the samples was noted at a wavelength of 546 nm. The final calculation was performed using the following formula:

$$c = 200 \text{ x } \delta A \text{ (sample) } / \delta A \text{ (standard) (mg/dL)}$$

blank consisted of 1000 µl of reagent only.

4.6.7 Estimation of Triglyceride Concentration

Reagents (R): Pipes buffer of 40 mmol/l of pH 7.0, 5 mmol/l of 4-Chlorophenol, ATP 1 mmol/l, 5 mmol/l of Magnesium ion, $\geq$ 1 U/mL of Peroxidase, $\geq$ 1 U/mL of Glycerol kinase, 0.4 mmol/l of 4-aminoantipyrine, $\geq$ 3.5 U/mL of Glycerol-3-phosphate oxidase, 0.05 % of sodium azide and 200 mg/dL or 2.28 mmol/l of standard.

Principle

The enzyme lipoprotein-lipase enzymatic activity causes hydrolysis of triglyceride. A colored phenazone is thus formed From Hydrogen peroxide (H_2O_2), 4-amino antipyrine, and 4-chlorophenol under the influence of the catalytic activity of peroxidase.

Procedure

For this assay, 10 μl of standard or serum were mixed with 1000 μl of regent. Contents were incubated for 5 min at 37 °C. The final absorbance was taken three times at a wavelength of 500 nm within 60 sec.

Using the followed formula, the final values were calculated as:

$$c = 200x \ \delta A \ (\text{sample})/ \ \delta A \ (\text{standard}) \ (\text{mg/dL})$$

blank consisted of 1000 μl of regent only.

4.6.8 Estimation of LDH-L

Reagent Composition

Reagent 1 (R1): R1 contained 2-Amino-2-methyl-propan-1-of 250 mmol/L of pH 9.4, L-Lactate 80 mmol/L and Sodium Azide 0.09 %.

Reagent 2 (R2): R2 contained NAD^+ 9 mmol/L

Principle

The principle is based on photometric detection of pyridine co-enzyme oxidation. The LDH activated can be detected using two reactions both lactate to pyruvate reaction (L-P. forward-reaction) and pyruvate to lactate reaction (P-L, backward-reaction). The presently used kit was designed for forwarding reaction thus lactate was oxidized to pyruvate with simultaneous reduction of NAD to NADH catalyzed by Lactate dehydrogenase. The rate of reduction of NAD was noted as a rise in absorbance which was directly related to the action of LDH in serum.

Procedure

WR (Working reagent) was produced by mixing R1 and R2 at a ratio of 4:1. 20 μl of distilled water or sample was gently mixed with 1000 μl of WR to run blank and sample. Contents were incubated at 37 °C for 1 min. At an interval of 1 min, three readings were recorded and then averaged.

The final value was calculated by using the given formula:

$$LDH [U/L] = \Delta A/min \; x \; 8095$$

4.7 Oxidative Stress and Antioxidants Enzymes Assays

For tissue biochemical analysis, tissue homogenates were prepared and evaluated for oxidative stress ROS, MDA assay, and defense markers SOD, POD, CAT, and reduced glutathione assay according to the previously published protocol with slight modifications.

4.7.1 Preparation of Tissue Homogenate

Tissue lysis/ extract buffer (pH. 07) was prepared by adding 5.95 g of HEPES, 0.1 g of sodium azide, 0.5 g of SDS, and 4.38 g of NaCl into 300 mL of distilled water and dissolved thoroughly using a magnetic stirrer. Following this 5 mL of Triton -X100 was added to this solution and the volume was raised to 500 mL. Various organs *viz.,* brain, kidney, liver, stomach, spleen, seminal vesicles, and testicular tissues were weighed (100 mg), minced in frosted petri plates, and homogenized further with the help of a hand-held glass homogenizer (GPE limited, UK) in 1mL extract buffer (Lysis buffer, pH. 7.0), to which 0.1mg of PMSF was also added. The homogenate was then centrifuged at 12204 *g* for 10 min to isolate the supernatant which was later collected in labeled autoclaved tubes (1.5 mL) and kept at -20 °C for biochemical investigations.

4.8 Investigation of Oxidative Stress

4.8.1 Estimation of Reactive Oxygen Species (ROS)

The ROS concentration in tissue homogenates was estimated following the protocol of Hayashi et al. (2007) (Hayashi et al., 2007). First, Sodium acetate buffer (0.1 M, pH.4.8) was prepared by adding 4.1 g of sodium acetate to 500 mL of distilled water. From this buffer, 100 mL were taken into another beaker and 10 mg of N.N-diethylpara phenyl diamine sulfate (DEPPD) were dissolved. This solution was named reagent 1. To make reagent 2, a stock solution of ferrous sulfate was made by dissolving 5 mg of ferrous sulfate in 1 mL of sodium acetate buffer, and 62.5 µL of this stock solution was pipette-picked and added to 125 mL of sodium acetate buffer. A working solution was prepared by adding reagent 1 and reagent 2 with a ratio of 1:25 (reagent 1: reagent 2) in a glass beaker and placed in the dark for almost 2 min.

To estimate ROS, hydrogen peroxide (H_2O_2, 30 % w/w, Sigma Aldrich) standards were prepared by serial dilutions of (0, 0.23, 0.46, 0.92, 1.87, 3.75, and 7.50 mg H_2O_2) from these standard solutions, 60 µL was taken and added to 1200 µL of 0.1M sodium acetate buffer (pH, 4.8) incubated for 5 minutes at 37 °C. A volume of 1680 µL reagent mixture was then, added to the incubated solution and heated for 1 min at 37 °C. Likewise, samples were prepared using the same procedure by adding 60 µL of tissue homogenate in 1200 µL of 0.1M sodium acetate buffer (pH, 4.8) incubated for 5 minutes at 37 °C. A volume of 1680 µL reagent mixture was then, added to the incubated solution and heated for 1 min at 37 °C. Absorbance was read at 505 nm on a UV-visible spectrophotometer (Agilent 8453, USA). Three readings for each sample were taken at 15-sec intervals for 180 sec. The standard curve was plotted and reported. One unit of ROS was equivalent to the concentration of hydrogen peroxide in the sample (1 unit = 1.0 mg H_2O_2/L).

4.8.2 Lipid Peroxidation Assay (TBARS)

Estimation of TBARS levels is used as an index of lipid peroxidation in tissue samples was done as described by Olszewska-Słonina et al. (2011) with modification (Olszewska-Słonina et al., 2011). Briefly, a solution mixture was prepared by adding 0.1 mL of tissue homogenate with 0.1 mL ascorbic acid (1.5 mM), 0.1 mL Tris- HCL (50 mM), 0.1 mL $FeSO_4$ (1mM), and 0.6 mL distilled water. The solution was then, incubated at 37 °C for 15 min. to this, 1 mL of thiobarbituric acid (TBA, 0.37% w/v) was added to stop the reaction. Afterward, 1 mL of trichloroacetic acid (TCA 10%) was added to each sample and the reaction mixtures were heated at 90 °C for 15 min in a water bath. After cooling, the mixtures were centrifuged at 1000 *g* for 10 min. The supernatant was separated and the amount of TBARS formed in each sample was estimated by measuring optical density at 532 nm. Results were expressed as nmol malonaldehyde/min/mg tissue at 37 °C using a molar extinction coefficient of 156 m mol/L/cm.

4.9 Antioxidant Enzyme Assays

4.9.1 Catalase Assay (CAT)

The activity of CAT in the tissues was determined according to Maehly (2006) with slight modifications (Maehly, 2006). Samples were prepared by adding 0.1 mL tissue

homogenate in 1.99 mL of 50 mM potassium phosphate buffer (pH.7) and 1 mL of H_2O_2 (5.9 mM), in a 3 mL cuvette. Absorbance was measured at 240 nm immediately for each sample at 15-sec and 30-sec intervals, then averaged. In the same way, instead of homogenate, distilled water was added to the reagent mixture to blank. The absorbance difference of 0.01 as U/min was regarded as one unit of CAT activity.

4.9.2 Superoxide Dismutase Assay (SOD)

Superoxide dismutase (SOD) activity was determined following the protocol of Azeemi et al. with modifications (Azeemi et al., 2009). A reagents mixture was prepared by adding 4.5 mL of L-methionine (9.9 mM), 3.5 mL of Triton X-100 (0.025%), and 3 mL of 57 µM nitro blue tetrazolium (NBT) in a volumetric flask and the final volume was raised to 100 mL with phosphate buffer saline (50 mM, pH. 7). For each sample, 1 mL of reagent mixture was transferred into a cuvette containing 20 µL of tissue homogenate and illuminated to the fluorescent lamp for 7 min followed by incubation at 37 °C for 5 min. The reaction was initiated through the addition of 10 µL of chilled riboflavin (0.9 µM) following incubation at 40 °C for 8 min. The amount of chromogen formed was measured by recording the absorbance at 560 nm using a spectrophotometer. The results were expressed in U/mg protein.

4.9.3 Peroxidase Enzyme Assay (POD)

The concentration of POD in the tissue homogenate was evaluated according to Maehly (2006) (Maehly, 2006). The reaction mixture was prepared by the addition of 2.5 mL of phosphate buffer (50 mM), 0.1 mL of tissue homogenate, and 0.1 mL of guaiacol (20 mM). The contents were quickly stirred to make a homogeneous solution, then 0.3 mL of H_2O_2 (40 mM) was added to initiate the reaction. Change in absorbance of the reaction solution at 470 nm was determined after 1 min. One unit of POD activity was defined as an absorbance change of 0.01 as U/min.

4.9.4 Reduced Glutathione (GSH) Estimation

Reduced Glutathione was measured as defined by Salbitani and Carfagnaet (2017) (Salbitani et al., 2017). The reagent mixture was prepared by adding 0.1 mL of disodium phosphate buffer (0.4 M), 0.1 mL of tissue homogenate, and 0.5 mL of DTNB (5,5-dithiobis (2-nitrobenzoic acid)) into a cuvette. DTNB also known as Ellman's

reagent was made by dissolving 40 mg of DTNB in 100 mL of 1% tri-sodium citrate. The absorbance of the yellow color was measured at 412 nm, and one-unit GSH activity was represented as μMol/g.

4.10 Histopathological Examination

For histopathological examination, neutral buffered formalin (10%) fixed tissues were dehydrated in escalating degrees of alcohol, cleared in xylene, and then placed in melted paraffin wax overnight. The tissue-filled paraffin blocks were then prepared and sliced into 5 μm thick slices using a microtome (Leica Biosystems, Buffalo Grove, IL, USA). The slices were mounted on glass slides, dried, deparaffinized, and stained with Ehrlich's hematoxylin and eosin counterstained eosin (H&E). Stained slides were then, mounted in DPX, observed, and imaged at 10x and 40x under an optical microscope (CX41-Olympus, Japan) equipped with a digital camera (Tucson, USB2.0 H series). The results were analyzed by a veterinary pathologist and reported.

4.11 Statistical Analysis

All data were presented as the mean±s.e. Initial and final body weights, absolute and relative organ weights at necropsy, and hematological, serum, and tissue biochemical parameters were examined using Analysis of Variance (ANOVA). All statistical analyses were performed using Sigma Plot 12.0. Multiple comparisons were performed by Tukey's test. For histologic analysis, the animals were sacrificed, the samples were obtained, and a histopathological assessment was performed to evaluate the normal and affected tissues. $P < 0.05$ was considered significant.

Results

4.12 Acute Oral Toxicity Study and Determination of LD$_{50}$

Based on the results obtained from a preliminary study performed on female mice aimed at finding the NpNF doses, which can exert toxic effects on female mice, a start dose of 1000 mg/kg was chosen for the current experiment as it was found that the doses of 30, 300, and 900 mg/kg of NpNF did not show any toxic signs.

Presently, therefore, female mice received an increasing dose of NpNF, with a start dose of 1000 mg/kg, and other groups received oral doses of 2000, 2500, 2700, and 3200 mg/kg. Results revealed that mice that received a 1000 mg/kg oral dose of NpNF showed no mortality or signs of toxicity within 14 days. On the other, one mouse was found dead in the 2000 mg/kg treatment group after 5 days of the dose administration, yet gross necroscopy revealed no clinical signs.

The mortality rate and acute toxicity were increased progressively as the dose increased from 2000 mg/kg to 3200 mg/kg, whereby 100% mortality was recorded in the 3200 mg/kg treatment group within 24 h. The experiment was stopped at this stage, and dose-response data (mortality vs dose) were subjected to the computerized Statistical Analysis System (SAS) for a correct estimation of LD$_{50}$ through probit analysis, which was found to be 2574.77 mg/kg with 95% confidence limits (2338- 2789 mg/kg) (Table 4.1, Fig. 4.2).

4.13 Subacute Toxicity Studies

4.13.1 Clinical Observation, Body Weight, and Feed Consumption

 In general, throughout the experiment, no mortality or evident clinical indications suggesting toxicity of NpNF were seen at any dosage. The functional behavior of all the treated groups (male and female mice) was comparable to the control group. Besides, the body weight, food consumption, and water intake of all mice in all treatment groups were found to be normal. There was an increase in body weight, of male mice in all treatment groups observed (at the weekly interval on day 7 and day 14). Yet, this increment was not statistically significant between genders and compared to control (Fig. 4.3 A, B).

4.13.2 Relative Organ Weight and Organ-to-Body Weight Ratios

The absolute and relative organ weight of male mice treated with NpNF is demonstrated in Fig. 4.4 (A, B, and C). As shown in Fig. 4.4, there was no significant difference observed in the absolute and relative organs weight such as brain, heart, liver, kidneys, stomach, spleen, testes, and seminal vesicles of treated male mice compared to those in the control group, at any dose level. Likewise, the absolute weight of the brain, heart, liver, kidneys, stomach, and spleen and their respective organ-to-body weight ratios were found to be insignificantly changed in females of all treatment groups compared to control Fig. 4.5 (A, B).

4.13.3 Hematological Parameters

Hematological parameters, that included RBC, Hb, MCV, MCH, MCHC, platelets, WBCs, neutrophils, lymphocytes, monocytes, eosinophils, and basophils of male and female treated mice are shown in Table 4.2 and Table 4.3 respectively.

Data revealed that a low dose (30 mg/kg) of NpNF did not alter any of the hematological parameters in both male and female treatment groups. There occurred, however, a slight decrease in MCV ($p<0.018$) and MCH ($p<0.004$), levels while a slight increase in platelets count ($p<0.001$), monocytes ($p<0.001$) and eosinophils ($p<0.05$) were observed in male mice treated with medium dose of NpNF. Other parameters including RBC, Hb, MCHC, WBCs, neutrophils, lymphocytes, and basophils remained unchanged. Female mice, on the other treated with the medium dose of NpNF, showed better tolerance against the same dose, given, with no change recorded in any of the hematological parameters compared to the control.

Male mice treated with the high dose of NpNF, showed a statistically significant difference in few parameters compared to the control. A significant decrease was observed in RBC ($p<0.01$), MCH ($p<0.002$), WBCs ($p<0.001$), while an increase was observed in the platelets count ($p<0.001$), monocytes ($p<0.001$) and eosinophils ($p<0.001$). Other parameters, however remained unchanged. Besides, examination of blood parameters in female high dose group revealed a significant decrease in RBCs ($p<0.01$), Hb ($p<0.05$), MCV ($p<0.001$), MCH ($p<0.01$), MCHC ($p<0.035$) while an increase was observed in platelets count ($p<0.001$), monocytes ($p<0.05$), and eosinophil ($p<0.01$).

4.13.4 Serum Biochemical Analyses

Presently, serum biochemical analyses were performed to assess any adverse effect of NpNF on serum ALT, AST, ALP, bilirubin (total and direct), creatinine, LDH, cholesterol, and triglycerides. Data revealed that the low and medium doses of NpNF did not alter any of the above-mentioned parameters in both male and female treatment groups (Table 4.4).

Any significant changes, if found, were only in the high dose treated groups in both genders. The levels of ALT and ALP were significantly increased in 1000 mg/kg-NpNF treated groups in both genders (ALT; $p<0.05$, ALP; $p<0.001$ in males while ALT; $p<0.05$, ALP; $p<0.012$ in females). The levels of AST, however, remained unchanged (Fig. 4.6, 4.7).

Moreover, the levels of total bilirubin increased significantly ($p<0.005$), in high-dose treated male mice, compared to the control, while direct bilirubin and creatinine levels remained statistically unchanged (Fig. 4.8). On the other, in the high-dose female group a significant increase in both total ($p<0.005$) and direct bilirubin ($p<0.002$) levels were detected, whereas creatinine levels did not change statistically (Fig. 4.9).

Assessment of serum lipids profile revealed that high-dose treated male mice showed a significant increase in cholesterol and triglyceride levels ($p<0.05$). Lactate dehydrogenase levels remained unchanged in high-dose treated mice (Fig. 4.10). In female mice, treatment with the same dose resulted in a significant increase ($p<0.017$) in cholesterol levels only, serum triglycerides and LDH levels remained unchanged (Fig. 4.11).

4.14 Oxidative Stress, and Antioxidants Enzymes Assays

4.14.1 Reactive Oxygen Species (ROS) and Lipid Peroxidation (LPO)

The effects of NpNF doses on oxidative stress parameters such as ROS and LPO in various tissues of male and female mice) were evaluated and are presented in Table 4.5; Fig. 4.12 and Table 4.6; Fig. 4.13 respectively. Results revealed that the low dose of NpNF in all tissues and, the medium dose in most of the tissues did not produce any oxidative stress in both genders.

Compared to control, as demonstrated in Fig. 4.12 (A, a) a considerable elevation in the brain ($p < 0.05$; $p < 0.002$) and heart ($p < 0.004$; $p < 0.001$) ROS levels was observed following treatment with 300 and 1000 mg/kg NpNF in male mice, respectively. Whereas, in liver and kidney tissues, the ROS concentration increased significantly ($p < 0.05$) in the high dose group only. Contrary to this, the ROS concentration remained unchanged in the stomach, spleen, testes, and seminal vesicles in treated mice at any dose level. In female mice (Fig. 4.13A), on the other, the ROS content elevated in brain tissue ($p < 0.05$) in both medium and high doses, whereas, in the heart, liver, stomach, and spleen, the ROS levels increased significantly ($p < 0.05$) only in the high dose. In kidneys, ROS levels elevated in all groups (low; $p < 0.05$, medium; $p < 0.044$ & high dose; $p < 0.012$).

Lipid peroxidation (LPO) was estimated using the malondialdehyde (MDA) index, a secondary end product of the polyunsaturated fatty acids oxidation. Presently, a significant increase ($p < 0.05$) was observed in the brain and stomach of medium and high-dose treated mice, while TBARS content in the kidney, spleen, and testes was elevated ($p < 0.001$) in the 1000 mg/kg treatment group only.

Moreover, in the heart, liver, and seminal vesicles, TBARS levels did not change when compared to the control. Furthermore, in female mice, brain tissues showed a significant increase ($p < 0.05$) in TBARS concentration following medium and high dose treatment whereas, a significant elevation ($p < 0.05$) was observed in remaining tissues only in the high dose group following 14-day treatment.

4.14.2 Assessment of Antioxidant Enzymes Activity

The antioxidant status of various tissues in male and female mice following administration of NpNF doses at 30, 300, and 1000 mg/kg is given in Tables 4.5 and 4.6 respectively.

In male mice, the administration of medium and high doses of NpNF resulted in a significant decrease in the brain ($p < 0.001$), spleen ($p < 0.001$), and seminal vesicles ($p < 0.002$) CAT activity. While in the liver and stomach, CAT concentration declined significantly ($p < 0.001$) in the high-dose treated group. CAT activity in the heart, kidneys, and testes remains unchanged compared to the control (Fig. 4.14 A, a).

The SOD content, as illustrated in Fig. 4.14 (B, b) decreased only in high-dose treated brain ($p<0.001$), liver ($p<0.001$), and stomach tissues ($p<0.019$) in male mice. Whereas these levels remained unchanged in the heart, kidney, spleen, testis, and seminal vesicles as compared to the control.

The activity of CAT in female mice treated with various doses of NpNF is shown in Fig. 4.15 A. Only the brain ($p<0.012$), liver ($p<0.01$), and stomach tissues ($p<0.029$) were affected with high dose (1000 mg/kg) of NpNF. These values were, however not affected in the heart, kidney, and spleen compared to the control. The content of another antioxidant enzyme of great significance, SOD, showed only a slight decrease in kidney tissue ($p<0.026$) while the level remained unchanged in all other tissues (Fig. 4.15 B).

Interestingly, the peroxidase enzyme (POD) content in male mice tissues was not affected following treatment with NpNF for 14 days, at any dose (Fig. 4.16 A, a). Likewise, GSH activity was not affected in any tissue except for a slight decrease, which was observed in the brain ($p<0.05$) of the high-dose treated group (4.16 B, b).

In female mice, POD activity was comparable to control in all tissues treated with low, medium, and high doses (Fig. 4.17 A). similarly, GSH levels remained unchanged in all tissues except the heart, where administration of 1000 mg/kg NpNF led to a slight decrease in GSH content (Fig. 4.17 B).

4.15 Histopathological Examination

All main organs (brain, heart, liver, kidney, stomach, spleen, testes, and seminal vesicles) were found to be normal on gross necropsy. While most microscopic observations in low and medium-dose-treated Balb/c mice were within the range of predicted pathology and appeared with equal severity and frequency in both treated and control animals.

In the brain, the H&E-stained sections (Fig. 4.18) of the mouse hippocampus from the control group demonstrated the regular architecture of the CA1 region (A). Mice treated with low dose NpNF showed similar histological architecture which was comparable to control mice (B). The medium and high dosage groups revealed pathologic abnormalities in the mouse hippocampal region. Pyramidal cells with vacuolated cytoplasm were seen in the majority of pyramidal neurons while vesicular nuclei with

distended chromatin and large nucleoli were observed in a few pyramidal cells (C, D). Likewise, microscopic examination of brain sections obtained from control female mice showed normal morphology of neurons in the hippocampal CA1 region (Fig. 4.19 A). The low-dose group exhibited evidence of moderate cytoplasmic swelling (B). In comparison to control mice, medium and high dosages showed moderate hippocampal damage. Cellular atrophy, shrinkage, and intensely pigmented and black nuclei with vacuolated cells were the most noticeable abnormalities (C, D).

Histopathology of the control heart showed normal myocardium, consisting of cross-striated fiber cells. Intercalated discs were visible between cardiac cells (Fig. 4.20 A). The low-dose and medium-dose treated mice showed similar histological features as shown by the control cardiac tissue, with no indication of adverse effects of NpNF on cardiomyocytes (Fig. 4.20 B, C). Whereas, in the high-dose treatment group, cardiac muscles showed a mild increase in cytoplasmic vacuolization, with no indication of myocardial degeneration (4.20 D).

Heart sections from the control mice groups (female) showed regular myocardium architecture (Fig. 4.21 A). Sections from low-dose-treated mice exhibited histological architecture similar to control (B). In medium dose-treated mice, however, mild to moderate scattered myocytic destruction was found (C), The myofibrils of mice in the high dose treatment group were found disorganized, with a considerable loss of striations and vascular dilatation (D).

Representative photomicrographs of liver tissues from control mice (A), treated with low dose (30 mg/kg) NpNF (B), treated with medium dose (300 mg/ kg) NpNF (C), and treated with high dose (1000 mg/kg) of NpNF (D) are shown in Fig. 4.22. Control sections from male mice showed the normal architecture of liver tissue. The liver of male mice treated with the low and medium dose of NpNF showed no or negligible changes in tissue architecture. Compared to control and other groups, significant histopathological changes were, however, observed in the only high-dose treated group. These changes included moderate cytoplasmic degeneration, Kupffer cells activation, and mild sinusoidal dilation with no indication of cellular necrosis observed. Normal liver cells with well-defined cellular structures were seen in control female liver sections (Fig. 4.23 A). Treatment with the low and medium doses of NpNF did not affect the normal histological architecture of liver tissue compared to the control (B,

C). The high-dose group liver, on the other hand, revealed mononuclear cell infiltration, hepatic cell necrosis, and central vein congestion (D).

Detailed histopathology of the kidney tissue of male and female mice is presented in Fig. 4.24 and Fig. 4.25 respectively. Control (Fig. 4.24 A) showed normal histology of the mouse kidney with glomeruli and the Bowman's capsule are lined by visceral and parietal cells in renal corpuscles. Mice treated with low and medium doses of NpNF showed no pathological alterations in renal tissue and the kidney's histological structure appeared normal (B, C). In contrast, mice treated with high dose-NpNF revealed minimal alterations in renal tissues represented by a mild degeneration of renal tubules only. Whereas glomeruli appeared normal with no indication of any adverse effect of NpNF dose (D).

In female mice, kidney sections from the control group showed normal tissue architecture (Fig. 4.25 A). In the kidney, exposure to the low dose treatment did not cause any adverse effects (B). Medium dose treated groups, however, showed mild atrophy of some glomerular tufts, showing large Bowman's space and sloughing of few tubular epithelial cells (C). Tubular degeneration, dilatation, glomerular shrinkage and degeneration, and capillary congestion were all observed in mice given a high dosage of NpNF (D).

Histology of the stomach, after H & E staining (Fig. 4.26), showed a normal intact gastric mucosa in control tissue (A). Stomach tissue from low-dose NpNF-treated mice demonstrated a normal gastric mucosa with negligible alteration in the mucosal lining (B). Stomach treated with medium-dose-NpNF showed moderate exfoliation of the cells in the mucosal layer compared to control, mainly at the level of foveolar and parietal cells that are ulcerated (C). Similar observations were found in the high-dose treated-NpNF. Moderate injuries to the gastric mucosa were noticed with no pronounced edema, inflammatory cell infiltration in the submucosal layer, or necrosis (C, D).

In control (Fig. 4.27 A) mice (female), the mucous secreting cells of the gastric pits and the gastric glands showed normal histology. Likewise, treatment with the low and medium doses of NpNF showed an intact gastric mucosa similar to that of control animals (B, C) with the continuous epithelial surface. Whereas the surface epithelial

cells were disrupted and became more reddish with moderate mucosal ulceration and dilated inter glandular spaces in the high-dose treatment (D).

Figure 4.28 shows the histopathological sections of the spleen tissue in male mice. A clear distinction between the red and white pulp, resting follicles, and marginal zones was evident in the spleen of control mice (A). In the low-dose group, the spleen showed normal histology with distinct red and white pulp areas (B). Male mice administered with medium and high doses of NpNF showed pathological lesions and deviation in splenic tissues compared to control mice. Medium dose induced a lower degree of lymphoid depletion with the presence of fewer numbers of megakaryocytes in splenic tissue (C) while treatment with high dose NpNF for 14 days led to lymphoid depletion indicated by the presence of a large number of megakaryocytes and hemosiderin phagocytic cells in splenic tissue (D). Histological examinations of the spleen sectioned from control, low and medium dose-NpNF treated female mice were found normal with no abnormality (Fig. 4.29 A, B, and C). In the high dose group, a mild fusion of red and white pulp is, however, observed with the disappearance of the marginal zone between red and white pulp resulting in the disorganization of splenic tissue (D).

The photomicrographs of testicular sections are shown in Fig. 4.30. The spermatogenic cells and Sertoli cells in the seminiferous tubules of the control, low and medium-dose NpNF treated mice were found to be structurally normal indicating the safety of NpNF doses (A, B, C). On the other hand, minor necrosis in certain seminiferous tubules and slight edema in interstitial tissue was seen after 14 days of high dosage exposure (D).

Finally, the photomicrograph representing control and treated seminal vesicles presented in Fig. 4.31, indicated that all groups including control (A), low dose (B), medium dose (C), and high dose (D) possessed the normal histological architecture typical of mice seminal vesicle. The walls of seminal vesicles in all groups were composed of well-defined smooth muscle and tall columnar epithelium with characteristic branching. Higher magnification showed tall columnar epithelium with secretory granules and normal basal nuclei.
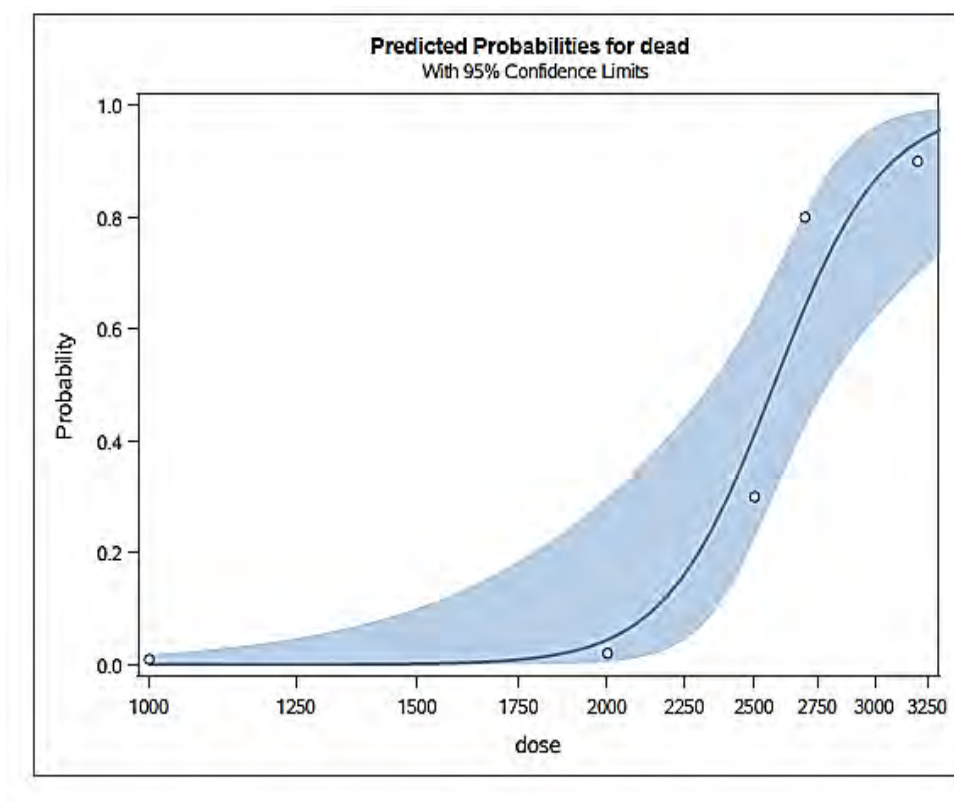
Fig. 4.2 Probit analysis graph/dose-response curve showing LD_{50} of naproxen nanoformulation (NpNF) in mice. Dose units mg/kg of mice.
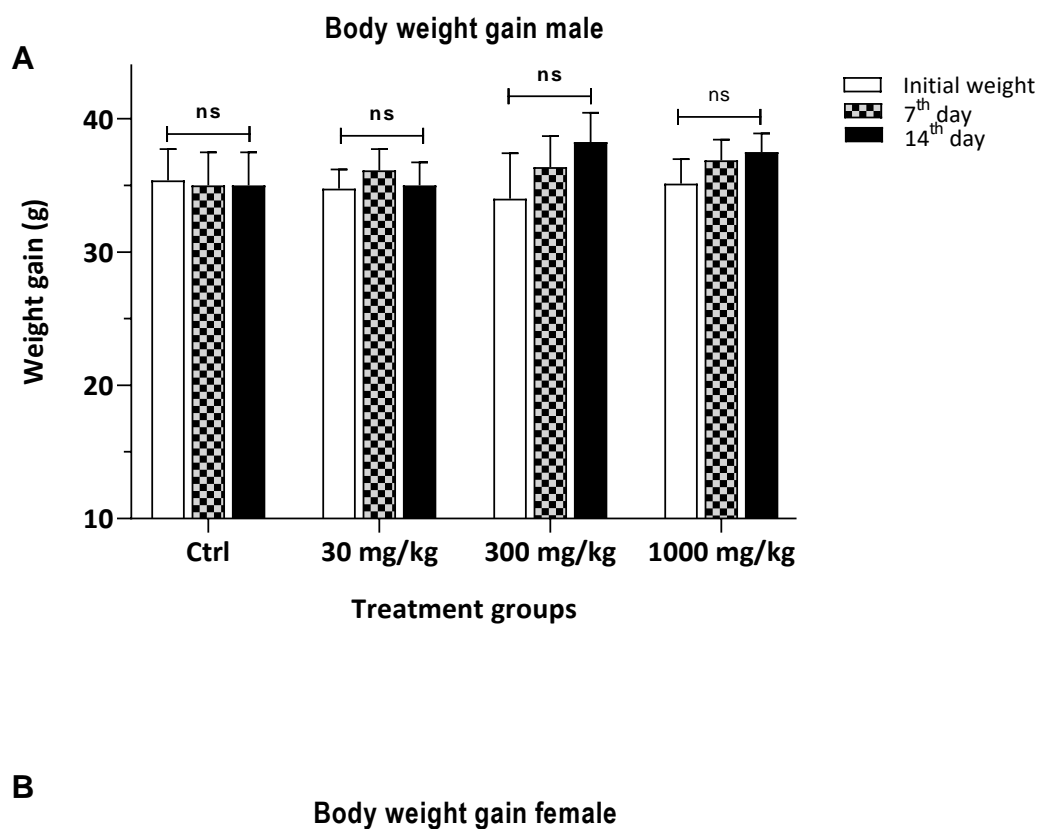
Fig. 4.3 Body weight changes of male and female mice treated with the increasing doses of NpNF during a 14-day repeat dose toxicity study. Values are expressed as mean ± s.e. (n = 6). ns= non-significant, compared with the control group.

A

B

C
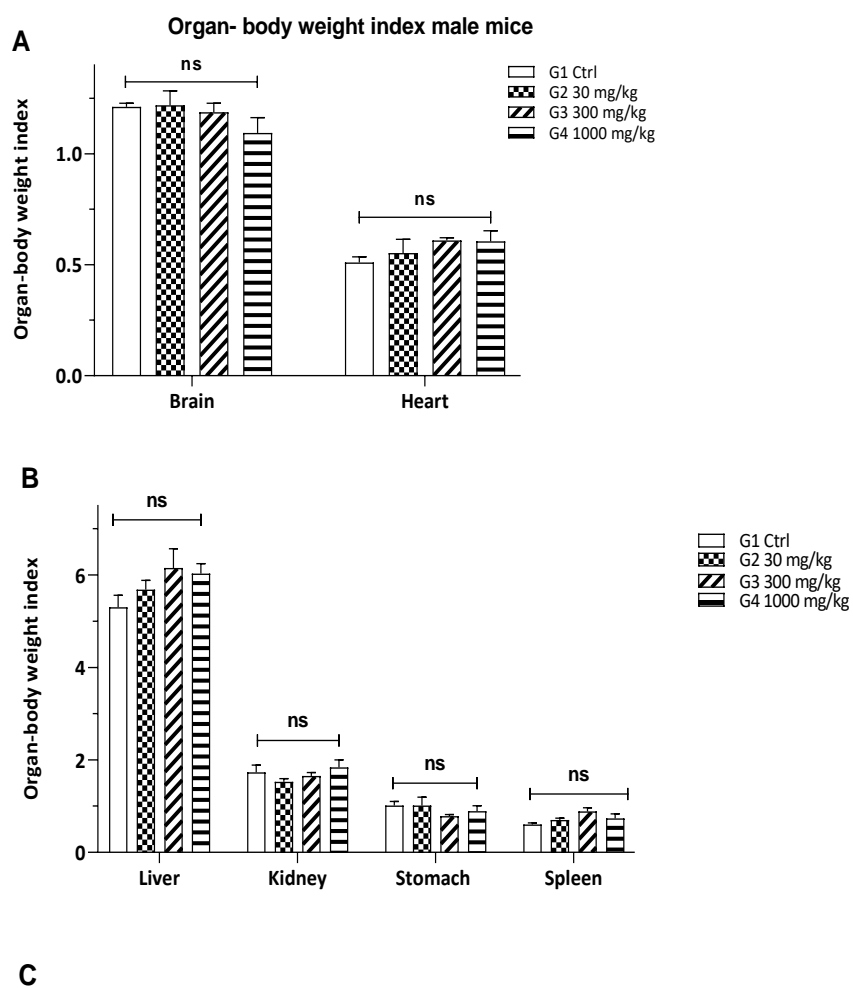
Fig. 4.4 Absolute and relative organ weights of male mice treated orally with the ascending doses of NpNF. Values are expressed as mean ± s.e. (n = 6). ns= non-significant, compared with the control group.

A

B
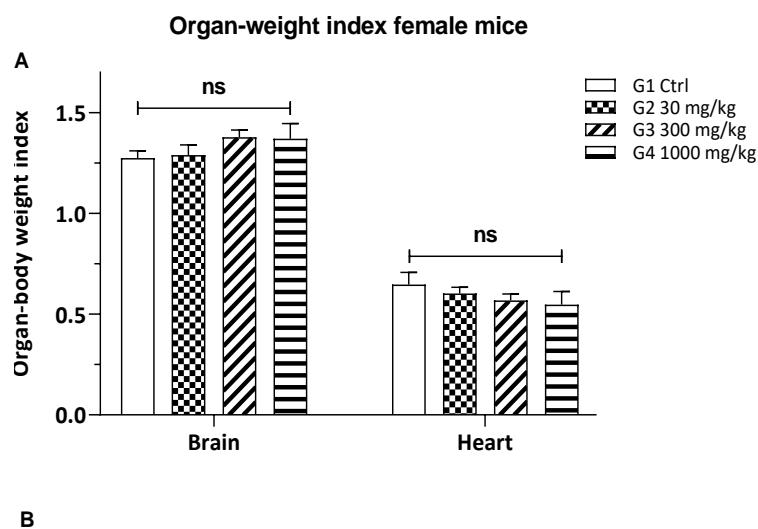
Fig. 4.5 Absolute and relative organ weights of female mice treated orally with the ascending doses of NpNF. Values are expressed as mean ± s.e. (n = 6). ns= non-significant, compared with the control group.
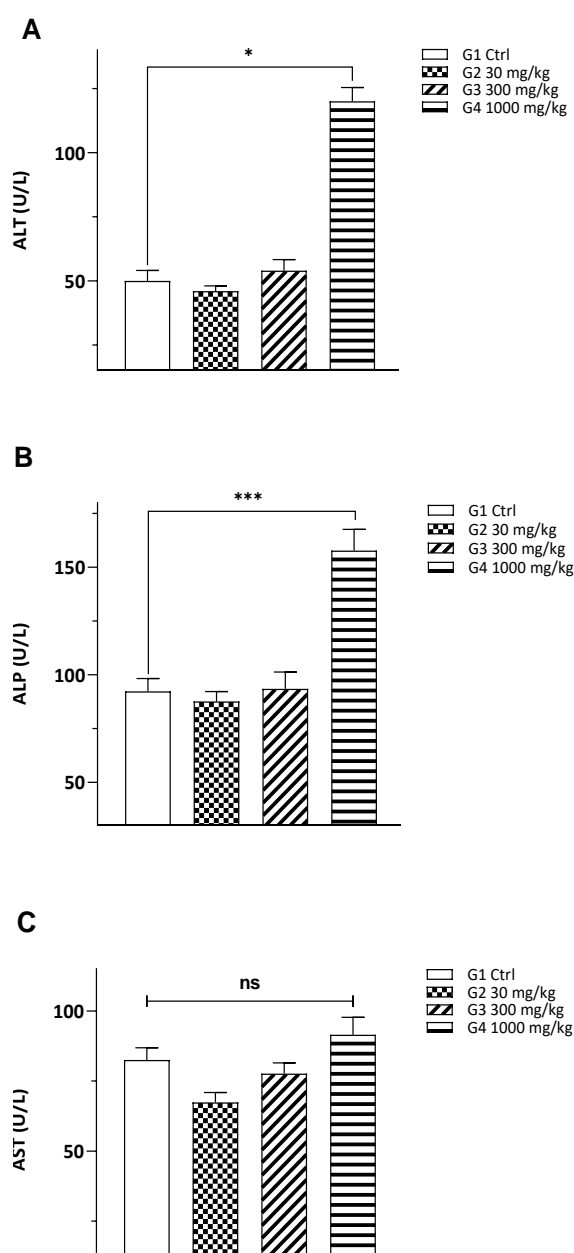
Fig. 4.6 Effects of NpNF doses on the serum ALT, ALP and AST levels in male mice (A) Serum ALT levels, (B) Serum ALP levels, (C) Serum AST levels. All values are expressed as mean ± s.e. (n = 6). *$p<0.05$, **$p<0.01$, ***$p<0.001$, ns=non-significant, compared with the control group; ALT, alanine aminotransferase; ALP, alanine phosphate; AST, aspartate aminotransferase.
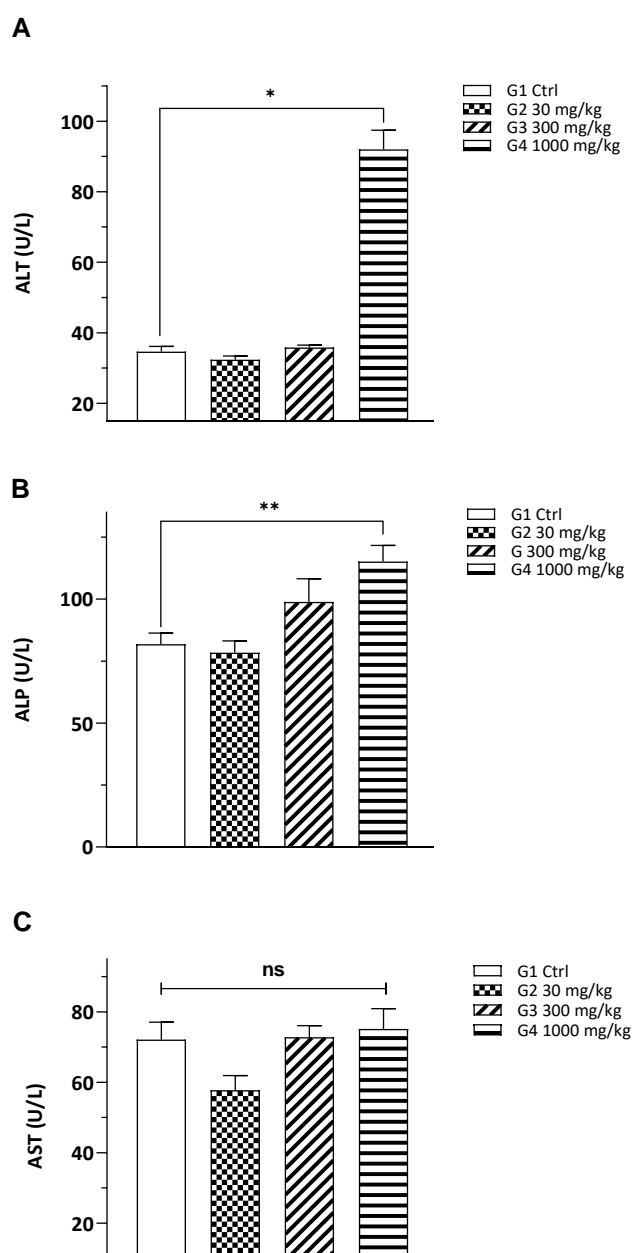
Fig. 4.7 Effects of NpNF doses on the serum ALT, ALP and AST levels in female mice (A) Serum ALT levels, (B) serum ALP levels, (C) Serum AST levels. All values are expressed as mean ± s.e. (n = 6). *$p < 0.05$, **$p < 0.01$, ***$p < 0.001$, ns= non-significant, compared with the control group; ALT, alanine aminotransferase; ALP, alanine phosphate; AST, aspartate aminotransferase.

A

B
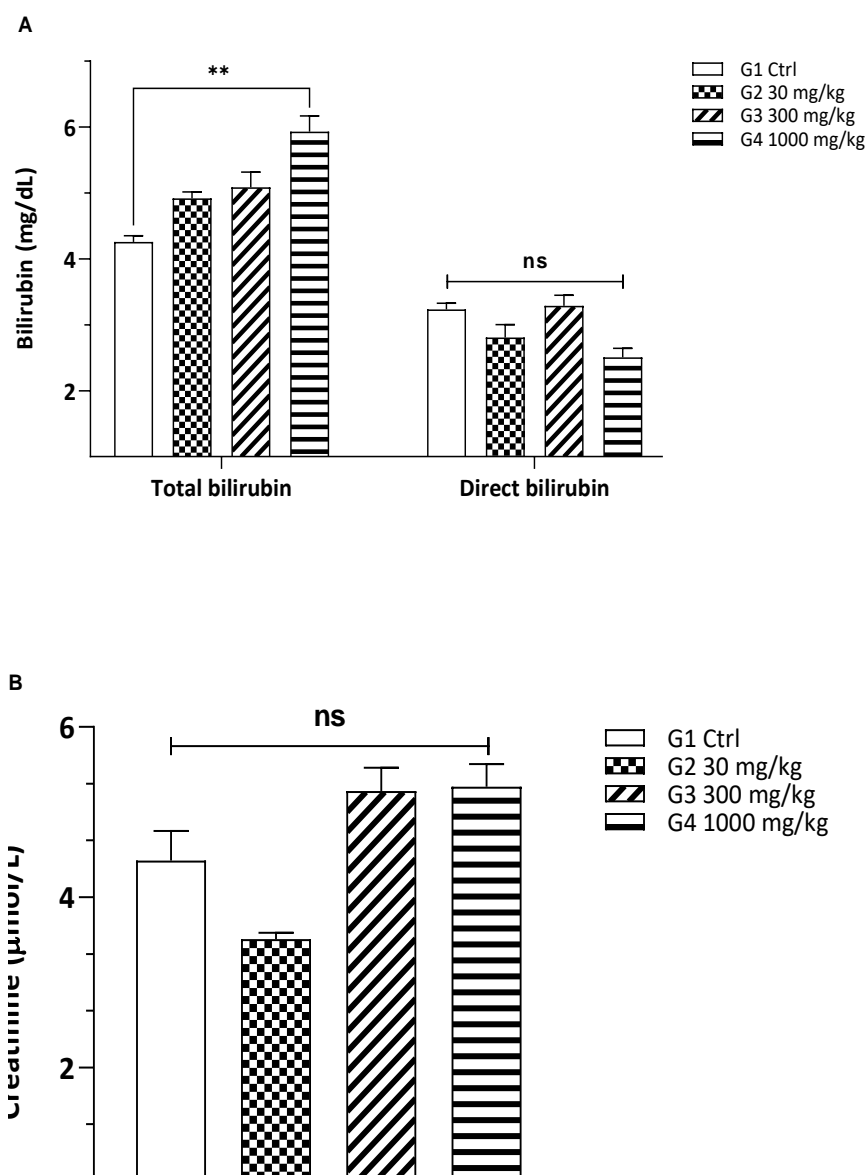
Fig. 4.8 Effects of NpNF doses on the serum bilirubin and creatinine levels in male mice (A) Serum bilirubin (total and direct) levels, (B) Serum creatinine levels. All values are expressed as mean ± s.e. (n = 6). *p<0.05, **p<0.01, ***p<0.001, ns= non-significant, compared with the control group.
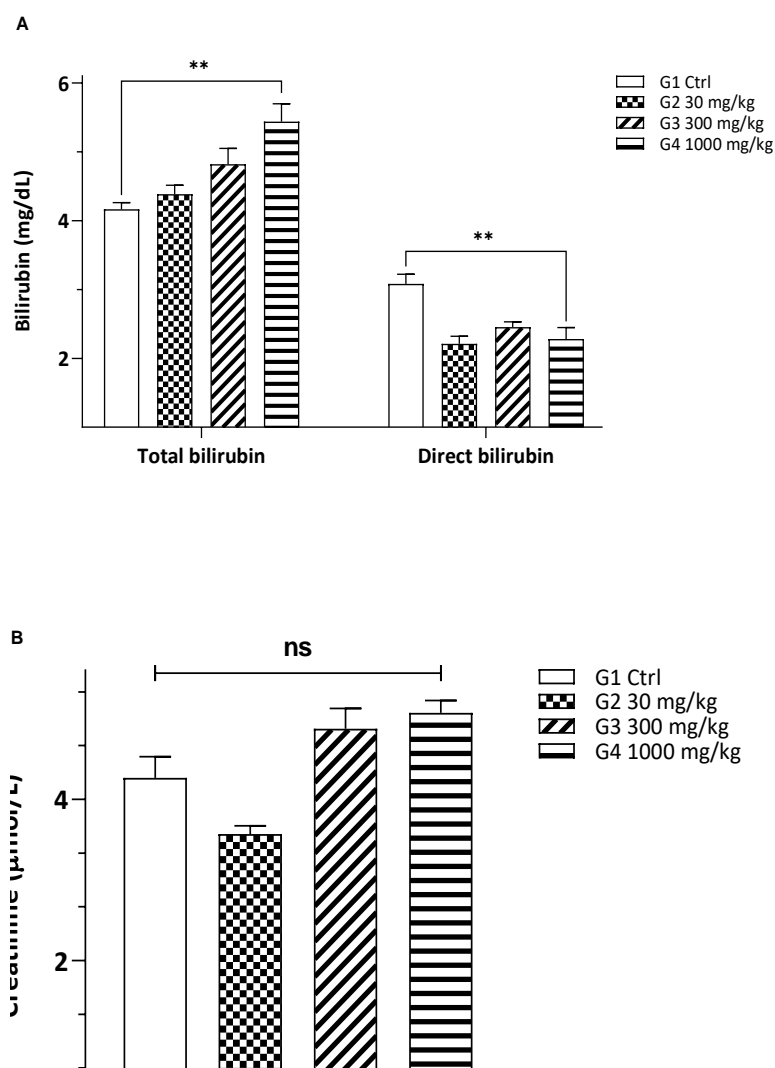
Fig. 4.9 Effects of NpNF doses on the serum bilirubin and creatinine levels in female mice (A) Serum bilirubin (total and direct) levels, (B) Serum creatinine levels. All values are expressed as mean $\pm$ s.e. (n = 6). *$p<0.05$, **$p<0.01$, ***$p<0.001$, ns= non-significant, compared with the control group.
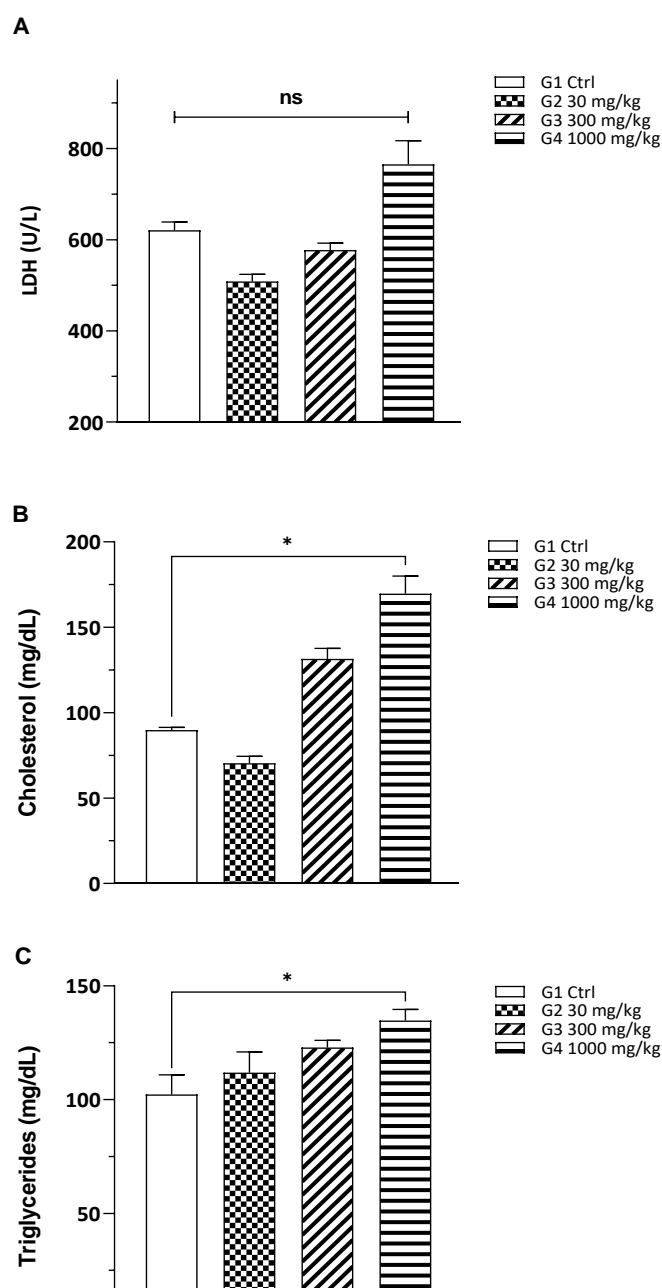
Fig. 4.10 Effects of NpNF doses on the serum LDH, cholesterol and triglycerides

levels in male mice (A) Serum LDH levels, (B) Serum cholesterol levels, (C)

serum triglycerides levels. All values are expressed as mean ± s.e. (n = 6).

*p<0.05, **p<0.01, ***p<0.001, ns= non-significant, compared with the

control group; LDH, lactate dehydrogenase.
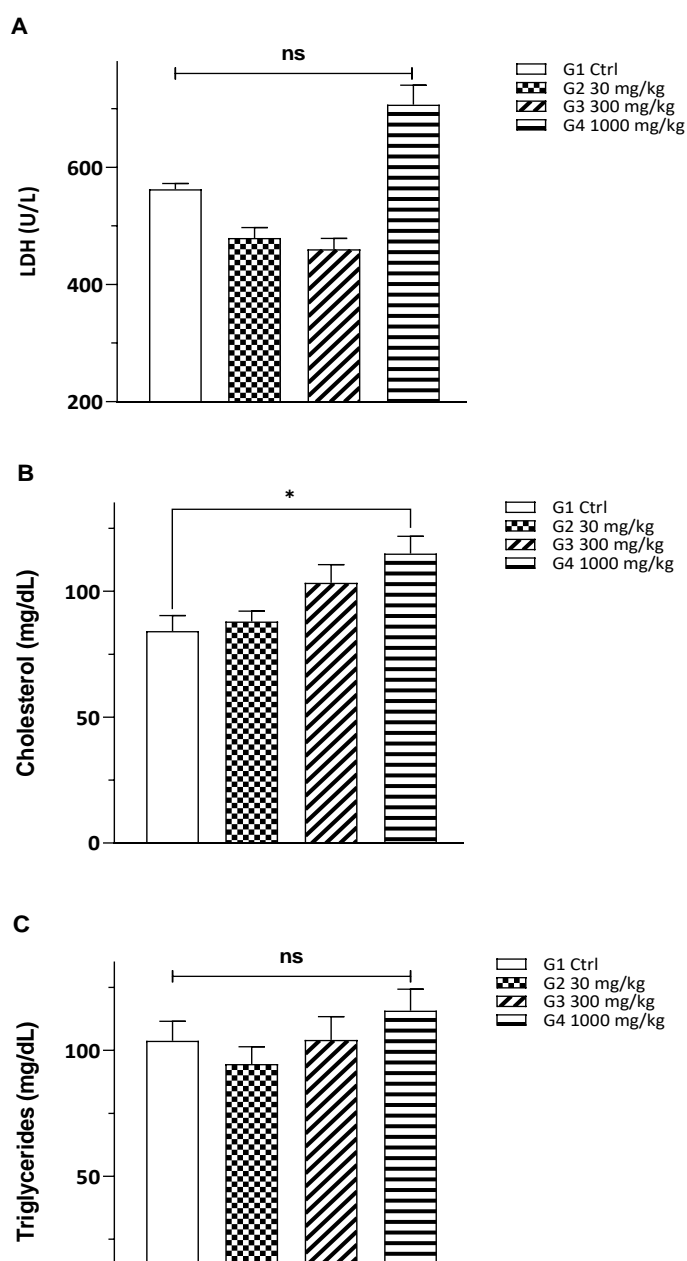
Fig. 4.11 Effects of NpNF doses on the serum LDH, cholesterol and triglycerides levels in female mice (A) Serum LDH levels, (B) Serum cholesterol levels, (C) Serum triglycerides levels. All values are expressed as mean ± s.e. (n = 6). *$p<0.05$, **$p<0.01$, ***$p<0.001$, ns= non-significant, compared with the control group; LDH, lactate dehydrogenase.
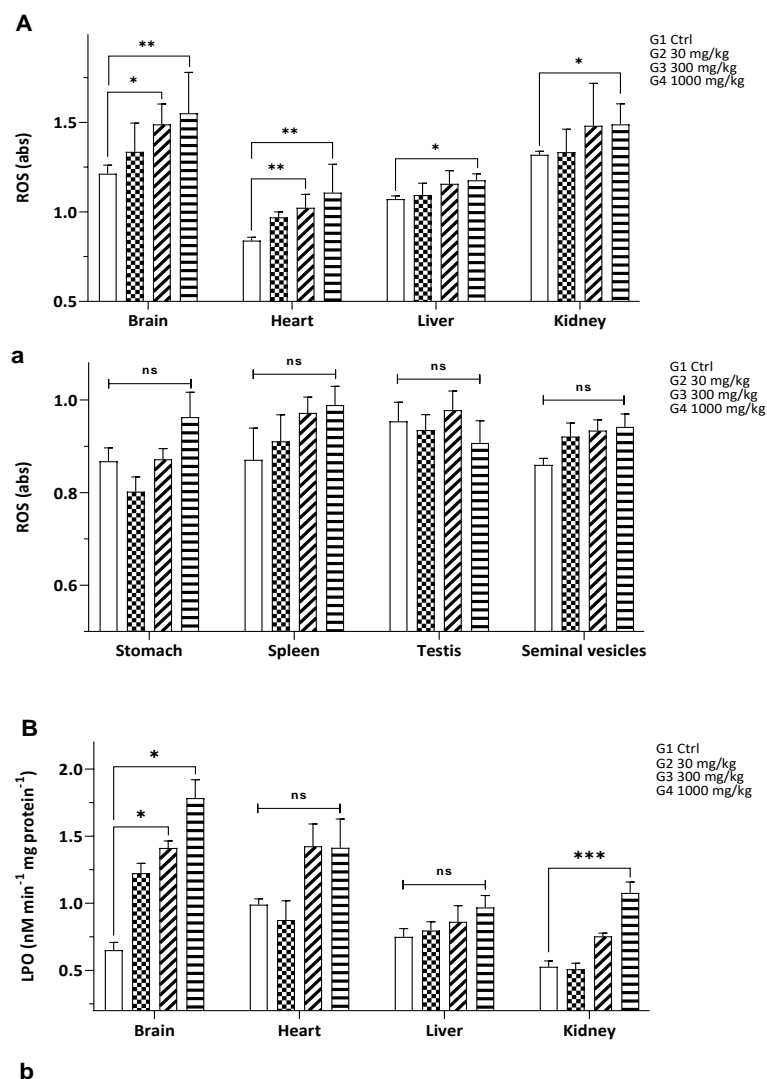
Fig. 4.12 Effects of NpNF doses on ROS (A, a) and LPO (B, b) levels in male mice tissues. All values are expressed as mean ± s.e. (n= 6). *p<0.05, **p<0.01, ***p<0.001, ns= non-significant, compared with the control group; ROS, reactive oxygen species; LPO, lipid peroxidase.
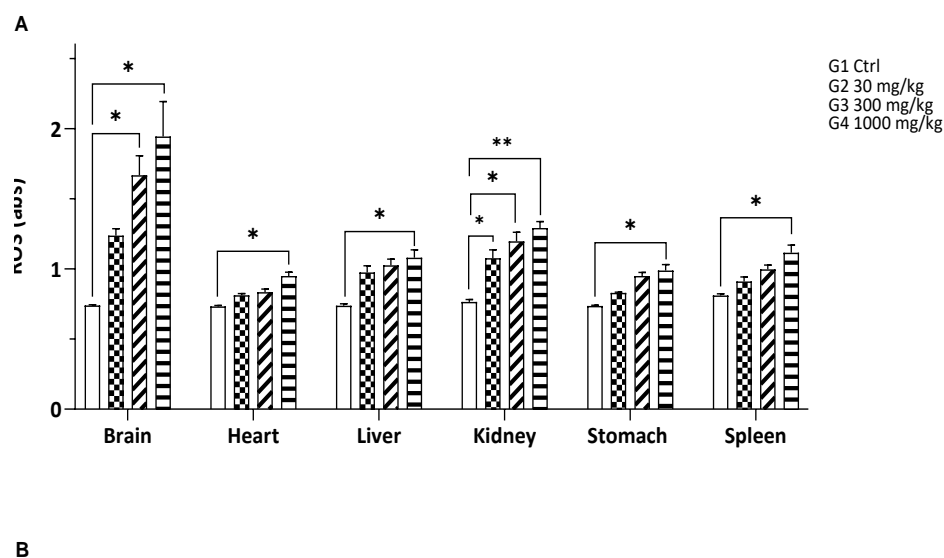
Fig. 4.13 Effects of NpNF doses on ROS (A) and LPO (B) levels in female mice tissues. All values are expressed as mean ± s.e. (n= 6). *p<0.05, **p<0.01, ***p<0.001, ns= non-significant, compared with the control group; ROS, reactive oxygen species; LPO, lipid peroxidase.
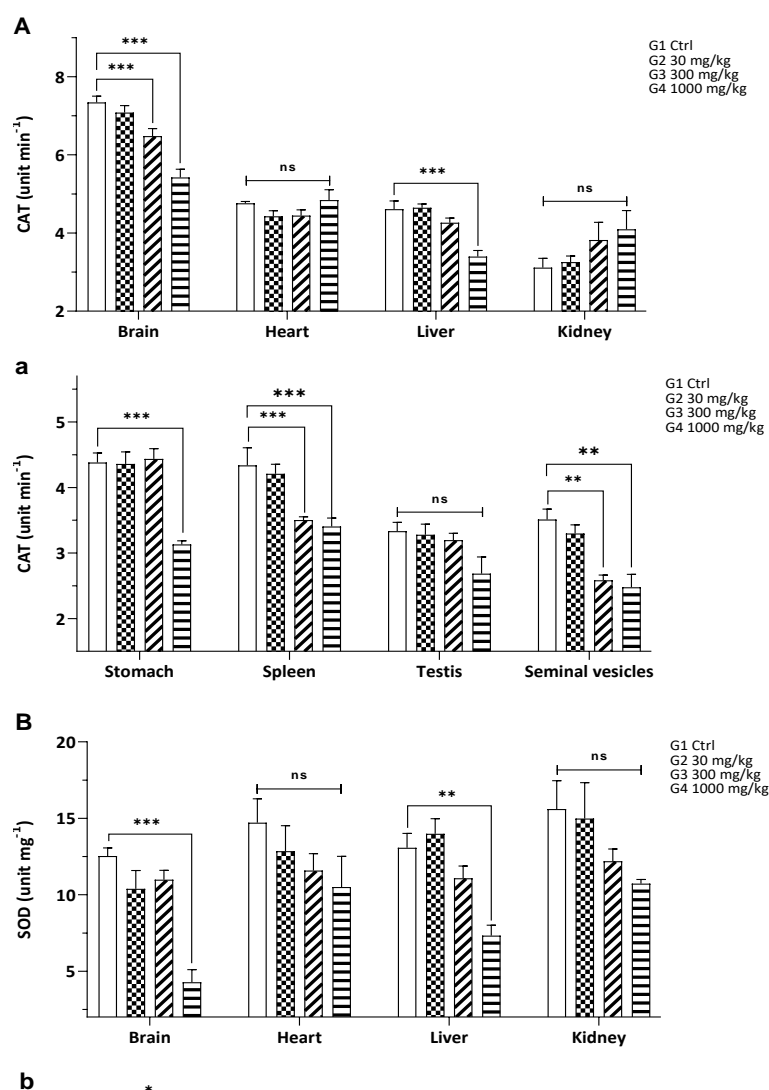
Fig. 4.14 Effects of NpNF doses on CAT (A, a) and SOD (B, b) levels in male mice
tissues. All values are expressed as mean ± s.e. (n= 6). *p<0.05, **p<0.01,
***p<0.001, ns= non-significant, compared with the control group; CAT,
catalase; SOD, superoxidase dismutase.
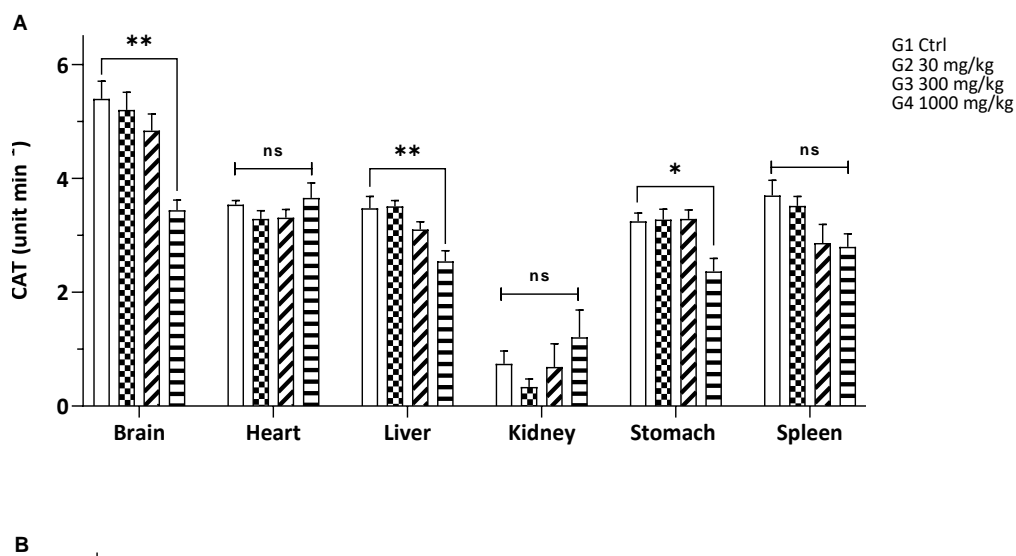
Fig. 4.15 Effects of NpNF doses on CAT (A) and SOD (B) levels in female mice tissues. All values are expressed as mean ± s.e. (n= 6). *p<0.05, **p<0.01, ***p<0.001, ns= non-significant, compared with the control group; CAT, catalase; SOD, superoxidase dismutase.
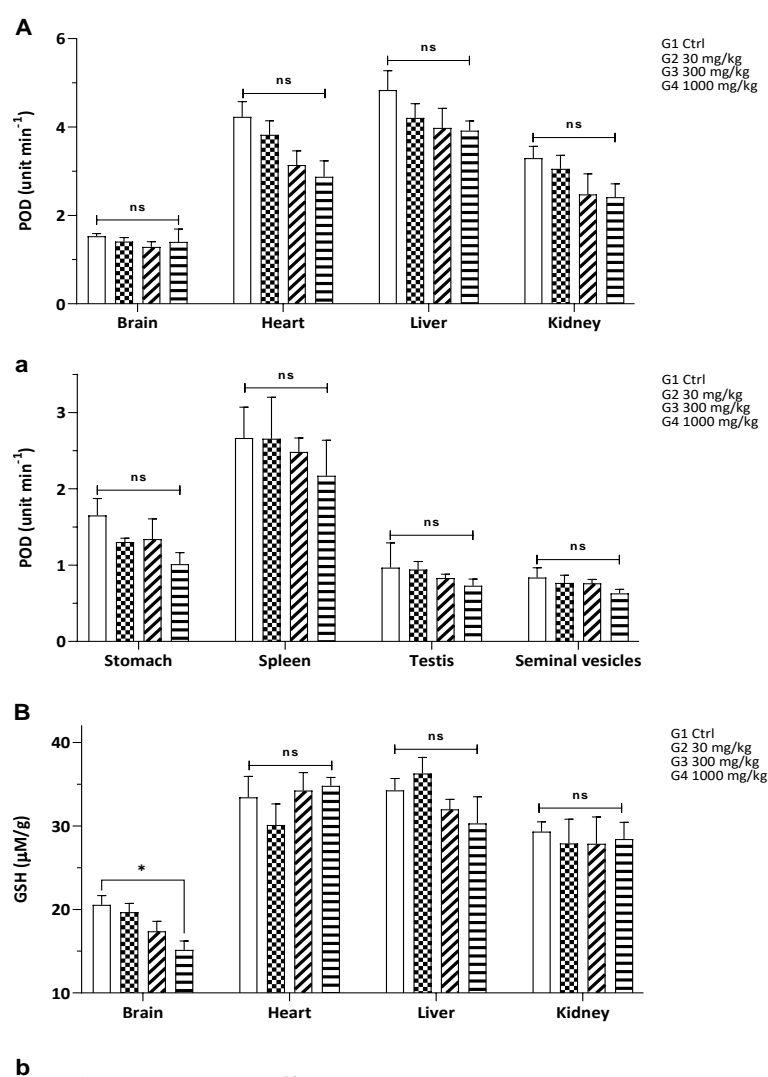
Fig. 4.16 Effects of NpNF doses on POD (A, a) and GSH (B, b) levels in male mice tissues. All values are expressed as mean ± s.e. (n= 6). *p<0.05, **p<0.01, ***p<0.001, ns= non-significant, compared with the control group; POD, peroxidase; GSH, glutathione enzyme.

A

B
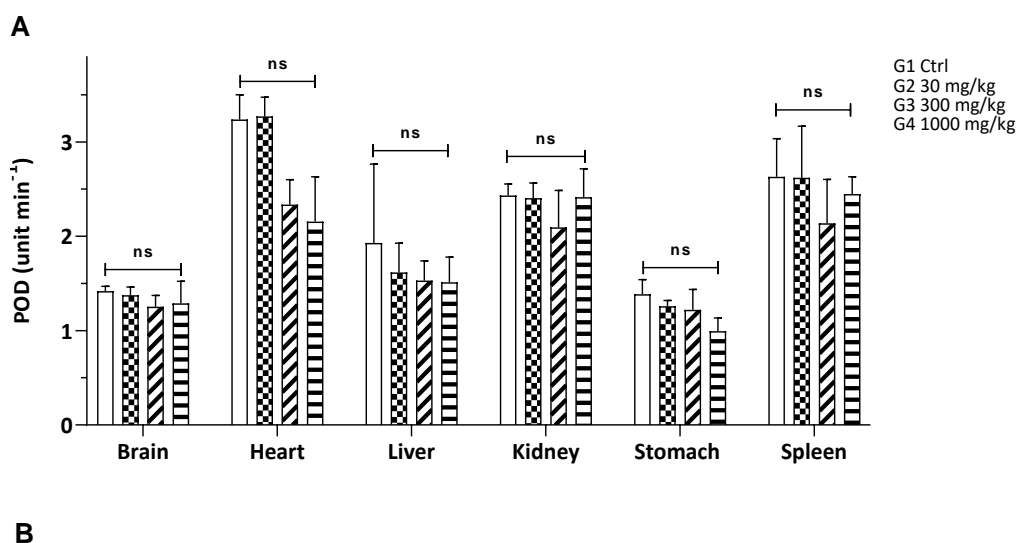
Fig. 4.17 Effects of NpNF doses on POD (A) and GSH (B) levels in female mice tissues. All values are expressed as mean ± s.e. (n= 6). *p<0.05, **p<0.01, ***p<0.001, ns= non-significant, compared with the control group; POD, peroxidase; GSH, glutathione enzyme.
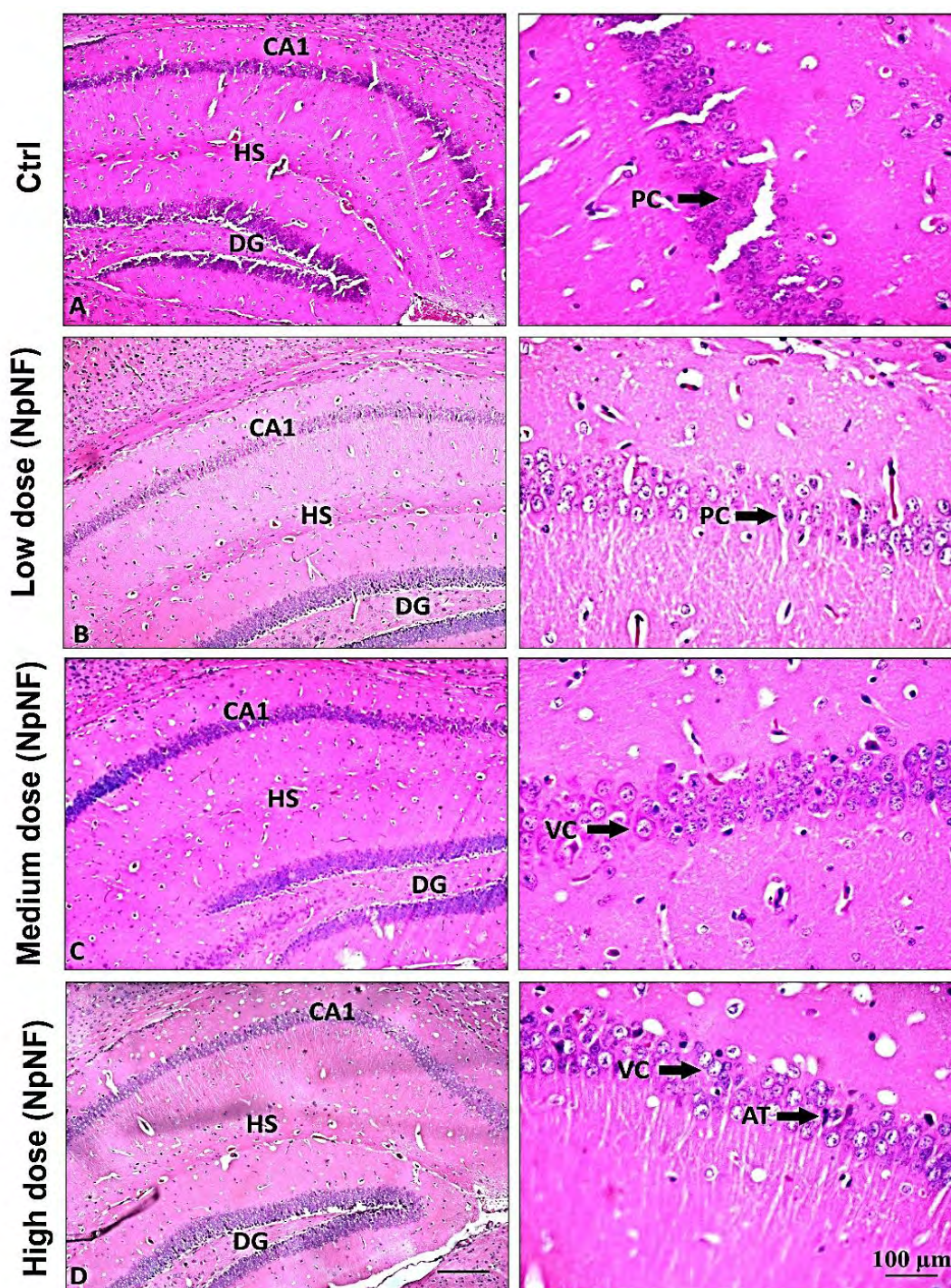
Fig. 4.18 Photomicrographs of control and NpNF treated brain sections of male mice (H&E) and the respective high magnification details of the CA1 subfield area of the hippocampus (A) normal brain, (B) treated with 30 mg/kg NpNF; (C) treated with 300 mg/kg NpNF and, (D) treated with 1000 mg/kg NpNF. HS= Hippocampal sulcus, DG= Dentate gyrus, PC= Pyramidal cell At= Atrophy of pyramidal cells, VC= Vacuolated cytoplasm. Magnification 10x (left column) and 40x (right column); Scale bar = 100 μm.
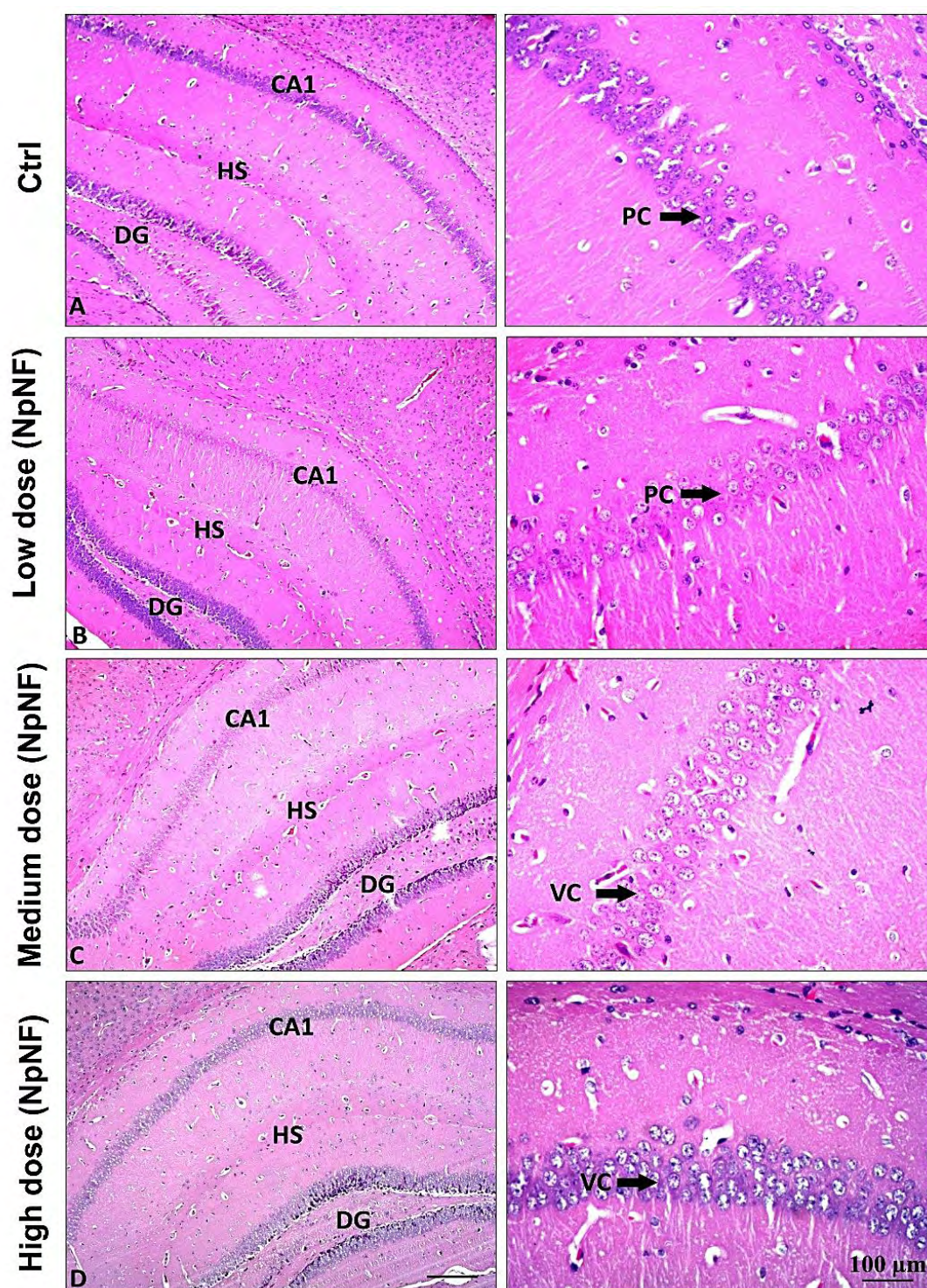
Fig. 4.19 Photomicrographs of control and NpNF treated brain sections of female mice stained with hematoxylin and eosin (H&E) (A) normal brain, (B) treated with 30 mg/kg NpNF; (C) treated with 300 mg/kg NpNF and, (D) treated with 1000 mg/kg NpNF. HS= Hippocampal sulcus, DG= Dentate gyrus, PC= Pyramidal cell VC= Vacuolated cytoplasm. Magnification 10x (left column) and 40x (right column); Scale bar = 100 μm.
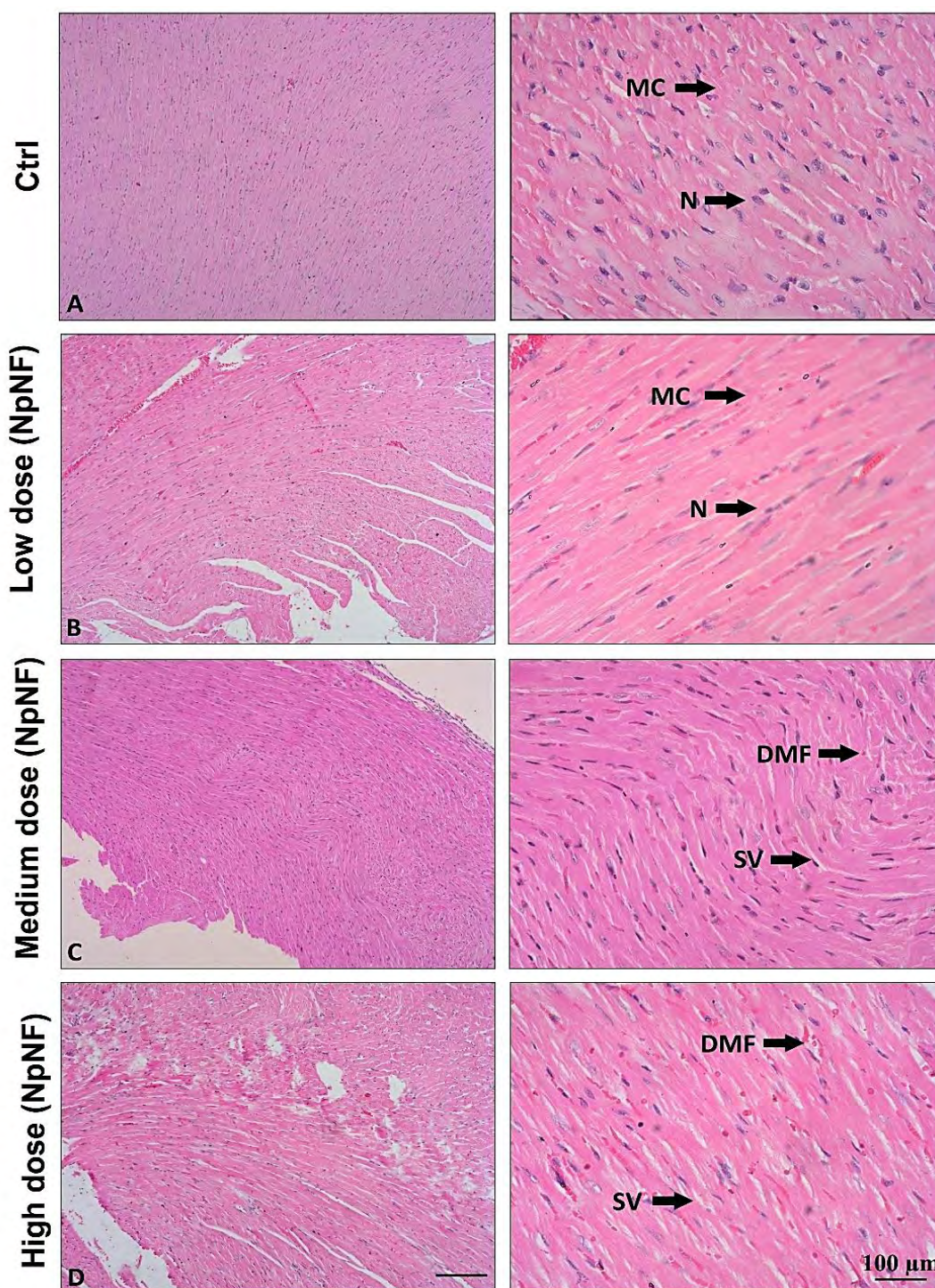
Fig. 4.20 Photomicrographs of control and NpNF treated heart sections of male mice stained with hematoxylin and eosin (H&E) (A) normal heart, (B) treated with 30 mg/kg NpNF; (C) treated with 300 mg/kg NpNF and, (D) treated with 1000 mg/kg NpNF. MC= Myocardial cells, N= Nucleus, SV= Sarcoplasmic vacuolation DMF= Degenerated muscle fibers. Magnification 10x (left column) and 40x (right column); Scale bar = 100 μm.
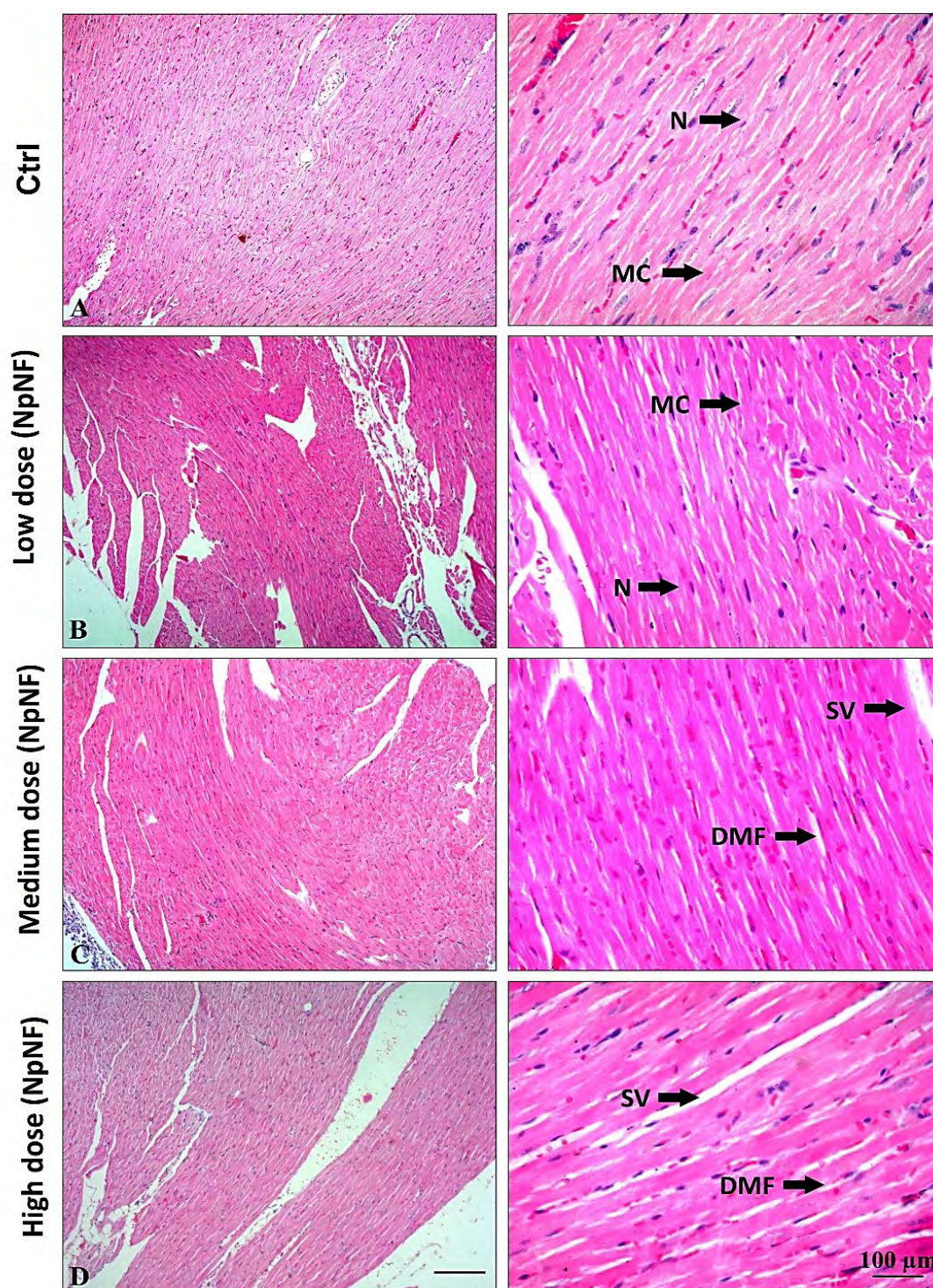
Fig. 4.21 Photomicrographs of control and NpNF treated heart sections of female mice stained with hematoxylin and eosin (H&E) (A) normal heart, (B) treated with 30 mg/kg NpNF; (C) treated with 300 mg/kg NpNF and, (D) treated with 1000 mg/kg NpNF. MC= Myocardial cells, N= Nucleus, SV= Sarcoplasmic vacuolation DMF= Degenerated muscle fibers. Magnification 10x (left column) and 40x (right column); Scale bar = 100 μm.
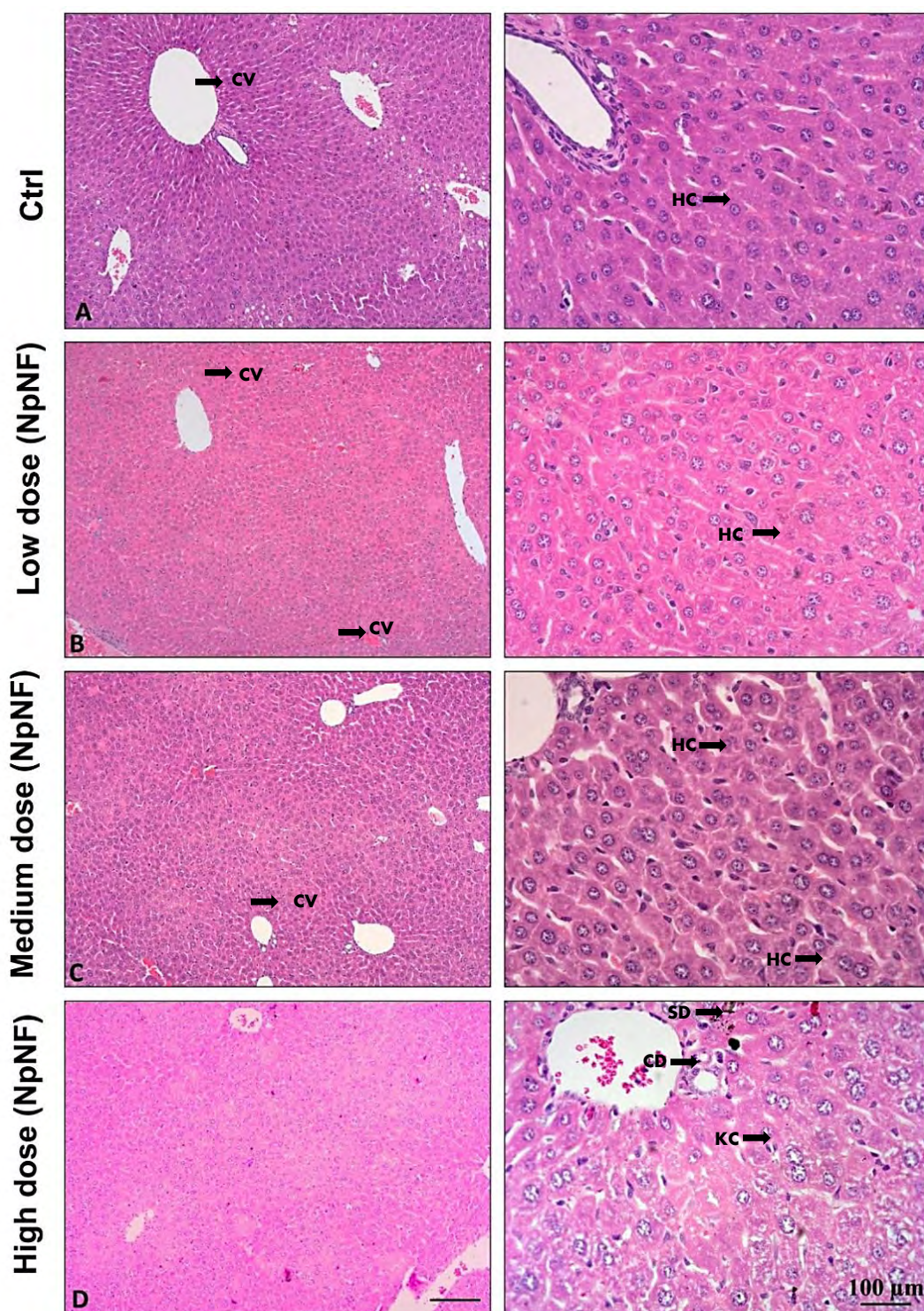
Fig. 4.22 Photomicrographs of control and NpNF treated liver sections of male mice stained with hematoxylin and eosin (H&E) (A) normal liver, (B) treated with 30 mg/kg NpNF; (C) treated with 300 mg/kg NpNF and, (D) treated with 1000 mg/kg NpNF. CV= Central vein, SD= Sinusoidal dilation, KC= Kupffer cell HC= Hepatic cells, CD= Cytoplasmic degeneration. Magnification 10x (left column) and 40x (right column); Scale bar = 100 μm.
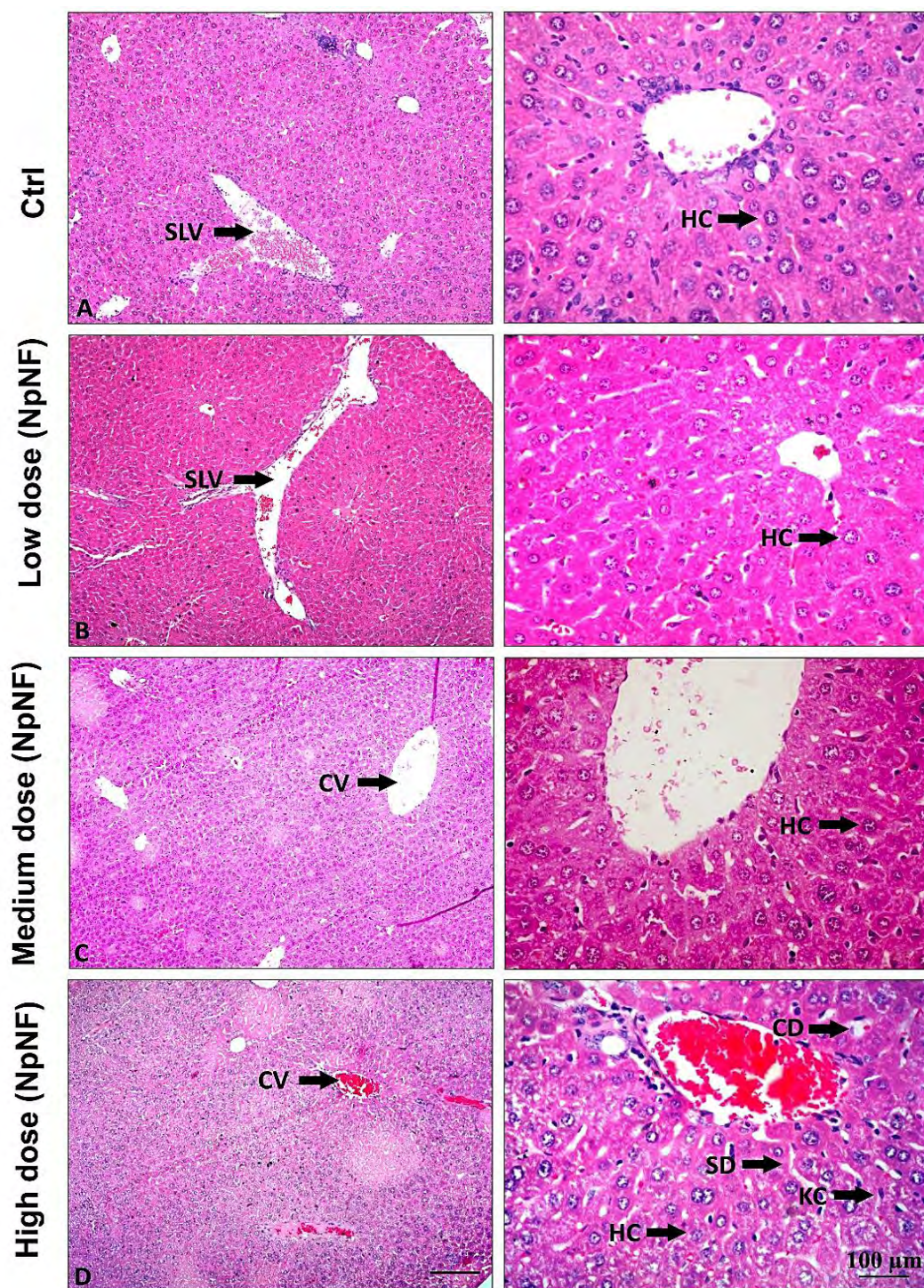
Fig. 4.23 Photomicrographs of control and NpNF treated liver sections of female mice stained with hematoxylin and eosin (H&E) (A) normal liver, (B) treated with 30 mg/kg NpNF (C) treated with 300 mg/kg NpNF and, (D) treated with 1000 mg/kg NpNF. SLV=Sub lobular vein, CV=Central vein, SD= Sinusoidal dilation, KC= Kupffer cell, HC= Hepatic cells, CD= Cytoplasmic degeneration. Magnification 10x (left column) and 40x (right column); Scale bar = 100 μm.
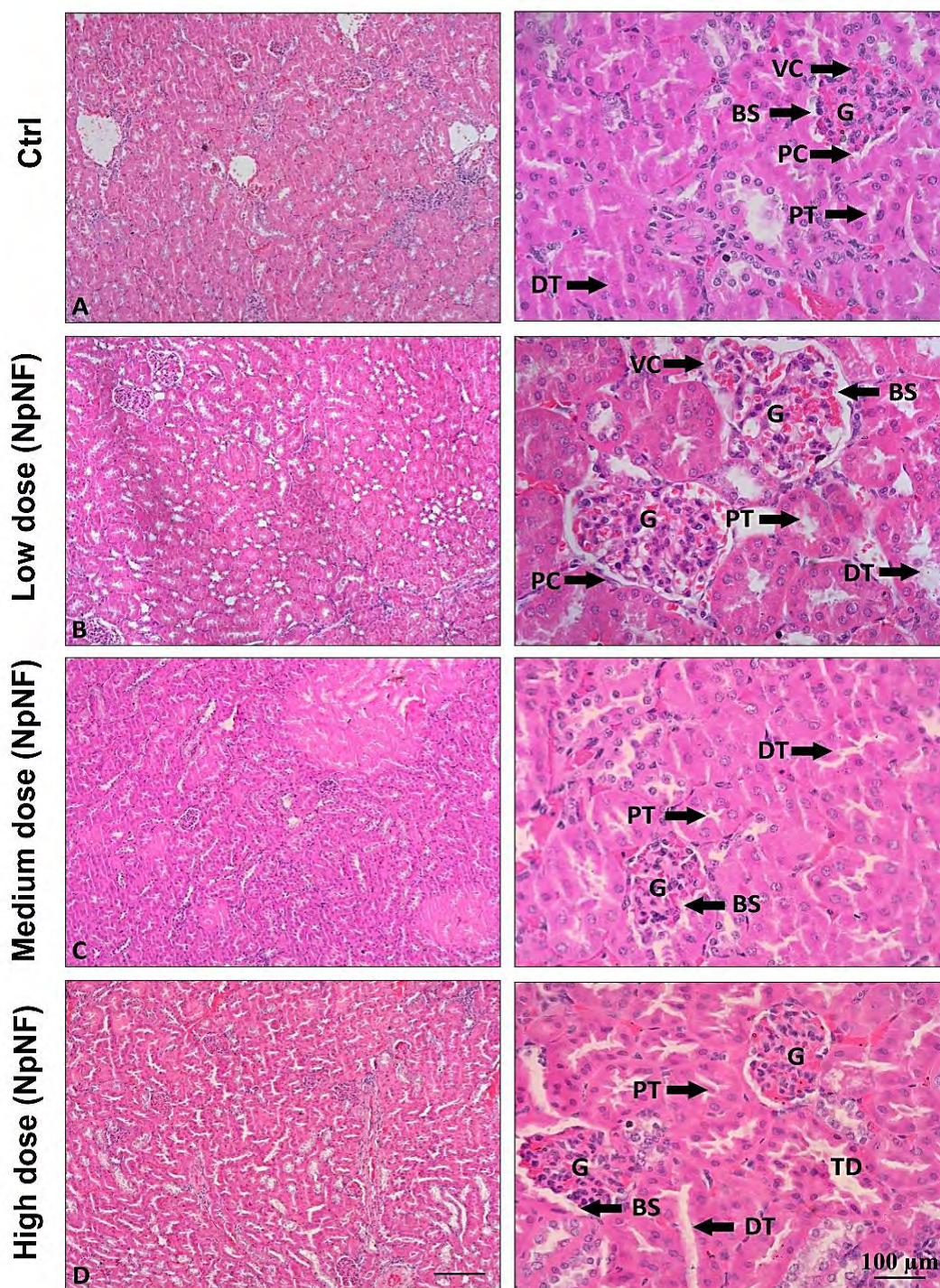
Fig. 4.24 Representative photomicrographs of control and NpNF treated kidney sections of male mice stained with hematoxylin and eosin (H&E) (A) normal kidneys, (B) treated with 30 mg/kg NpNF (C) treated with 300 mg/kg NpNF and, (D) treated with 1000 mg/kg NpNF. G= Glomeruli, BS= Bowman's spaces, PC= Parietal cell, VC= Visceral cells, DT= Distal tubule, PT= Proximal tubule TD= Tubular Dilation. Magnification 10x (left column) and 40x (right column); Scale bar = 100 μm.
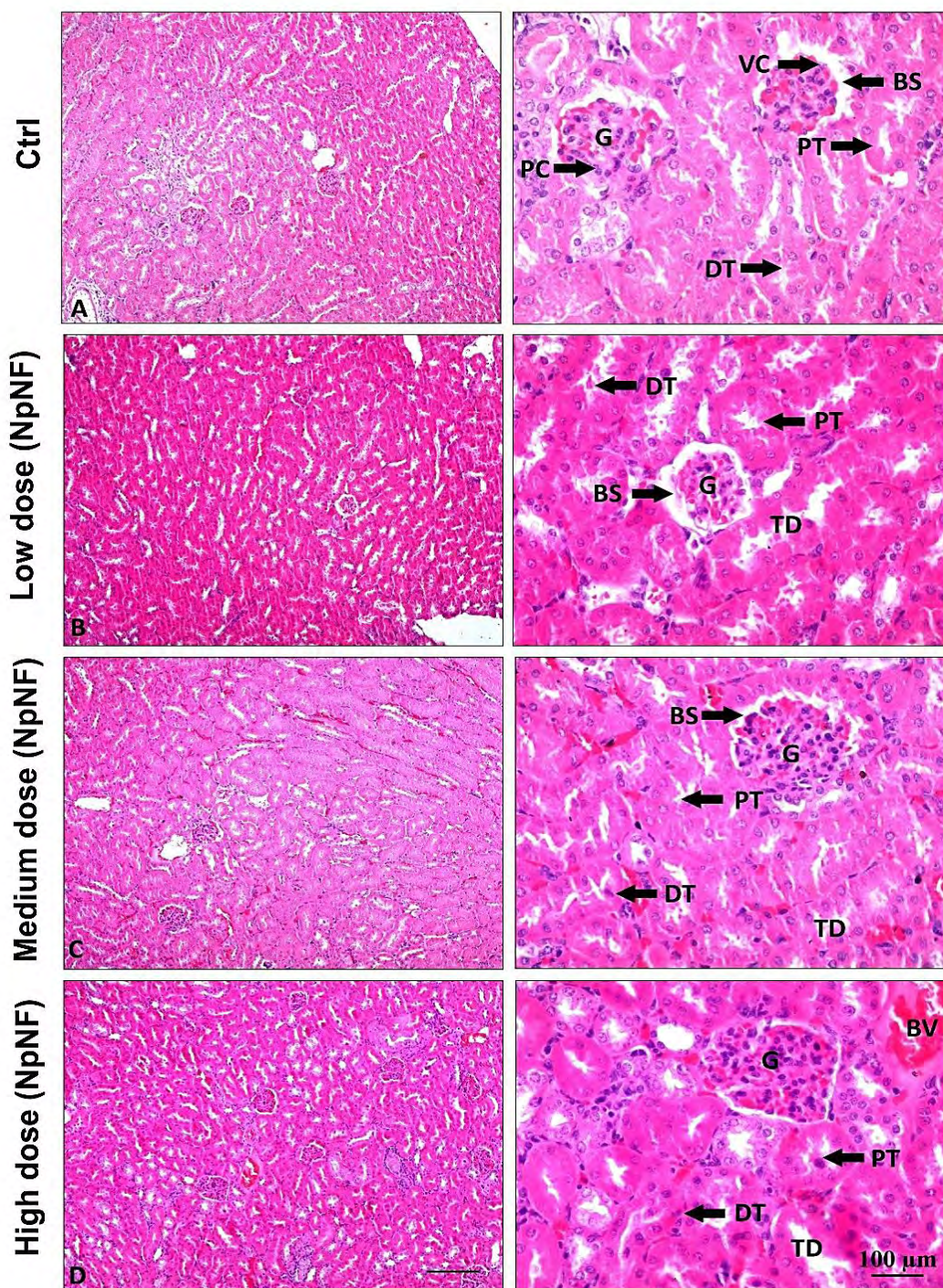
Fig. 4.25 Photomicrographs of control and NpNF treated kidney sections of female mice stained with hematoxylin and eosin (H&E) (A) normal kidney, (B) treated with 30 mg/kg NpNF (C) treated with 300 mg/kg NpNF and, (D) treated with 1000 mg/kg NpNF. G= Glomeruli, BS= Bowman's spaces, PC= Parietal cell, VC= Visceral cells, DT= Distal tubule, PT= Proximal tubule TD= Tubular Dilation, BV= Blood vessel. Magnification 10x (left column) and 40x (right column); Scale bar = 100 μm.
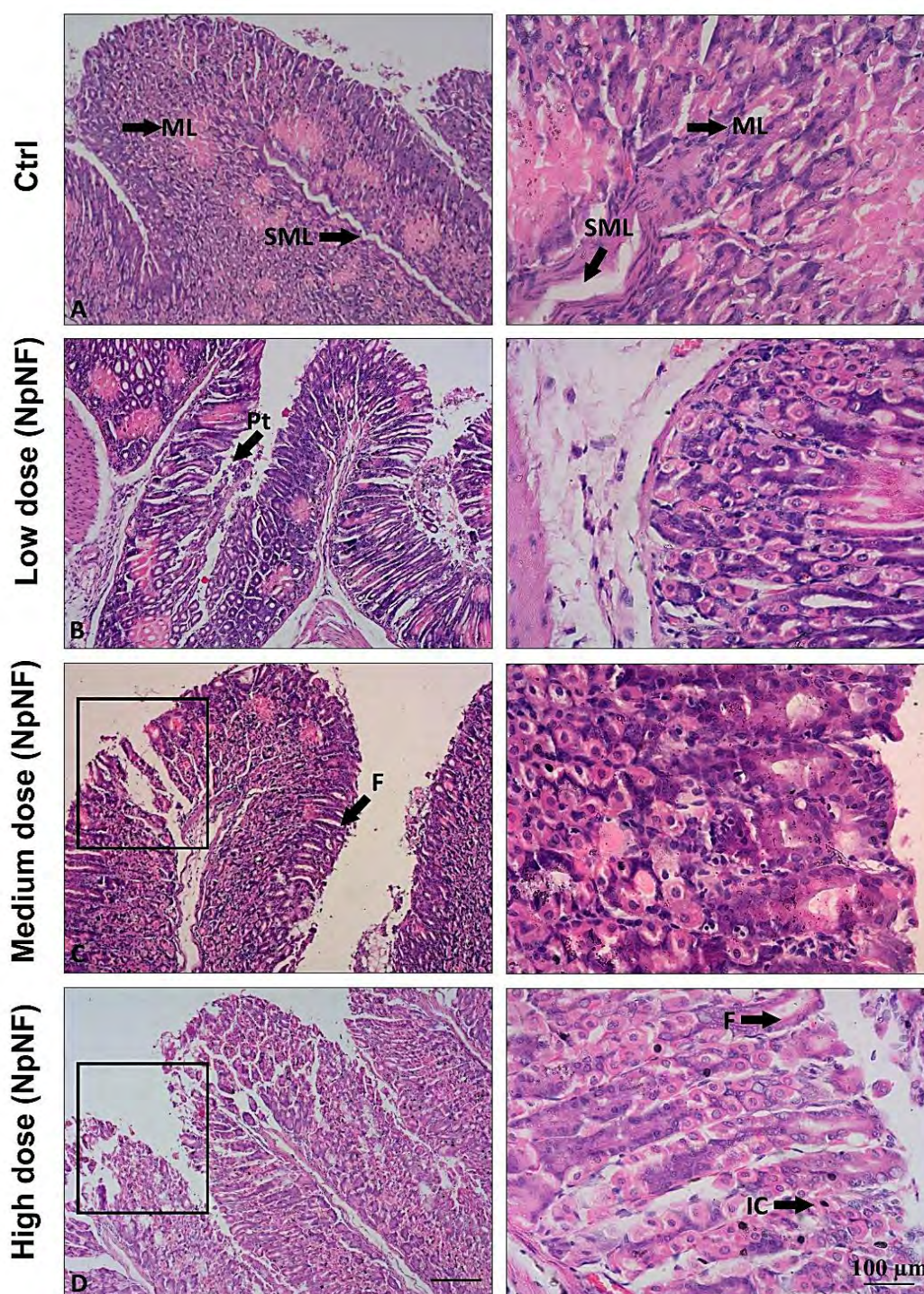
Fig. 4.26 Photomicrographs of control and NpNF treated stomach sections of male mice stained with hematoxylin and eosin (H&E) (A) normal stomach, (B) treated with 30 mg/kg NpNF (C) treated with 300 mg/kg NpNF and, (D) treated with 1000 mg/kg NpNF. ML= Mucosal layer, SML= Sub-mucosal layer, F= Foveolar cells P= Gastric pits, IC= Inflammatory cells, Square shape indicates gastric ulceration. Magnification 10x (left column) and 40x (right column); Scale bar = 100 μm.
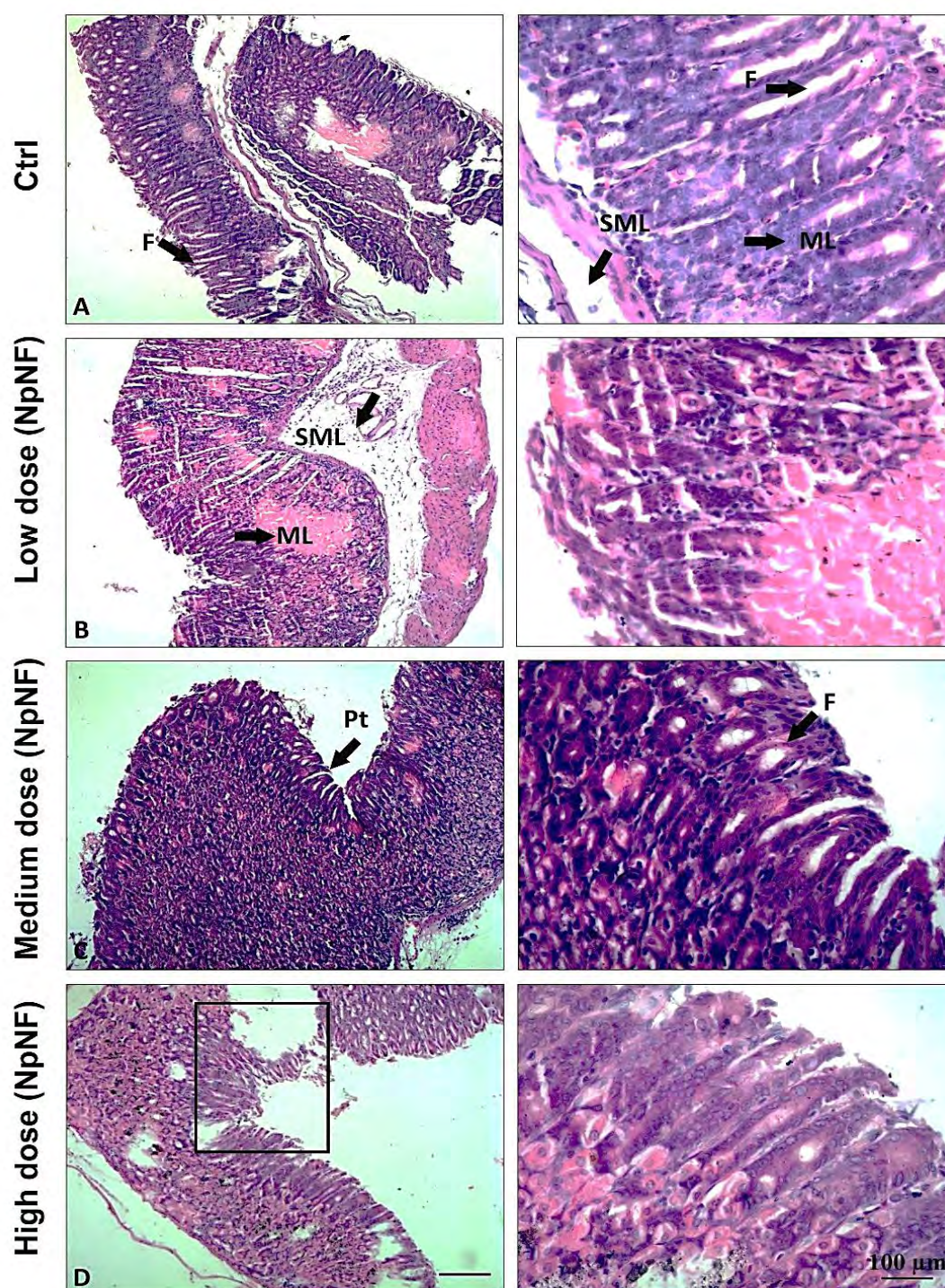
Fig. 4.27 Photomicrographs of control and NpNF treated stomach sections of female mice stained with hematoxylin and eosin (H&E) (A) normal stomach, (B) treated with 30 mg/kg NpNF (C) treated with 300 mg/kg NpNF and, (D) treated with 1000 mg/kg NpNF. ML= Mucosal layer, SML= Sub-mucosal layer, F= Foveolar cells, P= Gastric pits, IC= Inflammatory cells, Square shape indicates gastric ulceration. Magnification 10x (left column) and 40x (right column); Scale bar = 100 μm.
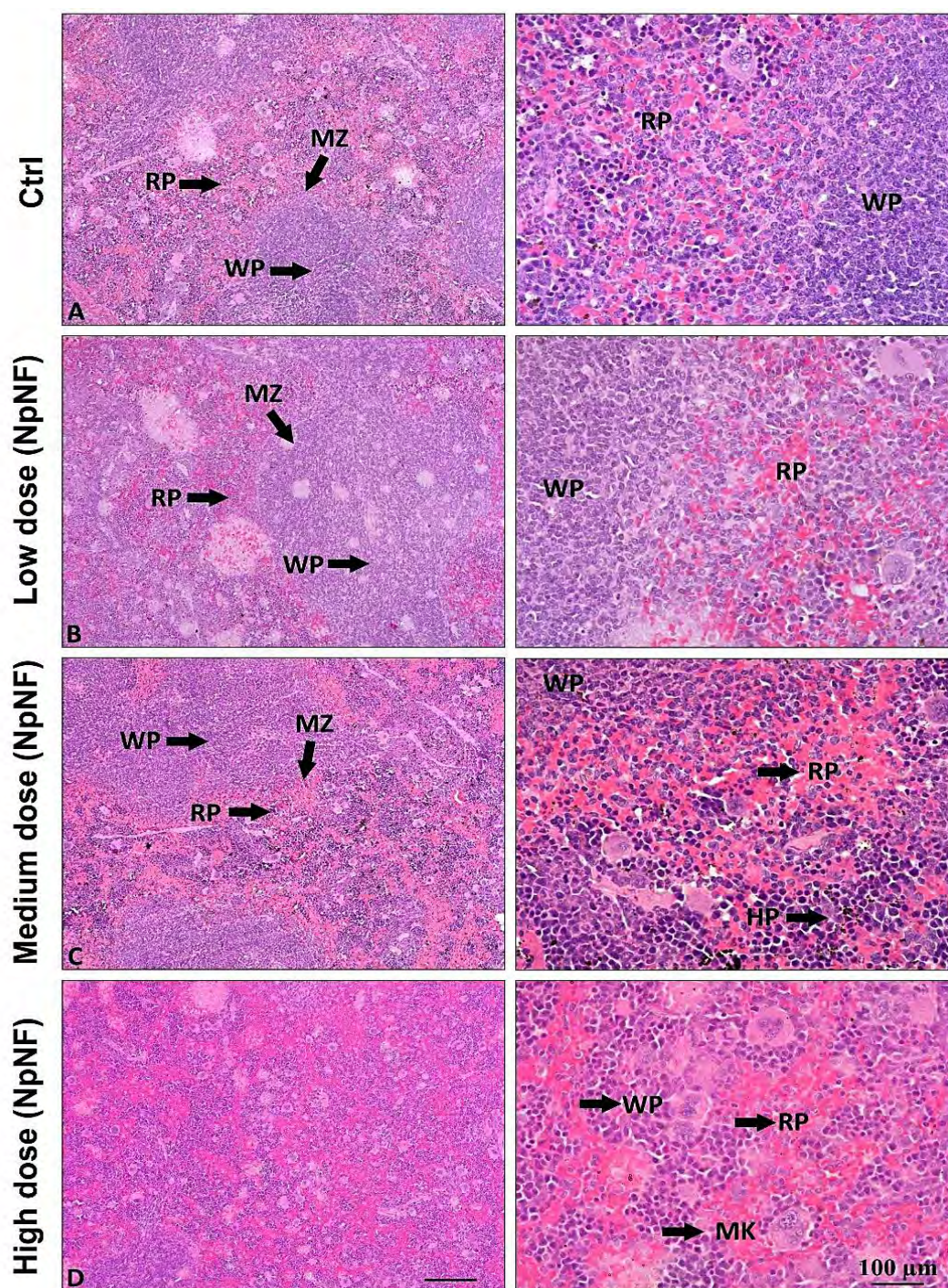
Fig. 4.28 Photomicrographs of control and NpNF treated spleen of male mice stained with hematoxylin and eosin (H&E) (A) normal spleen, (B) treated with 30 mg/kg NpNF (C) treated with 300 mg/kg NpNF and, (D) treated with 1000 mg/kg NpNF. RP= Red pulp, WP= White pulp, MZ= Marginal zone, Hp= Hematopoiesis, MK= Megakaryocyte. Magnification 10x (left column) and 40x (right column); Scale bar = 100 µm.
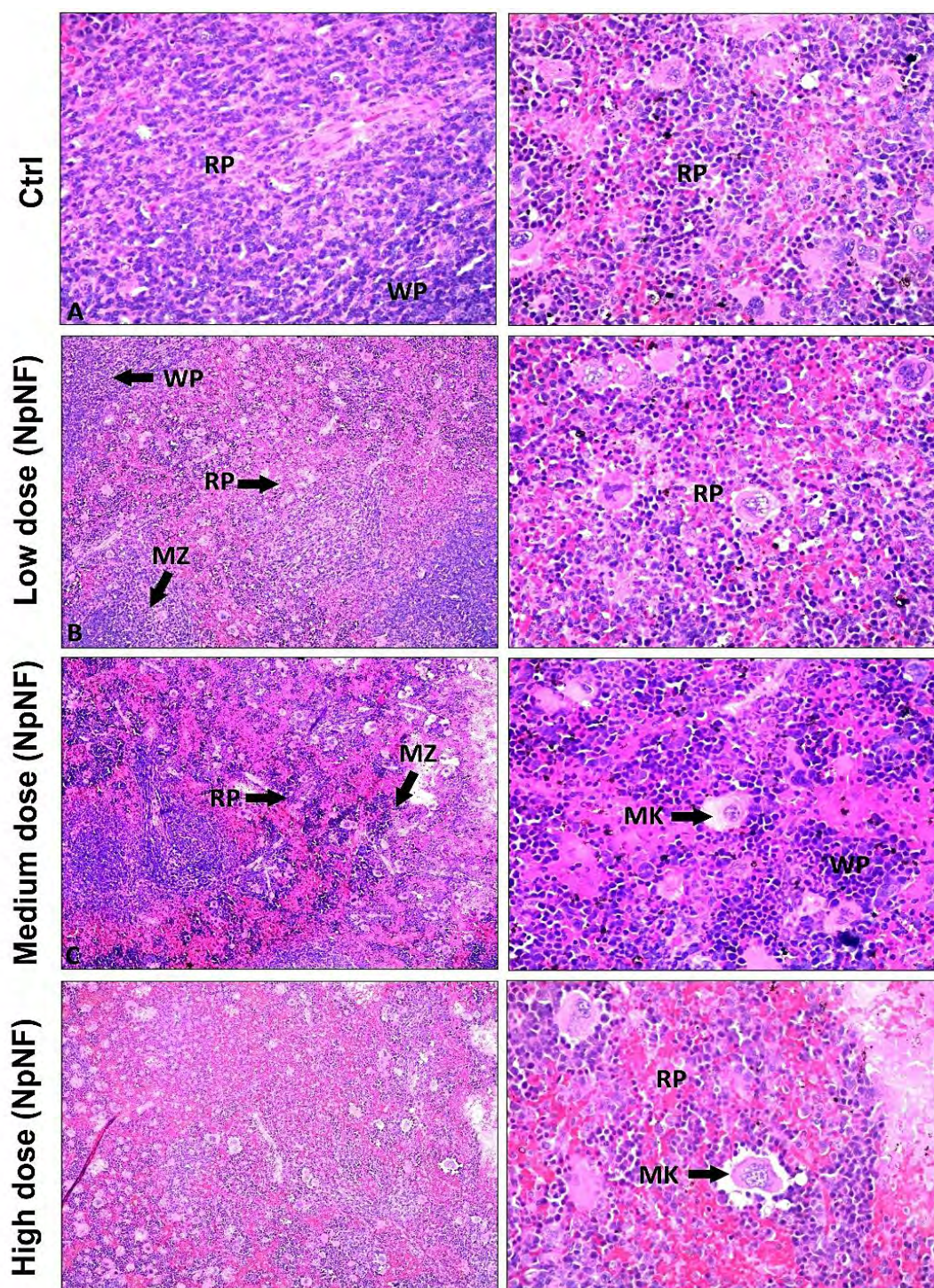
Fig. 4.29 Photomicrographs of control and NpNF treated spleen sections of female mice stained with hematoxylin and eosin (H&E) (A) normal spleen, (B) treated with 30 mg/kg NpNF (C) treated with 300 mg/kg NpNF and, (D) treated with 1000 mg/kg NpNF. RP= Red pulp, WP= White pulp, MZ= Marginal zone, MK= Megakaryocyte. Magnification 10x (left column) and 40x (right column); Scale bar = 100 μm.
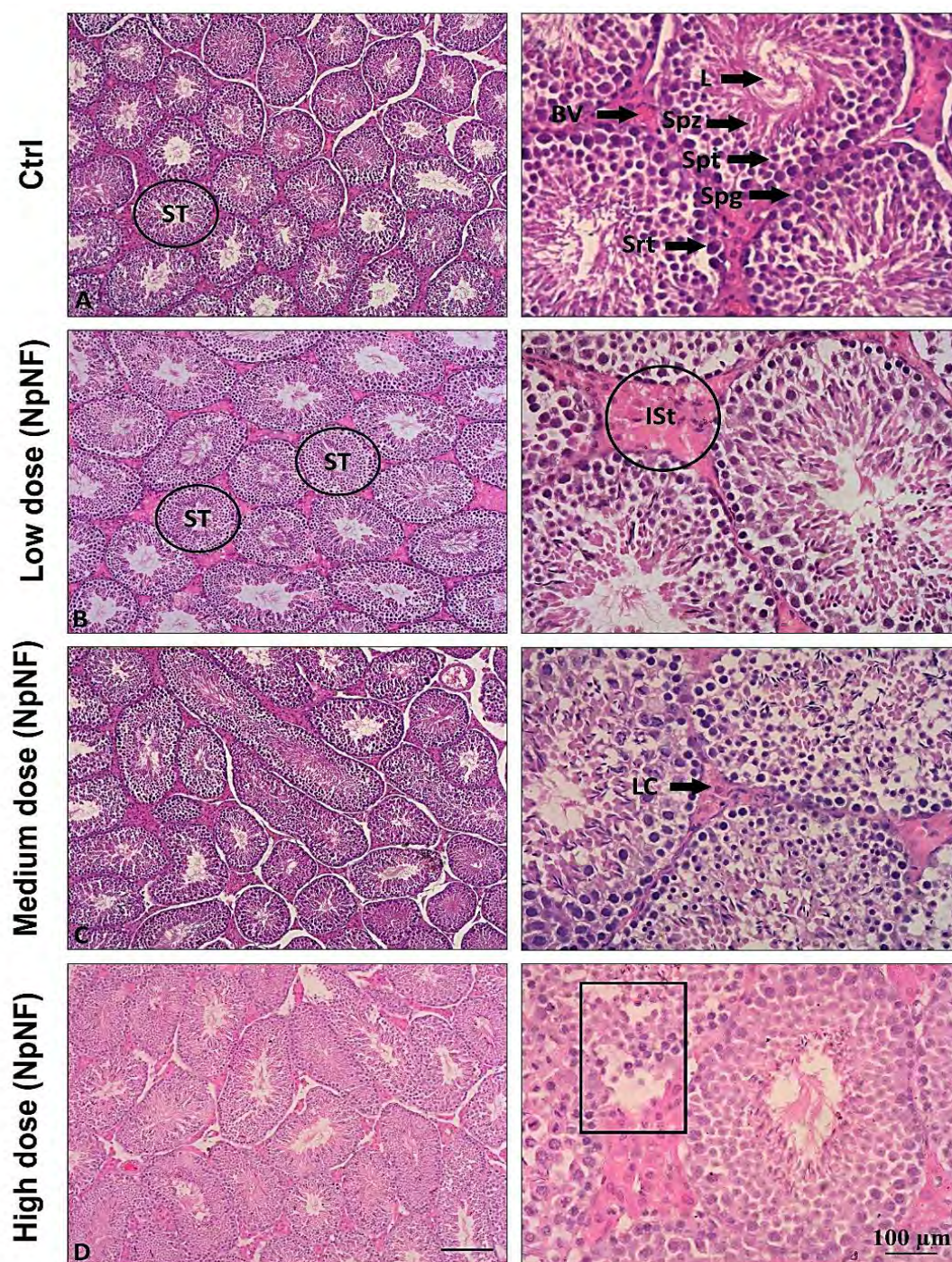
Fig. 4.30 Photomicrographs of control and NpNF treated testes sections of male mice stained with hematoxylin and eosin (H&E) (A) normal testes, (B) treated with 30 mg/kg NpNF (C) treated with 300 mg/kg NpNF and, (D) treated with 1000 mg/kg NpNF. ST= Seminiferous tubules, L= Lumen, Spz= Spermatozoa, Spt= Spermatid, Spg= Spermatogonia, ISt= Interstitial stroma, LC= Leydig cells, Srt= Sertoli cell, BV= Blood vessel, square shape= Tissue necrosis. Magnification 10x (left column) and 40x (right column); Scale bar = 100 μm.
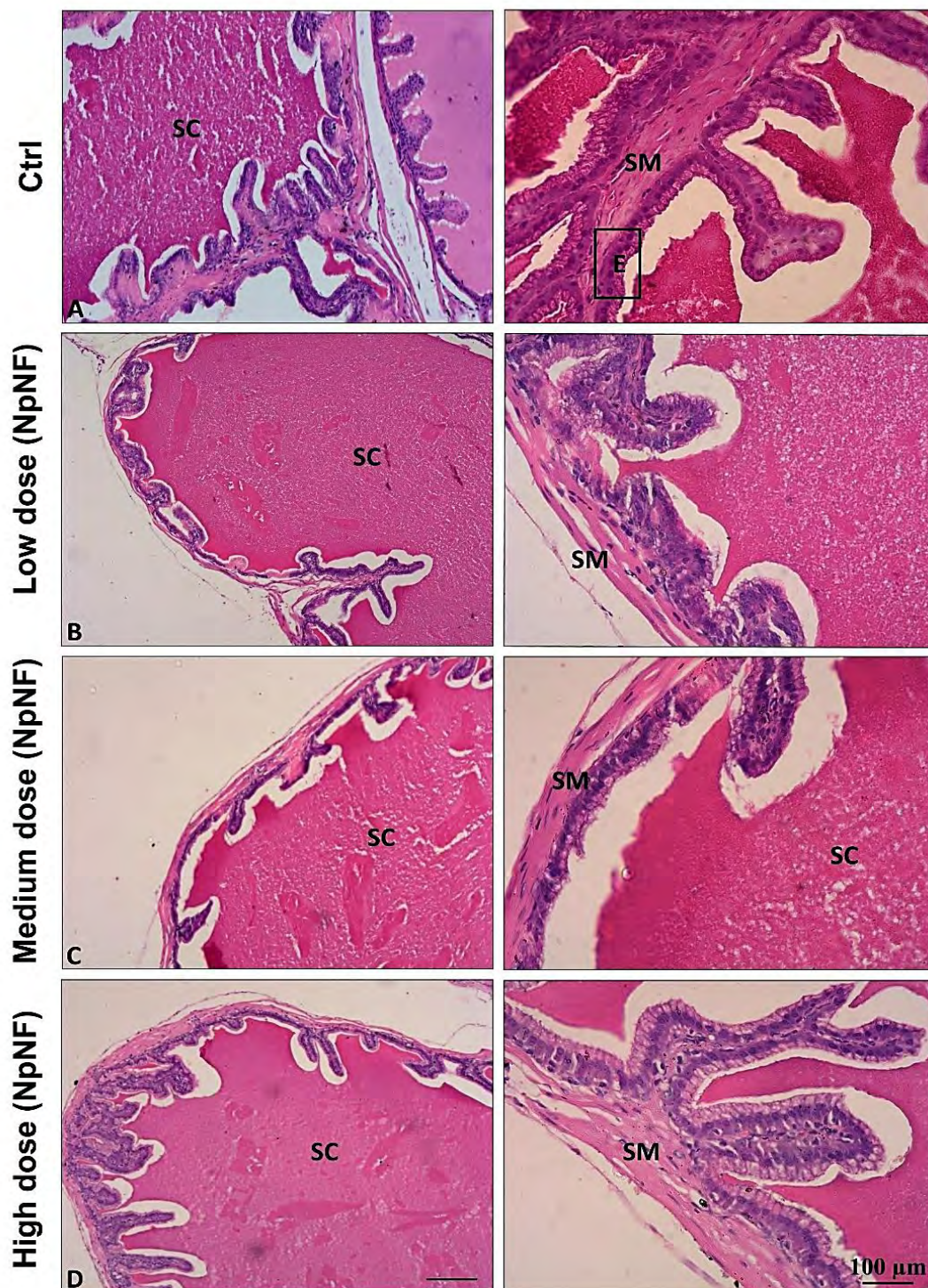
Fig. 4.31 Photomicrographs of control and NpNF treated seminal vesicles sections of male mice stained with hematoxylin and eosin (H&E) (A) normal seminal vesicles, (B) treated with 30 mg/kg NpNF (C) treated with 300 mg/kg NpNF and, (D) treated with 1000 mg/kg NpNF. SM= Smooth muscles, E= Tall columnar epithelium, SC= Secretory cells. Magnifiction 10x (left column) and 40x (right column); Scale bar = 100 μm.

Table 4.1 Probit analysis shows the percent probability of mice death from NpNF dose with 95% fiducial limits.

Probit Analysis on dose			
Probability	dose	95% Fiducial Limits	
0.10	2150.33493	1497.06765	2358.56144
0.20	2298.15527	1788.85101	2475.78062
0.30	2401.98558	2003.54145	2569.75305
0.40	2490.58804	2183.48868	2667.79245
0.50	2574.77052	2338.30796	2789.98317
0.60	2661.79838	2468.83516	2959.45338
0.70	2759.98460	2580.54439	3203.35836
0.80	2884.68029	2689.42988	3573.22221
0.90	3082.98168	2829.91209	4259.39502

Table 4.2 Hematological values of male mice treated orally with NpNF for 14 days. Values are mean ±s.e.

Parameters	Control	Low dose NpNF (30 mg/kg)	Medium dose NpNF (300 mg/kg)	High dose NpNF (1000 mg/kg)
RBC (M/µL)	07.65 ± 0.13	07.08 ± 0.23	07.00 ± 0.07	06.94 ± 0.17[b]
Hb (g/dL)	13.30 ± 0.13	12.70 ± 0.13	12.00 ± 0.32	11.00 ± 0.10
MCV (fL)	68.00 ± 3.01	69.70 ± 2.06	57.95 ± 1.58[c]	57.40 ± 1.36
MCH (pg)	23.57 ± 0.41	21.51 ± 0.99	19.35 ± 0.76[b]	18.95 ± 0.71[b]
MCHC (g/dL)	39.23 ± 2.19	41.43 ± 2.19	34.35 ± 1.05	33.48 ± 1.29
Platelets (µLx10^5)	03.61 ± 0.18	03.71 ± 0.12	04.54 ± 0.22[b]	06.98 ± 0.36[a]
WBC (µLx10^4)	01.16 ± 0.04	01.26 ± 0.03	01.29 ± 0.02	00.73 ± 0.01[a]
Neutrophils (%)	15.16 ± 0.40	17.16 ± 0.86	14.83 ± 0.70	19.58 ± 1.08
Lymphocytes (%)	72.00 ± 1.03	70.33 ± 2.30	67.66 ± 2.10	60.41 ± 1.89
Monocytes (%)	05.00 ± 0.28	05.50 ± 0.48	08.50 ± 0.18[a]	08.00 ± 0.28[a]
Eosinophil (%)	05.50 ± 0.20	05.00 ± 0.28	07.00 ± 0.46[c]	10.00 ± 0.25[a]
Basophil (%)	02.35 ± 0.15	02.00 ± 0.17	02.57 ± 0.17	02.02 ± 0.12

Different superscripts a, b and c in a column show significant difference at ***$p<0.001$, **$p<0.01$ & *$p<0.05$ from control (n=6/group).

Table 4.3. Hematological values of female mice treated orally with naproxen nano formulation for 14 days. Values are mean ±s.e.

Parameters	Control	Low dose NpNF (30 mg/kg)	Medium dose NpNF (300 mg/kg)	High dose NpNF (1000 mg/kg)
RBC (M/µL)	07.10 ± 0.11	07.02 ± 0.23	07.01 ± 0.12	06.83 ± 0.14[b]
Hb (g/dL)	12.26 ± 0.09	11.94 ± 0.10	10.86 ± 0.05[c]	10.50 ± 0.18[c]
MCV (fL)	64.60 ± 1.78	62.05 ± 2.00	58.16 ± 1.68	52.43 ± 1.83[a]
MCH (pg)	22.31 ± 0.41	21.26 ± 0.99	18.73 ± 0.76	17.68 ± 0.71[b]
MCHC (g/dL)	39.05 ± 2.19	39.40 ± 2.19	34.43 ± 1.05	30.25 ± 1.29[c]
Platelets (μLx10^5)	02.30 ± 0.18	02.06 ± 0.09	03.29 ± 0.20	05.01 ± 0.27[a]
WBC (μLx10^4)	01.15 ± 0.03	01.03 ± 0.02	0.915 ± 0.02	0.560 ± 0.01
Neutrophils (%)	19.67 ± 0.40	20.50 ± 0.86	21.00 ± 0.70	21.67 ± 1.28
Lymphocytes (%)	72.08 ± 3.76	70.83 ± 2.67	67.00 ± 2.60	64.33 ± 1.47
Monocytes (%)	04.25 ± 0.28	04.33 ± 0.48	06.00 ± 0.18	07.50 ± 0.28[c]
Eosinophil (%)	03.00 ± 0.20	04.00 ± 0.28	05.00 ± 0.46	08.00 ± 0.25[b]
Basophil (%)	01.00 ± 0.15	00.61 ± 0.17	01.00 ± 0.17	01.00 ± 0.12

Different superscripts a, b and c in a column show significant difference at ***p<0.001, **p<0.01 & *p<0.05 from control (n=6/group)

Table 4.4. Effect of naproxen sodium nanoformulation (NpNF) on serum biochemical status of male and female mice treated for 14 days. Values are presented as mean ± s.e.

Parameters	Sex	Control	Low dose NpNF (30 mg/kg)	Medium dose NpNF (300 mg/kg)	High dose NpNF (1000 mg/kg)
ALT (U/L)	M	50.00 ± 4.07	46.00 ± 2.00	54.00 ± 4.25	120.0 ± 5.34[c]
	F	34.67 ± 1.45	32.33 ± 1.05	35.83 ± 0.65	92.00 ± 5.46[c]
AST (U/L)	M	82.55 ± 4.29	67.40 ± 3.50	77.67 ± 3.81	91.50 ± 6.22
	F	72.14 ± 4.93	57.80 ± 4.12	72.83 ± 3.29	75.17 ± 5.76
ALP (U/L)	M	92.32 ± 5.96	87.63 ± 4.55	93.50 ± 7.79	157.7 ± 9.88[a]
	F	81.80 ± 4.49	78.43 ± 4.69	98.90 ± 9.28	115.1 ± 6.52[b]
Total bilirubin (mg/dL)	M	04.25 ± 0.09	04.91 ± 0.09	05.08 ± 0.23	05.93 ± 0.23[b]
	F	04.16 ± 0.07	04.38 ± 0.13	04.81 ± 0.22	05.43 ± 0.25[b]
Direct bilirubin (mg/dL)	M	03.23 ± 0.09	02.80 ± 0.19	03.28 ± 0.15	02.50 ± 0.13
	F	03.08 ± 0.14	02.21 ± 0.11	02.45 ± 0.07	02.28 ± 0.16[b]
Creatinine(μmol/L)	M	04.43 ± 0.34	03.51 ± 0.07	05.24 ± 0.27	05.29 ± 0.26
	F	04.26 ± 0.26	03.57 ± 0.10	04.87 ± 0.25	05.07 ± 0.15
LDH (U/L)	M	620.8 ± 18.2	508.6 ± 15.3	577.6 ± 15.0	765.6 ± 51.6
	F	562.6 ± 9.67	479.2 ± 17.8	460.2 ± 18.2	706.7 ± 33.3
Cholesterol (mg/dL)	M	89.81 ±1.59	70.45 ± 4.03	131.4 ± 6.19	169.7 ± 10.3[c]
	F	84.20 ± 6.14	88.00 ± 4.13	103.4 ± 7.17	115.0 ± 6.83[c]
Triglycerides (mg/dL)	M	102.2 ± 8.67	111.8 ± 9.11	122.8 ± 3.12	134.6 ± 4.94[c]
	F	103.8 ± 7.78	94.60 ± 6.82	104.2 ± 9.17	115.8 ± 8.54

Different superscripts a, b and c in a column show significant difference at ***p<0.001, **p<0.01 & *p<0.05 from control (n=6/group).

Table 4.5 Oxidative stress and antioxidant enzyme activity in male mice tissues following 14-day exposure to 30 mg/kg, 300 mg/kg, and 1000 mg/kg doses of naproxen nanoformulation (NpNF). Values are mean ± s.e.

Groups	Tissues	ROS (abs)	TBARS (nM min⁻¹ mg protein⁻¹)	SOD (unit mg⁻¹)	POD (unit min⁻¹)	CAT (unit min⁻¹)	GSH (µMol/g)
Control	Brain	1.21 ± 0.04	0.65 ± 0.05	12.53 ± 0.53	1.53 ± 0.05	7.34 ± 0.16	20.55 ± 1.11
Low dose		1.33 ± 0.16	1.22 ± 0.07	10.39 ± 1.19	1.41 ± 0.08	7.08 ± 0.17	19.68 ± 1.03
Medium dose		1.49 ± 0.11^c	1.41 ± 0.01^c	10.98 ± 0.61	1.28 ± 0.11	6.48 ± 0.18^a	17.39 ± 1.19
High dose		1.55 ± 0.22^b	1.78 ± 0.13^c	04.28 ± 0.82^a	1.40 ± 0.28	5.42 ± 0.21^a	15.10 ± 1.05^c
Control	Heart	0.84 ± 0.01	0.99 ± 0.04	14.71 ± 1.56	4.23 ± 0.34	4.76 ± 0.04	33.43 ± 2.51
Low dose		0.97 ± 0.03	0.87 ± 0.14	12.85 ± 1.66	3.82 ± 0.31	4.42 ± 0.14	30.13 ± 2.51
Medium dose		1.02 ± 0.07^b	1.42 ± 0.16	11.59 ± 1.09	3.14 ± 0.32	4.44 ± 0.14	34.26 ± 2.13
High dose		1.10 ± 0.15^b	1.41 ± 0.21	10.51 ± 2.00	2.87 ± 0.36	4.84 ± 0.26	34.80 ± 1.00
Control	Liver	1.07 ± 0.01	0.75 ± 0.06	13.08 ± 0.92	4.83 ± 0.43	4.61 ± 0.21	34.27 ± 1.41
Low dose		1.09 ± 0.06	0.79 ± 0.06	13.98 ± 0.98	4.20 ± 0.32	4.64 ± 0.09	36.30 ± 1.91
Medium dose		1.15 ± 0.07	0.86 ± 0.12	11.08 ± 0.78	3.98 ± 0.44	4.26 ± 0.11	32.01 ± 1.18
High dose		1.17 ± 0.03^c	0.96 ± 0.08	07.33 ± 0.67^b	3.92 ± 0.21	3.39 ± 0.15^a	30.30 ± 3.20
Control	kidney	1.32 ± 0.01	0.52 ± 0.04	15.60 ± 1.81	3.29 ± 0.26	3.11 ± 0.23	29.34 ± 1.16
Low dose		1.33 ± 0.12	0.50 ± 0.04	14.98 ± 2.34	3.05 ± 0.30	3.25 ± 0.15	27.91 ± 2.90
Medium dose		1.48 ± 0.23	0.75 ± 0.02	12.19 ± 0.79	2.47 ± 0.46	3.82 ± 0.45	27.86 ± 3.21
High dose		1.49 ± 0.11^c	1.07 ± 0.08^a	10.72 ± 0.27	2.41 ± 0.30	4.09 ± 0.47	28.43 ± 2.00

Different superscripts a, b and c in a column show significant difference at ***$p<0.001$, **$p<0.01$ & *$p<0.05$ from control (n=6/group).

Continued…

Control	stomach	0.86 ± 0.02	0.54 ±0.04	11.41 ± 0.73	1.65 ± 0.22	04.38 ± 0.14	05.69 ± 0.20
Low dose		0.80 ± 0.03	0.65 ± 0.09	10.56 ± 0.69	1.30 ± 0.05	04.36 ± 0.18	06.64 ± 0.30
Medium dose		0.87 ± 0.02	0.98 ± 0.11[c]	08.39 ± 0.80	1.34 ± 0.26	04.43 ± 0.15	05.94 ± 0.47
High dose		0.96 ± 0.05	1.08 ± 0.10[c]	07.09 ± 1.36[c]	1.01 ± 0.15	03.13 ± 0.05[a]	05.73 ± 0.29
Control	Spleen	0.87 ± 0.06	0.35 ± 0.06	03.34 ± 0.73	2.66 ± 0.40	04.34 ± 0.26	09.15 ± 0.80
Low dose		0.91 ± 0.05	0.47 ± 0.03	02.60 ± 0.44	2.65 ± 0.54	04.21 ± 0.14	08.52 ± 0.57
Medium dose		0.97 ± 0.03	0.48 ± 0.03	02.06 ± 1.10	2.48 ± 0.18	03.50 ± 0.04[a]	06.24 ± 0.57
High dose		0.98 ± 0.04	0.93 ± 0.08[a]	01.70 ± 0.85	2.17 ± 0.46	03.40 ± 0.13[a]	06.25 ± 0.36
Control	Testis	0.95 ± 0.04	0.54 ± 0.05	09.02 ± 1.19	0.96 ± 0.32	03.33 ± 0.13	03.67 ± 0.11
Low dose		0.93 ± 0.03	0.68 ± 0.07	07.14 ± 1.80	0.94 ± 0.10	03.28 ± 0.16	03.67 ± 0.16
Medium dose		0.97 ± 0.04	0.73 ± 0.05	06.76 ± 0.64	0.83 ± 0.05	03.19 ± 0.10	03.35 ± 0.29
High dose		0.90 ± 0.04	1.03 ± 0.08[a]	06.37 ± 1.35	0.73 ± 0.08	02.68 ± 0.25	03.86 ± 0.43
Control	Seminal vesicles	0.86 ± 0.01	0.56 ± 0.09	09.52 ± 1.44	0.83 ± 0.12	03.51 ± 0.15	02.71 ± 0.61
Low dose		0.92 ± 0.02	0.70 ± 0.05	08.84 ± 1.56	0.76 ± 0.10	03.30 ± 0.12	02.46 ± 0.47
Medium dose		0.93 ± 0.02	0.75 ± 0.08	07.88 ± 0.95	0.76 ± 0.05	02.58 ± 0.07[b]	02.41 ± 0.68
High dose		0.94 ± 0.02	0.80 ± 0.07	06.54 ± 1.48	0.63 ± 0.05	02.47 ± 0.19[b]	03.16 ± 0.37

Different superscripts a, b and c in a column show significant difference at ***$p<0.001$, **$p<0.01$ & *$p<0.05$ from control (n=6/group).

Table 4.6 Oxidative stress and antioxidant enzyme activity in female mice tissues following 14-day exposure to 30 mg/kg, 300 mg/kg, and 1000 mg/kg doses of naproxen nanoformulation (NpNF). Values are mean ± s.e.

Groups	Tissues	ROS (abs)	TBARS (nM min^{-1} mg protein^{-1})	SOD (Unit mg^{-1})	POD (Unit min^{-1})	CAT (Unit min^{-1})	GSH (µMol/g)
Control	Brain	00.73 ± 0.00	00.59 ± 0.03	09.87 ± 0.35	01.41 ± 0.05	05.39 ± 0.31	17.22 ± 1.25
Low dose		01.23 ± 0.04	00.63 ± 0.02	07.52 ± 1.82	01.37 ± 0.08	05.20 ± 0.31	16.67 ± 0.88
Medium dose		01.66 ± 0.13[c]	00.95 ± 0.05[c]	06.78 ± 1.33	01.25 ± 0.11	04.84 ± 0.28	15.16 ± 1.80
High dose		01.94 ± 0.25[c]	01.63 ± 0.09[c]	05.93 ± 1.85	01.28 ± 0.23	03.44 ± 0.18[b]	14.74 ± 0.72
Control	Heart	00.73 ± 0.00	00.60 ± 0.04	09.65 ± 0.71	03.23 ± 0.26	03.53 ± 0.07	35.57 ± 1.42
Low dose		00.81 ± 0.01	00.72 ± 0.02	09.20 ± 0.43	03.27 ± 0.20	03.29 ± 0.14	32.76 ± 0.70
Medium dose		00.83 ± 0.02	00.81 ± 0.08	09.45 ± 0.52	02.33 ± 0.26	03.31 ± 0.14	31.79 ± 1.57
High dose		00.95 ± 0.02[c]	00.96 ± 0.09[c]	08.43 ± 0.65	02.15 ± 0.47	03.65 ± 0.26	30.13 ± 0.56[c]
Control	Liver	00.73 ± 0.01	00.58 ± 0.03	11.56 ± 0.96	01.93 ± 0.83	03.47 ± 0.21	29.63 ± 0.21
Low dose		00.97 ± 0.04	00.66 ± 0.07	10.63 ± 1.70	01.61 ± 0.30	03.51 ± 0.09	28.87 ± 0.15
Medium dose		01.02 ± 0.04	00.89 ± 0.08	09.72 ± 0.24	01.53 ± 0.20	03.10 ± 0.13	26.95 ± 0.66
High dose		01.07 ± 0.05[c]	00.97 ± 0.08[c]	07.95 ± 0.30	01.51 ± 0.26	02.54 ± 0.18[b]	26.40 ± 1.60
Control	kidney	00.76 ± 0.01	00.45 ± 0.02	09.77 ± 0.73	02.43 ± 0.12	00.74 ± 0.22	27.72 ± 0.54
Low dose		01.07 ± 0.05[c]	00.58 ± 0.02	07.39 ± 1.12	02.40 ± 0.15	00.33 ± 0.13	26.15 ± 0.92
Medium dose		01.19 ± 0.06[c]	00.77 ± 0.03	07.12 ± 0.86	02.09 ± 0.39	00.68 ± 0.40	25.97 ± 1.23
High dose		01.29 ± 0.04[b]	00.87 ± 0.03[c]	04.76 ± 1.30[c]	02.41 ± 0.30	01.21 ± 0.47	24.46 ± 1.12

Continued…

Control	Stomach	00.73 ± 0.00	00.53 ± 0.01	05.96 ± 1.56	01.38 ± 0.15	03.26 ± 0.14	07.90 ± 0.21
Low dose		00.82 ± 0.00	00.72 ± 0.05	04.34 ± 0.87	01.25 ± 0.06	03.27 ± 0.18	07.33 ± 0.73
Medium dose		00.95 ± 0.02	01.05 ± 0.07	04.02 ± 0.70	01.22 ± 0.21	03.29 ± 0.15	07.47 ± 0.70
High dose		00.98 ± 0.04^{c}	01.12 ± 0.06^{c}	03.86 ± 1.19	00.99 ± 0.13	02.37 ± 0.22^{c}	06.48 ± 0.41
Control	Spleen	00.81 ± 0.01	00.35 ± 0.03	03.98 ± 1.05	02.63 ± 0.40	03.69 ± 0.26	07.48 ± 0.44
Low dose		00.91 ± 0.03	00.48 ± 0.02	03.62 ± 0.80	02.62 ± 0.54	03.51 ± 0.16	06.21 ± 0.44
Medium dose		00.99 ± 0.03	00.52 ± 0.03	03.53 ± 0.59	02.13 ± 0.46	02.86 ± 0.32	06.41 ± 0.59
High dose		01.15 ± 0.05^{c}	00.94 ± 0.07^{c}	02.90 ± 1.47	02.44 ± 0.18	02.79 ± 0.22	06.81 ± 2.42

Different superscripts a, b and c in a column show significant difference at ***$p<0.001$, **$p<0.01$ & *$p<0.05$ from control (n=6/group)

Discussion

Recent advances in the discovery and development of new pharmaceuticals have posed a challenge to science. The availability of new treatment methods necessitates the development of techniques that ensure their safety in humans (Rizvi and Saleh, 2018; Mitra, 2022). Before human safety investigations, non-clinical toxicity studies are conducted based on the performance of a particular animal species (Parveen et al., 2012).

As mentioned in earlier chapters, compared to the free form of drug, naproxen sodium incorporated in the MgO NPs exhibited a high anti-inflammatory effect against experimental mice. This efficacy of the nanoparticulate formulation is attributed to the alteration of the drug biodistribution by nanocarriers (Mitra, 2022). However, apart from this beneficial effect, the binding of naproxen sodium to the nanoparticles could also exert an influence on its toxicological profile. The main objective of the present study, therefore, was to investigate the toxicological profile of newly synthesized NpNF thoroughly using the rodent model.

A dose range-finding (DRF) study or the maximum tolerated dosage, is generally the initial *in vivo* toxicity (OECD, 1987) investigation for a novel chemical conducted in rodent species. This test enables the determination of the dose at which target organ toxicity is expected to occur, but without the need for further research due to the animals' morbidity and mortality (Gao et al., 2017).

In the present study, the acute toxicity evaluation showed that the oral LD_{50} value of NpNF was 2574 mg/kg and based on the LD_{50} value it could be categorized as safe (category 5; no warning on label) according to the Global Harmonized System for classifying hazardous chemicals (GSH) (Persson et al., 2017). Furthermore, the ratio between the minimal effective dose (1 mg/kg) reported earlier in this study and the lethal dose of NpNF (2574.77 mg/kg) indicates that it has a larger therapeutic window. The most interesting finding of the current research is that using MgO NPs as drug carriers and nano sizing worked together to lower therapeutic doses of NpNF and increase its safety by minimizing organ toxicities. Moreover, according to USA Food and Drug Administration (FDA), USA, the LD_{50} of naproxen sodium, (currently used to formulate nanoformulation) is 1200 mg/kg in mice. Although the toxicity of free-

form naproxen sodium has not been thoroughly investigated and reported in the literature, however, when compared to the reported LD_{50} of free-form NPRS, it is evident that the NpNF is safer than NPRS (FDA, 2011).

Since treatment-related toxicity was not evidenced during the acute toxicity evaluation of NpNF, therefore, a range 14-day repeated dose range-finding study was conducted to evaluate the effect of NpNF on key metabolic markers of males and females mice. This was done to provide comprehensive toxicological data on this novel nanoformulation. The selected doses (30, 300, and 1000 mg/kg b.w.) in this study were chosen based on two criteria, firstly, to assess the range of toxicological outcomes that could be observed by administering the lowest possible dose to the recommended highest daily oral dose (1000 mg/kg b.w/day). Secondly, to establish no observed adverse effect level (NOAEL) using the outcomes from dose-response toxicity data. The highest dose selected was approximately 11 times that of recommended daily dose of conventional naproxen sodium recommended for therapeutic purposes (Brutzkus, 2022). Whereas the medium dose was almost 3 times of recommended dose.

The lack of clinical symptoms of toxicity, morbidity, or mortality in all treatment groups (males and female mice) after 14 days of daily dose administration suggests that the NpNF is unlikely to be toxic. Daily observations of the animals' behavior (overall health status and clinical symptoms of toxicity) revealed no change. All animals in all treatment groups studied had their behavior defined as usual for the species.

In general, change in the body weight of an animal has been used to predict the detrimental effects of drugs or compounds (Liu et al., 2016). Furthermore, the relative organ weight reveals whether or not the organ has been injured. Excessive atrophy is prevalent in affected tissues and is indicated by the change in organ-body index (Bailey et al., 2004). If a chemical induces a mass drop of more than 10%, it is regarded as toxic, and this condition may be viewed as a sign of toxicity even if no other changes occur (Schultze et al., 2022). The body weight and relative organ weights of the treated mice did not change substantially from those of the control groups in the current investigation. It shows that the NpNF did not affect the animals' appetites or development. Furthermore, daily food and water intake were determined to be normal, indicating that administration of the test item did not produce stress in animals of both genders at any dosage level.

The examination of hematological parameters gives useful information on the adverse effects of foreign drugs on the hematopoietic system (Petterino and Argentino-Storino, 2006), since this system is among the most vulnerable to hazardous substances, particularly in the bone marrow, which produces red blood cells (Wu et al., 2018).

The decreased amount of red blood cells and WBCs in the male and females high dose treatment group accompanied by an increase in platelets in 1000 mg/kg b.w indicates that at increased doses, NpNF may have antianemia and immunomodulatory actions. (Petterino and Argentino-Storino, 2006). Even though the exact mechanism by which NpNF raises or reduces certain hematological indicators was not determined in this investigation, this effect is assumed to be a direct action of the NpNF on the hematopoietic system. The slight difference in other parameters, including MCV, MCH, MCHC, monocytes, and eosinophils indicates all of these metrics were determined to be within the species' normal physiological range. Furthermore, the hematological system of the experimental animals was visibly preserved, and blood's capacity to deliver oxygen to tissues was retained throughout this investigation.

The normal physiological functioning of the liver and kidney is of critical importance, with one being needed for metabolism and the other for waste product excretion, respectively (Das et al., 2015). It is necessary to know the status of these two significant organs to evaluate the toxicity of any new drug (Press et al., 2017), which may be confirmed by biochemical estimation (Fu et al., 2020).

Presently, in both genders, the subacute exposure to the higher dose (1000 mg/kg) of NpNF produced a significant increase in ALT, ALP, and bilirubin levels whereas, AST a most widely used hepatocellular injury marker (Kang, 2013) and serum creatinine remained unchanged. The increase in alkaline phosphatase (ALP) enzyme suggests that the impact is more selective for hepatobiliary than hepatocellular alterations. (Mangalampalli et al., 2017). Furthermore, the rise in total and direct bilirubin levels in both genders provides strong evidence that the effects are more of a functional parameter connected to hepatobiliary system disruption. Furthermore, an elevated creatinine level indicates impaired renal function (Washington and Van Hoosier, 2012), but was found to be unaffected following NpNF treatment at any dose level in both genders. Based on the biochemical findings, it is safe to conclude that NpNF, when delivered at the highest possible dose, may cause liver tissue damage, unlike other anti-

inflammatory drugs that have reported renal toxicities at recommended therapeutic doses (Menkes, 1989). Therefore, it can be concluded that the consumption of NpNF may have no toxicity effects on kidney tissues even at the highest dose (1000 mg/kg) administered.

Presently, moderate elevation in total serum cholesterol level was observed only in the high dose-NpNF exposed mice (male & female). This elevation might be related to cholestasis caused by an obstruction of the hepatic bile ducts, which causes a decrease or halt of bile secretion to the duodenum (Abatan et al., 2009). On the other, triglyceride levels were found to be within the normal range like the control group in both genders.

Lactate dehydrogenase (LDH), another important enzyme, present in almost all body tissues, is usually identified at higher-than-normal levels when released into blood fluids during cellular and tissue injuries. This test is, therefore, performs to detect tissue alterations and for the diagnosis of heart attack, anemia, trauma, muscle damage, shock, and liver disease (Farhana A, 2022). Interestingly, serum LDH levels were found to be normal in the experimental mice (both genders) following treatment with 30, 300, and 1000 mg/kg NpNF for 14-days.

Chemically reactive oxygen-containing molecules, commonly known as free radicals (ROS), are produced as byproducts of normal metabolic activities. These reactive species, if not controlled by the cellular process, can induce damage to important cellular entities such as DNA, protein, and lipid (Deavall et al., 2012). Furthermore, oxidative stress can cause lipid peroxidation, which transforms unsaturated lipids into polar lipid hydroperoxides in cell membranes thus altering the structures of DNA, protein, and other macromolecules. Examples include malondialdehyde (MDA), 2-propenal (acrolein), and isoprostanes (Deavall et al., 2012).

In the present study, ROS and LPO were measured in all vital tissues obtained from NpNF-treated male and female mice. Data revealed that the highest dose of NpNF significantly altered the oxidant-antioxidant balance in most of the tissues. Contrary to this, a low dose of naproxen nanoformulation did not show any adverse effect on any tissue biochemical parameter. However, a medium dose of NpNF has induced oxidative stress in a few tissues only along with disruption in antioxidants status.

There have been a few reports suggesting nanoparticles can pass through the blood-

brain barrier and reach the central nervous system (Shrivastava et al., 2014). Considering this, one of the major focuses of the present study was to study the potential role of NpNF in the induction of brain oxidative stress and alterations in antioxidant levels in the mouse. Data showed increased production of ROS and lipid peroxidation following exposure to medium and high doses of NpNF, suggesting that these nanoparticles caused oxidative stress in both male and female mice.

In the present study also, the activities of SOD, CAT, and GSH, were significantly inhibited in the groups exposed to the high dose of NpNF in all tissues from male and female mice, whereas POD remained unaffected. The brain, which accounts for only 2 % of the overall body weight, consumes 20% of all oxygen required by the body. Neuronal activity is almost exclusively obtained from ATP generated in the mitochondria, rather than depending on glycolysis. Mitochondria convert O_2 to H_2O to make ATP (Cui et al., 2004) but incomplete O_2 oxidation generates O_2 and H_2O_2, which are promptly regulated under normal conditions but overproduced in conditions of mitochondrial failure caused by neuroinflammation (Wang and Michaelis, 2010). In the present study, the oxidant-antioxidant imbalance found in the brain tissue following administration of nanoformulation in high doses (300- 1000 mg/kg/day) suggests that if organ systems are burdened with medications, chemicals, and nanostructures, the fine balance of antioxidant defense systems may be compromised (Cui et al., 2004).

NSAIDs cause cardiotoxicity by producing reactive oxygen species (ROS), which causes DNA damage and death in cardiac cells, as well as circulatory dysfunction (Fanelli et al., 2013). Presently, results revealed that in male mice, a high dose of NpNF caused a slight increase in ROS levels. Whereas antioxidants status remained unchanged and appeared in the normal range as that of untreated mice. Furthermore, the medium dose appeared to be completely safe by not disrupting any of the oxidant-antioxidant levels in heart tissue. In female mice, contrary to what was observed in male mice heart tissues, ROS and LPO levels increased compared to the control in the high dose group only. While GSH levels decreased significantly. Hence, from these results, it may be reasonable to assume that the current formulation is considerably safer than its conventional analog.

When subjected to NSAIDs for extended periods, the liver, and kidneys, the two most critical organs in maintaining the homeostasis and physiological state in the human

body, are extremely susceptible to oxidative damage (Bindu et al., 2020). In the present investigation, results revealed that in the liver of male mice, the level of CAT and SOD while in female mice CAT content declined significantly compared to the control. Whereas an increase in both ROS and LPO levels was observed in the same dose group. Medium and low doses, on the other, were found safe for liver tissues.

In kidneys, male mice showed a significant increase in ROS and LPO levels in the high dose group. Meanwhile, the antioxidant status remained unchanged. In females, however, SOD levels decreased significantly along with elevation in ROS and LPO levels. Results from a previous study evaluating the effect of naproxen on different tissues in experimental rats revealed that the treatment with 38.91 and 65.78 mg/kg (b.w) naproxen for 14 days led to a significant decrease in GSH levels in the liver, and kidney tissues while increased lipid peroxidation (Ahmad et al., 2018). Contrary to these findings, naproxen nanoformulation proved to be safe for liver or kidney tissues at doses, 5-9 times the conventional drug.

NSAIDs caused mucosal damage in stomach tissues via an "ion trapping" mechanism. The majority of nonsteroidal anti-inflammatory drugs (NSAIDs) are weak organic acids. They are non-ionized and lipid-soluble in gastric juice. These NSAIDs permeate into the cytoplasm of stomach mucosal epithelial cells, where the pH is neutral. Basic pH, NSAIDs are re-ionized, which makes them relatively lipophobic. As a result, NSAIDs become trapped and build within cells, causing cellular damage (Matsui et al., 2011). Currently, naproxen sodium nanoformulation was developed to reduce the mucosal damage caused by NSAIDs (Musumba et al., 2009). The data from stomach and spleen biochemical assays showed that, in male mice, administration of the highest dose only i.e.,1000 mg/kg/day increased LPO, while a decrease in CAT and SOD was observed. The ROS level was, however, unaffected. Female mice on the other showed an elevation in stomach ROS and LPO levels but led to a significant decrease in CAT concentration. GSH and POD activity remained unaffected in both genders. It is important to highlight in the view of current findings that, though consisting of naproxen sodium, showed no adversities against the stomach at 300 mg/kg/day, whereas several reports are indicating the ulcerative effects of NSAIDs administered at standard doses (McEvoy et al., 2021).

In male mice, spleen, after treatment with 1000 mg/kg NpNF a decrease in CAT activity

while the increase in lipid peroxidase may be attributed to excessive use of antioxidant enzyme to scavenge free radicle under NpNF induced oxidative stress. Whereas, in female mice, antioxidants level was found unaffected devoid of dose concentration administered. However, ROS and LPO activity increased significantly indicating oxidative stress caused by high doses.

Previous research on the impact of nonsteroidal anti-inflammatory drugs (NSAIDs) on male fertility and spermatogenesis has shown varying findings. Based on the results of these studies, it is suggested that prostaglandin's physiological role in the process of spermatogenesis may have inhibitory effects on the entire process due to NSAID induce inhibition in COX activity. However, in most of the studies, the fact that NSAIDs can cause oxidative stress in reproductive tissues remained overlooked. From this point of view, testicular tissues and seminal vesicles were assessed for oxidative stress and antioxidant activity. Data revealed that a high dose of naproxen nanoformulation caused moderated elevation in testicular LPO levels only. Whereas, in seminal vesicles, CAT activity decreased compared to the control. The activity of other enzymes was not affected in any dose group. A previous study evaluating reproductive toxicity of naproxen sodium reported that the administration of 10 mg/kg of naproxen sodium to mice for 35 days, motility and damage to seminiferous tubules, however, this effect was attributed to the inhibition of prostaglandins, which play a key role in reproductive functions (Uzun et al., 2014). Current findings suggest the reproductive safety of NpNF, at doses 100 times of conventional naproxen sodium.

Since histopathology is a common endpoint in the toxicological bioassays (Wolf and Maack, 2017), an in-depth microscopic analysis of various organs obtained from male and female experimental mice was performed for histopathological effects induced by NpNF. Although tissues from each treatment group were evaluated for histopathological changes, however, findings from the medium (300) and high dose groups (1000 mg/kg) will be discussed here. As mice exposed to the low dose of NpNF did not show any morphological alterations in any tissues.

Following 1000 mg/kg administration in male and female mice, histological examination revealed substantial neurodegeneration in the hippocampus CA1 region. The neurons in the medium-dose group were rather well maintained, with just little damage in the CA1 sector observed. As adverse effects were not observed in 300 mg/kg

dose groups, it is assumed that NpNF is neurotoxic only at higher doses (1000 mg/kg) administered for 14-days.

Mild to moderate (1000 mg/kg) abnormalities in heart muscle architecture were seen in the medium and high dosage groups. Conjugation of the drug with nanoparticles in the present study might have reduced its cardiotoxic effect, and the phenomenon is often ascribed to a favorable modification of drug bioavailability due to a predominant characteristic of drug delivery systems (Fojtu et al., 2017). The polymeric coating on NpNF is most likely to further mitigate the cardiotoxicity (Pereverzeva et al., 2019).

The activation of Kupffer cells and the formation of tiny monocytic infiltrations were two distinct effects observed in the liver of high-dose-treated (male and female mice). It's likely that loading the drug into nanoparticles made the incorporated drug less accessible to hepatocytes and thus, decreasing its toxicity (Pereverzeva et al., 2019). The impacts of naproxen nanoformulation in mice kidneys were much more apparent in the tubular system, although glomeruli appeared to be unaffected, according to the pathomorphological investigation. Since mitochondria are a primary producer of reactive oxygen species (ROS) and are abundant in kidney proximal tubule which makes, these cells are predisposed to oxidative stress (Abdeen et al., 2019; Tirichen et al., 2021).

The pathological changes in the stomach obtained from male and female mice after treatment showed that the gastric mucosa presented not only atrophic but also necrotic lesions (high dose group). As previously observed, all NSAIDs, except aspirin, exacerbate stomach motility at therapeutic dosages, resulting in gastric lesions (Musumba et al., 2009). The protection of gastric mucosal from such adversities in the present study may be attributed to the low dosage of drugs in nanoformulation.

The pathological changes in the spleen (male and female mice) were less pronounced in the animals treated with NpNF higher doses. The testes of the animals treated with NpNF exhibited less severe damage to the interstitial stroma. Whereas seminal vesicles showed near to normal morphology.

The current results suggest that NSAID-induced systemic toxicity can be minimized by incorporating the drug into MgO NPs. Presently only the highest dose administered (1000 mg/kg) showed signs of toxicity in both male and female mice. The reduced

toxicity of naproxen nanoformulations is most likely due to the drug's altered biodistribution mediated by nanoparticles. According to the findings, conjugating naproxen with MgO nanoparticles greatly reduced the risk of organ damage, thereby improving the drug's safety profile.

Moreover, under the stated experimental conditions, some aspects of the toxicity were observed associated with the medium dose (300 mg/kg). Using existing technological tools or identifying indices that are crucial for determining the no-observed-adverse-effect level (NOAEL), the NOAEL of NpNF was regarded as lower than 300 mg/kg in this study. Moreover, the present investigation could provide a guideline for selecting doses for the sub-chronic and chronic study, which may be more clinically relevant. In conclusion, whereas acute oral treatment of NpNF is unlikely to produce toxicity, repeated administration may have a long-term cumulative harmful effect on mice.

Finally, this study provides very valuable data on the acute and subacute toxicity profile of NpNF. However, additional toxicity data (chronic, mutagenicity, reproductive and carcinogenicity study) of NpNF are urgent to investigate to confirm the risk of NpNF for long-term exposure.

Chapter 5

A comparative study of naproxen nanoformulation vs naproxen: effects on target organs at therapeutic doses in Balb/c mice

Summary

NSAIDs cause multiple organ pathologies such as gastrointestinal tract ulcers and bleeding renal complications, hepatotoxicity, and impairment of cardiovascular tissues. Fabrication of nano-drug formulations with the help of nanotechnology can reduce drug systemic toxicity by increasing drug solubility. In this specific investigation, the safety of naproxen nanoformulations compared to its free form at therapeutic doses in healthy mice was elevated. While naproxen sodium caused severe damage to the heart, liver, kidney, and stomach tissues, oral administration of coated and uncoated naproxen nanoformulations succeeded in preventing tissue damage through the restoration of all biochemical, histological, and immunohistochemical alterations to near control levels.

Introduction

Nonsteroidal anti-inflammatory drugs, also known as NSAIDs, are indicated for the treatment of acute and chronic inflammatory conditions (Rainsford, 2007). Anti-inflammatory drugs including paracetamol, naproxen, acetylsalicylic acid, ibuprofen, and diclofenac sodium are usually, considered well-tolerated if only used for a short period (Fendrick and Greenberg, 2009). However, regular use of NSAIDs causes multiple organ pathologies such as gastrointestinal tract ulcers and bleeding (Wallace, 2012), renal complications, hepatotoxicity (O'Connor et al., 2003; Hörl, 2010), and impairment of cardiovascular tissues (Fanelli et al., 2013).

Even though the toxicity of NSAIDs is primarily attributed to their pharmacological mode of action (cyclooxygenase inhibition) (Bindu et al., 2020), there are, however, substantial indications that prostaglandin-independent mechanisms are also involved. For instance, "NSAIDs trapping" is a phenomenon where acidic NSAIDs with a low pKa accumulate due to high pH inside stomach cells. This effect of ion trapping leads to gastro-duodenal ulcers and bleeding, one of the major side effects of NSAIDs, reported to date. Alarmingly, gastric ulcers have been reported frequently among short-term (1-2 weeks) NSAID users. Secondly, another mechanism by which NSAIDs exert their toxic effect is their ability to act as gastro irritants which cause uncoupling mitochondrial oxidative phosphorylation thus inhibiting the electron transport chain inside gastric epithelium (Matsui et al., 2011). This generates reactive oxygen species, halts ATP production, and causes calcium ions toxicity within cells. Together all, may result in the oxidization of cellular lipids, proteins, and nucleic acids and lead to tissue impairment or organ dysfunction.

Cell death is also known as apoptosis or necrosis may happen due to the initiation of the various cellular signaling cascade in response to ROS generation in affected cells (Sandoval-Acuña et al., 2012). Moreover, it has been reported that anti-inflammatory drugs can activate tumor necrosis factor-alpha (TNF-α), one of the leading inflammatory cytokines produced during inflammations. Which then, induces cellular apoptosis by activating effector caspases or initiating the mitochondrial apoptotic pathway (Gebril et al., 2020). Moreover, the elevated level of proinflammatory mediators such as tumor necrosis factor (TNF-α), interleukin-6 (IL-6), interleukin 8 (IL-8), and interleukin -1β (IL-1β), following NSAIDs induce gastric inflammation

(Ackermann, 2017), further strengthens the ideas that NSAIDs cause gastric inflammation through tropical irritant effect (Watanabe et al., 2004)

Moreover, NSAIDs induced gastric mucosal injury through functional alteration such as reduced mucosal blood flow, hypermotility of the stomach, and microvascular damage. This is believed to be caused by NSAIDs' function to prevent prostaglandins synthesis through cyclooxygenase inhibition (Musumba et al., 2009). Prostaglandins are a group of physiologically active lipids present in mammalian tissues and take part in various functions such as contraction of smooth muscles, platelet aggregation, renin release, and play a critical role in immune and inflammatory response (Ricciotti and FitzGerald, 2011). In gastric mucosa, prostaglandin regulates mucosal blood flow, inhibition of which leads to gastric ulcers and erosions (Whittle, 2003).

Apart from their gastrotoxic effects, increasing evidence suggests that the frequent use of NSAIDs among patients and in healthy populations has increased the risk of cardiovascular disorders (Pirlamarla and Bond, 2016). Given the fact that the NSAIDs work by inhibiting cyclooxygenase, and their resultant products i.e., prostaglandins and thromboxane, this mechanism of NSAIDs action, leads to atherosclerosis, increase vascular thrombosis, and other cardiovascular effects (Fanelli et al., 2013). Besides, NSAIDs exert their cardiotoxic effect through upregulation of the nonsteroidal activated gene-1, inhibition of the Akt signaling pathway which promotes cell survival, downregulation of the NF-κB pathway, and oppression and alteration of the Bcl and p53 pathways respectively. All of which are involved in the cellular apoptotic process and lead to cardiovascular complications including cardiovascular infractions, stroke, and cardiovascular death (Ghosh et al., 2015).

In the liver, there are three major events believed to be responsible for NSAID-induced tissue destruction including the production of reactive drug metabolites that cause mitochondrial injury, obstruction of biliary flow also known as cholestasis, and formation of protein-duct adducts. Additionally, NSAID exposure for long period causes hepatocellular injuries due to abnormal biliary secretions and oxidative stress (Boelsterli, 2002). The abnormal production of NSAID metabolites interferes with the oxidative phosphorylation in mitochondria and results in the production of free radicals, which cause mitochondrial injury, disruption of hepatocyte membranous structures, and ultimate cell death through apoptosis (Woolbright and Jaeschke, 2018).

Altered electrolyte balance, worsening of renal functions and kidney failure due to impaired nephrons, and papillary necrosis are a few of the renal disorders reported against chronic NSAID use (Nies, 1988). Additionally, patients taking NSAIDs for chronic inflammatory conditions like musculoskeletal pain, arthritis, and chronic pain are at increased risk of renal damage and acute kidney failure than others, who do not take NSAIDs frequently (Lucas et al., 2019).

The first mechanism behind NSAIDs mediated renal failure is NSAIDs' function to inhibit the synthesis of prostaglandins involved in vasodilation thus decreasing blood flow to the kidney glomeruli. Reduction in renal blood flow results in severe deterioration of kidneys (Dixit et al., 2010). The second mechanism associated with the NSAIDs inducing renal injury is the direct toxic effect of the drug on kidney tissues, generally known as acute interstitial nephritis (AIN). In acute interstitial nephritis, kidneys suffer from inflammatory cell infiltration and tubulointerstitial damage, which lead to acute renal failure (Ulinski et al., 2004). Worldwide, about 15% of patients with renal conditions as the immunological response of the body against NSAIDs have reported taking NSAIDs only for short period i.e., 1 week.

Despite all kinds of organ toxicities, the therapeutic use of NSAIDs is unavoidable due to their potent therapeutic effects. It is, therefore, frequently recommended by clinical practitioners and drug regulatory authorities, and organizations to discontinue NSAID use or decrease the dose. However, lowering drug-related organ damage seems not practical or effective, especially when NSAIDs are used for chronic inflammatory diseases (Bindu et al., 2020). Thus, relatively safe usage of these drugs in the form of nanoformulation is the need of time which can prevent the risk of organ failure (Al-Lawati et al., 2019).

Fabrication of nano-drug formulations with the help of nanotechnology offers several advantages over its conventional free forms. The conjugation of drugs with a nano delivery system only reduces drug systemic toxicity by increasing drug solubility but as a consequence improves the therapeutic action *via* increased absorption of the drug through biological membranes (Kermanizadeh et al., 2018).

From this perspective, naproxen nanoformulations with an aim of better therapeutic activity and lesser toxicity were prepared successfully and evaluated thoroughly for

their therapeutic potential and acute and sub-acute toxicity in earlier studies performed. In this specific investigation, we aimed to assess the safety of naproxen nanoformulations compared to its free form at therapeutic doses in healthy mice, with a special interest in cardiac, GIT, hepatic, and renal tissues. This set of hematological, serum, and tissue biochemical assays was performed on tissues obtained from the treatment groups. Moreover, histomorphometry and histology of tissues were also performed to evaluate histopathological changes in tissues.

To provide further insights into the underlying pathogenetic mechanisms of naproxen/naproxen nanoformulation, the gene expression of pro-inflammatory cytokines (TNF α, IL-6, IL-1β) was studied through RT-PCR. Moreover, protein expressions of COX-2, i-NOS, NF κB, and caspase-3 were also studied through immunohistochemistry to provide a detailed mechanistic understanding. Finally, to analyze the impact of polymeric coating on nanoformulation, the individual effect of non-coated naproxen formulation was also investigated. Moreover, to avoid any potential bias the effects of MgO NPs used as drug carriers were studied as well.

Materials and Methods

5.1 Chemicals and Reagents

The antibodies used in the current study, the anti-COX, anti-iNOS, anti- NF-κB, anti-caspase-3, and anti-rabbit IgG H&L (HRP) were purchased from Santa Cruz Biotechnology (Santa Cruz, CA, USA). For real-time PCR, template (RNA), primers oligo $(T)_{18}$, random hexamers, dNTPs, M-MuLV reverse transcriptase, M-MuLV buffer, and nuclease-free water (NF H_2O) were purchased from Sigma Aldrich (Sigma Aldrich (St. Louis, Missouri, USA). All other chemicals used for tissue biochemical assays were of pure quality available and obtained from bonafide suppliers. Whereas serum biochemical analyses were performed using commercial kits (LAB KIT, Spain).

5.2 Experimental Animals

Healthy male BALB/c, mice (6–7-week-old) were procured from the National Institute of Health (NIH), Islamabad, and used in the current study. Mice were kept under pathogen-free standard laboratory conditions with temperature (22 °C ± 1.5 °C), relative humidity (60% ± 10%), and a 12-hour light/dark cycle in the animal house facility, Department of Animal Sciences, Quaid-i-Azam University, Islamabad and offered with standard rodent feed and clean water *ad libitum*. The animals were acclimatized to laboratory conditions for 7 days before the commencement of the experiment. The "Bioethical Committee (BEC)" at Quaid-i-Azam University approved the current study's animal handling and experimental procedures (BEC-FBS QAU2021-298). The related guidelines for the use and treatment of laboratory animals were strictly followed.

Doses for each treatment group were calculated according to the bodyweight of experimental mice, suspended in deionized water (<10 mL/kg), and administered orally for 14 days, through gavage. Control mice received an equal quantity of distilled/deionized water.

5.3 Dose Selection and Experimental Design

Findings from animal studies can be used to understand and anticipate human first dosage during the discovery phase of drug development (Robinson et al., 2008).

Allometric scaling allows scientists to interchange dosages between species during research, tests, and clinical trials by considering the differences in pharmacokinetics and pharmacodynamics among species (Timbadiya et al., 2015; Nair and Jacob, 2016; Narayanan et al., 2019). As a result, a dose-by-factor technique is employed in research when extrapolation of dosage between species is essential (Dorato and Buckley, 2006). The animal equivalent dosage (AED) for an established or therapeutically relevant treatment can be calculated by multiplying or dividing the human dose (mg/kg) by the K_m ratio, where K is a number that is unique to each species (Nair and Jacob, 2016).

$$AED \ (mg \ / \ kg) \ = Human \ does \ (mg \ / \ kg) \ \times \ Km \ ratio \ (1)$$

K_m is estimated by dividing the average body weight (kg) of species by its body surface area (m^2).

Hence, in the present study, using these allometric scales, the animal equivalent dose (AED) of naproxen sodium (available clinically) for mice was calculated by either dividing or multiplying the human dose (mg/kg) by the factor of 0.081 or 12.3 respectively.

For this, the therapeutic dose of naproxen sodium recommended for human use for the treatment of inflammatory diseases (e. g, for arthritis associated with rheumatic disease) was searched thoroughly and it was found to be 750 mg- 1 g/day for an adult human (70 kg, Merck manual for professional use) (MSD). The human therapeutic dose was then converted into an animal equivalent dose by first converting this dose into mg/kg, (750/70= 10.7 mg/kg) and adding the obtained value in the following standard formula.

$$AED \ (mg/kg)mice \ = 10.7 \ (mg/kg) \times \ 12.3 \ = 131.78 \ mg/kg$$

The doses obtained were further confirmed through an online dose conversion calculator developed by a group of researchers (Janhavi et al., 2022).

An equivalent quantity of naproxen nanoformulations (UNF and CNF) were administered to other treatment groups for the comparison of experimental outcomes. While, to elucidate any particular effect which can be caused by nMgO (drug carrier), present in the nanoformulation, a blank nMgO treatment group was added. The mice in this group were administered with nMgO equal to the quantity of these NPs used to

formulate naproxen nanoformulation (42 %, calculated previously).

Briefly, after 1 week of acclimatization, the mice were randomly divided into five groups (n= 8 mice/group). The control group received distilled/deionized water (<10 mL/kg), while mice in the treatment groups received oral doses of naproxen sodium NPRS; model drug (131.78 mg/kg), nMgO (55.34 mg/kg), uncoated nanoformulation (131.78 mg/kg) and coated nanoformulation (131.78 mg/kg) suspended in deionized water, administered through oral gavage for 14 days.

5.4 Clinical Observations, Body Weight, and Food Consumption

All animals were subjected to detailed clinical observation once before the initial dosage and at least once a week after that. These observations were obtained employing a grading scale outside the home cage in a predefined area. During the second exposure week, both the control and test animals were subjected to a modified in-house functional observation battery of tests, which included home-cage observations, hand-held observations, stimulus-response, and other additional measures. Bodyweight for each animal was recorded was measured the day before medication began, then once a week after that, and lastly on necropsy day. Feed consumption is measured and documented regularly.

5.5 Collection of Blood and Tissues

The mice were thoroughly anesthetized with ether for *ex vivo* experiments, and blood samples were taken from the heart of the mice on the last day of the experiments. Serum was collected by centrifugation and preserved at−80 °C for biochemical assays. After serum collection, anesthetized mice were killed through cervical dislocation, followed by the immediate isolation of the heart, liver, kidneys, and stomach.

These tissues were appropriately trimmed of any adherent, and their wet weight was taken immediately. Approximately 100 mg of each tissue was then, cut, rinsed with ice-cold saline solution, and kept at − 20 °C for tissue homogenate preparation. Whereas 10 mg of each tissue was cut and added immediately to 1 mL of TRIZOL reagent and stored at 4 °C for gene expression studies. The remaining tissues were fixed in a 10 % neutral buffered formalin solution for histopathological and immunobiological studies.

5.6 Calculation of Organ–Body Index

The organ–body weight index for the heart, liver, kidneys, and stomach was calculated according to the following formula:

$$\text{Organ} - \text{body weight index (\%)} = \text{Wet organ weight}/\text{Body weight} \times 100 \quad (2)$$

5.7 Determination of Serum Biochemical and Hematological Parameters

The effect of naproxen sodium and its nanoformulations on vital organs such as the liver and kidney were evaluated through plasma bio-chemical analysis of alanine aminotransferase (ALT), aspartate aminotransferase (AST), alkaline phosphatases (ALP), bilirubin (total and direct), and creatinine level. Lipid profile was assessed in all treatment groups through serum cholesterol and triglycerides analysis. Lactate dehydrogenase (LDH) assay, also known as LDH release assay was used to assess the cell death/cytotoxicity through measurement of LDH levels in plasma. All biochemical assays were performed on an automatic chemistry analyzer (Agilent-8453, California, U.S.A.) using commercially available kits (LAB KIT diagnostic kits Spain) (Procedure details for each assay have been provided in chapter 4).

Hematological parameters such as erythrocyte count (RBC), hemoglobin (Hb), mean corpuscular volume (MCV), hematocrit (HCT), and mean corpuscular hemoglobin (MCH), mean corpuscular hemoglobin concentration (MCHC), platelets, neutrophils, lymphocytes, monocytes, eosinophils, and basophils. Total leukocyte count and differential leukocytes were also evaluated. The results were compared among treatment groups and with the control group.

5.8 Tissue Biochemical Analyses: Homogenate Preparation, Oxidative Stress, and Antioxidant Enzyme Assays

Tissue homogenates were prepared and analyzed for tissue oxidative stress and antioxidant enzyme activities as explained in chapter 4.

5.9 Assessment of Ulcerogenic Activities

Stomachs were taken immediately after decapitation, opened along the larger curvature, cleansed with ice-cold saline, pressed dry with filter paper, and placed flat on cardboard

to be examined for gross lesions.

5.9.1 Determination of Ulcer Index

Each lesion was measured along its greatest length, and the total of the lengths per stomach was represented as ulcer index (mm).

5.9.2 Determination of Preventive Index

The percentage inhibition of stomach mucosal damage caused by the test medication/formulation is the preventative index of each drug. Equation 3 was used to determine it:

Protection percentage (%) = [(ulcer index positive control/ulcer index treated] x 100 (3)

5.10 Histopathological Examination

To study the test compounds-induced histopathological alterations, H & E staining of the targeted organs, including the heart, liver, kidneys, and stomach, was done according to a previously published technique (Ahmad et al., 2021). Following fixation, the tissues were dehydrated in graded ethanol series from 70 % to 100 %. The tissues were then, cleaned with xylene and infiltrated in molten paraffin wax overnight. The infiltrated tissues were then, embedded in a paraffin wax block and the microtomy (Leica, USA) was performed to obtain 4-5-μm thick sections. The sectioned tissues were then placed on slides, deparaffinized using absolute xylene (100 %), and finally, rehydrated with ethanolic concentrations (70–100 %) and distilled water. Later, the slides were incubated with hematoxylin for 10 min then washed in running tap water for 5 min. and immersed in an eosin solution for 5–10 min, followed by a careful rinse in tap water and were air-dried. The slides were then dehydrated using graded ethanol (70%, 95%, and 100%), mounted in DPX, observed, and photographed at 10x and 40x under an optical microscope (CX41-Olympus, Japan) equipped with a digital camera (Tucson, USB2.0 H series). The data were evaluated and reported by a veterinary pathologist.

5.11 Immunohistochemical Analysis

The immunohistochemical staining was performed to investigate the effect of test

compounds on the expression of NF-κB, iNOS, COX2, and cleaved-caspase 3 proteins in the heart, liver, kidney, and stomach. Briefly, the paraffin-embedded tissue slices (4 μm) were treated with xylene, and alcohol and quenched by 3% H_2O_2 in menthol to inactivate endogenous peroxidase. Following washing with phosphate-buffered saline (PBS) the tissue was treated with normal goat serum (NGS), primary antibodies i.e., rabbit polyclonal (anti-NF-κB, anti-iNOS, anti COX2, and anti-caspase 3), and secondary antibodies (Abcam, Shanghai, China). Immunoreactivity was determined according to the manufacturer's protocol.

The intensity of the immunostaining was calculated as the fraction of DAB-positive immunoreactive area in 6 fields/section calculated in HPF (100x) and presented as the area percentage of immunopositive cells to the total area of the microscopic field using ImageJ software and compared to the control.

5.12 RNA Extraction and Real-Time PCR Analysis

5.12.1 RNA extraction and Quantification

Tissues from the heart, liver, kidneys, and stomach were weighed (10 mg), added to 1 mL TRIZOL reagent, and stored at 4 °C. Each tissue was then homogenized with a glass homogenizer (wrapped with aluminum foil) at room temperature. Following homogenization, the homogenate was transferred to the fresh Eppendorf tubes and was allowed to stand for 5 min at room temperature.

- **Phase separation**

A volume of 0.2 mL cold chloroform was added to each Eppendorf tube, vortexed quickly for 15 seconds, then incubated at room temperature for 2 minutes. After that, the samples were centrifuged at 12,000 *g* for 15 min at 4 °C. The mixture was separated into lower red, phenol-chloroform interphase, and an RNA-containing colorless upper aqueous phase. The top aqueous phase was then transferred into a new chilled tube with care.

- **RNA precipitation**

To precipitate the RNA from the aqueous phase, a volume of 0.2 mL chilled isopropanol was added into the aqueous phase containing tubes and mixed well by

shaking. The tubes were then, incubated for 10 min on ice and centrifuged at not more than 12,000 g for 10 min at 4 °C. The precipitated RNA appeared gel-like pellet on the side and the bottom of the tube was then recovered and suspended in 1 mL chilled 75% ethanol without dissolving or mixing it.

- **RNA wash**

Tubes containing RNA pellet and chilled ethanol (75%) were then, centrifuged again at 7,500 g for 5 min at 4 °C. The supernatant was discarded, and the RNA pellet was washed again using the same procedure. After the final wash, the ethanol was recovered completely from each sample and the pellets in tubes were dissolved in 20 µL RNAse-free water.

- **RNA quantification**

In the present study, a nanodrop plate was used to assess the quality and quantity of RNA. (Skanit RE 4.1, Thermo Scientific). Absorbance was measured at 260, 280, and 320 nm, with a ratio of 260/280 greater than 1.6 indicating high-quality RNA, and RNA quantities ranging from 800 to 1200 ng/µL. The RNA extraction technique was repeated three times.

- **cDNA Synthesis**

The RNA was converted to cDNA using a commercially available cDNA synthesis kit (Vivantis cDSK01-050, Malaysia) according to the manufacturer's protocol. Briefly, the RNA- primer mixture was prepared by mixing all reagents in the centrifuge tubes and centrifuged briefly. Table 5.1 shows components of the RNA primer mix.

Table 5.1 Preparation of RNA-primer mixture

Reagents	Stock Conc.	Working Conc.	Vol/reaction	Vol/n
Total RNA			7 µL*	
Primers	40 µM	4 µM	1 µL	
DNTPs	10 mM	1 Mm	1 µL	
NF H$_2$0			1 µL	
Final Volume			10 µL	

"n" is the number of reactions *Depending on the concentration of RNA.

The mixture was then incubated at 65 °C for 5 min and chilled for 2 min on ice. To this,

10 µL of cDNA synthesis mix (Table 5.2) was added, mixed gently, and centrifuged for a few sec. The whole mixture was then, incubated at 42 °C for 60 min. Following this step, the temperature was raised to 85 °C for 5 min. The tubes were then, chilled using ice and centrifuged for a few sec.

Table 5.2 Volume of each reagent taken during the preparation of the cDNA Synthesis Mix

Reagents	Stock Conc.	Working Conc.	Vol/reaction	Vol/n
M-MuLV Reverse Transcriptase	5000U	100 U	0.2 µL	
M-MuLV buffer	10X	2X	2 µL	
NF H$_2$0			7.8 µL	
Final Volume			10 µL	

"n" is the number of reactions

The synthesized cDNA obtained was then, stored at -20 °C for further processing. The sequence of primers used for PCR reaction is given in Table 5.3

Table 5.3 Primers used in the study

Primers	Sequence (5'-3')
GAPDH-FW	GTATGACAACAGCCTCAAGAT
GAPDH-RW	GTCCTTCCACGATACCAAAG
IL6-FW	GTGTGTGTGTGTGTGTGTAATC
IL6-RW	CCATTATGCCCAGCCTTATCT
IL1β-FW	CCAGGAGAGGAGTTGGTTATTC
IL1β-RW	GGACGTCATCAGGCTTCTTT
TNF-α-FW	ATGGGAGACGAGGGAGATAAG
TNF-α-RW	CGTCCAACCTCAGCATCTTT

- **Real-Time – PCR**

Real-time polymerase chain reactions were performed on Mic PCR (BioMolecular System) using template cDNA, forward & reverse Primer, 2X HOT SYBR Green qPCR Mix (Solar Bio Cat No. SR1110), and nuclease-free water. The details of reagents used in PCR reaction are given in Table 5.4, whereas conditions optimized for PCR reaction are mentioned in Table 5.5.

Table 5.4 Optimized concentrations of reagent used in PCR reaction

PCR Reagents	Stock Conc.	Working Conc.	Vol/Rec	Vol. x (n)
cDNA template	-	1:10	2.6 µL	
P_F	10 µM	0.2 µM	0.2 µL	
P_R	10 µM	0.2 µM	0.2 µL	
Eva Green	2X	1X	5 µL	
PCR H_2O			2 µL	
Final Volume			10 µL	

"n" indicates the number of reactions

Table 5.5 Optimized conditions for the PCR reaction

Steps	Sub-cycles	Conditions	PCR cycles
Initial Denaturation		95 °C, 12 min	1
PCR Cycles	Denaturation	95 °C, 15 sec	
	Primer annealing	61°C, 20 sec	40
	Primer extension	72 °C, 20 sec	
Hold		95 °C, 15 sec	

- **Representative graphs of Real-time PCR**

Cycling Graph
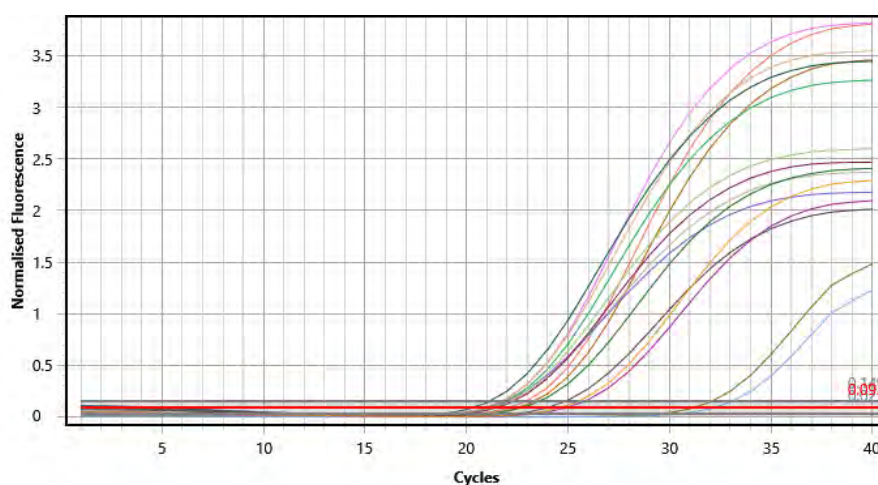
Fig. 5.1 Real-time cycling graphs showing normalized fluorescence on Y-axis and Cycles (Cq) on X-axis. Peaks are showing different samples against the threshold.

Melt Curve Graph
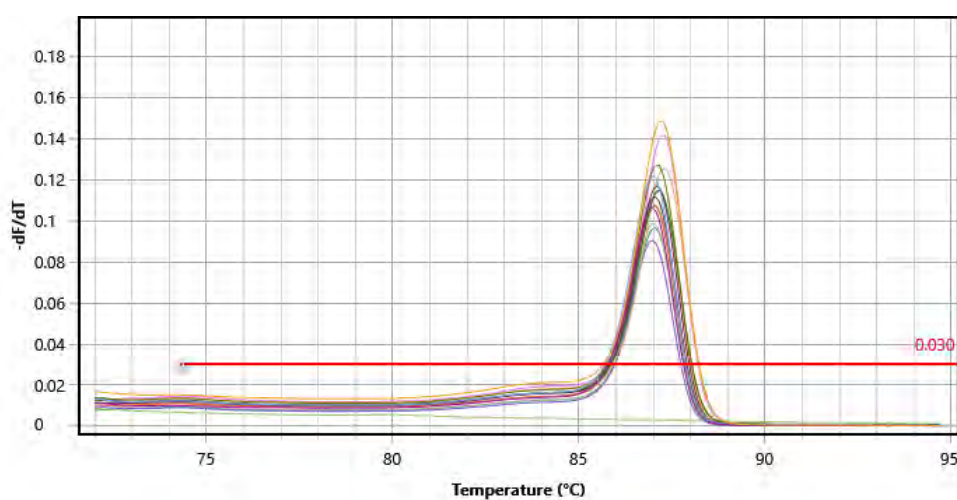
Fig. 5.2 Melt analysis graph; First derivative curve plotted as dF/dT (y-axis) against temperature (°C, x-axis), Depicting amplification of desired product only. In the case of dimer formation, there are double peaks between 75 °C to 80 °C in the temperature range.

5.13 Statistical Analysis

Data are presented as the mean ± s.e. initial and final body weights, absolute and relative organ weights at necropsy and hematological, serum, and tissue biochemical parameters were analyzed by Analysis of Variance (ANOVA). All statistical analyses were performed using SigmaPlot 12.0 (Microscoft Inc. USA). Multiple comparisons were performed by the Tukey test. For histologic analysis, the animals were sacrificed, and the samples were obtained. Image J software was used to carry out morphometry of normal and affected tissues. $p < 0.05$ was a statistically significant difference.

Results

5.14 Clinical Observations, Body Weight, and Food Consumption

In general, no mortality or obvious clinical signs suggestive of systemic toxicity associated with the given treatment were observed throughout the study. One mortality, however, was observed in the free NPRS treated group after 10-days, which upon gross microscopic examination revealed ulceration of major organs: the liver and stomach. The functional behavior of all the treated groups was compared with the control group. Besides, the body weight, food consumption, and water intake of all mice treated with repeated oral doses were found to be normal as well.

The body weight of mice in all treatment groups was found comparable to that of the control group except for the free NPRS treatment group where a gradual decrease in body weight was observed throughout the study ($p<0.01$) Fig. 5.3 A. Food consumption and water intake, however, remained unchanged in nanoformulation and were comparable to control mice. Whereas mice in the free NPRS group showed a low intake.

5.15 Relative Organ Weight and Organ-to-Body Weight Ratio

The absolute and relative organ weight of mice treated with free NPRS, nMgO, UNF, and CNF is demonstrated in Fig. 5.3 (B). As shown, there was no significant difference in the absolute and relative organs weight such as heart, liver, kidneys, and stomach of nMgO, UNF and CNF treated male mice compared to those from the control group. However, in the free NPRS treated group, a significant decrease ($p<0.05$) in heart and kidney weight while a significant increase in stomach and liver weight ($p<0.05$) was observed as compared to the control.

5.16 Hematological Parameters

Hematological parameters, including RBC, Hb, MCV, MCH, MCHC, platelets, WBCs, neutrophils, lymphocytes, monocytes, eosinophils, and basophils of treated mice are shown in Table 5.6.

Overall, significant changes were observed in RBC, MCH, MCHC, and platelet levels in all treatment groups when compared to the control. Data revealed that the

administration of free NPRS led to significant change in all hematological parameters with a considerable decrease in RBC (p<0.001), Hb (p<0.001), MCV (p<0.05), MCH (p<0.001), MCHC (p<0.001), WBC (p<0.001) and lymphocytes (p<0.001), while an increase in platelets counts (p<0.001), neutrophils (p<0.001) and monocytes (p<0.001) occurred as compared to the control.

Coated naproxen nanoformulation on the other, showed significant alteration in RBC (p<0.001), MCH (p<0.05), MCHC (p<0.05), platelets (p<0.001) and eosinophils (p<0.05) as compared to the control. Moreover, a comparison among free NPRS and other treatment groups revealed that the administration of naproxen nanoformulations presented a better hematological profile than NPRS at the same doses administered.

5.17 Serum Biochemical Analyses

Presently, serum biochemical analyses were performed to assess any adverse effect of free NPRS, nMgO, UNF, and CNF on serum ALT, AST, ALP, and bilirubin (total and direct), creatinine, LDH, cholesterol, and triglycerides (Table 5.7).

The liver, kidney, and structural membrane injury biomarkers were monitored, with no significant increase in the mean ALT, AST, ALP, creatinine, total bilirubin, and direct bilirubin levels in the mice treated with nMgO, coated and uncoated naproxen nanoformulation as compared to the baseline value and the mean serum level in those given normal saline (Fig. 5.4). Any significant change, if observed was only in the free NPRS treated group, where an administration of NPRS at clinical doses caused a significant increase in serum ALT (p<0.001), AST (p<0.001), ALP (p<0.019), and creatinine (p<0.05) levels as compared to the control. Whereas a considerable decrease in serum bilirubin (p<0.015) was observed following NPRS treatment. In brief, nMgO, and naproxen nanoformulations showed serum biochemical values nearing normal and better tolerance to the doses administered.

Assessment of serum lipids (Fig. 5.5) revealed that free NPRS-treated male mice showed a significant increase in cholesterol (p<0.001) and triglyceride levels (p<0.005). In contrast on the other, treatment with naproxen nanoformulations and nMgO caused no change in lipid profile as compared to the control. Lactate dehydrogenase levels remained unchanged in all treatment groups.

5.18 Oxidative stress, and Antioxidants Enzyme Assays

5.18.1 Reactive Oxygen Species (ROS) and Lipid Peroxidation (LPO)

The effects of free NPRS and its nanocarrier and nanoformulations on oxidative stress parameters such as ROS and LPO in various tissues of male mice the heart, liver, kidney, and stomach were evaluated and presented in Table 5.8; Fig. 5.6 (A, B) respectively.

Compared to control, as demonstrated in Fig. 5.6 A, a considerable elevation in the heart ($p < 0.001$) ROS level was observed following treatment with free NPRS. Treatment with nMgO and naproxen nanoformulation, on the other, did not affect heart ROS level and the values obtained were comparable to the control group and significantly lower ($p < 0.001$) than the free NPRS. A considerable decrease in ROS levels ($p < 0.048$) was observed in the coated nanoformulation group as compared to its uncoated form.

Likewise, ROS levels in liver tissues elevated significantly ($p < 0.001$) following treatment with free NPRS. Whereas liver ROS concentration remained unaffected in other treatment groups compared to the control and showed a significant decrease ($p < 0.001$) when compared statistically with NPRS treated group at the same doses administered. Among all groups, coated nanoformulation-treated mice showed ROS levels corresponding to those of control mice.

In kidney tissue, ROS concentration elevated significantly ($p < 0.008$) in the NPRS dose group only. On the contrary, ROS concentration remained unchanged in the nMgO, UNF, and CNF-treated mice. A similar pattern of ROS levels was observed in stomach tissues as well where treatment with NPRS led to significant elevation ($p < 0.016$) in ROS levels. Whereas coated naproxen nanoformulation did not cause any effect on stomach ROS and values obtained were a comparable control group of mice.

Lipid peroxidation (LPO) was estimated using the malondialdehyde (MDA) index, a secondary end product of the polyunsaturated fatty acids oxidation. Presently, a significant rise in the liver ($p < 0.003$) and kidney ($p < 0.05$) LPO levels were observed in mice treated with NPRS, whereas in comparison to the control, TBARS content in the same tissues was found unaffected in nMgO, UNF and CNF treated groups. The

TBARS level in heart and stomach tissues remained unaffected in all treatment groups.

5.18.2 Assessment of Antioxidant Enzymes Activity

The antioxidant status of various tissues in male mice following administration of NPRS, nMgO, UNF, and CNF is given in Table 5.8.

In male mice, the administration of NPRS resulted in a major decrease in the heart ($p < 0.001$), liver ($p < 0.001$), kidney ($p = 0.001$), and stomach ($p < 0.002$) CAT Activity. While in the nMgO and naproxen nanoformulations treated groups, the CAT activity was comparable to that shown by control in all tissues. Intergroup comparison showed that the mice treated with CNF did not show any decrease in CAT enzyme activity as compared to the control (Fig. 5.7 A).

Likewise, the SOD content, as illustrated in Fig. 5.7 (B) decreased significantly in the heart ($p < 0.003$), liver ($p < 0.001$), and kidneys ($p < 0.018$) of NPRS-treated mice. While mice dosed with a similar quantity of naproxen nanoformulations did not show alter SOD content in any tissues and the values obtained for SOD, in nMgO, and nanoformulation treated tissues were comparable to control mice tissues. In the stomach, SOD content remained unchanged in all treatment groups as compared to the control.

As shown in Fig. 5.8 A, the POD level in mice hearts treated with nMgO, UNF, and CNF, was found equivalent to control mice, whereas NPRS-treated hearts presented a highly significant decrease ($p < 0.001$) in the POD activity. Liver tissue on the other, when treated with NPRS and its uncoated nanoformulation showed a considerable decrease ($p < 0.001$) in the POD content as compared to the control, however, this effect was more pronounced in NPRS-treated groups ($p < 0.001$) as compared to other treatment. In kidneys, the POD activity was affected only in NPRS treated group and showed a significant decline ($p < 0.05$) as compared to the control and coated nanoformulation. Likewise, stomach POD levels decreased in NPRS treated group only as compared to the control ($p < 0.009$) and CNF ($p < 0.01$).

As shown in Fig. 5.8 B, GSH levels, another non-enzymatic antioxidant of great significance decreased significantly following treatment with NPRS ($p < 0.05$) in the heart tissues, compared to the control, nMgO, UCF, and CNF. Moreover, the GSH

activity presented by nMgO, UNF, and CNF was comparable to those of control mice. In the liver, the GSH levels declined in all treatment groups except CNF, where the activity remained unchanged and almost similar to control mice. The GSH content in kidneys declined significantly in all treatment groups ($p<0.001$) when compared with the control kidneys, however, the lowest level was found in the kidneys of NPRS ($p<0.001$) treated group compared to the nMgO, UNF, and CNF.

5.19 Assessment of Ulcerogenic Activities

At the end of the current experiments, the stomach of each animal was assessed for gross morphological changes following various treatments, Fig. 5.9 (A-F). It was revealed that the stomach of the control group showed normal mucosa without any injuries (Fig. 5.9 A). However, the NPRS-exposed group showed bloody streaks injuries ranging from 14 to 18 mm in length (Fig. 5.9 B), showing a significant increase ($p<0.001$) in ulcer index as compared to the control. Pretreatment with nMgO (drug carrier), and naproxen nanoformulations both coated and uncoated effectively protected the mucosal layer, without any significant difference in ulcer index from the control group (Fig. 5.9 C, D, & E) with a significant decrease ($p<0.001$) of ulcer index compared to NPRS-exposed group.

In terms of percent protection of the mucosal layer, the data obtained (Fig. 5.9 G) from nMgO, UNF, and CNF treatment groups were analyzed, using NPRS treated group as the positive control. Results revealed that the nMgO protected stomach mucosa by 81% ($p<0.001$), while UNF protected stomach mucosa by 84% ($p<0.001$) compared to the NPRS treated group. Likewise, mice pre-treated with CNF prevented any stomach injury by 83% ($p<0.001$) compared to the NPRS-treated mice.

5.20 Histopathological Examination

Gross necropsy of all the major organs, heart, liver, kidney, and stomach was found to be normal in control mice.

Histological study of control mice heart showed normal cellular architecture of cardiac myocardial cells, the cardiomyocytes with one centrally placed nucleus. Cardiac muscles showed intercalated discs which are the specialized junction between cardiac cells (Fig. 5.10 A).

On the other, histological sections of the heart obtained from the mice given free NPRS showed remarkable changes such as degradation in cardiac muscle with vacuolization and edema formation in multiple areas. This intercellular vacuolation of different sizes in heart sections disrupted the myofilaments arrangement and loss of striations (5.10 B). Mild damage in heart muscle fibers in blank nMgO treated groups was observed (5.10 C). Whereas, in uncoated nanoformulation-treated mice, cardiac muscles showed a mild increase in myocardial muscle fiber degeneration (5.10 D). Coated nanoformulation (CNF), on the other, showed a comparatively better arrangement of the muscle with minimum damage (5.10 D).

A representative photomicrograph of liver tissues from control mice (A), treated with NPRS (B), treated with nMgO (C), treated with UNF (D), and treated with CNF (E) is shown in Fig. 5.11. In male mice, control sections showed normal tissue with an intact central vein surrounded by hexagonal hepatocytes. The sinusoidal space appeared normal as pale spaces between the hepatocytes in routine hematoxylin and eosin (H&E) staining. Compared to control and other groups there occurred, however, greater histopathological changes in the liver tissues from NPRS treated mice. These changes included the appearance of micro and macro vesicles, cytoplasmic degeneration, necrotic foci, Kupffer cells activation, and infiltration of inflammatory cells. The liver of male mice treated with the nMgO, UNF, and CNF showed no or negligible changes in tissue architecture. There were no mononuclear cell infiltrations, sinusoidal or central vein dilatation, or hepatocyte degeneration.

The detailed histopathology of the kidney tissue of control and treated mice are shown in Fig. 5.12. Control kidney (Fig 5.12 A) showed normal histological with renal cortex surrounded by numerous renal corpuscles, each made up of glomeruli and the Bowman's capsule, which is lined by visceral and parietal cells. While Bowman's space was normally placed. The renal corpuscles are surrounded by normal proximal and distal convoluted tubules. Furthermore, mice treated with NPRS (Fig. 5.12 B) revealed marked tubular degeneration and dilatation, edema exudate, necrosis, and infiltration of inflammatory cells. On the contrary, minimal alteration in renal tissues represented mild degeneration of renal tubules with a normal renal cortex, and glomeruli were observed in mice treated with nMgO, UNF, and CNF (Fig. 5.12 C, D & E).

Microscopic examination of the stomach, after H & E staining (Fig. 5.13), showed that

the control mice maintained a normal intact gastric mucosa complement of mucosal lineage: chief cells that produce pepsinogen, parietal cells in the intermediate- zone, and foveolar mucus-producing cells. The control stomach did not show any signs of cellular congestion, or degeneration of mucosal lining and lacked any inflammatory infiltrate in the submucosal area (A).

Severe exfoliation of the gastric epithelial cells along with disruption of the mucosal layer and dilated inter glandular spaces of the stomach compared with that of control, and other treatment groups, mainly at the level of foveolar and parietal cells that are eroded (ulcers) were found in the NPRS treated mice (B). On the contrary, the stomach treated with the nMgO demonstrated a normal gastric mucosa with negligible alteration in the mucosal lining (C). Stomach treated with UNF showed the mucous secreting cells of the gastric pits and the gastric glands showed normal histology typical of mice gastric tissues (D), similarly, treatment with CNF showed an intact gastric mucosa similar to that of control animals (E).

5.21 Immunohistological Detection of COX2, iNOS, NF-Kβ, And Cleaved-Caspase -3 in Target Tissues

The expression and localization of common inflammatory and apoptotic markers were studied in the heart, liver, kidneys, and stomach of control/nontreated and treated mice.

As a potent marker of inflammation, currently, the expression of COX-2 was examined through immunohistology in heart sections (Fig. 5.14 A). Data revealed that the positively stained cardiomyocytes following NPRS treatment, in terms of percent area were found to be the highest among all treatment groups (16.36 ± 0.389 %) ($p<0.001$), followed by the untreated group showing $9.84 \pm 0.40\%$ COX-2 positive areas. Interestingly, treatment with nMgO, UNF, and CNF caused the activation of COX-2 expression in heart sections only in $6.0 \pm 0.40\%$ $7.0 \pm 0.40\%$ and $5.0 \pm 0.40\%$ percent area which was significantly lower than that of shown by control ($p<0.001$).

In terms of the percent reduction in COX-2 expressed area, a comparison among treatment groups showed that treatment with nMgO, UNF, and CNF led to a significant decline in COX-2 expression ($p<0.001$) by 62%, 56.25%, 68.75% compared to the NPRS treatment.

Inducible nitric oxide synthase (iNOS) expression was also studied in the present study to determine the role of immune response in the induction of cardiomyopathies following different treatments. Results indicated that NPRS treatment led to an overexpression of iNOS ($p < 0.001$), in cardiomyocytes compared to the control, nMgO, UNF, and CNF treated mice (Fig. 5.14 B). In control mice, the percent area of positively stained for iNOS was found to be 17.89 % ± 0.41, whereas in nMgO, UNF and CNF treated mice, the same was found to be 21.0% ± 0.41, 13.0% ± 1.30, and 8.0% ± 0.29, respectively. When compared with NPRS-treated mice, a significant reduction in i-NOS expression was found following nMgO (44.73%), UNF (63.55%), and CNF (78.94%) treatment.

The expression of apoptotic marker cleaved activated caspase-3 which is absent under normal conditions and detectable only during cell apoptosis was used successfully, to detect the activation of the apoptotic mechanism within tissues (Fig. 5.14 C). Using the active cleaved caspase-3, a higher number of positive cardiomyocytes were observed ($p < 0.001$) in NPRS-treated heart tissues compared to the untreated control and other treatment groups ($p < 0.001$). On the other, compared to the control, the number of cardiomyocytes positive for cleaved- caspase-3 declined by 52% in CNF treated heart tissue section. Similarly, the numbers of cleaved caspase-3 activated cardiomyocytes were reduced by 65% and 77% in UNF and nMgO treated groups respectively.

In terms of percent area, positive staining for cleaved caspase-3 was observed in heart sections, the untreated/ control groups showed 21.0% ± 1.075, NPRS; 43.0± 0.86, nMgO; 9.96 ± 0.52, UNF; 15.76 ± 0.55 and, CNF; 20.62 ± 0.09. These results indicated that the positively stained cardiomyocytes in groups other than NPRS were not statistically different from untreated sections. However, compared to control, NPRS-treated hearts showed a significant increase ($p < 0.001$) in cleaved caspase-3 expression by 53.61%.

In liver tissue (Fig. 5.15), the highest NF-κB expression with a positive percent area of 75.11 ± 2.481 ($p < 0.001$) was found in NPRS-treated mice compared to all other treatment groups, while NF-κB expression decreased clearly in UNF and CNF treated groups with positively stained areas found to be 15.2 ± 1.82 % and 15.25 ± 0.8% respectively. These levels were markedly lower than those shown by NPRS treated group and were nearly equivalent to the control group (19.79 ± 0.75). However, nMgO

treated group showed a relatively higher level of NF-κB expression (p<0.001) as compared to the control, UNF, and CNF.

Likewise, an expression of COX-2 in liver tissues indicated that the number of positively stained hepatocytes in terms of percent area was found to be highest in the NPRS treatment group; 53.36 ± 3.15 (p<0.001). Whereas treatment with the same dose downregulated the expression of COX-2 enzyme with 14.79 ± 1.59 % (p<0.001) positively stained hepatocytes in nMgO treated group (p<0.001), 22.15±2.04 % following UNF treatment and 23.43±1.50 % caused by CNF treatment. Statistically, UNF, CNF, and nMgO treatment led to significantly lowered COX-2 expression as compared to the NPRS treated group and the results obtained were comparable to those shown by the control groups, 20.79±1.19 %. As regards the percent decrease in COX-2 expression showed by nMgO, UNF, and compared to CNF, NPRS treatment, a decline of 73.5 %, 58.49 %, and 56.6 % respectively, was noticeable.

Expression of cleaved caspase-3 levels revealed that NPRS caused the highest level of apoptosis in mice liver tissues, with 36.15±0.98 % apoptotic hepatocytes, while treatment with nMgO, UNF, and CNF caused only, 14±0.51 %, 10.23±0.38 %, and 21.2 ±1.15 % hepatocytic apoptosis. When compared statistically, the apoptosis level in nMgO, UNF, and CNF were comparable to those found in the control liver, while the highest (p<0.001) levels were found in NPRS-treated hepatocytes compared to all groups.

Immunohistochemical analysis showed that COX-2 expression in kidneys (Fig. 5.16 A) was downregulated by UNF and CNF, while treatment with NPRS led to a significant elevation in COX-2 levels (p<0.001) in experimental mice. As indicated in the data obtained, the percent COX-2-stained area in NPRS-treated kidney sections was 55.52 ± 2.44 %, while it was found to be 30±1.25 %, 25.84±1.08 %, and 17.03±0.64 % in nMgO, UNF, and CNF treated kidney tissues. Surprisingly, in control kidneys, the positively stained area was found to be 32±0.83%, which indicated that results from nMgO, UNF, and CNF were comparable to those of control.

The percent positive area for iNOS in NPRS-treated kidneys was highest among all groups (38.78 ± 1.50). While treatment with UNF and CNF significantly downregulated the iNOS expression with only 14.65±0.38 and 11.68±0.47 percent positive area. In

control mice, 11±1.16 % of the total area was found to be i-NOS positive (Fig. 5.16 B).

Moreover, significant elevation (p<0.001) in cleaved caspase-3 expression was found when the mice were treated with NPRS compared to UNF and CNF administered groups as shown in Fig. 5.16 (C). Lastly, the stomach tissues obtained from various treatment groups were also studied for COX-2, iNOS, and cleaved caspase-3 immunostaining (Fig. 5.17). In NPRS treated group, intense and severe COX-2 (34±1.42 percent-stained area), i-NOS (38.43±0.55), and cleaved caspase-3 (43.11±0.86) immunoreactivity were detected in the stomach mucosa, foveola epithelium and parietal cells, and vascular endothelium near to submucosa. However, this activity effectively declined (p<0.001) in stomach tissues following treatment with UNF and CNF as shown in Fig. 5.17 (A, B, C). Statistically, compared to NPRS, treatment with UNF led to a significant decline (p<0.001) in 32% percent COX-2 expression (23±0.76 positive stained area), whereas treatment with CNF, caused a 47% decrease (p<0.001) in COX-2 expression (18.75±1.14), in stomach tissues. nMgO on the other resulted in a percent decrease (p<0.001) by 55% (15±1) compared to the NPRS treatment. In control mice, the COX-2 positive area was found to be 25±0.55%.

Similar results were obtained for iNOS expression in stomach tissues following NPRS, nMgO, UNF, and CNF treatment. Protein expression analysis revealed that iNOS expression significantly upregulated following NPRS treatment (38.43±0.55). While a significant downregulation was observed in nMgO (21.49±1.30), UNF (13.85±0.54), and CNF (08.05±0.29) compared to the NPRS. Where, the values observed in nMgO, UNF, and CNF neared control (17.89±0.41).

Likewise, cleaved caspase-3 tissue expression was found to be highest in NPRS (43.11±0.86) treatment group compared to the control (21.96±1.07), nMgO (9.96±0.52), UNF (15.76±0.55), and CNF (20.62±0.90). As indicated in the data, treatment with UNF and CNF led to a significant decrease in gastric cell apoptosis.

5.22 Effect of Experimental Doses on the mRNA Expression of IL-6, IL1β, and TNF-α in Mice Tissues

To understand the underlying molecular mechanisms, behind pathological changes and cellular damage observed in treated animals, following various treatments, the expression of pro-inflammatory cytokines IL-6, IL1β, and TNF-α mRNA was studied

in the heart, and liver, kidney, and stomach tissues.

In the heart tissue (Fig. 5.18), NPRS exposure significantly increased IL-6 (A), IL1β (B), and TNF-α (C) gene expression as compared to the control group ($p < 0.001$), nMgO, UNF, and CNF. In contrast, there was no significant difference in the levels of IL-6, IL1β, and TNF-α observed between the nMgO, UNF, and CNF group and control. Comparison among UNF and CNF treated groups showed that the CNF suppressed/downregulated all three cytokine expressions more efficiently ($p < 0.05$-0.01) than its uncoated form.

In liver tissue (Fig. 5.19), a similar pattern of IL-6 (A), IL1β (B), and TNF-α (C) mRNA expression levels was observed, where the mRNA expression of all the three cytokines markedly increased ($p < 0.001$) following treatment with NPRS, compared to the control. Whereas there was no significant difference in the levels of IL-6, IL1β, and TNF-α mRNA expression was found between the nMgO, UNF, and CNF group and control. Although the levels of IL-6, IL1β, and TNF-α decreased significantly ($p < 0.05$) in UNF and CNF groups.

Following NPRS treatment, the assessment of IL-6, IL1β, and TNF-α mRNA through real-time PCR demonstrated increased ($p < 0.001$) expression in the kidney tissues (Fig. 5.20) when compared with the control. While the levels of these cytokines remained unaffected in nMgO, UNF and CNF treated groups and values obtained were comparable to those of control. Compared to NPRS treated group, the mRNA levels for the same cytokines were decreased in UNF and CNF treatment groups. Moreover, the expression level of IL-6, IL1β, and TNF-α were found lower ($p < 0.05$) in the kidneys of the CNF-treated group compared to UNF.

Compared to the control, in the stomach (Fig. 5.21), the IL-6 (A), IL1β (B), and TNF-α (C) mRNA expression levels were significantly higher only in the NPRS group ($p < 0.001$). In contrast, the mRNA expression of IL-6, IL1β, and TNF-α mRNA was significantly lower in the nMgO, UNF, and CNF ($p < 0.01$-0.001) group than in the NPRS-only group, and levels were found to compare to those of control tissues. Additionally, the treatment with CNF led to a significant decline in IL-6, IL1β, and TNF-α mRNA expression compared to its uncoated form (UNF).

A

B
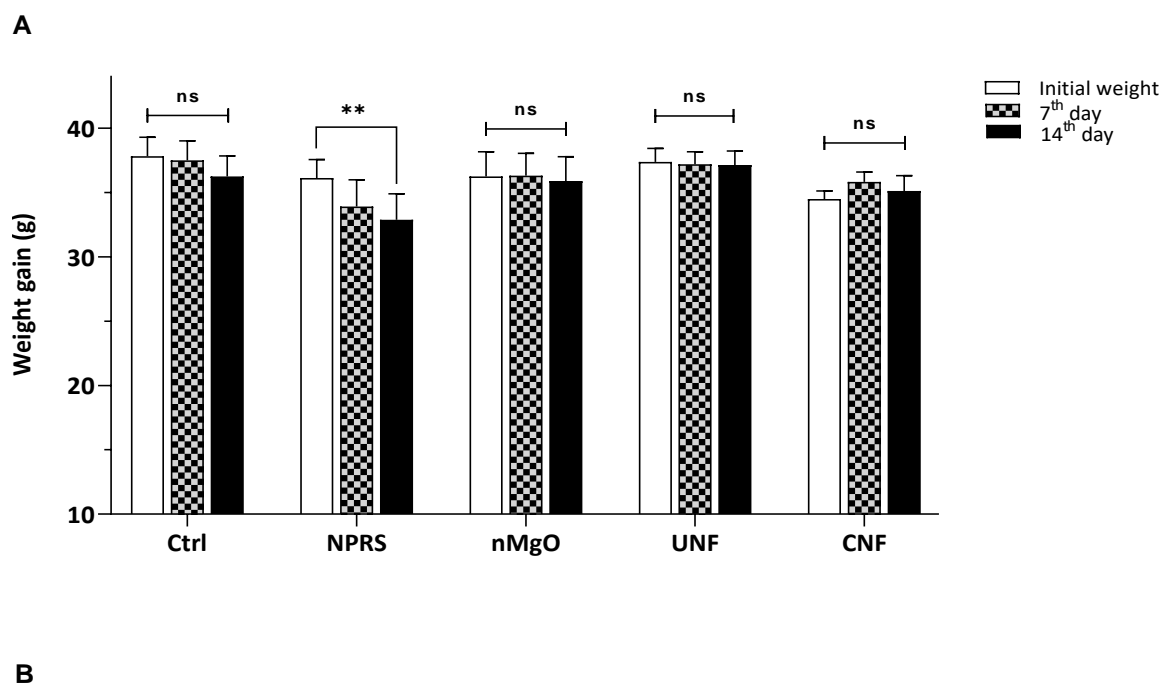
Fig. 5.3 Body weight changes of mice treated with the naproxen sodium (NPRS), blank nMgO, uncoated naproxen nanoformulation (UNF), and coated naproxen nanoformulation (CNF) (A). Absolute and relative organ weights of heart, liver, kidneys, and stomach of treatment groups. Values are expressed as mean±s.e. (n = 8). *p<0.05, **p<0.01, ***p<0.001, ns= non-significant, compared with the control (B).
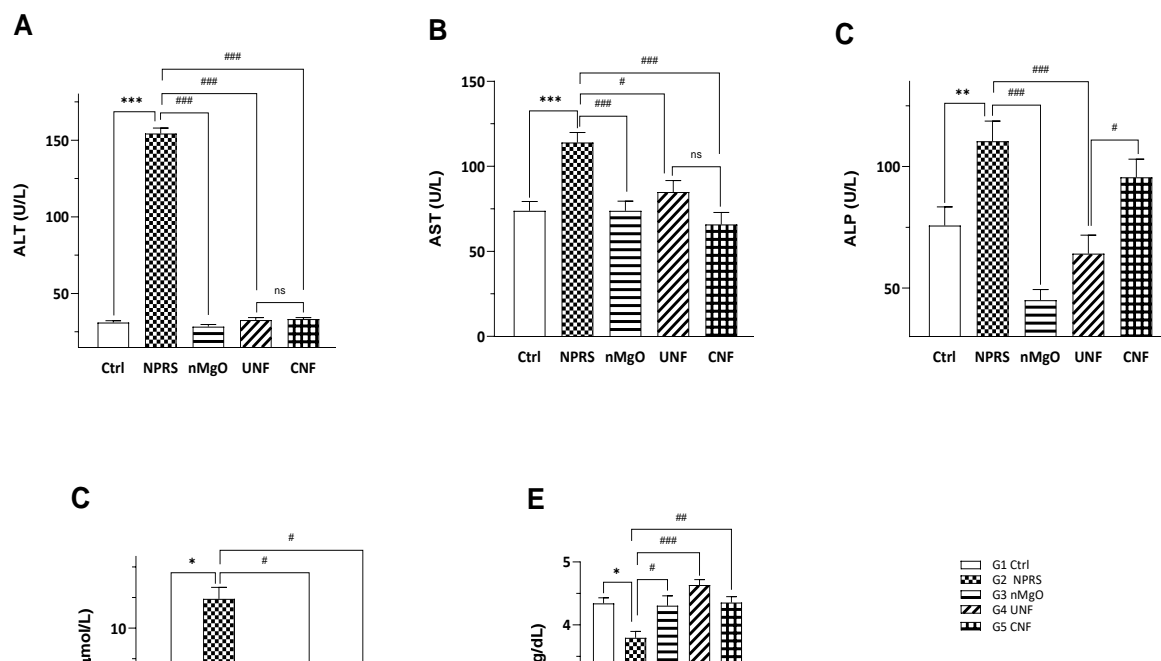
Fig. 5.4 The effect of NPRS, nMgO, UNF and CNF on the serum ALT, AST, ALP, serum creatinine and bilirubin (total and direct) levels in male mice (A) Serum ALT levels, (B) Serum AST levels, (C) Serum ALP levels, (D) Serum creatinine, (E) Serum bilirubin levels. All values are expressed as mean±s.e. (n = 8). *p<0.05, **p<0.01, ***p<0.001, compared with the control. Whereas #p<0.05, ##p<0.01, ###p<0.001, among treatment groups other than the control. ns= non-significant; ALT, alanine aminotransferase; ALP, alanine phosphate; AST, aspartate
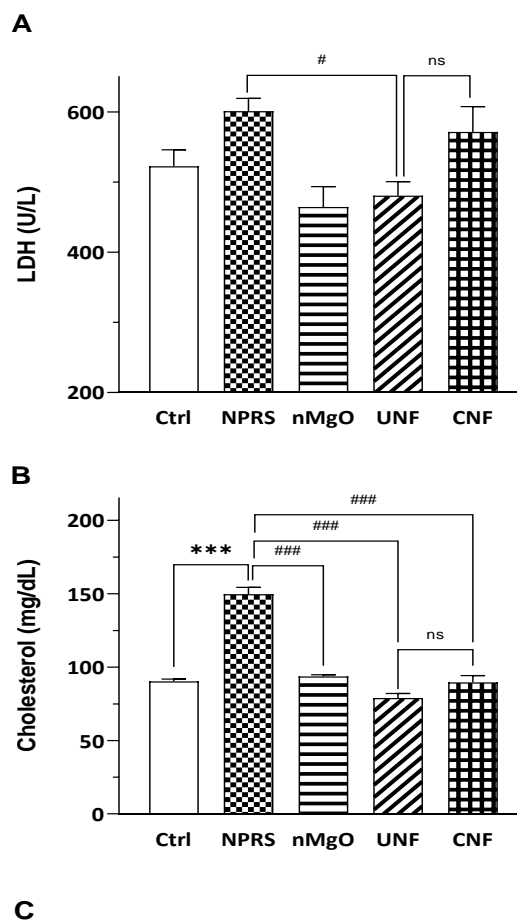
Fig. 5.5 The effect of NPRS, nMgO, UNF and CNF on the serum LDH, cholesterol and triglycerides levels in male mice (A) Serum LDH levels, (B) Serum cholesterol, and (C) Serum triglycerides levels. All values are expressed as mean±s.e. (n = 8). *p<0.05, **p<0.01, ***p<0.001, compared with the control. Whereas #p<0.05, ##p<0.01, ###p<0.001, among treatment groups other than the control. ns= non-significant; LDH, lactate dehydrogenase.

A

B
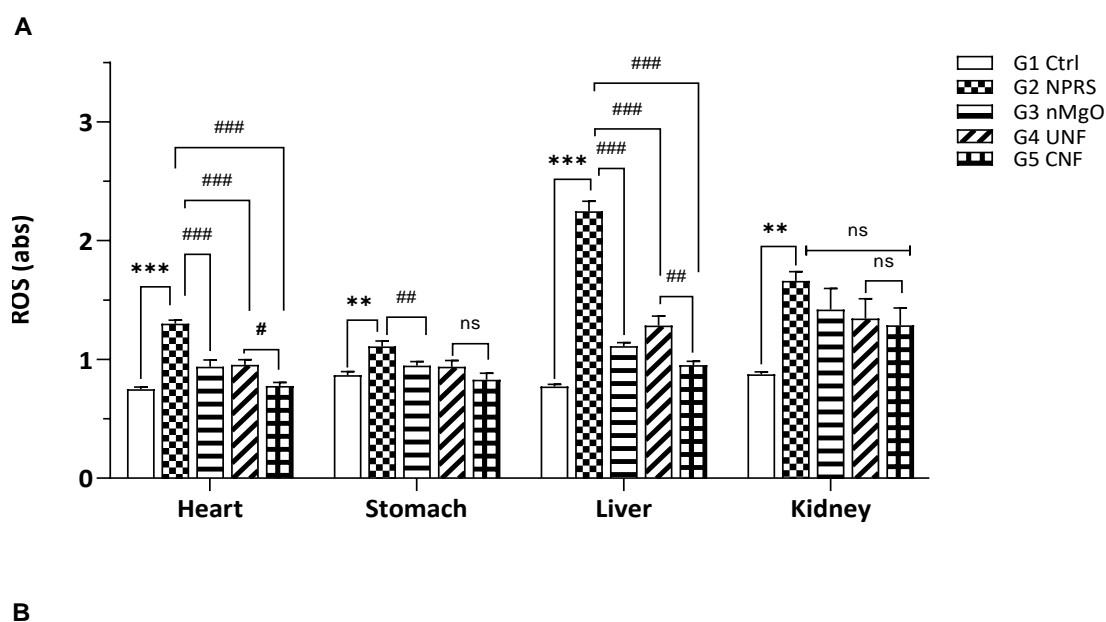
Fig. 5.6 The effect of NPRS, nMgO, UNF and CNF on ROS (A) and LPO (B) levels in male mice tissues. All values are expressed as mean±s.e. (n= 8). *p<0.05, **p<0.01, ***p<0.001, compared with the control. Whereas #p<0.05, ##p<0.01, ###p<0.001, among treatment groups other than the control. ns= non-significant; ROS, reactive oxygen species; LPO, lipid peroxidase.

A

B
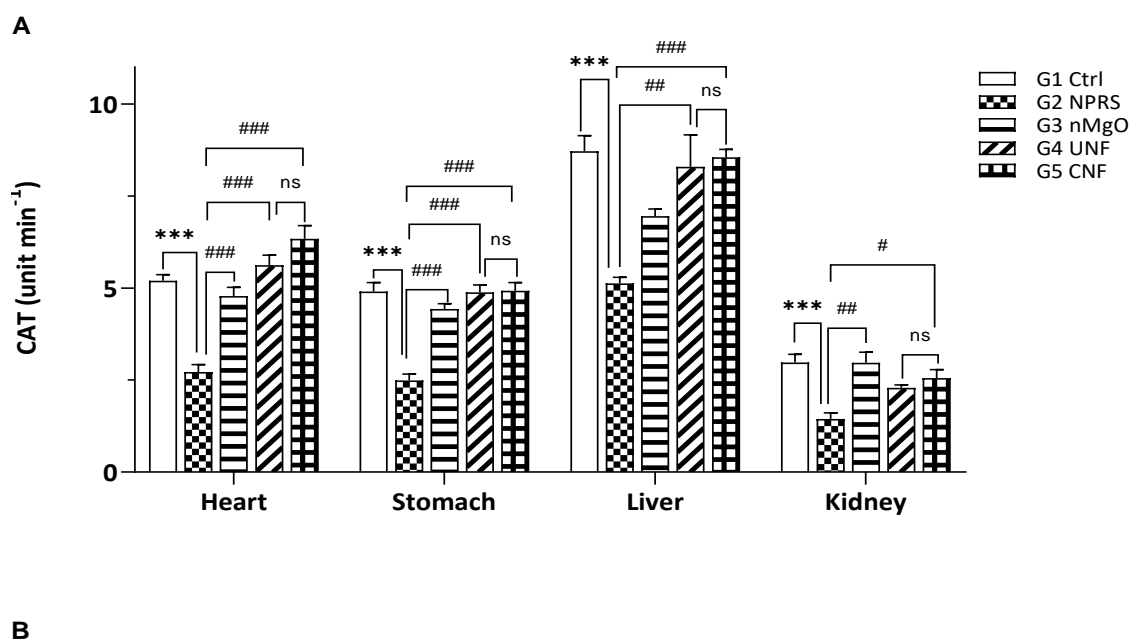
Fig. 5.7 The effect of NPRS, nMgO, UNF and CNF on CAT (A) and SOD (B) levels in male mice tissues. All values are expressed as mean±s.e. (n= 8). *p<0.05, **p<0.01, ***p<0.001, compared with the control. Whereas #p<0.05, ##p<0.01, ###p<0.001, among treatment groups other than the control. ns= non-significant, CAT, catalase; SOD, superoxidase dismutase.

A

B
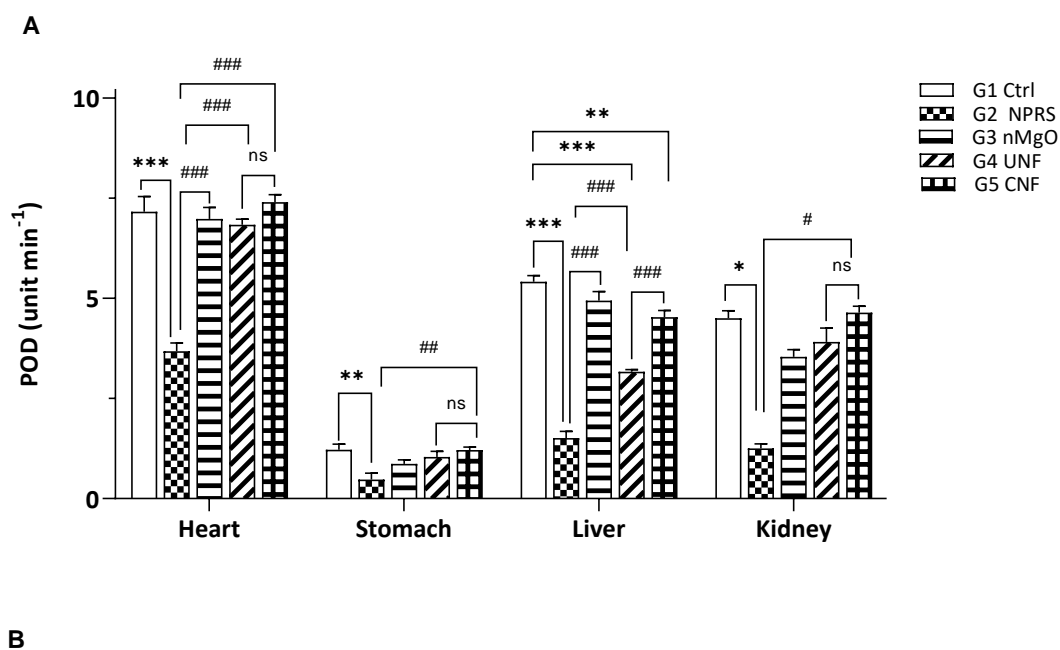
Fig. 5.8 The effect of NPRS, nMgO, UNF and CNF on POD (A) and GSH (B) levels in male mice tissues. All values are expressed as mean±s.e. (n= 8). *p<0.05, **p<0.01, ***p<0.001, compared with the control. Whereas #p<0.05, ##p<0.01, ###p<0.001, among treatment groups other than the control, ns= non-significant; POD, peroxidase; GSH, glutathione enzyme.
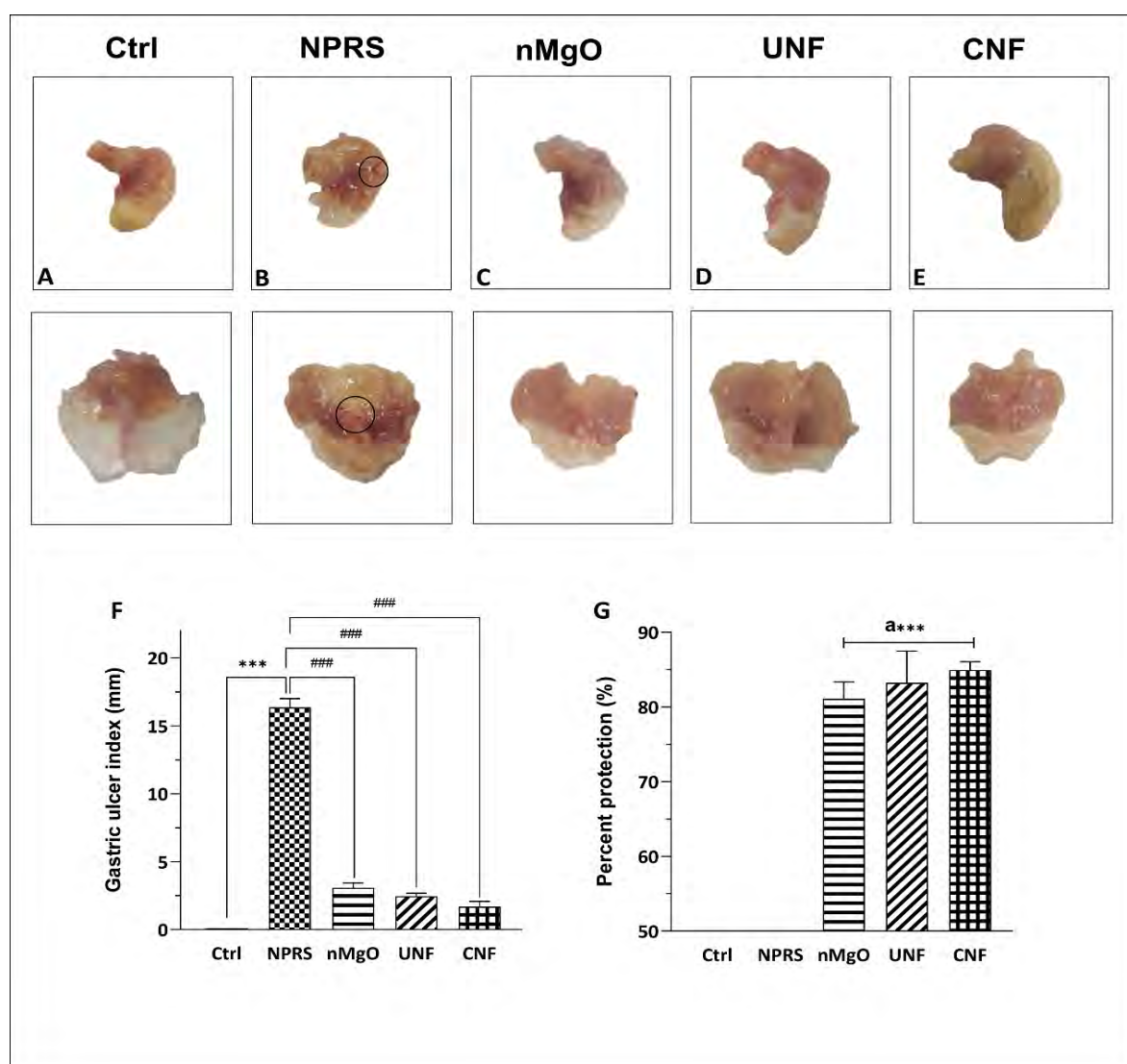
Fig. 5.9 Evaluation of naproxen sodium (NPRS), its nanocarrier (nMgO), and nanoformulation (UNF, CNF) induced stomach ulcer following 14-day oral treatment. Macroscopic morphology of the gastric mucosa of mice challenged with various treatments (A-E). The mean gastric ulcer index of each group (F). Percent inhibition in stomach ulcers compared to the model drug (NPRS). Each column represents the mean±s.e.(n= 6). *p<0.05, **p<0.01, ***p<0.001, compared with the control, whereas a*** versus NPRS (p < 0.001).

Fig. 5.10 Representative photomicrographs of control and treated heart sections of male mice stained with hematoxylin and eosin (H&E) (A) normal heart, (B) treated with Naproxen sodium; (C) treated with blank magnesium oxide nanoparticles; (D) treated with uncoated naproxen nanoformulation and, (E) treated with coated naproxen nanoformulation. MC= Myocardial cells, N= Nucleus, SV= Sarcoplasmic vacuolation DMF= Degenerated muscle fibers. Magnification 10x (left column) and 40x (right column); Scale bar = 100 μm.
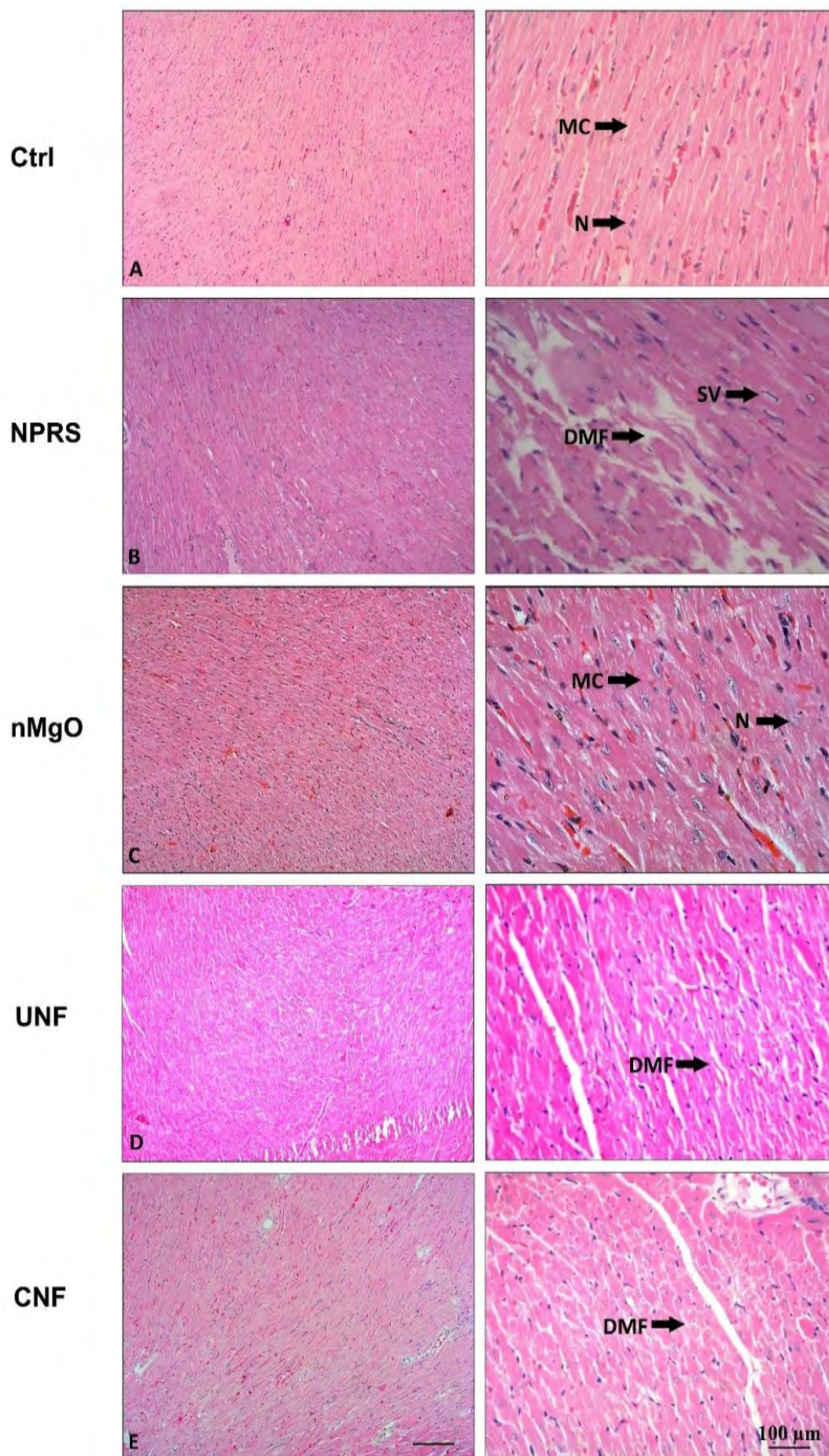
Fig. 5.11 Representative photomicrographs of control and treated liver sections of male mice stained with hematoxylin and eosin (H&E) (A) normal liver, (B) treated with Naproxen sodium; (C) treated with blank magnesium oxide nanoparticles; (D) treated with uncoated naproxen nanoformulation and, (E) treated with coated naproxen nanoformulation. CV= Central vein, SD= Sinusoidal dilation, KC= Kupffer cell, HC= Hepatic cells, IFC= Inflammatory cell concentrate. Magnification 10x (left column) and 40x (right column); Scale bar = 100 μm.
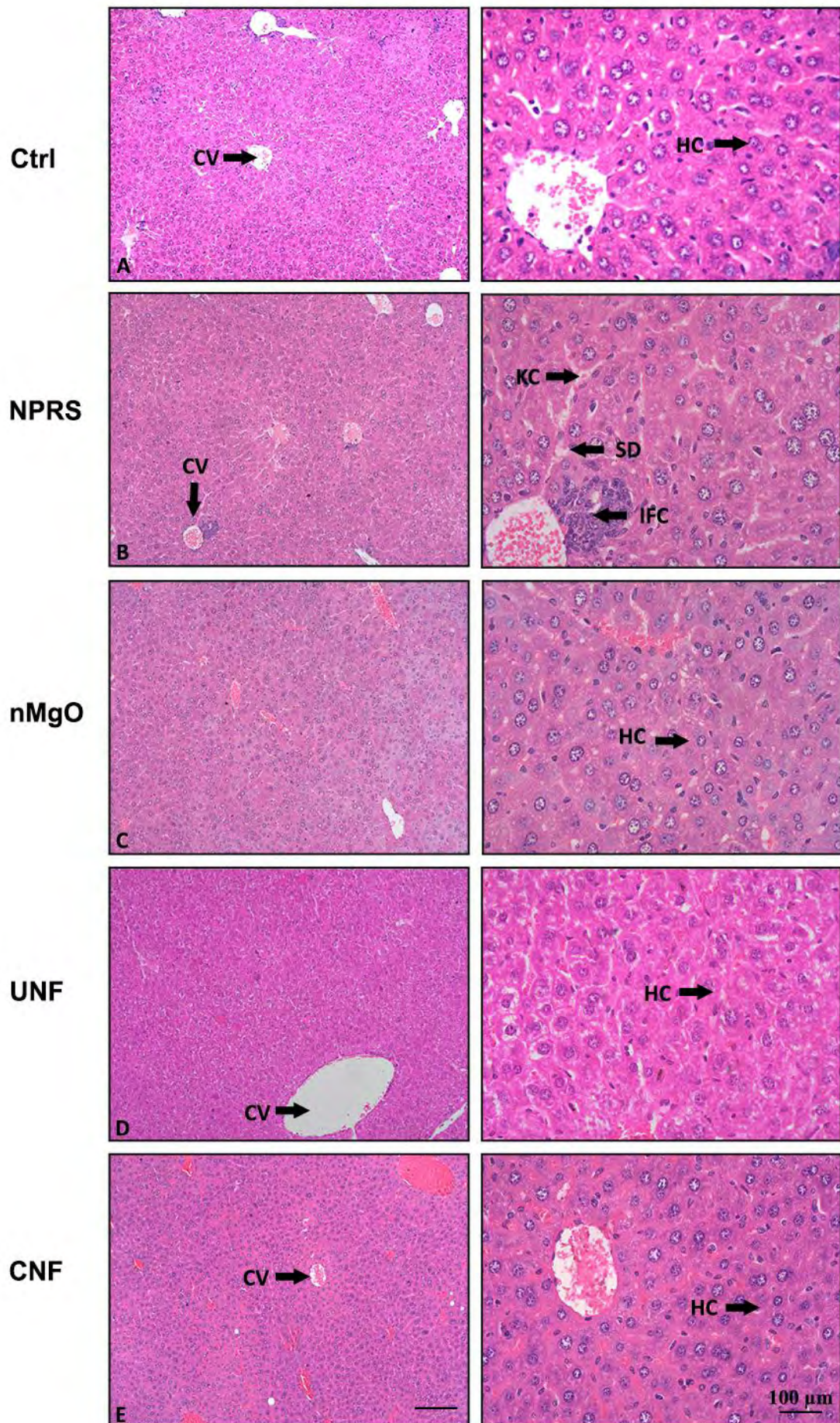
Fig. 5.12 Representative photomicrographs of control and treated kidney sections of male mice stained with hematoxylin and eosin (H&E) (A) normal kidney, (B) treated with Naproxen sodium; (C) treated with blank magnesium oxide nanoparticles; (D) treated with uncoated naproxen nanoformulation and, (E) treated with coated naproxen nanoformulation. G= Glomeruli, BS= Bowman's spaces, VC= Visceral cell, DT= Distal tubule, PT= Proximal tubule TD= Tubular Dilation, IFC= Inflammatory cell infiltrate. Magnification 10x (left column) and 40x (right column); Scale bar = 100 μm.
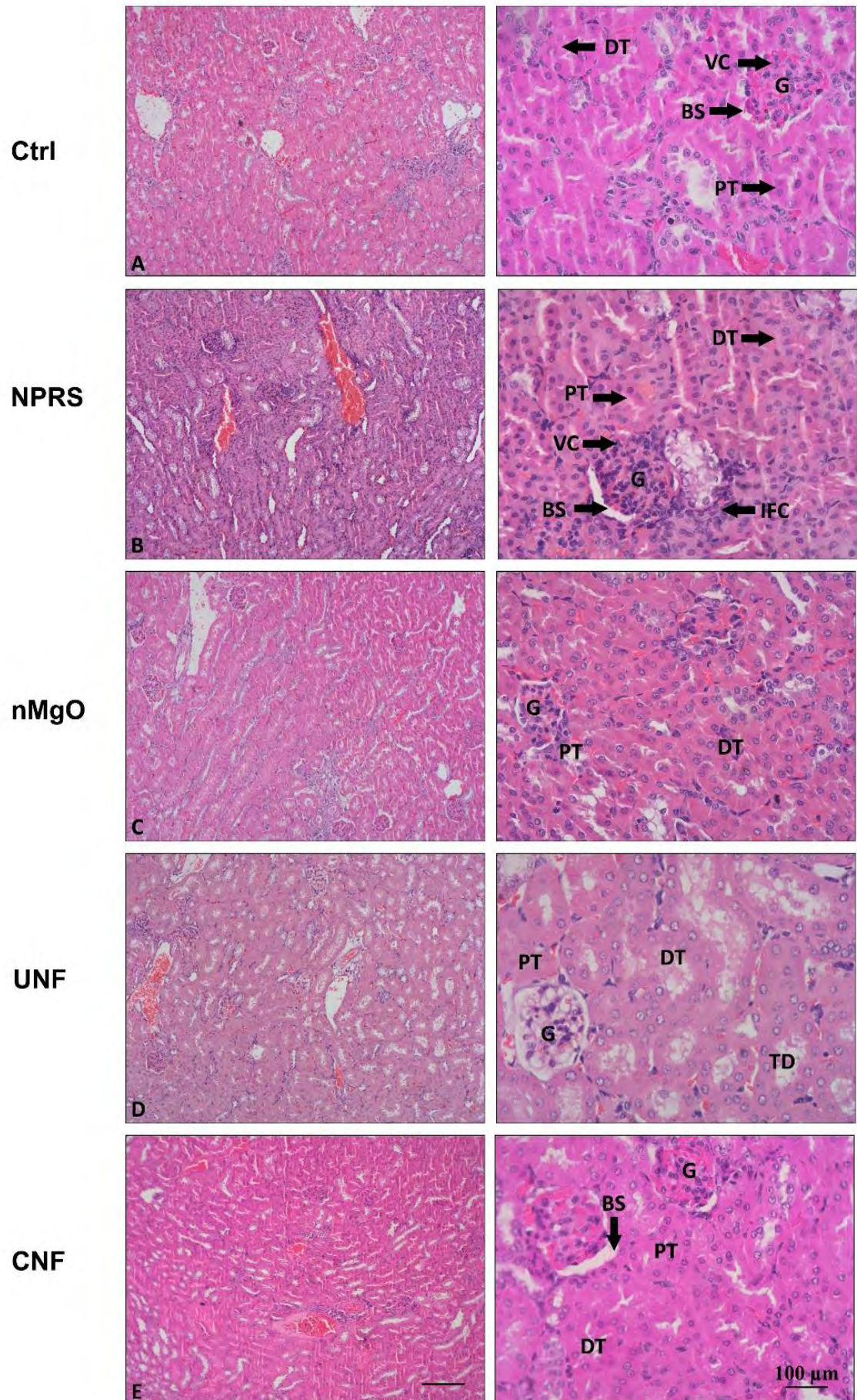
Fig. 5.13 Representative photomicrographs of control and treated stomach sections of male mice stained with hematoxylin and eosin (H&E) (A) normal stomach, (B) treated with Naproxen sodium; (C) treated with blank magnesium oxide nanoparticles; (D) treated with uncoated naproxen nanoformulation and, (E) treated with coated naproxen nanoformulation. ML= Mucosal layer, SML= Sub-mucosal layer, F= Foveolar cells P= Gastric pits, Square shape indicates gastric ulceration. Magnification 10x (left column) and 40x (right column); Scale bar = 100 μm.
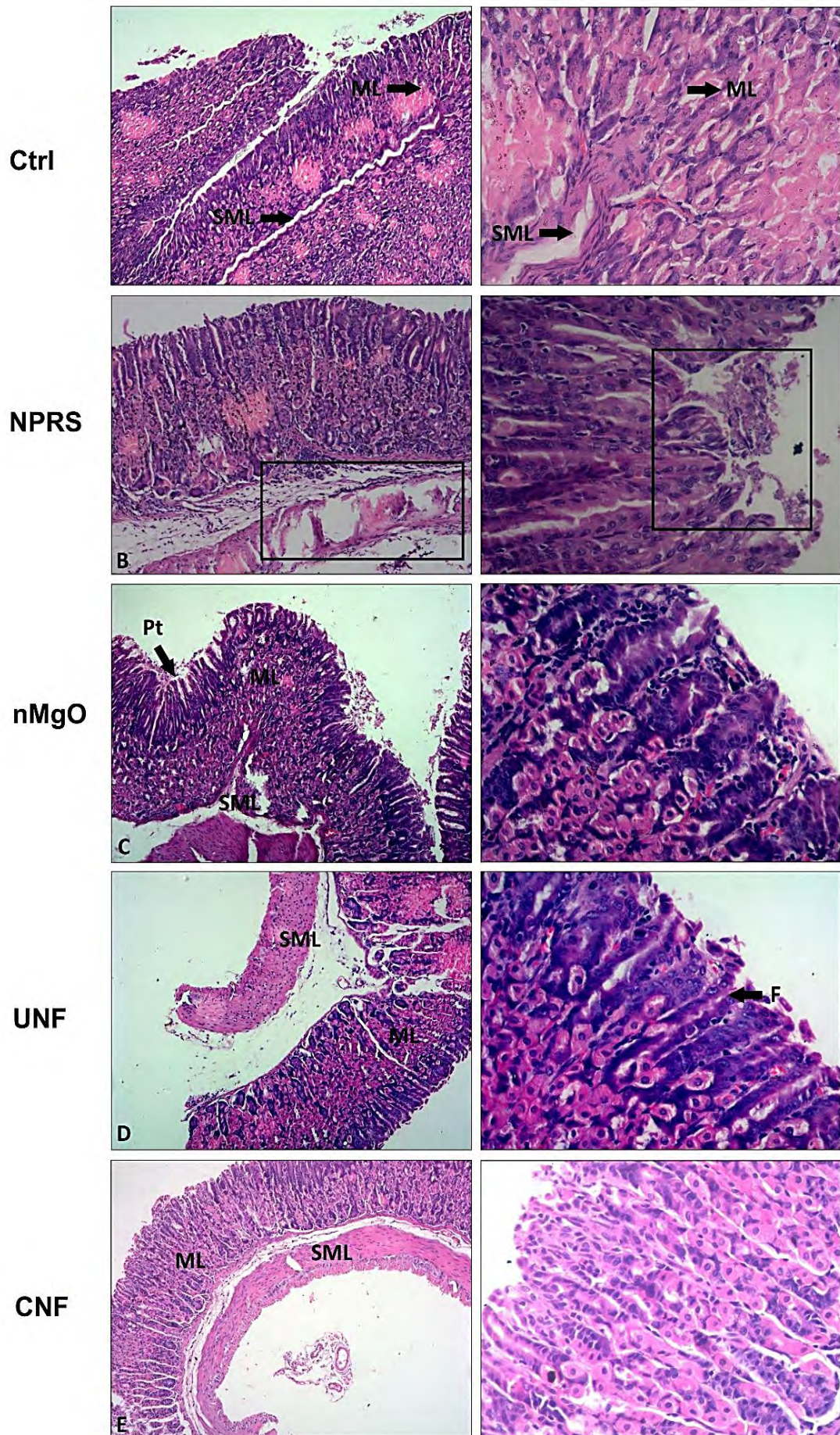
Fig. 5.14. The IHC positive staining (% area) of COX-2 (A), i-NOS (B) and cleaved caspase-3 (C) in heart tissue following treatment with NPRS, nMgO, UNF and CNF. All values are expressed as mean±s.e.(n= 6). $*p < 0.05$, $**p < 0.01$, $***p < 0.001$, compared with the control. Whereas #p<0.05, ##p<0.01, ###p<0.001, among treatment groups other than the control, ns= non-significant.
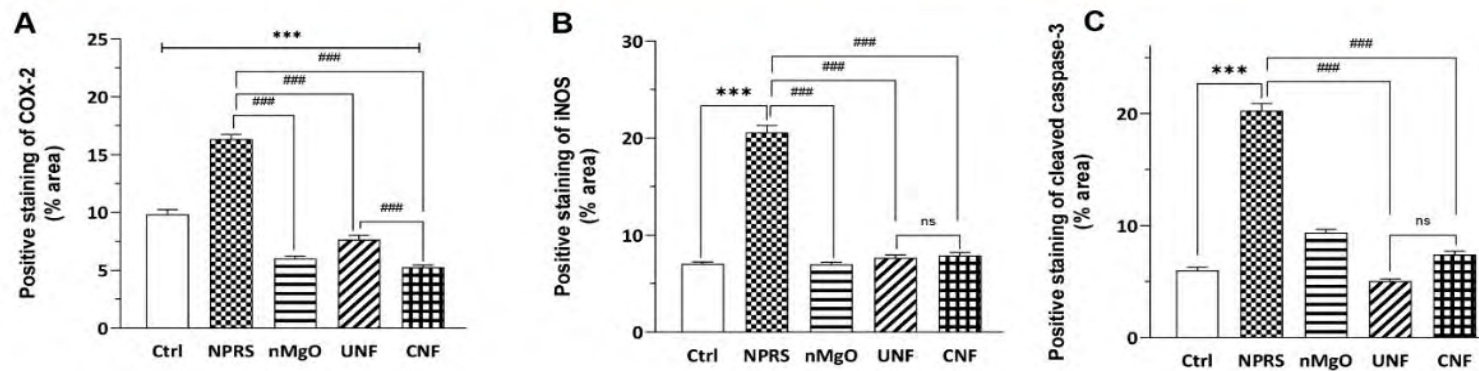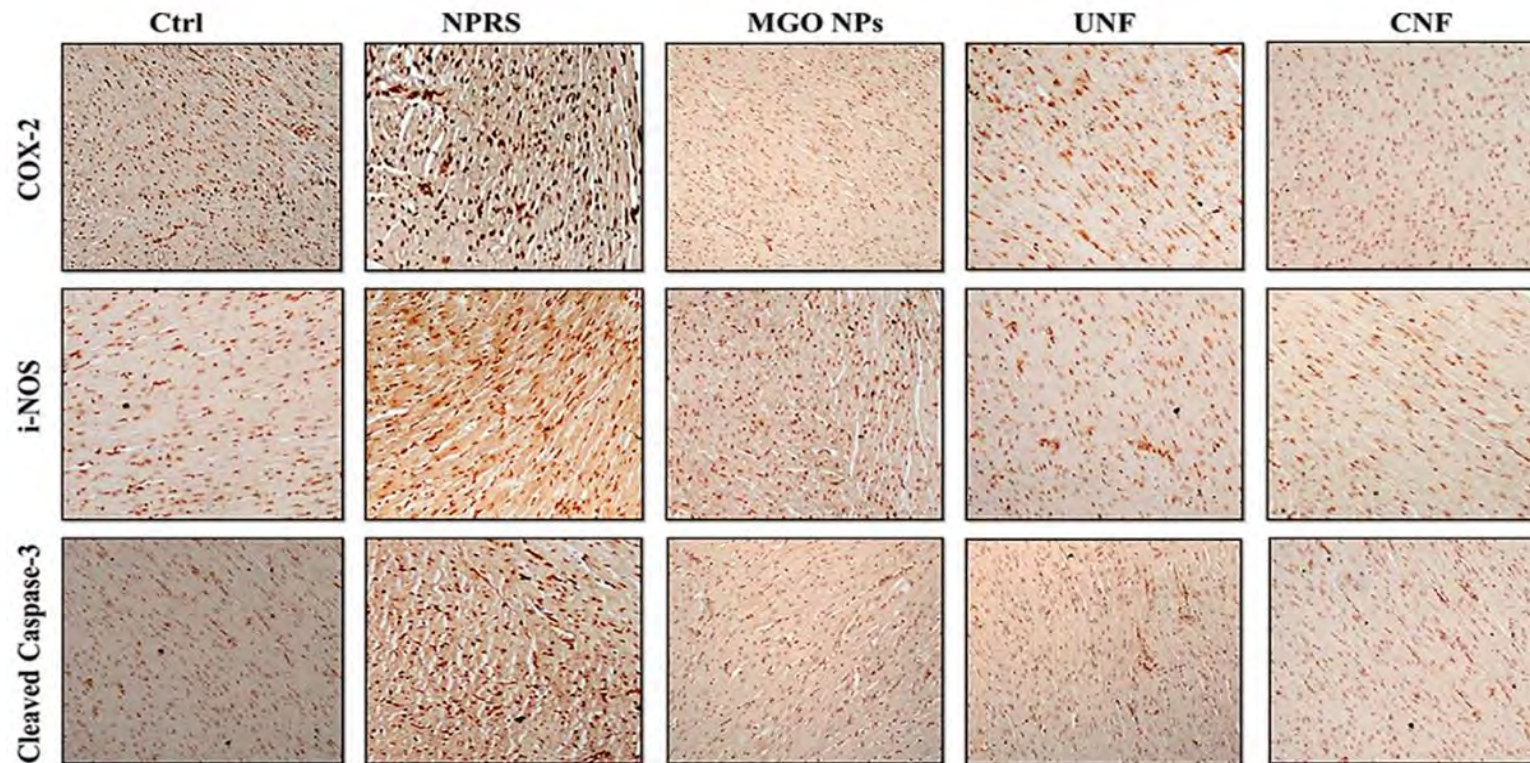
Fig. 5.15 The IHC positive staining (% area) of NFκB (A), COX-2 (B) and cleaved caspase-3 (C) in liver tissue following treatment with NPRS, nMgO, UNF and CNF. All values are expressed as mean±s.e. (n= 6). $*p<0.05$, $**p<0.01$, $***p<0.001$, compared with the control. Whereas $\#p<0.05$, $\#\#p<0.01$, $\#\#\#p<0.001$, among treatment groups other than the control, ns= non-significant.
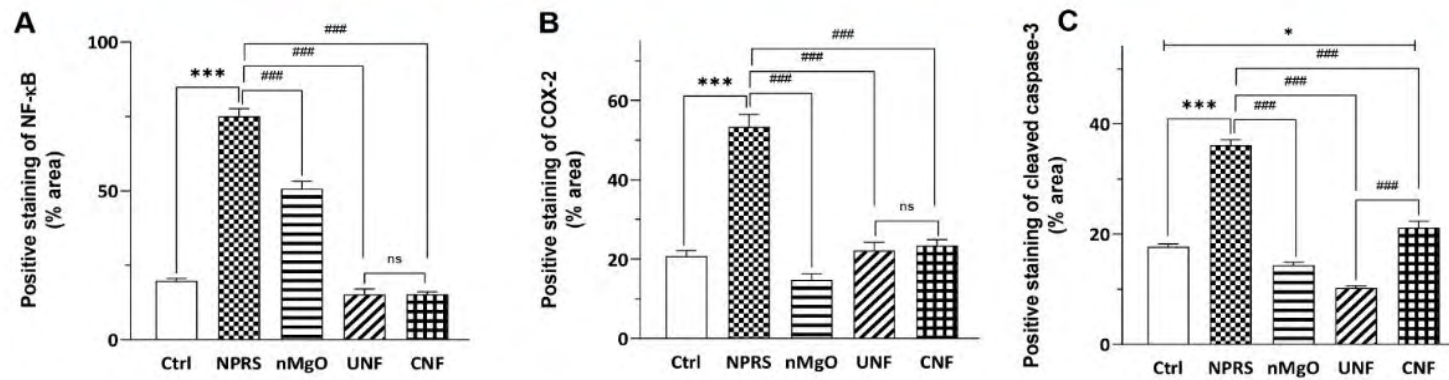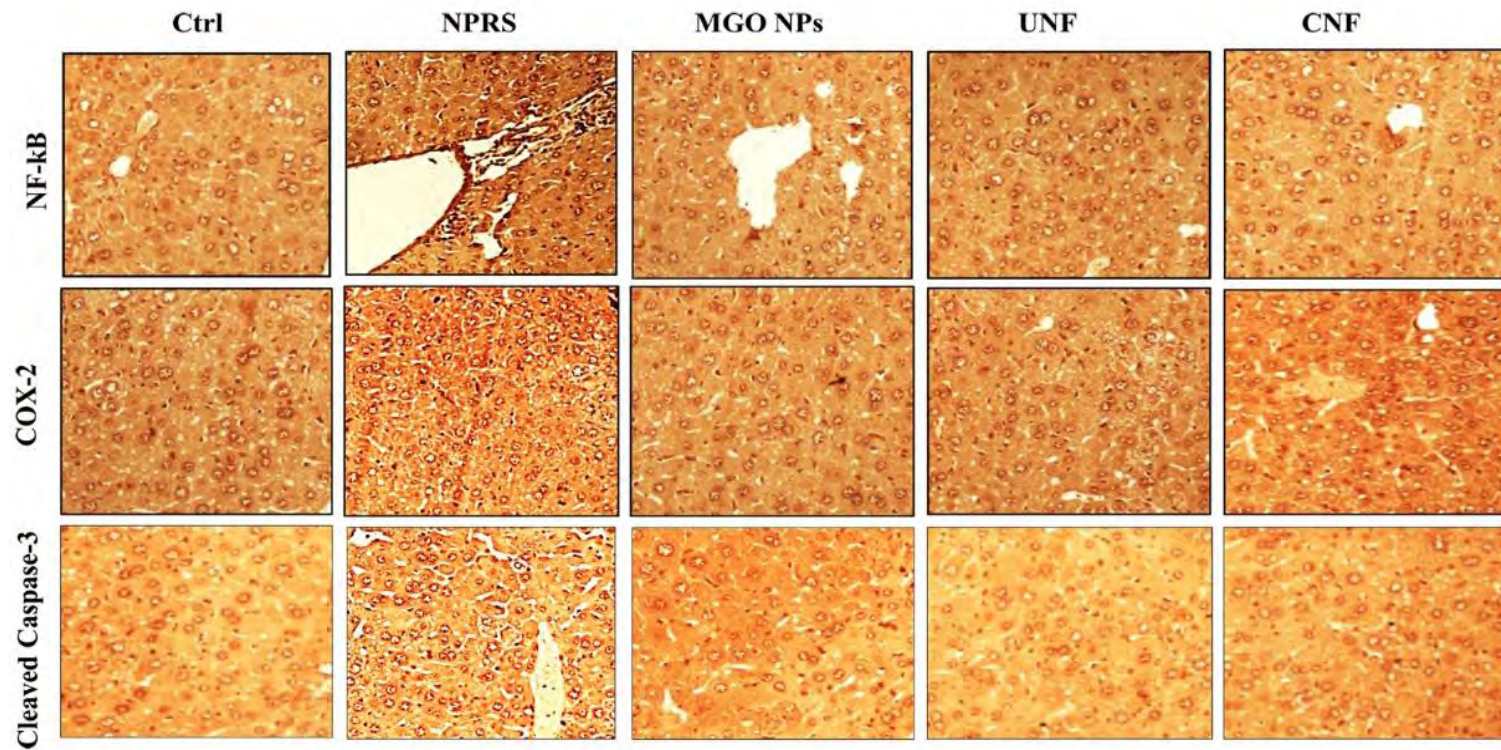
Fig. 5.16 The IHC positive staining (% area) of COX-2 (A), i-NOS (B) and cleaved caspase-3 (C) in kidney tissue following treatment with NPRS, nMgO, UNF and CNF. All values are expressed as mean±s.e. (n= 6). $*p<0.05$, $**p<0.01$, $***p<0.001$, compared with the control. Whereas $\#p<0.05$, $\#\#p<0.01$, $\#\#\#p<0.001$, among treatment groups other than the control, ns= non-significant.
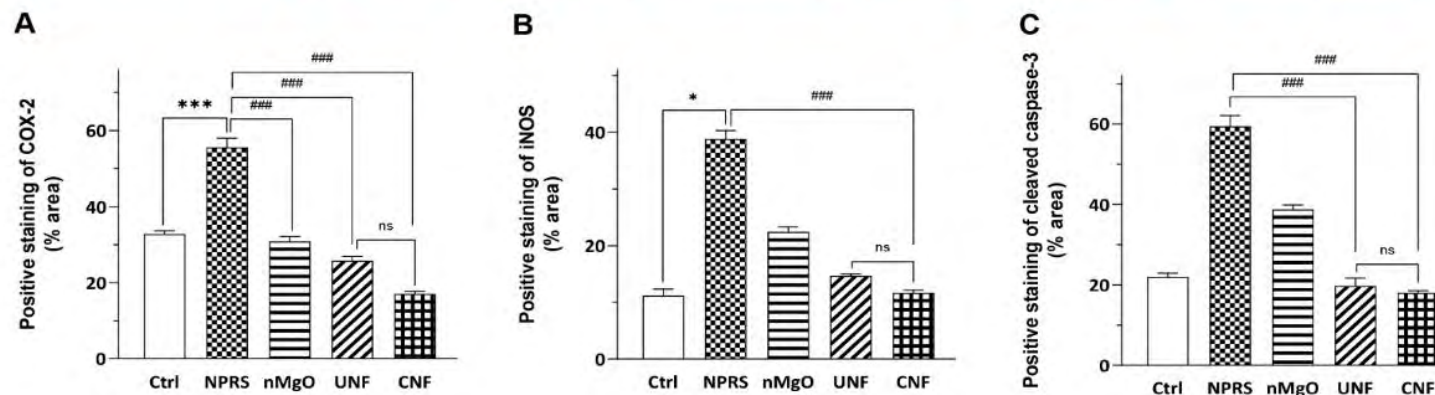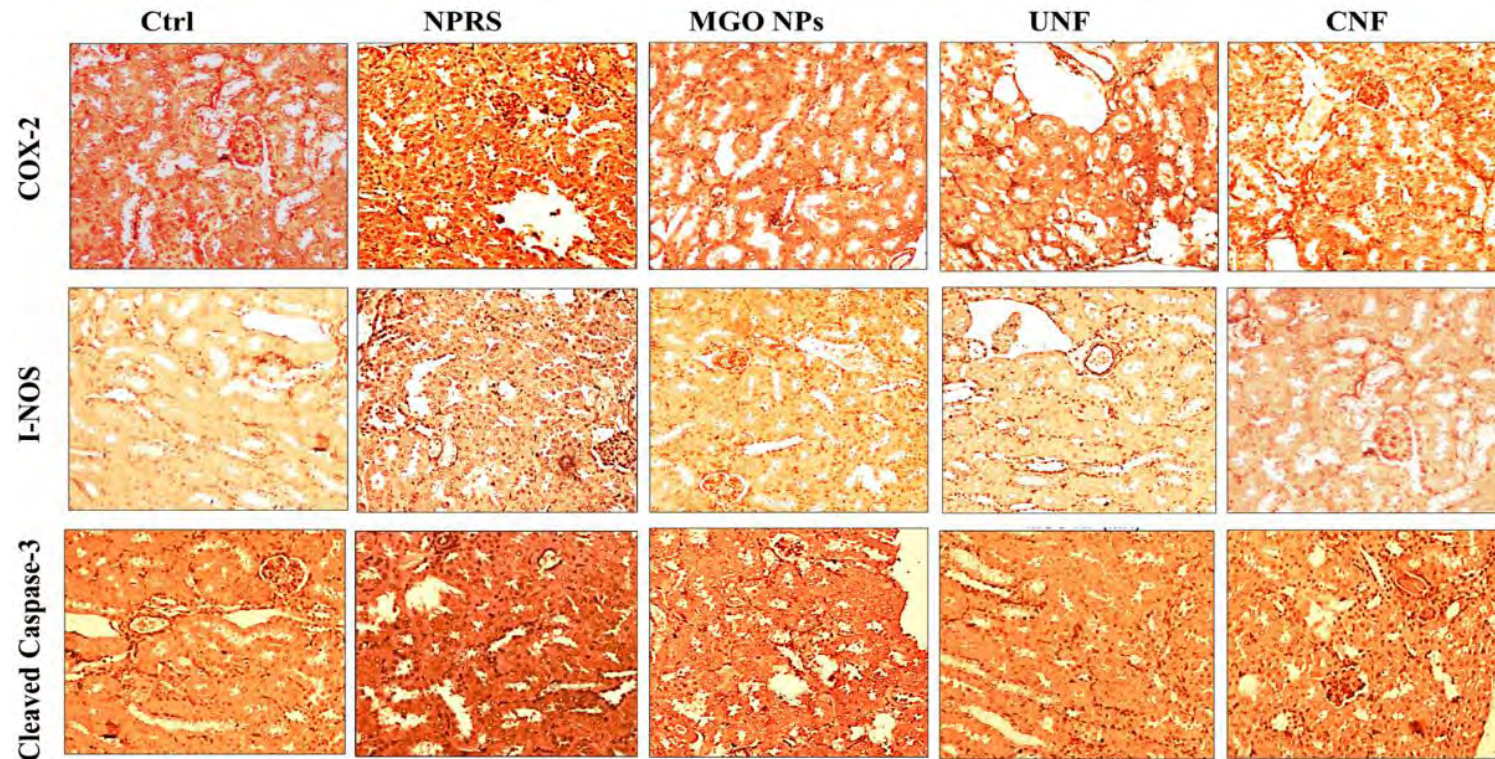
Fig. 5.17 The IHC positive staining (% area) of COX-2 (A), i-NOS (B) and cleaved caspase-3 (C) in stomach tissue following treatment with NPRS, nMgO, UNF and CNF. All values are expressed as mean±s.e. (n= 6). $*p<0.05$, $**p<0.01$, $***p<0.001$, compared with the control. Whereas $\#p<0.05$, $\#\#p<0.01$, $\#\#\#p<0.001$, among treatment groups other than the control, ns= non-significant.
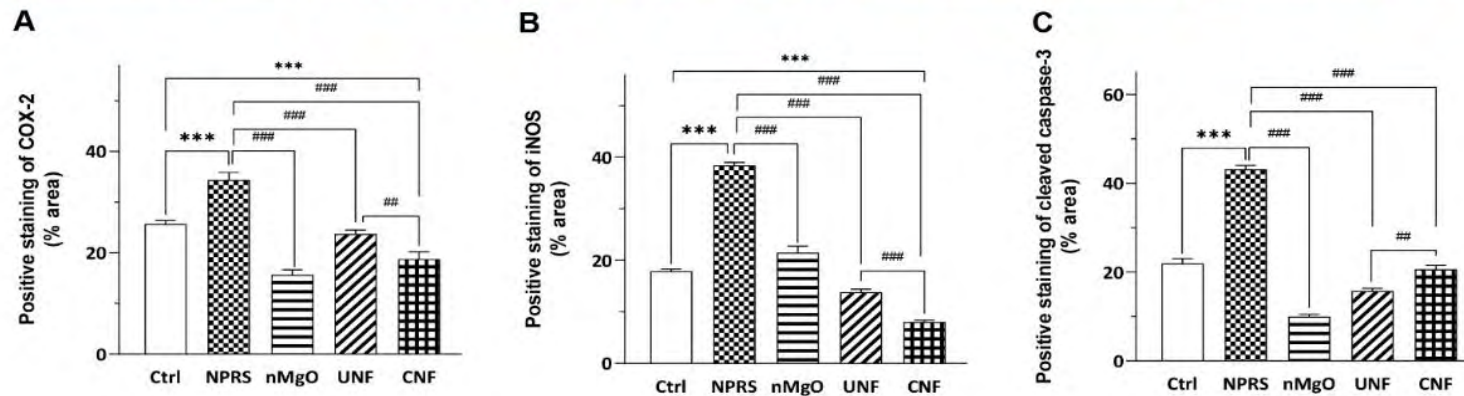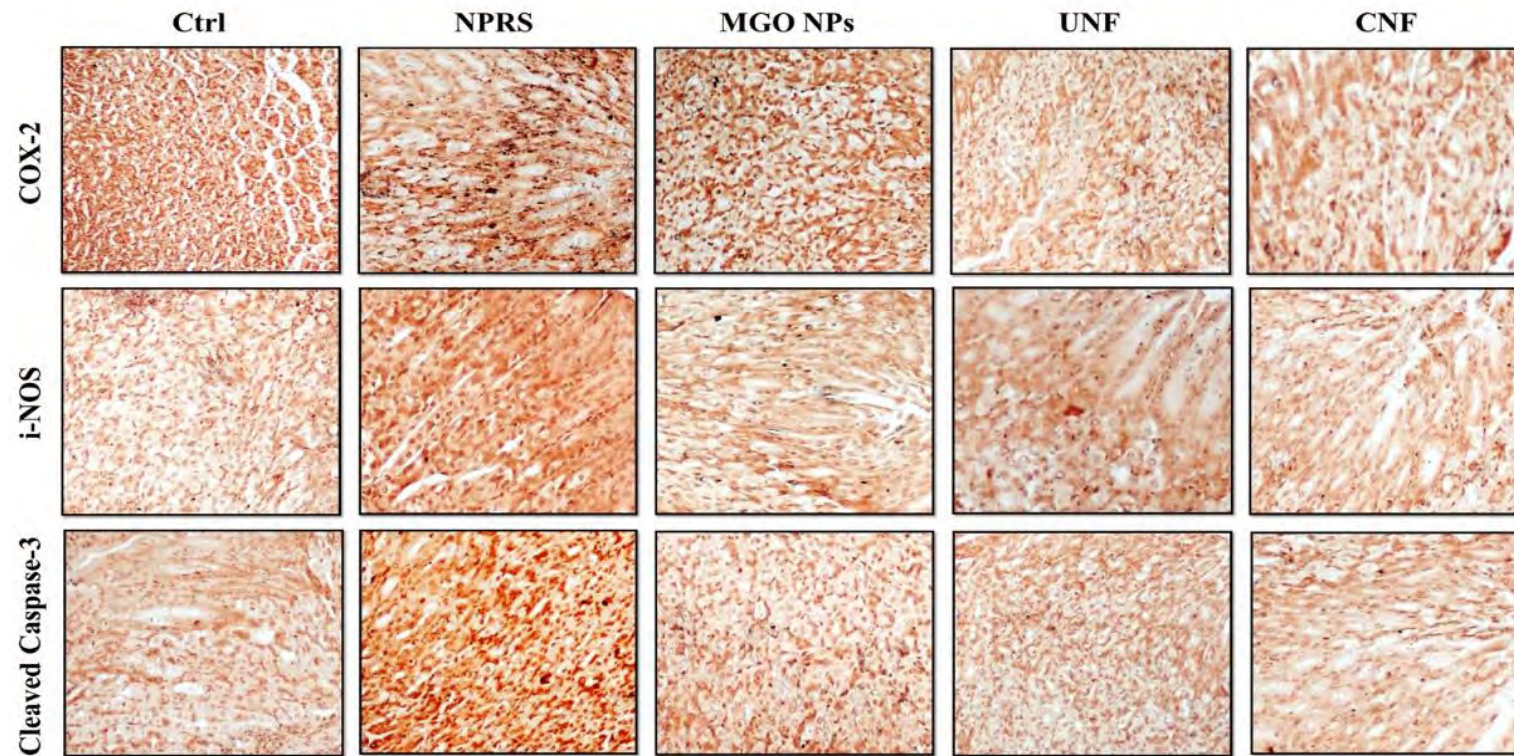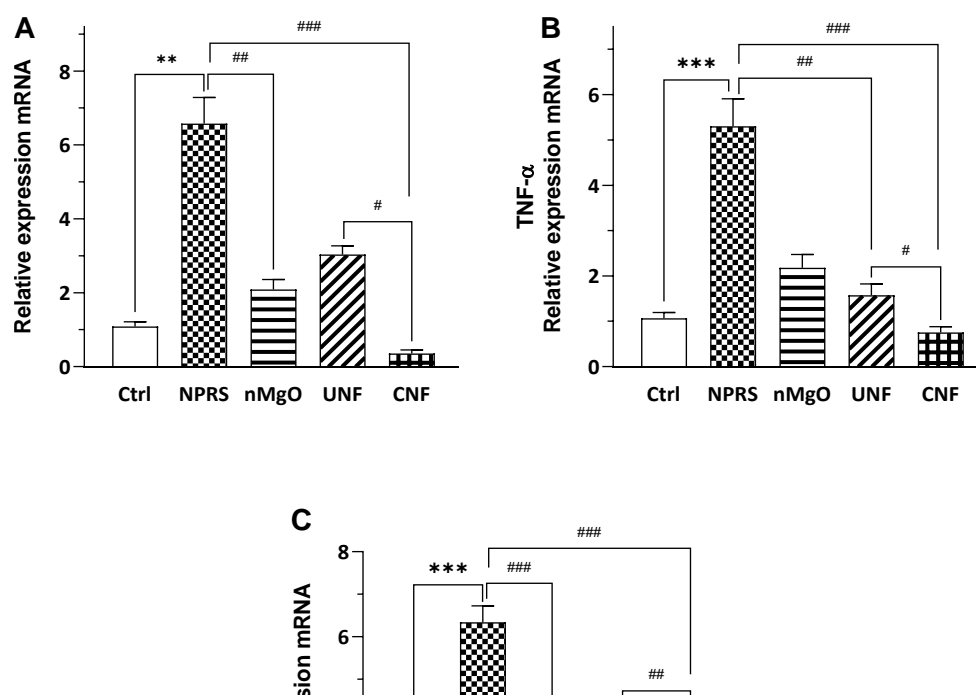
Fig. 5.18 mRNA expression of IL-6 (A), IL-β (B), and TNF-α (C) in the heart tissues of mice. The mRNA levels were measured, and data were normalized to GAPDH. The expression of mRNA in the control group was designated as 1, and the others were expressed as folds compared to the control. All values are expressed as mean±s.e. (n= 08). *p<0.05, **p<0.01, ***p<0.001, compared with the control. Whereas #p<0.05, ##p<0.01, ###p<0.001, among treatment groups other than the control, ns= non-significant.
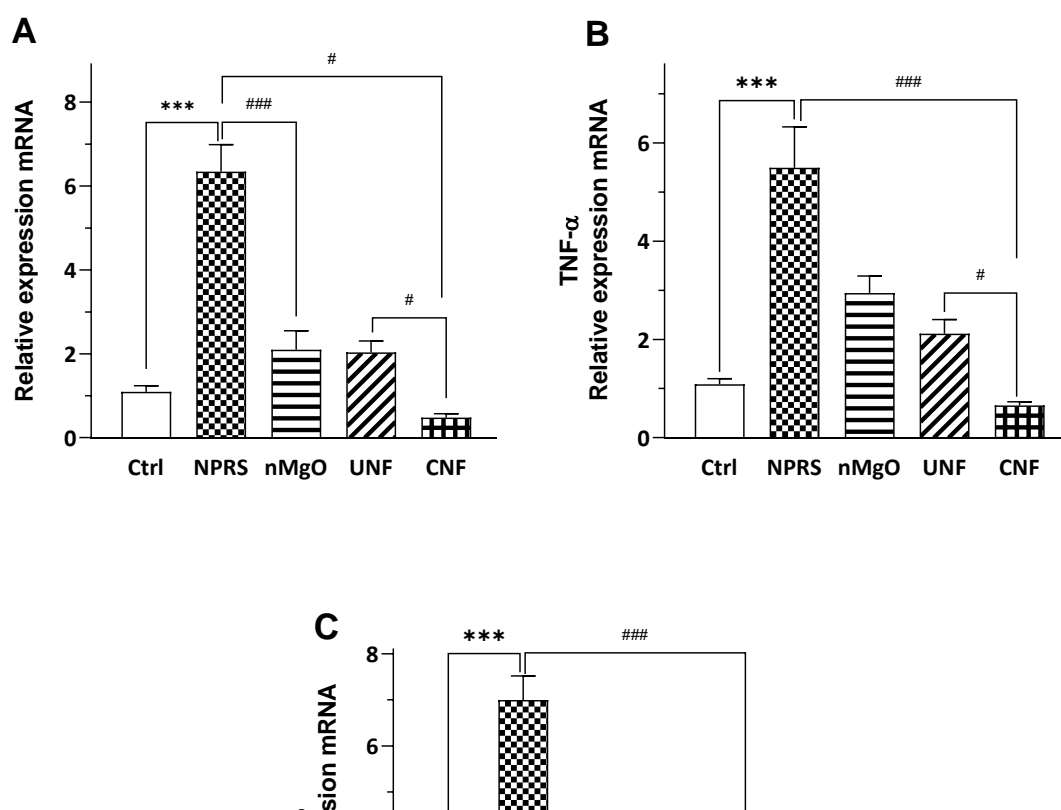
Fig. 5.19 mRNA expression of IL-6 (A), IL-β (B), and TNF-α (C) in the liver tissues of mice. The mRNA levels were measured, and data were normalized to GAPDH. The expression of mRNA in the control group was designated as 1, and the others were expressed as folds compared to the control. All values are expressed as mean±s.e. (n= 08). *$p < 0.05$, **$p < 0.01$, ***$p < 0.001$, compared with the control. Whereas #$p < 0.05$, ##$p < 0.01$, ###$p < 0.001$, among treatment groups other than the control, ns= non-significant.
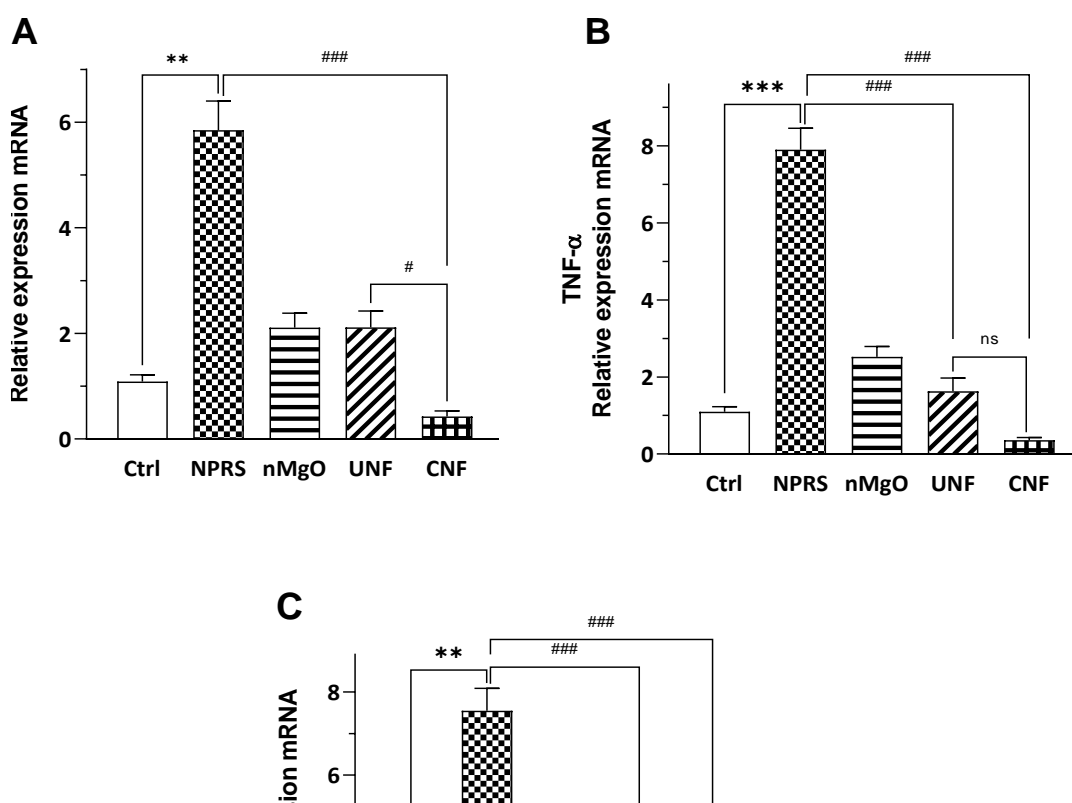
Fig. 5.20 mRNA expression of IL-6 (A), IL-β (B), and TNF-α (C) in the kidney tissues
of mice. The mRNA levels were measured, and data were normalized to
GAPDH. The expression of mRNA in the control group was designated as 1,
and the others were expressed as folds compared to the control. All values are
expressed as mean±s.e. (n= 08). *p<0.05, **p<0.01, ***p<0.001, compared
with the control. Whereas #p<0.05, ##p<0.01, ###p<0.001, among treatment
groups other than the control, ns= non-significant.
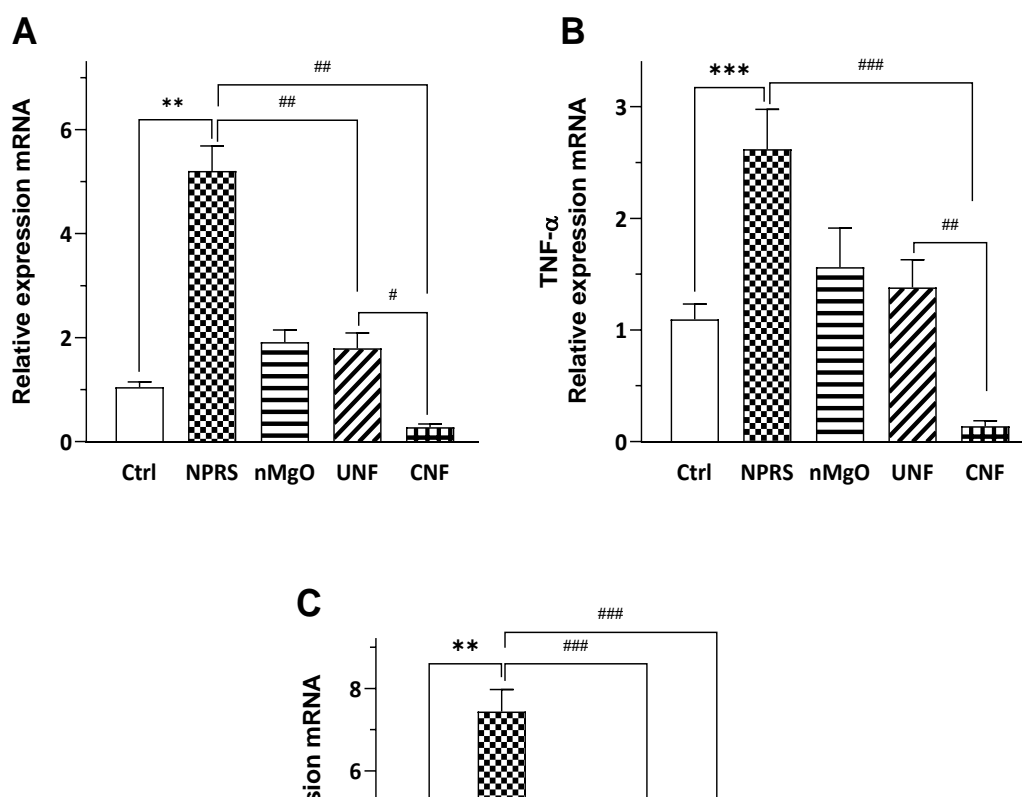
Fig. 5.21 mRNA expression of IL-6 (A), IL-β (B), and TNF-α (C) in the stomach tissues of mice. The mRNA levels were measured, and data were normalized to GAPDH. The expression of mRNA in the control group was designated as 1, and the others were expressed as folds compared to the control. All values are expressed as mean±s.e. (n= 08). *$p<0.05$, **$p<0.01$, ***$p<0.001$, compared with the control. Whereas #$p<0.05$, ##$p<0.01$, ###$p<0.001$, among treatment groups other than the control, ns= non-significant

Table 5.6 Effect of coated naproxen nanoformulation (CNF) on hematological parameters of male mice treated orally for 14 days. Values are expressed as mean±s.e compared with the negative control, NPRS (positive control), nMgO, and UNF.

Parameters	Control	NPRS	nMgO	UNF	CNF
RBC (M/µL)	07.47 ± 0.10	05.43 ± 0.09$^{\downarrow a***}$	06.59 ± 0.10$^{\downarrow a***,\uparrow b***}$	06.57 ± 0.15$^{\downarrow a,\uparrow b***}$	06.56 ± 0.12$^{\downarrow a,\uparrow b***}$
Hb (g/dL)	12.56 ± 0.19	09.30 ± 0.44$^{\downarrow a***}$	10.68 ± 0.34$^{\downarrow a***,\uparrow b*}$	11.64 ± 0.26$^{\uparrow b***}$	11.98 ± 0.24$^{\uparrow b***}$
MCV (fL)	66.80 ± 0.90	52.68 ± 0.95$^{\downarrow a*}$	55.88 ± 0.99	55.90 ± 1.06	58.46 ± 2.03
MCH (pg)	23.63 ± 0.40	16.83 ± 0.25$^{\downarrow a***}$	18.66 ± 0.27$^{\downarrow a**}$	18.25 ± 0.48$^{\downarrow a*}$	19.43 ± 0.23$^{\downarrow a*,\uparrow b***}$
MCHC (g/dL)	36.78 ± 0.63	29.53 ± 0.53$^{\downarrow a***}$	33.95 ± 0.62$^{\downarrow a**,\uparrow b***}$	33.80 ± 0.51$^{\downarrow a**,\uparrow b***}$	34.31 ± 0.49$^{\downarrow a*,\uparrow b***}$
Platelets (µLx10^5)	03.68 ± 0.33	14.00 ± 0.28$^{\uparrow a***}$	05.71 ± 0.02$^{\uparrow a***,\downarrow b***}$	07.29 ± 0.28$^{\uparrow a***,\downarrow b***}$	08.71 ± 0.23$^{\uparrow a***,\downarrow b***}$
WBC (µLx10^4)	01.28 ± 0.07	00.46 ± 0.03$^{\downarrow a***}$	01.83 ± 0.03	01.91 ± 0.04	01.67 ± 0.09$^{\uparrow b*}$
Neutrophils (%)	11.42 ± 0.66	24.50 ± 0.67$^{\uparrow a***}$	18.50 ± 0.31$^{\uparrow a***,\downarrow b***}$	13.33 ± 0.84$^{\downarrow b***}$	12.66 ± 0.66$^{\downarrow b***}$
Lymphocytes (%)	77.08 ± 1.89	61.83 ± 2.96$^{\downarrow a***}$	68.83 ± 2.37$^{\downarrow a*}$	73.00 ± 1.98$^{\uparrow b***}$	74.00 ± 1.57$^{\uparrow b***}$
Monocytes (%)	04.66 ± 0.33	07.66 ± 0.42$^{\uparrow a***}$	05.16 ± 0.40$^{\downarrow b**}$	06.66 ± 0.21$^{\downarrow b*}$	04.50 ± 0.22$^{\downarrow b***,d*}$
Eosinophil (%)	05.50 ± 0.50	05.00 ± 0.00	06.33 ± 1.20	06.00 ± 0.10	07.00 ± 1.15$^{\uparrow a*}$
Basophil (%)	01.33 ± 0.21	01.00 ± 0.12	01.16 ± 0.30	01.00 ± 0.36	01.83 ± 0.40

Different superscripts indicate statistical significance (at ***$p<0.001$, **$p<0.01$ & *$p<0.05$) between groups with a, b, c, and d representing significant difference with the control, NPRS, nMgO, and UNF, respectively (n=8/group).

Table 5.7 Effect of naproxen sodium nanoformulation (CNF) on serum biochemical status of male mice treated for 14 days. Values are presented as mean ± s.e. and compared with the control, NPRS, nMgO, and UNF.

Parameters	Control	NPRS	nMgO	UNF	CNF
ALT (U/L)	31.02 ± 1.19	154.0 ± 3.59$^{\uparrow a***}$	28.33 ± 1.45$^{\downarrow b**}$	32.71 ± 1.54 $^{\downarrow b***}$	33.33 ± 0.97$^{\downarrow b***}$
AST (U/L)	73.83 ± 5.48	114.0 ± 5.89$^{\uparrow a***}$	73.83 ± 5.67$^{\downarrow b**}$	84.83 ± 6.75$^{\downarrow b*}$	65.83 ± 7.04$^{\downarrow b***}$
ALP (U/L)	75.71 ± 7.67	110.0 ± 8.25$^{\uparrow a**}$	45.00 ± 4.38$^{\downarrow b***}$	64.14 ± 7.64$^{\downarrow b**}$	95.57 ± 7.44$^{\uparrow d*}$
Total bilirubin (mg/dL)	04.34 ± 0.08	03.79 ± 0.10$^{\downarrow a**}$	04.30 ± 0.15$^{\uparrow b*}$	04.63 ± 0.08$^{\uparrow b***}$	04.35 ± 0.09$^{\uparrow b**}$
Direct bilirubin (mg/dL)	02.27 ± 0.06	01.98 ± 0.16	02.59 ± 0.20	02.10 ± 0.06	02.05 ± 0.03
Creatinine(μmol/L)	04.63 ± 0.34	11.59 ± 0.61$^{\uparrow a*}$	06.92 ± 0.74	04.56 ± 0.33$^{\downarrow b*}$	05.27 ± 0.64$^{\downarrow b*}$
LDH (U/L)	522.0 ± 23.6	601.0 ± 18.1	464.0 ± 29.1	480.0 ± 19.8$^{\downarrow b*}$	571.0 ± 36.1
Cholesterol (mg/dL)	90.27 ± 1.67	149.0 ± 4.51$^{\uparrow a***}$	93.62 ± 1.11$^{\downarrow b***}$	78.89 ± 3.06$^{\downarrow b***}$	89.59 ± 4.65$^{\downarrow b***}$
Triglycerides (mg/dL)	71.82 ± 2.38	88.20 ± 3.59$^{\uparrow a**}$	74.61 ± 2.17$^{\downarrow b*}$	75.09 ± 3.83$^{\downarrow b*}$	74.82 ± 2.09$^{\downarrow b*}$

Different superscripts indicate statistical significance at ***$p<0.001$, **$p<0.01$ & *$p<0.05$ between groups with a, b, c, and d representing significant difference with the control, NPRS, nMgO, and UNF, respectively. (n=8/group).

Table 5.8 Oxidative stress parameters in male mouse tissue homogenate following 14-day exposure to coated nanoformulation of naproxen sodium (CNF). Values are presented as mean ± s.e. and compared with the control, NPRS, nMgO, and UNF.

Groups	Tissues	ROS (abs)	TBARS (nM min^{-1} mg protein^{-1})	SOD (unit mg^{-1})	POD (unit min^{-1})	CAT (unit min^{-1})	GSH (µMol/g)
Control	Heart	0.74 ± 0.02	0.99 ± 0.04	24.14 ± 1.79	7.15 ± 0.38	5.20 ± 0.16	38.60 ± 0.89
NPRS		1.30 ± 0.03$^{\uparrow a***}$	1.46 ± 0.11	10.65 ± 1.49$^{\downarrow a**}$	3.68 ± 0.20$^{\downarrow a***}$	2.71 ± 0.20$^{\downarrow a***}$	14.94 ± 0.69$^{\downarrow a*}$
nMgO		0.94 ± 0.06$^{\downarrow b***}$	0.81 ± 0.04$^{\downarrow b*}$	21.43 ± 2.08	6.98 ± 0.28$^{\uparrow b***}$	4.78 ± 0.23$^{\uparrow b***}$	31.78 ± 1.67$^{\uparrow b*}$
UNF		0.96 ± 0.04$^{\downarrow b***}$	0.90 ± 0.10$^{\downarrow b*}$	22.47 ± 2.73$^{\uparrow b**}$	6.83 ± 0.14$^{\uparrow b***}$	5.62 ± 0.26$^{\uparrow b***}$	33.44 ± 0.63$^{\uparrow b*}$
CNF		0.78 ± 0.03$^{\downarrow b***,\downarrow d*}$	0.64 ± 0.05$^{\downarrow b*}$	25.18 ± 1.74$^{\uparrow b***}$	7.39 ± 0.18$^{\uparrow b***}$	6.34 ± 0.35$^{\uparrow b***}$	34.07 ± 1.60$^{\uparrow b*}$
Control	Stomach	0.87 ± 0.03	0.54 ± 0.04	06.01 ± 0.86	1.22 ± 0.14	4.90 ± 0.25	06.28 ± 0.18
NPRS		1.11 ± 0.05$^{\uparrow a**}$	0.72 ± 0.08	03.69 ± 0.46	0.47 ± 0.16$^{\downarrow a**}$	2.49 ± 0.17$^{\downarrow a***}$	03.13 ± 0.07$^{\downarrow a*}$
nMgO		0.95 ± 0.03	0.56 ± 0.04	02.68 ± 0.15$^{\downarrow a*}$	0.86 ± 0.09	4.43 ± 0.14$^{\uparrow b***}$	03.53 ± 0.27$^{\downarrow a*}$
UNF		0.94 ± 0.05	0.54 ± 0.07	04.20 ± 0.78	1.03 ± 0.14	4.88 ± 0.20$^{\uparrow b***}$	04.22 ± 0.33$^{\downarrow a*}$
CNF		0.83 ± 0.05$^{\downarrow b**}$	0.33 ± 0.05$^{\downarrow b***}$	06.09 ± 0.38	1.21 ± 0.07$^{\uparrow b**}$	4.92 ± 0.22$^{\uparrow b***}$	06.01 ± 0.40$^{\uparrow b*}$
Control	Liver	0.77 ± 0.02	0.80 ± 0.05	22.72 ± 2.18	5.40 ± 0.15	8.72 ± 0.41	32.47 ± 0.69
NPRS		2.62 ± 0.08$^{\uparrow a***}$	1.03 ± 0.05$^{\uparrow a**}$	05.80 ± 0.96$^{\downarrow a***}$	1.51 ± 0.16$^{\downarrow a***}$	5.12 ± 0.16$^{\downarrow a***}$	16.86 ± 1.86$^{\downarrow a*}$
nMgO		1.11 ± 0.03$^{\downarrow b***}$	0.90 ± 0.05	15.10 ± 1.12$^{\uparrow b**}$	4.94 ± 0.22$^{\uparrow b***}$	6.95 ± 0.19	14.07 ± 0.66$^{\downarrow a*}$
UNF		1.28 ± 0.08$^{\downarrow b***}$	0.84 ± 0.04$^{\downarrow b**}$	19.56 ± 2.09$^{\uparrow b***}$	3.16 ± 0.05$^{\uparrow b***}$	8.29 ± 0.87$^{\uparrow b**}$	19.02 ± 0.37$^{\downarrow a*}$
CNF		0.95 ± 0.03$^{\downarrow b***,d**}$	0.82 ± 0.02$^{\downarrow b**}$	23.91 ± 0.63$^{\uparrow b***}$	4.52 ± 0.17$^{\uparrow b***,d**}$	8.55 ± 0.21$^{\uparrow b***}$	26.12 ± 1.08$^{\uparrow b*}$

Control	kidney	0.88 ± 0.02	0.53 ± 0.04	09.50 ± 0.43	4.50 ± 0.18	2.97 ± 0.22	34.54 ± 1.01
NPRS		$1.66 \pm 0.08^{\uparrow a**}$	$1.51 \pm 0.14^{\uparrow a*}$	$06.70 \pm 0.68^{\downarrow a**}$	$1.25 \pm 0.11^{\downarrow a*}$	$1.44 \pm 0.16^{\downarrow a***}$	$08.68 \pm 0.80^{\downarrow a***}$
nMgO		1.42 ± 0.18	$0.63 \pm 0.05^{\downarrow b*}$	08.26 ± 0.58	3.54 ± 0.17	$2.97 \pm 0.28^{\uparrow b**}$	$22.48 \pm 1.02^{\downarrow a***,\uparrow b***}$
UNF		1.35 ± 0.17	0.70 ± 0.06	08.36 ± 0.29	3.91 ± 0.34	2.29 ± 0.07	$14.55 \pm 0.34^{\downarrow a***,\uparrow b***}$
CNF		1.29 ± 0.15	$0.65 \pm 0.06^{\downarrow b*}$	08.83 ± 0.53	$4.63 \pm 0.16^{\uparrow b*}$	$2.55 \pm 0.23^{\uparrow b*}$	$29.53 \pm 1.28^{\downarrow a**,\uparrow b***,\uparrow d***}$

Different superscripts indicate statistical significance (at ***$p<0.001$, **$p<0.01$ & *$p<0.05$) between groups with a, b, c, and d representing significant difference with the control, NPRS, nMgO, and UNF, respectively. (n=8/group).

Discussion

The purpose of the current investigation was to evaluate the safety of coated naproxen nanoformulation (CNF) in healthy mice at clinical doses compared to its conventional free-form naproxen sodium at therapeutic doses. The purpose of the comparison was to assess if naproxen nanoformulation proves to be better than its conventional form in terms of cardiovascular, GIT, hepatic, and renal safety. The findings from this study, which are lacking in the scientific literature will appear to serve as a guide in dose selection and understanding of the safety margin of the formulation for clinical application. Heart, liver, stomach, and kidney tissues that are considered the main target of NSAIDs toxicity, were thoroughly examined through various tissue and serum biochemical assays and studied for the change in expression of proinflammatory, inflammatory, and apoptotic markers as well. Together all data obtained from the current results indicated that naproxen nanoformulation proved to be a promising alternative to its conventional free form.

Generally, a decrease in body weight is an indicator of cellular disturbance and a biomarker for safety in toxicity studies (Saleem et al., 2017). However, no body weight loss was observed in mice given a daily human equivalent dose of CNF for 14 days. In contrast, free NPRS-treated mice showed a considerable loss in body weight likely due to anorexia, homeostatic body function, and metabolic imbalance of the electrolyte (Gregus, 2015).

Similarly, the organ-body weight index is another sensitive parameter that is used widely to determine the safety of new drugs, and a comparison of organ weights between treated and untreated groups of animals has conventionally been used to evaluate the toxic effect of the synthesized compound (Karabulut and Barlas, 2018). In the present study, naproxen nanoformulations, either coated or coated and magnesium oxide nanoparticles did not affect organ weight indicating the safety of current formulations and MgO nanoparticles. Whereas NPRS treated group showed a treatment-related effect on organs weight, with a noticeable increase in liver and stomach weight index, while a significant decrease was found in heart and kidneys weight index. Since there is such a study available previously that can indicate the effect of NPRS on the organ-bodyweight index, therefore a comparison of results is not possible. However, a careful interpretation of the results can be useful to predict the

toxicity of the compound.

According to Bindu et al. (2007), the decreased heart weight whenever, found in toxicity/safety studies is usually without a microscopic correlate and is often associated with bodyweight decreases secondary to treatment. As for NPRS treatment, a significant weight loss in experimental mice has been observed so the decrease in heart weight might be attributed to an overall loss in body weight (Bindu et al., 2020).

On the other hand, alterations in liver weight may suggest treatment-related changes including hepatocellular hypertrophy (e.g., enzyme induction or peroxisome proliferation) especially an increase in liver weight whenever observed in short-term studies indicate that the test compound might possess a potent hepatic enzyme-inducing potential (Sellers et al., 2007). Since the kidneys are target organs of chemical toxicity; it correlates well with histopathological changes. Therefore, changes in kidney weight caused by the NPRS treatment reflect renal toxicity, tubular hypertrophy, or chronic progressive nephropathy (Greaves, 2012). These effects were further confirmed through serum and tissue toxicity markers. Increased stomach weight observed with NPRS treatment compared to the control groups suggest the occurrence of hypertrophied mucosa due to the inflammation caused by a topical irritant, an effect peculiar to NSAIDs class of drugs (Atkinson and Fudin, 2020).

The present study showed that the clinical dose of NPRS caused a drastic decrease in RBC, Hb, MCV, MCH, MCHC, WBC, and lymphocyte count/ content while significantly increased platelets, neutrophils, and monocytes compared to the control and coated naproxen nanoformulation. Given that these hematological changes have a higher predictive value for human toxicity (Arika et al., 2016), the destructive effect of NPRS on blood cells at therapeutic doses implies its toxic nature and indicated that NPRS like other NSAIDs such as diclofenac sodium, ibuprofen, paracetamol that can cause hematological disorders even at therapeutic doses (Kawazoe et al., 2017).

Contrary to this, naproxen nanoformulations and MgO nanoparticles examined in the current study for their hematological effects showed that the administration of nMgO caused a significant decline in RBC count, Hb levels, MCH, and lymphocytes count, and increased platelets counts and neutrophil percentages only. While uncoated naproxen nanoformulation decreased RBCs, MCH, MCHC, and inclination were

observed in platelets count. likewise, coated naproxen nanoformulation also resulted in a decreased RBC, MCH, MCHC, and increased platelets count. Though a statistical comparison of RBCs level found in the uncoated and coated nanoformulation group (6.56-6.59 M/µL) with the control, (07.47 M/µL) might indicate mild anemia, according to the reported literature anemia is declared only if RBCs levels less than 3.5 M/µL are found in the hematological test. Both of these nanoformulations, however, didn't affect WBCs and their differential count indicated immunoprotection. A mild increase in platelet level compared to control found in nMgO, and nanoformulated groups don't necessarily indicate thrombocytosis.

The ALT, AST, and ALP are serum biochemical markers used to assess liver function and predict hepatocellular injury. The present findings as regards increase in NPRS-induced ALT, AST, and ALP serum levels are consistent with previous findings that NSAIDs such as diclofenac, ibuprofen, and paracetamol cause significant alteration in serum biochemical parameters (Gomaa, 2018). This effect may be attributed to an acidic moiety or reactive metabolites of NPRS that bind to host proteins causing cellular injury (Bessone, 2010; Kishida et al., 2012).

Bilirubin, which is the excretory product formed by the catabolism of heme and normally conjugated by the liver to form bilirubin diglucuronide and excreted through the bile, is elevated when there is a significant liver impairment caused by drugs (Rodwell and Murray, 2018). Presently elevation in serum bilirubin in NPRS-treated mice in the present study indicates NPRS led to severe anemia and correlates with the histological tissue findings in liver tissue. Moreover, creatinine is a non-protein nitrogenous substance formed from creatine and phosphocreatine during muscle metabolism and removed from the blood by glomerular ultrafiltration of the kidneys, and any abnormalities that decrease glomerular filtration rate will result in increased serum creatinine (Dhanvijay et al., 2013). Currently, naproxen associated increased level of serum creatinine agrees with Odangowei et al. (2020) who concluded that an increase in serum creatinine by NSAIDs reflects a marked decrease in glomerular filtration rate and indicates kidney injury (Ogidi et al., 2020).

The significant elevation observed in serum total cholesterol in NPRS treated group may be due to hepato-biliary impairment, protein-losing nephropathy, and impaired cholesterol metabolism. These findings are in accord with (Orinya et al., 2016). Serum

triglyceride level was found to be increased in NPRS-treated mice compared to the control and other treatment groups and may be associated with liver impairment (Mendenhall and Mortiaux, 1962). Interestingly, serum LDH levels were found to be normal in the experimental mice in all treatment groups.

On the other, at the same doses, coated and uncoated naproxen nanoformulations did not show any alteration in all of the above-mentioned tissue toxicity makers and all values obtained were comparable to that of the control. It, therefore, seems that the slow release of the NPRS from the nMgO might have prevented excessive interaction of the NPRS with normal cells.

Reactive oxygen species (ROS) generation induces oxidative stress and is associated with cell death, a general mechanism of NSAIDs-induce tissue toxicity reported in past studies (Ghosh et al., 2015; Ahmad et al., 2018). As demonstrated by Ahmad et al. (2018) naproxen treatment at 38 mg/kg and 65 mg/kg doses induces a significant increase in lipid peroxidation and ROS levels in the brain, kidney, and liver tissues of experimental rats (Ahmad et al., 2018), in line with this, the results of the present study showed that the NPRS treatment at therapeutic dose caused a significant elevation in ROS and LPO levels in heart, liver, kidneys, and stomach tissues.

The antioxidant system of the body is a defense against free radicals and reactive species. This defense when affected by toxins, radicals, reactive oxygen species, and reactive nitrogen species, caused up/downregulation of several antioxidant enzymes (Birben et al., 2012). Therefore, the increased lipid peroxidation and ROS level and decreased glutathione, SOD, CAT, and POD activities in the heart, liver, kidney, and stomach tissues following NPRS treatment in the present study indicate a possible involvement of NPRS-induced oxidative stress that altered antioxidant level in all tissues. The involvement of ROS in organ toxicity has been reported widely for diclofenac, ketoprofen, piroxicam, naproxen, and many other NSAIDs (Ghosh et al., 2015). In contrast to results obtained from NPRS-treated tissues, the treatment of mice with coated and uncoated nanoformulations not only maintained the antioxidant defense systems in all tissues studied but also did not induce oxidative stress in the heart, and liver, kidney, and stomach tissues. The binding of NPRS to MgO nanoparticles considerably increases the drug's aqueous solubility and thus its dissolution and/or increases the drug's permeability through biological membranes

leading to faster onset of action reducing the manifestations of the drug toxicity (Kermanizadeh et al., 2018). This observation correlates with the results of earlier studies that demonstrated the improved toxicological profile of ibuprofen sodium conjugated to PEGylated gelatin nanoparticles (mean size ~ 200 nm) (Narayanan et al., 2013).

As known and accepted widely irrespective of their mechanism of action, prolonged exposure to any class of NSAIDs has been shown to have potential adverse effects on cardiovascular events in patients with or without preexisting cardiovascular conditions (Amer et al., 2010). Presently, the administration of NPRS at clinical dose induced cardiotoxicity on the myocardial tissue in the treated mice. An observation which was similar to that by Pathan et al. (2010) revealed that the experimental rats were given NPRS (50 mg/kg/day) for five days showed a significant increase in oxidative stress and decreased the activity of antioxidant enzymes along with disruption in biochemical parameters the serum LDH and induced cardiomyopathies (Pathan et al., 2010).

Uncoated and coated nanoformulation both did not alter the normal histological structure of the myocardial tissue in mice at clinical doses except for minor dilation in cardiac muscle arrangement that was observed in UNF treated group. Similar results were found in another study that encapsulation of diclofenac sodium, another NSAID with high cardiotoxicity profile, into the polymeric micelle showed decreased signs of cardiotoxicity compared to the free drug (Al-Lawati et al., 2018).

The one major risk that has always been associated with the short- or long-term use of NSAIDs, is gastrointestinal mucosal injury (Conaghan, 2012). Presently, the effect of NPRS on mice stomachs was examined through macroscopic and microscopic examination of tissues. It was found in the gross examination of tissue that the administration of NPRS to mice caused severe hemorrhagic lesions along with an increased ulcer score. Whereas microscopic examination revealed extensive histopathological changes, such as vascular congestion, edema, degeneration of epithelial cells, intracellular infiltration, and increased apoptosis of gastric epithelia. However, NPRS entrapped in MgO nanoparticles and coated with PVA significantly reduced gastritis-associated changes within the gastric mucosa, as evidenced by a decrease in the gastric ulcer score, maintained mucosal fold in the gastric wall with no signs of leucocyte infiltration.

The gastric mucosal layer is the first line of defense for the stomach against external stimuli, and its motility can affect the development of gastric lesions (Orlando, 2010). NSAIDs can cause damage to the gastroduodenal mucosa via the topical irritant effect on the epithelium, suppression of gastric prostaglandin synthesis, and reduction of gastric mucosal blood flow (Wallace, 2000). To reduce these side effects, similar to the present study, several other nano delivery systems including liposomes and nanoparticles have been reported to demonstrate GI protection against ulceration associated with non-selective NSAIDs such as aceclofenac, naproxen sodium, and diclofenac (Chime et al., 2013; Sarfraz et al., 2019; Jianxian et al., 2020).

Despite the overall low incidence of NSAID-induced hepatotoxicity, their widescale use makes them an important cause of drug-induced liver injury. In the present study, the hepatotoxic effect of NPRS was also studied and compared with that of nanoformulations. Present, the administration of NPRS induced marked histological aberrations evident by the presence of a pyknotic nucleus, cellular disintegration in the form of vacuolization, and infiltration of inflammatory cells (Kupffer cells). Whereas administration of the same doses of naproxen nanoparticulate formulations maintained the cellular integrity of the liver tissues and therefore, it is possible that the loading of NPRS in nanoparticles leads to a different distribution of the drug in the liver making the incorporated drug less accessible to hepatocytes and thus reducing its toxicity.

Presently, congestion, glomerular atrophy with Bowman's gap enlargement, epithelial disintegration in tubular structures, and mononuclear cell infiltration in kidney tissues, were observed in the NPRS-treated group suggesting apoptotic events. The renal adverse effects have been reported widely for non-selective COX, as well as for COX-2 selective, inhibitors in literature (Sharma and Jawad, 2005). The present findings seem to be consistent with other researchers who found that the classical NSAIDs, diclofenac, and naproxen, cause the most marked defects, overall, in renal development including edema, kidney hypoperfusion, hypertension, and renal maldevelopment (Olliges et al., 2011). The naproxen nanoparticulate formulation, on the other, did not affect the normal tissue architecture of kidneys when treated at the same clinical doses. These results are supported by earlier findings in the present study, that administration of nanoformulation maintained the delicate balance of antioxidant enzymes in kidney tissues.

In continuation with the aforementioned evaluation of NPRS-induced toxic effects and comparison of results with its nanoformulations through various assays, one major goal of the present study was to explore further, the underlying molecular and pathophysiological mechanisms by which inflammatory cytokines, apoptosis inducers, and inflammatory regulators could be involved in the onset of tissue injury /toxicity.

For this, the protein expressions of COX-2, i-NOS, NF-κB, and cleaved caspase-3 were studied in control and treated heart, liver, kidney, and stomach tissues through immunohistochemistry while, and mRNA expression of IL6, IL 1β, and TNF α, were studied through real-time PCR in treated and control tissues.

NPRS-induced cardiotoxicity observed in the present study is considered to be the result of increased oxidative stress that induces upregulation of pro- cytokines, such as tumor necrosis factor-alpha (TNF-α), interleukin-1beta (IL-1β), and interleukin-6 (IL-6) (Poljsak et al., 2013). COX-2, which is present at low or undetectable levels in most tissues, may be quickly and strongly activated in response to inflammatory signals or other stresses (Streicher and Wang, 2008). The same mechanism was observed in the NPRS-induced upregulation of the COX-2 enzyme in cardiomyocytes indicating NPRS-induced inflammatory stress that might induce COX-2 production. Caspase 3 is a well-known component of the cellular death pathway. Stimuli having a membrane receptor-activated or mitochondrial origin such as free radicles can activate it (Condorelli et al., 2001). The current study found that overexpression of caspase-3 reduced heart function, indicating a possible role of caspase-3 in tissue damage.

In cardiac tissues treated with naproxen nanoformulation, the levels of proinflammatory cytokines, COX-2, iNOS, and caspase -3 were found to be near baseline nearing the control tissues suggesting that the incorporation of the drug in nanoparticles has prevented the direct drug contact with the heart tissues while coating with the PVA has further improved the safety of nanoparticulate formulation (El-Sisi et al., 2020).

NPRS-induced cardiotoxicity, on the other hand, is thought to be the consequence of enhanced oxidative stress, inflammation, cardiomyocyte apoptosis, and mitochondrial abnormalities. As a result, increased oxidative stress, mediated by the production of reactive oxygen species (ROS), is thought to play a key role in the NPRS-induced upregulation of pro-cytokines such as tumor necrosis factor-alpha (TNF- α),

interleukin-1beta (IL-1), and interleukin-6 (IL-6). These cytokines are believed to play a role in congestive heart failure pathogenesis (CHF) (Birmingham and Buvanendran, 2013).

Nonsteroidal anti-inflammatory drugs (NSAIDs) including aspirin, ibuprofen, naproxen, sulindac, ketoprofen, mefenamic acid, and indomethacin are some of the aggressive chemical compounds causing GI mucosal damage (Matsui et al., 2011). As reported by Kokura et al. (2000) the increased production of TNF- α, which augments neutrophil-derived superoxide generation and the production of IL-1, is associated with aspirin-induced inflammation in the stomach mucosa (Kokura et al., 2000). In a previous study, a significant increase in inflammatory mediators IL-6, TNF-α, and COX-2 was observed in BALB/c mice with gastric mucosal damage induced by indomethacin (Wang et al., 2019). Consistent with these studies, the increased expression of COX-2 found in NPRS-treated mice indicated a strong correlation between upregulation of COX-2 expression and gastric injury in the current study. Moreover, the protein expression study of iNOS and caspase-3 in NPRS and its nanoparticulate formulations indicated that the NPRS led to a significant increase in the iNOS and caspase-3 expression in the stomach tissues. While the levels of iNOS and caspase-3 were found low in nanoformulations treated mice.

Piotrowski et al. (1999) showed that in animals receiving an ulcerogenic dose of indomethacin, there was a 12-fold increase in gastric epithelial expression of iNOS activity compared with controls, and this increase was positively correlated with damage to the epithelium (Piotrowski et al., 1999). Interestingly, similar results were found in the present study where iNOS upregulation in gastric tissue treated with NPRS, may be involved in gastric damage. However, encapsulation of NPRS in MgO NPs and subsequent coating has prevented the formation of ulcers significantly as shown by the low level of iNOS expression. These results as regards NPRS-induce gastric toxicity through activation of caspase-3 corroborated well with another study in which indomethacin caused significant apoptosis in parietal cells through activation of TNF-α and caspase-3 (Gebril et al., 2020).

In the present study, immunostaining of NFκB in liver tissues from control, naproxen nanoformulation, NPRS, and MgO NPs treated groups were assessed. Results revealed that the NPRS significantly upregulated the expression of NFκB protein in treated liver

tissues suggesting its role in liver toxicity (More et al., 2017). It has been well documented that NF-κB when activated, is transferred into the nucleus, and carries out the transcription of inflammatory cytokines (TNF-α), interleukins (ILs), and other mediators of apoptosis and fibrosis (Iqubal et al., 2020). TNF-α is a critical factor in liver injury and plays a significant role in inducing hepatic apoptosis (Shimizu et al., 2005). Similar to the previous studies, the role of these cytokines in NPRS-induced liver injury was assessed in terms of their mRNA expression in liver tissues. As expected, the expression of TNFα, IL-1β, and IL-6 was found to be the highest in NPRS-treated liver tissues. While treatment with the naproxen nanoformulations significantly suppressed cytokines mRNA levels and prevented liver damage (Tanaka et al., 2014).

COX-2 is an important molecule in the progress of hepatic fibrosis and may play a critical role in liver inflammation, autophagy, and cell senescence (Yang et al., 2020). Presently the elevated expression of COX-2 in liver hepatocytes following NPRS treatment is suggestive of the critical role played by COX-2 in tissue inflammation and injury (Lu et al., 2018). While COX-2 levels were downregulated in liver tissues treated with naproxen nanoformulations. In the present study, cleaved caspase-3, a marker of cellular apoptosis (Hasan, 2019) was found to be abundant in the livers of male mice treated with a clinical dose of NPRS. While downregulated expression of caspase-3 in hepatocytes of naproxen nanoformulation-treated mice livers suggests the hepatoprotective role of hepatocellular damage, cell death, and pro-inflammatory signaling (Thapaliya et al., 2014).

The downregulation of inflammatory cytokines, NFκB, COX-2, and caspase-3, the major contributors to liver injury, in naproxen nanoformulation treated liver tissues may be attributed to the slow and constant release of NPRS from nanoparticles (Abo-zalam et al., 2021) and its PVA coating seems to prevent off-target side effects.

In kidney tissue, the increased expression of COX-2 might be caused by liver inflammation as indicated by the increased level of mRNA expression of pro-inflammatory cytokines interleukin-1β, 1L-6, and TNF-α (Zhang et al., 2017). Cytokines activate as a response to kidney injury and induce the synthesis of (nitric oxide) by iNOS (inducible NO synthase) and initiate inflammation (Zamora et al., 2000). Whereas IL-6 is produced in response to proinflammatory signals including

TNF-α by endothelial cells as a common response to tissue injury and organ failure (Sherwood and Toliver-Kinsky, 2004). Moreover, the activation of caspase-3 following indomethacin intake in a previous study resulted in mitochondrial malfunction and intracellular inflammatory signaling pathway activation (Chen et al., 2021).

Presently, the NPRS-induced renal complications can be ascribed to the activation and upregulations of IL-6, IL 1β, and TNFα in response to ROS-mediated cellular injury and then, subsequent elevated expression of iNOS, COX-2, and caspase-3. Contrary to this, naproxen nanoformulations showed a significant decline in the above-mentioned regulators and inflammatory mediators suggesting a nephroprotective role. Consistent with the encouraging findings regards nanoformulations, in a different study, Harirforoosh et al. (2016) found free diclofenac resulted in higher renal necrosis compared to vehicle, whereas diclofenac encapsulated in poly(lactic-co-glycolic) (PLGA) nanoparticles did not affect renal morphology (Harirforoosh et al., 2016).

Lastly, after administration of the placebo nanoparticles (nMgO) at the dosage level of 55.34 mg/kg/day (equivalent to the amount used in NPRS nanoformulation), did not show any adverse or toxic effects in any of the tissues studied, and all the physiological values were found to be near baseline or as detected in control mice. The safety and biocompatibility of nMgO observed in the present study are attributed to a particular advantage associated with the use of nMgO as drug carriers that, once taken, nMgO, are successfully metabolized into Mg^{2+} and OH^- ions, which are excreted from biological systems, preventing tissue accumulation and resultant toxicities. Overall, nanomedicine appears to be a promising technique for NSAID administration that is both effective and safe.

In summary, our results indicate that ROS-induced upregulation of TNF-α, IL-1β, and IL-6 accompanied by increased expression of COX-2, iNOS and caspase-3 contributed together to inducing tissue toxicities.

Contrary to this, naproxen nanoformulations either coated or uncoated significantly downregulated the expressions of the above-mentioned cytokines and inflammatory mediators, hence suggesting a protective role. although both forms of nanoformulation either coated or uncoated showed tissue protection, however, coated nanoformulation was found to be more efficient in terms of prevention of organs from drug-induced

damage. This superiority of CNF may be attributed to PVA coating which might have favorably altered the pKa profile and biodistribution of NPRS in healthy mice thus preventing tissue toxicity.

To sum up, the present study demonstrates that the naproxen nanoformulation holds significant promise in safeguarding organs against potential toxic effects associated with the administration of the drug in its free form, which otherwise resulted in severe detrimental impacts. Apart from that, this study has placed significant emphasis on evaluating the impact of coating on nanoformulation, a critical consideration. The objective was to ascertain whether the introduction of a coating material could avert potential toxicity arising from direct exposure to the uncoated nanoformulation. The comprehensive analysis of this objective, encompassing various parameters, has unequivocally demonstrated that the introduction of a polymeric coating confers enhanced organ safety upon the nanoformulation, also as investigated for therapeutic activity in chapter 3, the inclusion of the coating further enhances the therapeutic effectiveness of the nanoformulation. This improvement can be attributed to the gradual release facilitated by its nanocarrier and the protective coating layer. Collectively, the findings indicate that the coated nanoformulation, referred to as CNF, surpasses its uncoated counterpart (UNF) in terms of both therapeutic efficacy and organ safety within the context of this study.

Finally, nanomedicine has the potential to reduce the toxicity of NSAIDs, and incorporating NSAIDs into nano delivery systems might be a viable alternative for the prevention and/or treatment of a variety of chronic inflammatory illnesses, including cancer. Nevertheless, one of the limitations of the present study is that the inhibitors or knock-out models to inhibit the molecular mechanisms involved in NPRS-induced tissue toxicity were used to validate the protective effect of its nanoformulations. However, the results of the current study shed light on the protective effect of naproxen nanoformulation and would foster further studies to further prove the current finding.

General Discussion

Inflammation is a body's natural response to any kind of noxious stimuli and is represented by the activation of an inflammatory cascade (Varela et al., 2018). This response involves various kinds of inflammatory cells that work together to resolve injury, however, if inflammation is left unchecked it further triggers an inflammatory cascade and leads to life-threatening conditions such as cancer (Ratan et al., 2022). To resolve inflammation there are two kinds of medication available to date: steroidal anti-inflammatory drugs and non-steroidal anti-inflammatory drugs. Steroidal anti-inflammatory drugs, as the name indicates are made up of synthetic steroids. Whereas non-steroidal anti-inflammatory drugs (NSAIDs) are a group of synthetic drugs that reduce pain, inflammation, and fever (Williams and Buvanendran, 2011). Despite being clinically effective and widely used, both types of anti-inflammatory medicines have major disadvantages. The long-term use of steroidal drugs is associated with behavioral disturbances, anxiety, sleeplessness, the elevation of the body sugar level, indigestion, weight gain, and a weak immune system whereas, the regular use of NSAIDs can potentially lead to gastrointestinal ulcers and bleeding cardiovascular effects, loss of kidney function and liver damage (Bindu et al., 2020). As a result, the use of steroids has been restricted to the treatment of serious medical disorders such as systemic lupus erythematosus (SLE) and autoimmune hepatitis when no other therapeutic options are available. NSAIDs, on the other hand, are routinely used to treat acute and chronic inflammatory illnesses, acute pain relief, and fever, making their usage unavoidable.

Nanotechnology is a rapidly evolving branch of science that provides plausible solutions to current challenges associated with drug toxicity, such as reduced effective treatment doses through nano-sizing and nano-drug delivery systems which prevents drugs from reaching off-target tissues (García et al., 2022). While nanosizing includes the reduction in drug particle size to increase its surface area and solubility, the drug delivery systems utilize synthesized NPs as drug carriers to produce low-dose formulations (Daraee et al., 2016). One of the major advantages of drug delivery systems is that they maintain plasma levels of drug for an extended period due to sustained release of drug from its carrier, thus favorably modulating the drug pharmacokinetic profile in such a way that desired therapeutic effect could be achieved with only little quantity of drug used (Çalış et al., 2019). In this context, numerous

nano-delivery systems have been researched thoroughly in preclinical investigations that include polymeric micelles, polymeric microspheres, liposomes, solid lipid nanoparticles, and dendrimers among other. Despite the preclinical success, the translation of the established nano delivery formulations for NSAIDs to clinical research has been extremely restricted (Martinho et al., 2011; Soares et al., 2018). This might be due to concerns of drug manufacturers about using comparatively expensive innovative delivery methods for NSAIDs that are used by patients on a long-term basis (Pandey and Jain, 2020). Massive production issues, as well as safety concerns and strict regulations, may have led to the minimal clinical usage of NSAIDs-based nanodrug delivery systems (Sainz et al., 2015). Second, polymeric nanoparticles as NSAID carriers have significant drawbacks, including high cost, precipitation, drug permeability, buildup in human tissues, cytotoxicity, and difficulty clearing from the circulatory system (Smet et al., 2013; Ghasemiyeh and Mohammadi-Samani, 2018; Vega et al., 2020). Thus, as an alternative, the use of metal oxides as drug carriers shows potential in drug delivery applications.

Metal oxide nanoparticles are highly stable and can be constructed according to the desired size, structure, and porosity. Metal oxide nanoparticles can incorporate hydrophilic and hydrophobic drugs efficiently which results in the effective delivery of drugs to target sites (Murthy et al., 2020). Moreover, the metal oxide can be used in implant, theragnostic, wound healing, cancer therapy, antimicrobial, and drug delivery applications (García et al., 2022) and unlike polymeric nanoparticles, metal oxides are available in a wide range of shapes and sizes. In this scenario, the present thesis reports for the first time the successful preparation and evaluation of metal oxide nanoparticles based on novel cost-effective, low-dose naproxen nanoformulation with an improved therapeutic profile compared to its conventional analog.

Magnesium is the second most frequent cation among trace elements, and it is essential for the normal functioning of a variety of human body systems and activities such as the regulation of glucose through insulin secretion, and various enzymatic and cell signaling activities (Jahnen-Dechent and Ketteler, 2012). In terms of its use in nanodrug delivery applications, magnesium oxide-based nanoparticles (MgO NPs) have suddenly acquired prominence as drug carriers, in the field of nanotechnology (Gajengi et al., 2017) due to several advantages associated with it such as mechanical strength, small

particle size, wide surface area, superior drug adsorption capabilities, along with bulk synthesis using simple techniques. Moreover, MgO NPs are proved to be anti-inflammatory, anti-bacterial, anti-viral, and anti-diabetic. Therefore, in the present work, we prepared amorphous natured MgO NPs with a hydrodynamic size range from 140-484 nm, as an initial step to prepare naproxen nanoformulation. The synthesis of MgO NPs was verified using XRD and UV-visible analyses. Following that using post-loading techniques, naproxen sodium was loaded on MgO NPs, and this formulation was termed uncoated nanoformulation (UNF). A ratio of NPRS: MgO NPs = 2: 3 was chosen based on a set of preliminary experiments and finalized. Presently, naproxen sodium (NPRS) was selected as a model anti-inflammatory drug due to its excellent therapeutic properties (Hsueh et al., 2020), but the use of NPRS has been limited due to certain gastrointestinal and other physiological complications reported widely at doses, indicated for the treatment of certain inflammatory diseases (500 mg to 1200 mg/day for an adult human) for long durations (from month to years) (Maniar et al., 2018). The size and surface charge of UNF was found to be ranging between 152 and 399 nm and -11.7 mV respectively. Most likely, this variation in size may be due to the agglomeration of drug-conjugated NPs.

Since post-loading is easy and universal for loading various drugs, these drugs-loaded nanoparticles may face challenges *in vivo* such as undesirable burst release due to the unspecific binding or adsorption of drugs on the particle surface (Rizvi and Saleh, 2018). Besides, soon after administration, the nanoparticles can form clusters whilst in the bloodstream. The absorption of plasma proteins on the surface of nanoparticles results in activation of the clearance mechanism by macrophage cells and the removal of nanoparticles from the blood circulation (Issa et al., 2011; Liu et al., 2011) which in turn, leads to a reduction in the nanoparticle-based therapeutic efficacy. Therefore, coating a thin layer of extra material such as a biocompatible polymer is a common and effective approach to mitigate the initial burst release and can prevent opsonization (Kayal and Ramanujan, 2010).

Present, the UNF was entirely coated with 2.5% polyvinyl alcohol and termed coated nanoformulation (CNF). Following PVA coating, a significant improvement and uniformity in the particle size were observed and particle size was found to be 161 nm. These findings suggested that polymeric coating over NP aggregates helped in particle

segregation and uniformity in particle size (Ventola, 2017). The particle size obtained in the current study for CNF (161 nm), is considered a suitable particle size for most nanotherapeutic applications. In terms of thermostability, both nanoformulations were found to be more thermostable than naproxen sodium alone suggesting the formation of a stable nanoformulation.

Drug encapsulation and loading studies were performed to analyze the drug-carrying potential of MgO NPs. The results revealed that nanoformulation holds 50.4% encapsulation efficiency while loading capacity was found to be 43.2%. As mentioned previously the NPRS to MgO NPs ratio was kept at 2: 3 current findings suggest that MgO NP is capable of adsorbing NPRS on its surface almost equal to its quantity added. Finally, drug release studies performed *in vitro* revealed that CNF showed a prolonged release of NPRS at pH 6.8 (> 95%) in 24 h. Minimum drug release was observed at acidic pH (1.2) over time. Used as a model drug in the current study, naproxen is among the acidic NSAIDs that tend to accumulate in the gastric cells at low pH, causing damage to the gastric lumen (Rodriguez-Stanley et al., 2006). The maximum release of NPRS at intestinal pH (6.8) and minimal release at stomach pH (1.2– 4.0) in the present study may be attributed to the conjugation of NPRS with MgO nanocarrier (Sarfraz et al., 2020).

The second objective of the present study was to test the anti-inflammatory, analgesic, and antipyretic potency of nanoformulation using various *in vitro* and *in vivo* models. *In vitro* hemolytic or membrane stability assay and protein denaturation inhibition assay, are two particular assays used worldwide, to analyze the anti-inflammatory effect of newly synthesized compounds (Wang et al., 2018). In both assays, the test compound is tested for its ability to prevent cellular membrane and protein from denaturation. Presently, naproxen nanoformulations either coated or non-coated acted as RBC membrane stabilizers and protected the RBC membranes from hemolysis. Similar results were found in protein denaturation inhibition that naproxen nanoformulation coated with PVA exhibited the highest inhibition potential against heat-induced protein denaturation in a concentration-dependent manner.

In the carrageenan-induced paw edema model, the release of 5-hydroxytryptamine, histamine, cyclooxygenase, and bradykinin characterize the initial phase of inflammation (0–2 hours after carrageenan injection), whereas increased production of

prostaglandins (PGs), free radicals production and neutrophil infiltration mark the subsequent second phase (2– 6 hours after carrageenan injection) (Vinegar et al., 1969). Again, in this model for *in vivo* anti-inflammatory evaluation, naproxen nanoformulation significantly alleviated paw edema in a dose-dependent manner. This effect was observed right after dose (CNF) administration (early phase of inflammation) and continued toward a later phase of inflammation. Moreover, the central, and peripheral analgesic activity of any test compound is determined by its ability to prevent pain in test animals.

At present two different pharmacological test models were employed to test the analgesic potential of nanoformulations; tail immersion test to evaluate central analgesic activity whereas, acetic-acid induced writhing to test the peripheral analgesic activity of test compounds. Immersion of mice tails in hot water initiate pain at the spinal level and the delay in response time for tail withdrawal is recorded (Hole and Tjølsen, 2007) whereas intraperitoneal ($\mu\mu$i.p.) injection of acetic acid to experimental animals results in a writhing response characterized by constrictions of abdominal muscles with stretching of hindlimbs (Gawade, 2012). Data from both studies suggested that CNF is a strong analgesic with potency higher than its conventional free form. Finally, nanoformulation was tested for its antipyretic potential. Besides being prescribed as potent anti-inflammatory and analgesic drugs, NSAIDs are also indicated to cure fever as antipyretics (Dangarembizi et al., 2018). Presently, the nanoformulation was analyzed for its antipyretic effect as well, using the brewer's yeast-induced pyrexia model. Remarkably, the antipyretic effect of CNF was found to be superior to the standard antipyretic drug paracetamol at doses ten times lower than paracetamol.

In all pharmacological investigations, the outcomes of naproxen nanoformulation were compared to diclofenac sodium, which was used as a positive control, and naproxen sodium which was used as a reference drug. Interestingly, the effect of coated nanoformulation was found to be superior to conventional drugs. Although equally effective activity was shown by uncoated nanoformulation, CNF was superior among all in terms of therapeutic efficiency. This effect may be ascribed to the slow release of naproxen from MgO NPs which maintained the drug's effective dose level in plasma necessary to show therapeutic effects. Taken together, these studies suggested that the naproxen nanoformulation is a potent anti-inflammatory, analgesic, and antipyretic

agent, with efficiency 10-times higher than conventional NSAIDs such as naproxen sodium, paracetamol, and diclofenac sodium at the same doses or even at low doses administered.

Any synthetic or natural compound that offers any potential use in humans or animals, is rigorously investigated for its toxicity in an animal model before its application (Parveen et al., 2012). After testing the therapeutic effects of CNF, we investigated the toxicological profile of CNF using the rodent model. Since MgO NPs-based nanoformulation is reported for the first time, acute toxicity testing was necessary to find out the lethal dose of LD_{50} in mice. Results when computed statistically, revealed that the oral LD_{50} of CNF in mice is 2574 mg/kg, and could be categorized as safe (category 5; no warning on label) according to the Global Harmonized System for classifying hazardous chemicals (GSH) (Persson et al., 2017). Furthermore, the ratio between the minimal effective dose (1 mg/kg) reported earlier in this study and the lethal dose of NpNF (2574.77 mg/kg) indicates that it has a larger therapeutic window. According to USA Food and Drug Administration (FDA), USA, the LD_{50} of naproxen sodium, (currently used to formulate nanoformulation) is 1200 mg/kg in mice. Although the toxicity of free-form naproxen sodium has not been thoroughly investigated and reported in the literature, however, when compared to the reported LD_{50} of free-form NPRS, it is evident that the CNF is safer than NPRS (FDA, 2011).

On the other hand, the repeat-dose toxicity studies usually conducted for 14-28 days hold great significance in the preclinical investigation, during drug development. These investigations serve to establish the extent to which medications might cause toxicity and also the amount at which they are regarded safe. The data from this study establish the drug dose at which no effects are observed (NOELs) or no-observed adverse effect levels (NOAELs) were detected along with other important aspects such as organ toxicity and estimating the dose for the initial human trials (Dorato and Engelhardt, 2005). Therefore, after acute toxicity testing, a 14-day repeated dose range-finding study was conducted using low dose (30 mg/kg), medium dose (300 mg/kg), and high dose (1000 mg/kg) to evaluate the effect of CNF on male and female mice using various assays. Data from hematological, serum biochemical (ALT, AST, ALP, LDH, bilirubin, creatinine, triglyceride, and cholesterol), tissue biochemical (ROS, LPO; CAT, POD, SOD, and reduced glutathione levels in all tissues), and tissue histology (brain, heart,

liver, stomach, spleen, kidney, testis, and seminal vesicles) from both male and female mice revealed that low dose produced no effects in any of the tissues tested. The administration of medium-dose however, mildly affected a few tissues in male and female mice whereas treatment of high dose significantly affected most of the tissues except testicular tissue and seminal vesicles. Using existing technological tools or identifying indices that are crucial for determining the no-observed-adverse-effect level (NOAEL), the NOAEL of CNF was regarded as lower than 300 mg/kg in this study.

Since the regular use of NSAIDs causes multiple organ pathologies such as gastrointestinal tract ulcers and bleeding (Wallace, 2012), renal complications, hepatotoxicity (O'Connor et al., 2003; Hörl, 2010), and impairment of cardiovascular tissues (Fanelli et al., 2013). The current study sought to determine if the new nanoformulation is safer than the conventional form at therapeutic levels in target tissues such as the heart, stomach, liver, and kidneys. Mice in uncoated nanoformulation, coated nanoformulation and naproxen sodium treatment groups received clinical dose whereas mice in MgO treated group received MgO NPs equal to the quantity present in the nanoformulation. In the current study, MgO NPs treated group was included to elucidate any effect that can be caused by the MgO NPs used as drug carriers in naproxen nanoformulation.

Given the hematological changes caused by any test compound have a higher predictive value for human toxicity (Arika et al., 2016), naproxen nanoformulations were examined in the current study for their hematological effects. Results showed that the administration of uncoated naproxen and coated naproxen nanoformulation mildly disrupted hematological parameters in comparison to naproxen sodium, administration of which caused a drastic decrease in RBC, Hb, MCV, MCH, MCHC, WBC, and lymphocyte count/ content while significantly increased platelets, neutrophils, and monocytes.

The ALT, AST, and ALP are serum biochemical markers used to assess the hepatocellular injury. Whereas bilirubin is an excretory product formed by the catabolism of heme and normally excreted through the bile. The elevated level of bilirubin depicts major liver impairment caused by drugs (Rodwell and Murray, 2018). The present findings as regards increase in ALT, AST, and ALP in NPRS treated serum levels are consistent with previous findings that NSAIDs such as diclofenac, ibuprofen,

and paracetamol cause significant alteration in serum biochemical parameters (Gomaa, 2018). Moreover, an elevated level of serum bilirubin in NPRS-treated mice indicates NPRS led to severe anemia and correlates well with the histological tissue findings in the present study.

Creatinine is a non-protein nitrogenous substance formed from creatine and phosphocreatine during muscle metabolism and removed from the blood by glomerular ultrafiltration of the kidneys, and any abnormalities that decrease glomerular filtration rate will result in increased serum creatinine (Dhanvijay et al., 2013). Currently, naproxen associated increased level of serum creatinine agrees with Odangowei et al. (2020) who concluded that an increase in serum creatinine by NSAIDs reflects a marked decrease in glomerular filtration rate and indicates kidney injury (Ogidi et al., 2020). Moreover, a significant increase in serum cholesterol and triglycerides levels in NPRS-treated mice may be due to hepato-biliary and (Orinya et al., 2016) liver impairment, respectively (Mendenhall and Mortiaux, 1962). Interestingly, it was found in the present study that coated and uncoated naproxen nanoformulations did not show any alteration in all of the above-mentioned tissue toxicity makers and all values obtained were comparable to that of the control. It, therefore, seems that the slow release of the NPRS from the MgO NPs might have prevented excessive interaction of the NPRS with normal cells.

Reactive oxygen species (ROS) generation induces oxidative stress and is associated with cell death, a general mechanism of NSAIDs-induce tissue toxicity reported well in past studies Likewise, lipid peroxidation leads to the disintegration of lipid membranes (Ghosh et al., 2015; Ahmad et al., 2018). Whereas the antioxidant system of the body is a defense against free radicals and reactive species. When affected by toxins, radicals, reactive oxygen species, and reactive nitrogen species, the antioxidant defense shows up or downregulation of several antioxidant enzymes (Birben et al., 2012). Therefore, the increased lipid peroxidation and ROS level and decreased glutathione, SOD, CAT, and POD activities in the heart, liver, kidney, and stomach tissues following NPRS treatment in the present study indicate a possible involvement of NPRS-induced oxidative stress that altered antioxidant level in all tissues. The involvement of ROS in organ toxicity has been reported widely for diclofenac, ketoprofen, piroxicam, naproxen, and many other NSAIDs (Ghosh et al., 2015).

In contrast, the treatment of mice with coated and uncoated nanoformulations not only maintained the antioxidant defense systems in all tissues studied but also did not induce oxidative stress in the heart, liver, kidney, and stomach tissues. The binding of NPRS to MgO nanoparticles might have considerably increased the drug's aqueous solubility and thus its dissolution and/or increases the drug's permeability through biological membranes leading to faster onset of action reducing the manifestations of the drug toxicity (Kermanizadeh et al., 2018).

The one major risk that has always been associated with the short- or long-term use of NSAIDs, is gastrointestinal mucosal injury (Conaghan, 2012). It was found in the gross examination of tissue that the administration of NPRS to mice caused severe hemorrhagic lesions along with an increased ulcer score. On the contrary, administration of uncoated and coated nanoformulation preserved the integrity of stomach tissues which was shown by the normal morphology of stomach tissue observed in both groups.

Tissue microscopy revealed that NPRS caused disorganization of the myofibrils with moderate loss of striations and vascular dilatation in heart tissues. Vascular congestion, edema, degeneration of epithelial cells, intracellular infiltration, and increased apoptosis of gastric epithelia were observed in gastric tissue. cellular disintegration in the form of vacuolization and infiltration of inflammatory cells were observed in liver tissue while in kidneys, congestion, glomerular atrophy with Bowman's gap enlargement, epithelial disintegration in tubular structures, and mononuclear cell infiltration was observed. Together histopathological findings demonstrated NPRS-induced tissue toxicity at therapeutic doses.

However, NPRS entrapped in MgO nanoparticles and coated with PVA significantly reduced gastritis-associated changes within the gastric mucosa, as evidenced by a decrease in the gastric ulcer score, maintained mucosal fold in the gastric wall with no signs of leucocyte infiltration. Moreover, uncoated and coated nanoformulation both did not alter the normal histological structure of the myocardial tissue in mice at clinical doses except for minor dilation in cardiac muscle arrangement that was observed in UNF treated group. Similar results were found in another study that encapsulation of diclofenac sodium, another NSAID with high cardiotoxicity profile, into the polymeric micelle showed decreased signs of cardiotoxicity compared to the free drug (Al-Lawati

et al., 2018). Moreover, administration of the same doses of naproxen nanoparticulate formulations maintained the cellular integrity of the liver tissues and did not affect the normal tissue architecture of the kidneys.

The mRNA expressions of pro-inflammatory cytokines such as TNFα, IL6, and IL1β associated with drug toxicity were also studied in the present investigation. It is suggested that oxidative stress induces upregulation of pro- cytokines, such as tumor necrosis factor-alpha (TNF-α), interleukin-1beta (IL-1β), and interleukin-6 (IL-6) (Poljsak et al., 2013). Present, a significant upregulation in TNFα, IL6, and IL1β mRNA expression in heart, liver, kidney, and stomach tissues from NPRS-treated mice confirms the idea that NPRS triggers the immune system through the production of ROS and further causes tissue toxicities.

Caspase-3 is a well-known component of cellular death and stimuli such as free radicles can activate it to cause apoptosis of cells (Condorelli et al., 2001). COX-2, on the other, is present at low or undetectable levels in most tissues, may be quickly and strongly activated in response to inflammatory signals or other stresses (Streicher and Wang, 2008), and cytokines induce the synthesis of (nitric oxide) by iNOS (inducible NO synthase) and initiate inflammation (Zamora et al., 2000). Presently, immunohistochemistry performed in the present study revealed that NPRS led to a strong expression of COX-2, iNOS, and caspase-3 in the heart, liver, kidney, and stomach tissues.

Presently, the NPRS-induced renal complications can be ascribed to the activation and upregulations of IL-6, IL 1β, and TNFα in response to ROS-mediated cellular injury and then, subsequent elevated expression of iNOS, COX-2, and caspase-3. Contrary to this, naproxen nanoformulations showed a significant decline in the above-mentioned regulators and inflammatory mediators suggesting a protective role. Lastly, after administration of the placebo nanoparticles (nMgO) at the dosage level of 55.34 mg/kg/day (equivalent to the amount used in NPRS nanoformulation), did not show any adverse or toxic effects in any of the tissues studied, and all the physiological values were found to be near baseline or as detected in control mice.

General Conclusion

Literature showed that the therapeutic use of NPRS is associated with dose-dependent organ toxicities. The present investigation reported that nanosizing using MgO NPs as nanocarrier enhanced the therapeutic efficacy and decreased the toxicity of the anti-inflammatory drug NPRS. This study is the first of its kind to report the preparation of non-toxic, cost-effective, and more potent therapeutic nanoformulation of NPRS (CNF). CNFwih size of 161 nm and surface charge -8 mV showed significant analgesic, anti-inflammatory, and antipyretic effects in mice at 10 to 90 times lower doses than conventional NPRS.

Acute and sub-acute toxicity studies determined that present nanoformulation is safe up to 300 mg/kg with moderate signs of toxicity showed at 1000 mg/kg oral dose in both male and female mice. Using existing technological tools or identifying indices that are crucial for determining the no-observed-adverse-effect level (NOAEL), the NOAEL of naproxen nanoformulation is regarded as lower than 300 mg/kg in this study. Whereas oral LD_{50} is found to be 2574.77 mg/kg in mice. Organ's safety studies among naproxen nanoformulations (UNF and CNF) and naproxen sodium alone at therapeutic doses revealed that naproxen indeed can cause organ damage through the activation of several proteins that are involved in organ inflammation and apoptosis. However, encapsulation of naproxen with MgO NPs significantly reduce drug-induced tissue toxicity and restored the level of inflammatory cytokines (IL6, IL1β, and TNF-α), iNOS, COX-2, and apoptotic proteins caspase-3 to the baseline levels.

Although, this study provides very valuable data on the acute and subacute toxicity profile of CNF, the long-term effect of CNF in mice were not studied. However, the present investigation could provide a guideline for selecting doses for the sub-chronic and chronic study, which may be more clinically relevant. Whereas acute oral treatment of naproxen nanoformulation is unlikely to produce toxicity, repeated administration may have a long-term cumulative harmful effect on mice. Additional toxicity data (chronic, mutagenicity, reproductive and carcinogenicity study) on CNF are urgent to investigate to confirm the risk of CNF for long-term exposure in comparative toxicity experiments.

Nevertheless, the protein inhibitors or knock-out models to inhibit the molecular

mechanisms involved in NPRS-induced tissue toxicity should be used to validate the protective effect of naproxen nanoformulations. However, the results of the current study shed light on the protective effect of naproxen nanoformulation and would foster further studies to prove the current finding. Lastly, MgO NPs may also be used as biocompatible drug carriers to enhance the therapeutic efficacy and reduced the toxicity of other therapeutic and anti-inflammatory drugs.

List of Publications

1. **Razzaq, A., Naz, S. S., Qureshi, I. Z., Rehman, F.-U. and Qaisar, S.** (2022). Synthesis of PVA capped naproxen conjugated MgO nanoparticles and its bioactivity screening. *Journal of Drug Delivery in Science and Technology*, 103429. **IF: 5.06**

2. **Razzaq, A., Qureshi, I. Z.** (2022). Naproxen sodium nanoparticles are less toxic and gastroprotective agents than the conventional NSAID drug naproxen sodium in Balb/c mice. *Toxicology and Applied Pharmacology*. **IF: 4.42**.

REFERENCES

Abadi, S.S.H., Moin, A. and Veerabhadrappa, G.H. (2016). fabricated microparticles: an innovative method to minimize the side effects of NSAIDs in arthritis. *Critical Review in Therapeutic Drug Carrier Systems*, *33*(5), pp.433-488.

Abasian, P., Ghanavati, S., Rahebi, S., Nouri Khorasani, S., and Khalili, S. (2020). Polymeric nanocarriers in targeted drug delivery systems: A review. *Polymers for Advanced Technologies*, *31*(12), pp.2939-2954.

Abatan, M.O., Lateef, I. and Taiwo, V.O, (2006). Toxic effects of non-steroidal anti-inflammatory agents in rats. *African Journal of Biomedical Research*, *9*(3).

Abbasi, E., Aval, S.F., Akbarzadeh, A., Milani, M., Nasrabadi, H.T., Joo, S.W., Hanifehpour, Y., Nejati-Koshki, K. and Pashaei-Asl, R. (2014). Dendrimers: synthesis, applications, and properties. *Nanoscale research letters*, *9*(1), pp.1-10.

Abdeen, A., Aboubakr, M., Elgazzar, D., Abdo, M., Abdelkader, A., Ibrahim, S. and Elkomy, A. (2019). Rosuvastatin attenuates piroxicam-mediated gastric ulceration and hepato-renal toxicity in rats. *Biomedicine & Pharmacotherapy*, *110*, pp.895-905.

AboulFotouh, K., Allam, A.A. and El-Badry, M. (2019). Self-emulsifying drug delivery systems: easy to prepare multifunctional vectors for efficient oral delivery. In *Current and Future Aspects of Nanomedicine*. IntechOpen.

Abo-Zalam, H.B., El-Denshary, E.S., Abdelsalam, R.M., Khalil, I.A., Khattab, M.M. and Hamzawy, M.A. (2021). Therapeutic advancement of simvastatin-loaded solid lipid nanoparticles (SV-SLNs) in treatment of hyperlipidemia and attenuating hepatotoxicity, myopathy, and apoptosis: Comprehensive study. *Biomedicine & Pharmacotherapy*, *139*, p.111494.

Ackermann, M.R. (2017). Inflammation and healing. In *Pathologic basis of veterinary disease*, pp. 73-131.

Ahmad, A., Ansari, M.M., Mishra, R.K., Kumar, A., Vyawahare, A., Verma, R.K., Raza, S.S. and Khan, R. (2021). Enteric-coated gelatin nanoparticles mediated oral delivery of 5-aminosalicylic acid alleviates severity of DSS-induced

ulcerative colitis. *Materials Science and Engineering: C*, *119*, p.111582

Ahmad, M.H., Fatima, M., Hossain, M. and Mondal, A.C. (2018). Evaluation of naproxen-induced oxidative stress, hepatotoxicity and in-vivo genotoxicity in male Wistar rats. *Journal of pharmaceutical analysis*, *8*(6), pp.400-406.

Ahmad, M.Z., Akhter, S., Jain, G.K., Rahman, M., Pathan, S.A., Ahmad, F.J. and Khar, R.K. (2010). Metallic nanoparticles: technology overview & drug delivery applications in oncology. *Expert opinion on drug delivery*, *7*(8), pp.927-942.

Ahmed, R. and Baig, M.A. (2009). A comparative study of single and double pulse laser induced breakdown spectroscopy. *Journal of Applied Physics*, *106*(3), p.033307.

Al Lawati, H. and Jamali, F. (2016). Onset of action and efficacy of ibuprofen liquigel as compared to solid tablets: A systematic review and meta-analysis. *Journal of Pharmacy & Pharmaceutical Sciences*, *19*(3), pp.301-311.

Alavi, M. and Nokhodchi, A. (2021). Micro-and nanoformulations of paclitaxel based on micelles, liposomes, cubosomes, and lipid nanoparticles: Recent advances and challenges. *Drug Discovery Today*.

Alfaro, A., León, A., Guajardo-Correa, E., Reuquen, P., Torres, F., Mery, M., Segura, R., Zapata, P.A. and Orihuela, P.A. (2019). MgO nanoparticles coated with polyethylene glycol as carrier for 2-Methoxyestradiol anticancer drug. *Plos one*, *14*(8), p.0214900.

Al-Lawati, H., Aliabadi, H.M., Makhmalzadeh, B.S. and Lavasanifar, A. (2018). Nanomedicine for immunosuppressive therapy: achievements in pre-clinical and clinical research. *Expert opinion on drug delivery*, *15*(4), pp.397-418.

Al-Lawati, H., Binkhathlan, Z. and Lavasanifar, A. (2019). Nanomedicine for the effective and safe delivery of non-steroidal anti-inflammatory drugs: A review of preclinical research. *European Journal of Pharmaceutics and Biopharmaceutics*, *142*, pp.179-194.

Al-Lawati, H., R Vakili, M., Jamali, F. and Lavasanifar, A. (2016). Polymeric micelles for the delivery of diclofenac and its ethyl ester derivative. *Pharmaceutical Nanotechnology*, *4*(2), pp.109-119.

Almeida Junior, S.D. (2019). In vivo methods for the evaluation of anti-inflammatory and antinoceptive potential. *BrJP*, *2*, pp.386-389.

Almontasser, A., Parveen, A. and Azam, A. (2019), Synthesis, Characterization and antibacterial activity of Magnesium Oxide (MgO) nanoparticles. In *IOP Conference Series: Materials Science and Engineering* *577* (1), p. 012051.

Amendola, V. and Meneghetti, M. (2009). Size evaluation of gold nanoparticles by UV−vis spectroscopy. *The Journal of Physical Chemistry C*, *113*(11), pp.4277-4285.

Amer, M., Bead, V.R., Bathon, J., Blumenthal, R.S. and Edwards, D.N. (2010). Use of nonsteroidal anti-inflammatory drugs in patients with cardiovascular disease: a cautionary tale. *Cardiology in review*, *18*(4), pp.204-212.

Anabitarte, F., Cobo, A. and Lopez-Higuera, J.M. (2012). Laser-induced breakdown spectroscopy: fundamentals, applications, and challenges. *International Scholarly Research Notices*, *2012. ISRN Spectroscopy, 2012*, p.285240.

Ananda, A., Ramakrishnappa, T., Archana, S., Yadav, L.R., Shilpa, B.M., Nagaraju, G. and Jayanna, B.K. (2022). Green synthesis of MgO nanoparticles using Phyllanthus emblica for evans blue degradation and antibacterial activity. *Materials Today: Proceedings*, *49*, pp.801-810.

Anselmo, N.A., Paskakulis, L.C., Garcias, R.C., Botelho, F.F.R., Toledo, G.Q., Cury, M.F.R., Carvalho, N.Z., Mendes, G.E.F., Iembo, T., Bizotto, T.S.G. and Cury, P.M. (2018). Prior intake of Brazil nuts attenuates renal injury induced by ischemia and reperfusion. *Brazilian journal of nephrology*, *40*, pp.10-17.

Arika, W.M., Nyamai, D.W., Musila, M.N., Ngugi, M.P. and Njagi, E.N.M. (2016). Hematological markers of in vivo toxicity. *Journal of Hematology & Thromboembolic Diseases*, **04**.

Aronoff, D.M. and Neilson, E.G., (2001). Antipyretics: mechanisms of action and clinical use in fever suppression. *The American journal of medicine*, *111*(4), pp.304-315.

Asanuma, M., Nishibayashi-Asanuma, S., Miyazaki, I., Kohno, M. and Ogawa, N. (2001). Neuroprotective effects of non-steroidal anti-inflammatory drugs by

direct scavenging of nitric oxide radicals. *Journal of neurochemistry*, *76*(6), pp.1895-1904.

Asha, A.B. and Narain, R. (2020). Nanomaterials properties. In *Polymer science and nanotechnology*, pp. 343-359.

Ashik, U.P.M., Kudo, S. and Hayashi, J.I. (2018). An overview of metal oxide nanostructures. *Synthesis of Inorganic Nanomaterials*, pp.19-57.

Athar, T. (2015). Smart precursors for smart nanoparticles. In W. Ahmed & M. J. Jackson (Eds.), *Emerging Nanotechnologies for Manufacturing (Second Edition)* (pp. 444-538). Boston: William Andrew Publishing.

Atkinson, T.J. and Fudin, J. (2020). Nonsteroidal antiinflammatory drugs for acute and chronic pain. *Physical Medicine and Rehabilitation Clinics*, *31*(2), pp.219-231

Axson, J.L., Stark, D.I, Bondy, A.L., Capracotta, S.S., Maynard, A.D., Philbert, M.A., Bergin, I.L. and Ault, A.P. (2015). Rapid kinetics of size and pH-dependent dissolution and aggregation of silver nanoparticles in simulated gastric fluid. *The Journal of Physical Chemistry C*, *119*(35), pp.20632-20641.

Azeemi, S.T.Y., Raza, S.M., Yasinzai, M. and Samad, A. (2009). Effect of different wavelengths on superoxide dismutase. *Journal of Acupuncture and Meridian Studies*, *2*(3), pp.236-238.

Bai, X. Smith, Z.L., Wang, Y. Butterworth, S. and Tirella, A. (2022). Sustained drug release from   smart nanoparticles in cancer therapy: A comprehensive review. *Micromachines*, *13*(10), 1623.

Baig, N., Kammakakam, I. and Falath, W. (2021). Nanomaterials: A review of synthesis methods, properties, recent progress, and challenges. *Materials Advances*, *2*(6), pp.1821-1871.

Bailey, S.A., Zidell, R.H. and Perry, R.W. (2004). Relationships between organ weight and body/brain weight in the rat: what is the best analytical endpoint?. *Toxicologic pathology*, *32*(4), pp.448-466.

Banerjee, A., Qi, J., Gogoi, R., Wong, J. and Mitragotri, S. (2016). Role of nanoparticle size, shape and surface chemistry in oral drug delivery. *Journal of Controlled Release*, *238*, pp.176-185.

Banik, A., Gogoi, P. and Saikia, M.D. (2012). Interaction of naproxen with β-cyclodextrin and its derivatives/polymer: experimental and molecular modeling studies. *Journal of Inclusion Phenomena and Macrocyclic Chemistry*, *72*(3), pp.449-458.

Bao, W.L., Wu, Q., Hu, B., Sun, D., Zhao, S., Shen, X., Cheng, H. and Shen, W. (2021). Oral nanoparticles of SNX10-shRNA plasmids ameliorate mouse colitis. *International Journal of Nanomedicine*, *16*, p.345-357.

Barani, M., Rahdar, A., Sargazi, S., Amiri, M.S., Sharma, P.K. and Bhalla, N. (2021). Nanotechnology for inflammatory bowel disease management: Detection, imaging and treatment. *Sensing and Bio-Sensing Research*, *32*, p.100417.

Barnes, P.J. (2006). How corticosteroids control inflammation: quintiles prize lecture 2005. *British journal of pharmacology*, *148*(3), pp.245-254.

Batista-Navarro, R.T. (2013). Biological Activity. *Encyclopedia of Systems Biology*, pp.110-110. New York, NY: Springer New York.

Bensman, A. (2020). Non-steroidal anti-inflammatory drugs (NSAIDs) systemic use: the risk of renal failure. *Frontiers in pediatrics*, *7*, p.517.

Bernardi, A., Zilberstein, A.C.C.V., Jäger, E., Campos, M.M., Morrone, F.B., Calixto, J.B., Pohlmann, A.R., Guterres, S.S. and Battastini, A.M.O. (2009). Effects of indomethacin-loaded nanocapsules in experimental models of inflammation in rats. *British journal of pharmacology*, *158*(4), pp.1104-1111.

Bessone, F. (2010). Non-steroidal anti-inflammatory drugs: What is the actual risk of liver damage?. *World journal of gastroenterology: WJG*, *16*(45), p.5651-5661.

Bessone, F., Hernandez, N., Roma, M.G., Ridruejo, E., Mendizabal, M., Medina-Cáliz, I., Robles-Díaz, M., Lucena, M.I. and Andrade, R.J. (2016). Hepatotoxicity induced by coxibs: how concerned should we be?. *Expert Opinion on Drug Safety*, *15*(11), pp.1463-1475.

Bhattacharjee, S. (2016). DLS and zeta potential–what they are and what they are not?. *Journal of controlled release*, *235*, pp.337-351.

Bhattacharjee, S., Rietjens, I.M., Singh, M.P., Atkins, T.M., Purkait, T.K., Xu, Z.,

Regli, S., Shukaliak, A., Clark, R.J., Mitchell, B.S. and Alink, G.M. (2013). Cytotoxicity of surface-functionalized silicon and germanium nanoparticles: the dominant role of surface charges. *Nanoscale*, *5*(11), pp.4870-4883.

Bhise, K.S., Dhumal, R.S., Paradkar, A.R. and Kadam, S.S. (2008). Effect of drying methods on swelling, erosion and drug release from chitosan–naproxen sodium complexes. *Aaps Pharmscitech*, *9*(1), pp.1-12.

Bindu, S., Mazumder, S. and Bandyopadhyay, U. (2020). Non-steroidal anti-inflammatory drugs (NSAIDs) and organ damage: A current perspective. *Biochemical pharmacology*, *180*, p.114147.

Bindu, S., Mazumder, S., and Bandyopadhyay, U. J. B. P. (2020). Non-steroidal anti-inflammatory drugs (NSAIDs) and organ damage: A current perspective. *Biochemical Pharmacology, 180*, p. 114147.

Birben, E., Sahiner, U.M., Sackesen, C., Erzurum, S. and Kalayci, O. (2012). Oxidative stress and antioxidant defense. *World allergy organization journal*, *5*(1), pp.9-19.

Birmingham, B. and Buvanendran, A. (2014). Nonsteroidal anti-inflammatory drugs, acetaminophen, and COX-2 inhibitors. In *Practical Management of Pain*, pp. 553-568.

Bishnoi, A., Kumar, S. and Joshi, N. (2017). Wide-angle X-ray diffraction (WXRD): technique for characterization of nanomaterials and polymer nanocomposites. In *Microscopy methods in nanomaterials characterization* (pp. 313-337). Elsevier.

Boelsterli, U.A. (2002). Mechanisms of NSAID-induced hepatotoxicity. *Drug safety*, *25*(9), pp.633-648.

Brand, M.D., Affourtit, C., Esteves, T.C., Green, K., Lambert, A.J., Miwa, S., Pakay, J.L. and Parker, N. (2004). Mitochondrial superoxide: production, biological effects, and activation of uncoupling proteins. *Free Radical Biology and Medicine*, *37*(6), pp.755-767.

Brune, K. and Hinz, B. (2004). The discovery and development of antiinflammatory drugs. *Arthritis & Rheumatism: Official Journal of the American College of Rheumatology*, *50*(8), pp.2391-2399.

Brutzkus JC, S. M., Varacallo M. (2022). *Naproxen*: StatPearls Publishing, Treasure Island (FL).

Çalış, S., Atar, K.Ö., Arslan, F.B., Eroğlu, H. and Çapan, Y. (2019). Nanopharmaceuticals as Drug-Delivery Systems: For, Against, and Current Applications. In *Nanocarriers for Drug Delivery* (pp. 133-154). Elsevier.

Cao, Y., Ma, Y., Tao, Y., Lin, W. and Wang, P. (2021). Intra-articular drug delivery for osteoarthritis treatment. *Pharmaceutics*, *13*(12), p.2166.

Carter, M. and Shieh, J. (2015). Chapter 2-animal behavior. *Guide to research techniques in neuroscience*, pp.39-71.

Caster, J.M., Stephanie, K.Y., Patel, A.N., Newman, N.J., Lee, Z.J., Warner, S.B., Wagner, K.T., Roche, K.C., Tian, X., Min, Y. and Wang, A.Z. (2017). Effect of particle size on the biodistribution, toxicity, and efficacy of drug-loaded polymeric nanoparticles in chemoradiotherapy. *Nanomedicine: Nanotechnology, Biology and Medicine*, *13*(5), pp.1673-1683.

Chandrakala, V., Aruna, V. and Angajala, G. (2022). Review on metal nanoparticles as nanocarriers: Current challenges and perspectives in drug delivery systems. *Emergent Materials*, pp.1-23.

Chen, C., Yang, J.S., Lu, C.C., Wu, Y.T. and Chen, F.A. (2021). Effect of Quercetin on Injury to Indomethacin-Treated Human Embryonic Kidney 293 Cells. *Life*, *11*(11), p.1134.

Chime, S.A., Attama, A.A., Builders, P.F. and Onunkwo, G.C. (2013). Sustained-release diclofenac potassium-loaded solid lipid microparticle based on solidified reverse micellar solution: in vitro and in vivo evaluation. *Journal of microencapsulation*, *30*(4), pp.335-345.

Communication from the Commission to the European Parliament, Second, t. C. a. t. E. E. a. S. C. o. t., and Nanomaterials., R. R. o. (2012). Types and uses of nanomaterials, including safety aspects.

Conaghan, P.G. (2012). A turbulent decade for NSAIDs: update on current concepts of classification, epidemiology, comparative efficacy, and toxicity. *Rheumatology international*, *32*(6), pp.1491-1502.

Condorelli, G., Roncarati, R., Ross Jr, J., Pisani, A., Stassi, G., Todaro, M., Trocha,

S., Drusco, A., Gu, Y., Russo, M.A. and Frati, G. (2001). Heart-targeted overexpression of caspase3 in mice increases infarct size and depresses cardiac function. *Proceedings of the National Academy of Sciences*, **98**(17), pp.9977-9982.

Cremers, D. A., Multari, R. A., and Knight, A. K. Laser-Induced Breakdown Spectroscopy. In *Encyclopedia of Analytical Chemistry* (pp. 1-28).

Croy, S.R. and Kwon, G.S. (2006). Polymeric micelles for drug delivery. *Current pharmaceutical design*, **12**(36), pp.4669-4684.

Cui, K., Luo, X., Xu, K. and Murthy, M.V. (2004). Role of oxidative stress in neurodegeneration: recent developments in assay methods for oxidative stress and nutraceutical antioxidants. *Progress in Neuro-Psychopharmacology and Biological Psychiatry*, **28**(5), pp.771-799.

D'Souza, S. (2014). A review of in vitro drug release test methods for nano-sized dosage forms. *Advances in Pharmaceutics*, **2014**, pp.304757.

D'Amour, F.E. and Smith, D.L. (1941). A method for determining loss of pain sensation. *Journal of Pharmacology and Experimental Therapeutics*, **72**(1), pp.74-9.

Dangarembizi, R., Erlwanger, K.H., Rummel, C., Roth, J., Madziva, M.T. and Harden, L.M. (2018). Brewer's yeast is a potent inducer of fever, sickness behavior and inflammation within the brain. *Brain, Behavior, and Immunity*, **68**, pp.211-223.

Daraee, H., Etemadi, A., Kouhi, M., Alimirzalu, S. and Akbarzadeh, A. (2016). Application of liposomes in medicine and drug delivery. *Artificial cells, nanomedicine, and biotechnology*, **44**(1), pp.381-391.

Das, N., Bhattacharyya, A., Paria, B. and Sarkar, S. (2015). Study on assessment of renal function in chronic liver disease. *Journal of Clinical and Diagnostic Research: JCDR*, **9**(3), p.OC09-OC12.

De Smet, L., Ceelen, W., Remon, J.P. and Vervaet, C. (2013). Optimization of drug delivery systems for intraperitoneal therapy to extend the residence time of the chemotherapeutic agent. *The Scientific World Journal*, **2013**. P.720858.

De Souza, R., Zahedi, P., Allen, C.J. and Piquette-Miller, M. (2010). Polymeric drug

delivery systems for localized cancer chemotherapy. *Drug delivery*, *17*(6), pp.365-375.

Deavall, D.G., Martin, E.A., Horner, J.M. and Roberts, R. (2012). Drug-induced oxidative stress and toxicity. *Journal of toxicology*, *2012*, pp.645460.

Desai, N. (2012). Challenges in development of nanoparticle-based therapeutics. *The AAPS journal*, *14*(2), pp.282-295.

Desjardins, P.J., Olugemo, K., Solorio, D. and Young, C.L. (2015). Pharmacokinetic properties and tolerability of low-dose SoluMatrix diclofenac. *Clinical Therapeutics*, *37*(2), pp.448-461.

Deuis, J.R., Dvorakova, L.S. and Vetter, I. (2017). Methods used to evaluate pain behaviors in rodents. *Frontiers in molecular neuroscience*, *10*, p.284.

Dhanvijay, P., Misra, A.K. and Varma, S.K. (2013). Diclofenac induced acute renal failure in a decompensated elderly patient. *Journal of Pharmacology and Pharmacotherapeutics*, *4*(2), pp.155-157.

Dingle, J.T., Gordon, J.L., Hazleman, B.L., Knight, C.G., Page Thomas, D.P., Phillips, N.C., Shaw, I.H., Fildes, F.J.T., OLIVER, J.E., Jones, G. and Turner, E.H. (1978). Novel treatment for joint inflammation. *Nature*, *271*(5643), pp.372-373.

Dixit, M., Doan, T., Kirschner, R. and Dixit, N. (2010). Significant acute kidney injury due to non-steroidal anti-inflammatory drugs: inpatient setting. *Pharmaceuticals*, *3*(4), pp.1279-1285.

Donati, M., Conforti, A., Lenti, M.C., Capuano, A., Bortolami, O., Motola, D., Moretti, U., Vannacci, A., Rafaniello, C., Vaccheri, A. and Arzenton, E. (2016). Risk of acute and serious liver injury associated to nimesulide and other NSAIDs: data from drug-induced liver injury case–control study in Italy. *British journal of clinical pharmacology*, *82*(1), pp.238-248.

Dorato, M.A. and Buckley, L.A. (2006). Toxicology in the drug discovery and development process. *Current protocols in pharmacology*, *32*(1), pp.10-3.

Dorato, M.A. and Engelhardt, J.A. (2005). The no-observed-adverse-effect-level in drug safety evaluations: use, issues, and definition (s). *Regulatory toxicology and pharmacology*, *42*(3), pp.265-274.

Dougall, I.G. and Unitt, J. (2015). Evaluation of the biological activity of compounds: techniques and mechanism of action studies. In *The Practice of Medicinal Chemistry* (pp. 15-43). Academic Press.

Drini, M. (2017). Peptic ulcer disease and non-steroidal anti-inflammatory drugs. *Australian prescriber*, *40*(3), p.91.

Duncan, B., Kim, C. and Rotello, V.M. (2010). Gold nanoparticle platforms as drug and biomacromolecule delivery systems. *Journal of controlled release*, *148*(1), pp.122-127.

Duncan, R. (2003). The dawning era of polymer therapeutics. *Nature reviews Drug discovery*, *2*(5), pp.347-360.

Dwyer, J. (2004). Dietary Reference Intakes (DRIs): Concepts and Implementation. In L. R. Johnson (Ed.), *Encyclopedia of Gastroenterology* (pp. 613-623). New York: Elsevier.

Elisha, I.L., Dzoyem, J.P., McGaw, L.J., Botha, F.S. and Eloff, J.N. (2016). The anti-arthritic, anti-inflammatory, antioxidant activity and relationships with total phenolics and total flavonoids of nine South African plants used traditionally to treat arthritis. *BMC complementary and alternative medicine*, *16*(1), pp.1-10.

El-Sisi, A.E., Sokkar, S.S., Ibrahim, H.A., Hamed, M.F. and Abu-Risha, S.E. (2020). Targeting MDR-1 gene expression, BAX/BCL2, caspase-3, and Ki-67 by nanoencapsulated imatinib and hesperidin to enhance anticancer activity and ameliorate cardiotoxicity. *Fundamental & Clinical Pharmacology*, *34*(4), pp.458-475.

Erhirhie, E.O., Ihekwereme, C.P. and Ilodigwe, E.E. (2018). Advances in acute toxicity testing: strengths, weaknesses and regulatory acceptance. *Interdisciplinary toxicology*, *11*(1), p.5.

EUBANK, W.R. (1951). Calcination studies of magnesium oxides. *Journal of the American Ceramic Society*, *34*(8), pp.225-229.

Evans, B.C., Nelson, C.E., Shann, S.Y., Beavers, K.R., Kim, A.J., Li, H., Nelson, H.M., Giorgio, T.D. and Duvall, C.L. (2013). Ex vivo red blood cell hemolysis assay for the evaluation of pH-responsive endosomolytic agents for cytosolic delivery of biomacromolecular drugs. *JoVE (Journal of Visualized*

Experiments), **(73)**, p.e50166.

Fadeel, B. (2019). The right stuff: on the future of nanotoxicology. *Frontiers in Toxicology*, p.1.

Falcaro, P., Ricco, R., Yazdi, A., Imaz, I., Furukawa, S., Maspoch, D., Ameloot, R., Evans, J.D. and Doonan, C.J. (2016). Application of metal and metal oxide nanoparticles@ MOFs. *Coordination Chemistry Reviews*, *307*, pp.237-254.

Falke, S. and Betzel, C. (2019). Dynamic light scattering (DLS). In *Radiation in Bioanalysis* (pp. 173-193). Springer, Cham.

Fanelli, A., Romualdi, P., Viganò, R., Lora Aprile, P., Gensini, G. and Fanelli, G. (2013). Non-selective non-steroidal anti-inflammatory drugs (NSAIDs) and cardiovascular risk. *Acta Biomed*, *84*(1), pp.5-11.

Farhana, A. and Lappin, S.L. (2022). Biochemistry, lactate dehydrogenase. In *StatPearls [Internet]*. StatPearls Publishing.

Farjadian, F., Ghasemi, A., Gohari, O., Roointan, A., Karimi, M. and Hamblin, M.R. (2019). Nanopharmaceuticals and nanomedicines currently on the market: challenges and opportunities. *Nanomedicine*, *14*(1), pp.93-126.

FDA. (2010). *M3(R2) Nonclinical Safety Studies for the Conduct of Human Clinical Trials and Marketing Authorization for Pharmaceuticals*. Center for Drug Evaluation and Research, Center for Biologics Evaluation and Research

FDA. (2011). (naproxen sodium) CONTROLLED-RELEASE TABLETS.

FDA. (2015). FDA Drug Safety Communication: FDA strengthens warning that non-aspirin nonsteroidal anti-inflammatory drugs (NSAIDs) can cause heart attacks or strokes.

Fendrick, A.M. and Greenberg, B.P. (2009). A review of the benefits and risks of nonsteroidal anti-inflammatory drugs in the management of mild-to-moderate osteoarthritis. *Osteopathic medicine and primary care*, *3*(1), pp.1-7.

Fernandes, M., RB Singh, K., Sarkar, T., Singh, P. and Pratap Singh, R. (2020). Recent applications of magnesium oxide (MgO) nanoparticles in various domains. *Advanced Materials Letters*, *11*(8), pp.1-10

Fiehn, C., Muller-Ladner, U., Gay, S., Krienke, S., Freudenberg-Konrad, S., Funk,

J., Ho, A.D., Sinn, H. and Wunder, A. (2004). Albumin-coupled methotrexate (MTX-HSA) is a new anti-arthritic drug which acts synergistically to MTX. *Rheumatology*, *43*(9), pp.1097-1105.

Fojtu, M., Gumulec, J., Stracina, T., Raudenska, M., Skotakova, A., Vaculovicova, M., Adam, V., Babula, P., Novakova, M. and Masarik, M. (2017). Reduction of doxorubicin-induced cardiotoxicity using nanocarriers: a review. *Current drug metabolism*, *18*(3), pp.237-263.

Foulkes, R., Man, E., Thind, J., Yeung, S., Joy, A. and Hoskins, C. (2020). The regulation of nanomaterials and nanomedicines for clinical application: Current and future perspectives. *Biomaterials science*, *8*(17), pp.4653-4664.

Fröhlich, E. (2012). The role of surface charge in cellular uptake and cytotoxicity of medical nanoparticles. *International journal of nanomedicine*, *7*, p.5577.

Frölich, J.C. (1997). A classification of NSAIDs according to the relative inhibition of cyclooxygenase isoenzymes. *Trends in Pharmacological Sciences*, *18*(1), pp.30-34.

Fruchon, S. and Poupot, R. (2017). Pro-inflammatory versus anti-inflammatory effects of dendrimers: The two faces of immuno-modulatory nanoparticles. *Nanomaterials*, *7*(9), p.251.

Fu, S., Wu, D., Jiang, W., Li, J., Long, J., Jia, C. and Zhou, T. (2020). Molecular biomarkers in drug-induced liver injury: challenges and future perspectives. *Frontiers in pharmacology*, *10*, p.1667.

Fullerton, J.N., O'Brien, A.J. and Gilroy, D.W. (2013). Pathways mediating resolution of inflammation: when enough is too much. *The Journal of pathology*, *231*(1), pp.8-20.

Gad, S. E. (2014). Prostaglandins. In P. Wexler (Ed.), *Encyclopedia of Toxicology (Third Edition)* (pp. 1120-1122). Oxford: Academic Press.

Gaikwad, V.L., Choudhari, P.B., Bhatia, N.M. and Bhatia, M.S. (2019). Characterization of pharmaceutical nanocarriers: in vitro and in vivo studies. In *Nanomaterials for drug delivery and therapy* (pp. 33-58). William Andrew Publishing.

Gajengi, A.L., Sasaki, T. and Bhanage, B.M. (2017). Mechanistic aspects of formation

of MgO nanoparticles under microwave irradiation and its catalytic application. *Advanced Powder Technology*, *28*(4), pp.1185-1192.

Gandotra, S. (2020). Lipid droplets in the immune response and beyond. In *Lipid Signaling and Metabolism* (pp. 173-196). Academic Press.

Gao, C.H., Mortimer, M., Zhang, M., Holden, P.A., Cai, P., Wu, S., Xin, Y., Wu, Y. and Huang, Q. (2019). Impact of metal oxide nanoparticles on in vitro DNA amplification. *PeerJ*, *7*, p.e7228.

Gao, S., Tian, B., Han, J., Zhang, J., Shi, Y., Lv, Q. and Li, K. (2019). Enhanced transdermal delivery of lornoxicam by nanostructured lipid carrier gels modified with polyarginine peptide for treatment of carrageenan-induced rat paw edema. *International journal of nanomedicine*, *14*, p.6135.

Gao, Y., Gesenberg, C. and Zheng, W. (2017). Oral formulations for preclinical studies: principle, design, and development considerations. In *Developing Solid Oral Dosage Forms* (pp. 455-495). Academic Press.

Gao, Y., Zuo, J., Bou-Chacra, N., Pinto, T.D.J.A., Clas, S.D., Walker, R.B. and Löbenberg, R. (2013). In vitro release kinetics of antituberculosis drugs from nanoparticles assessed using a modified dissolution apparatus. *BioMed research international*, *2013*, p.136590.

Garcia, C., Feve, B., Ferre, P., Halimi, S., Baizri, H., Bordier, L., Guiu, G., Dupuy, O., Bauduceau, B. and Mayaudon, H. (2010). Diabetes and inflammation: fundamental aspects and clinical implications. *Diabetes & metabolism*, *36*(5), pp.327-338.

García, M. C., Torres, J., Dan Córdoba, A. V., Longhi, M., and Uberman, P. M. (2022). 2 - Drug delivery using metal oxide nanoparticles. In K. Mondal (Ed.), *Metal Oxides for Biomedical and Biosensor Applications* (pp. 35-83): Elsevier.

Gaudiuso, R., Dell'Aglio, M., De Pascale, O., Senesi, G.S. and De Giacomo, A. (2010). Laser induced breakdown spectroscopy for elemental analysis in environmental, cultural heritage and space applications: a review of methods and results. *Sensors*, *10*(8), pp.7434-7468.

Gawade, S. (2012). Acetic acid induced painful endogenous infliction in writhing test on mice. *Journal of Pharmacology and Pharmacotherapeutics*, *3*(4), p.348.

Ge, Z.J., Zeng, Y.M. and Tan, Y.F. (2005). Effects of intrathecal 6-hydroxydopamine, α1 and α2 adrenergic receptor antagonists on antinociception of propofol in mice. *Acta Pharmacologica Sinica*, *26*(2), pp.186-191.

Gebril, S.M., Ito, Y., Shibata, M.A., Maemura, K., Abu-Dief, E.E., Hussein, M.R., Abdelaal, U.M., Elsayed, H.M., Otsuki, Y. and Higuchi, K. (2020). Indomethacin can induce cell death in rat gastric parietal cells through alteration of some apoptosis-and autophagy-associated molecules. *International Journal of Experimental Pathology*, *101*(6), pp.230-247.

Gerberich, W.W., Jungk, J.M. and Mook, W.M. (2003). The bottom-up approach to materials by design. In *Nano and Microstructural Design of Advanced Materials* (pp. 211-220). Elsevier Science Ltd.

Ghasemiyeh, P. and Mohammadi-Samani, S. (2018). Solid lipid nanoparticles and nanostructured lipid carriers as novel drug delivery systems: Applications, advantages and disadvantages. *Research in pharmaceutical sciences*, *13*(4), p.288.

Ghosh, R., Alajbegovic, A. and Gomes, A.V. (2015). NSAIDs and cardiovascular diseases: role of reactive oxygen species. *Oxidative medicine and cellular longevity*, *2015*, 536962.

Giannini, C., Ladisa, M., Altamura, D., Siliqi, D., Sibillano, T. and De Caro, L. (2016). X-ray diffraction: a powerful technique for the multiple-length-scale structural analysis of nanomaterials. *Crystals*, *6*(8), p.87.

Goh, J.Z., Tang, S.N., Chiong, H.S., Yong, Y.K., Zuraini, A. and Hakim, M.N. (2015). Evaluation of antinociceptive activity of nanoliposome-encapsulated and free-form diclofenac in rats and mice. *International journal of nanomedicine*, *10*, p.297.

Goldstein, J.L. and Cryer, B. (2015). Gastrointestinal injury associated with NSAID use: a case study and review of risk factors and preventative strategies. *Drug, healthcare and patient safety*, *7*, p.31-41.

Gomaa, S. (2018). Adverse effects induced by diclofenac, ibuprofen, and paracetamol toxicity on immunological and biochemical parameters in Swiss albino mice. *The journal of basic and applied zoology*, *79*(1), pp.1-9.

Gopalan, C., and Kirk, E. (2022). Inflammation. In C. Gopalan & E. Kirk (Eds.), *Biology of Cardiovascular and Metabolic Diseases* (pp. 53-66): Academic Press.

Gorodetsky, R. (2014). Salicylates. In P. Wexler (Ed.), *Encyclopedia of Toxicology (Third Edition)* (pp. 208-210). Oxford: Academic Press.

Grand, J., Augui. , B. and Le Ru, E.C. (2019). Combined extinction and absorption UV–visible spectroscopy as a method for revealing shape imperfections of metallic nanoparticles. *Analytical chemistry*, *91*(22), pp.14639-14648.

Greaves, P. (2012). Chapter 10 - Urinary Tract. In P. Greaves (Ed.), *Histopathology of Preclinical Toxicity Studies (Fourth Edition)* (pp. 537-614). Boston: Academic Press.

Green, G.A. (2001). Understanding NSAIDs: from aspirin to COX-2. *Clinical cornerstone*, *3*(5), pp.50-59.

Gregus, Z. (2015). Mechanisms of Toxicity. In C. D. Klaassen & J. B. Watkins Iii (Eds.), *Casarett & Doull's Essentials of Toxicology, 3e*. New York, NY: McGraw-Hill Education.

Guo, C.G. and Leung, W.K. (2020). Potential strategies in the prevention of nonsteroidal anti-inflammatory drugs-associated adverse effects in the lower gastrointestinal tract. *Gut and liver*, *14*(2), p.179-189.

Gupta, A.K. and Gupta, M. (2005). Synthesis and surface engineering of iron oxide nanoparticles for biomedical applications. *biomaterials*, *26*(18), pp.3995-4021.

Gupta, A.K., Parasar, D., Sagar, A., Choudhary, V., Chopra, B.S., Garg, R. and Khatri, N. (2015). Analgesic and anti-inflammatory properties of gelsolin in acetic acid induced writhing, tail immersion and carrageenan induced paw edema in mice. *PloS one*, *10*(8), p.e0135558.

Gupta, A.K., Parasar, D., Sagar, A., Choudhary, V., Chopra, B.S., Garg, R. and Khatri, N. (2015). Analgesic and anti-inflammatory properties of gelsolin in acetic acid induced writhing, tail immersion and carrageenan induced paw edema in mice. *PloS one*, *10*(8), p.e0135558.

Hamimed, S., Jebli, N., Sellami, H., Landoulsi, A. and Chatti, A. (2020). Dual Valorization of Olive Mill Wastewater by Bio-Nanosynthesis of Magnesium

Oxide and Yarrowia lipolytica Biomass Production. *Chemistry & biodiversity*, *17*(3), p.e1900608.

Harirforoosh, S., West, K.O., Murrell, D.E., Denham, J.W., Panus, P.C. and Hanley, G.A. (2016). Examination of the pharmacodynamics and pharmacokinetics of a diclofenac poly (lactic-co-glycolic) acid nanoparticle formulation in the rat. *European Review for Medical and Pharmacological Sciences*, *20*(23), pp.5021-5031.

Hasan, A.U.H. (2019). Evaluation of in vitro and in vivo therapeutic efficacy of Ribes alpestre Decne in Rheumatoid arthritis. *Brazilian Journal of Pharmaceutical Sciences*, *55*.

Hayashi, I., Morishita, Y., Imai, K., Nakamura, M., Nakachi, K. and Hayashi, T. (2007). High-throughput spectrophotometric assay of reactive oxygen species in serum. *Mutation Research/Genetic Toxicology and Environmental Mutagenesis*, *631*(1), pp.55-61.

He, Y., Ingudam, S., Reed, S., Gehring, A., Strobaugh, T.P. and Irwin, P. (2016). Study on the mechanism of antibacterial action of magnesium oxide nanoparticles against foodborne pathogens. *Journal of nanobiotechnology*, *14*(1), pp.1-9.

Hegazi, N.M., Sobeh, M., Rezq, S., El-Raey, M.A., Dmirieh, M., El-Shazly, A.M., Mahmoud, M.F. and Wink, M. (2019). Characterization of phenolic compounds from Eugenia supra-axillaris leaf extract using HPLC-PDA-MS/MS and its antioxidant, anti-inflammatory, antipyretic and pain killing activities in vivo. *Scientific Reports*, *9*(1), pp.1-12.

Helmy, H.S., El-Sahar, A.E., Sayed, R.H., Shamma, R.N., Salama, A.H. and Elbaz, E.M. (2017). Therapeutic effects of lornoxicam-loaded nanomicellar formula in experimental models of rheumatoid arthritis. *International journal of nanomedicine*, *12*, p.7015-7023.

Hilário, M.O.E., Terreri, M.T. and Len, C.A. (2006). Nonsteroidal anti-inflammatory drugs: cyclooxygenase 2 inhibitors. *Jornal de pediatria*, *82*, pp.S206-S212.

Hinz, B., and Pahl, A. (2007). Cyclooxygenase-1. In S. J. Enna & D. B. Bylund (Eds.), *xPharm: The Comprehensive Pharmacology Reference* (pp. 1-5). New York:

Elsevier.

Hitkari, G., Singh, S. and Pandey, G. (2019). Nanoparticles: an emerging weapon for mitigation/removal of various environmental pollutants for environmental safety. In *Emerging and Eco-Friendly Approaches for Waste Management* (pp. 359-395). Springer, Singapore.

Hole, K., and Tjølsen, A. (2007). Tail Flick Test. In R. F. Schmidt & W. D. Willis (Eds.), *Encyclopedia of Pain* (pp. 2392-2395). Berlin, Heidelberg: Springer Berlin Heidelberg.

Hörl, W.H. (2010). Nonsteroidal anti-inflammatory drugs and the kidney. *Pharmaceuticals*, *3*(7), pp.2291-2321.

Hsueh, M.F., Bolognesi, M.P., Wellman, S.S. and Kraus, V.B. (2020). Anti-inflammatory effects of naproxen sodium on human osteoarthritis synovial fluid immune cells. *Osteoarthritis and cartilage*, *28*(5), pp.639-645.

Hurley, R. (2007). Anemia and red blood cell disorders. In *Immigrant medicine* (pp. 611-623). WB Saunders.

Hussaini, A., Solorio, D. and Young, C. (2016). Pharmacokinetic properties of low-dose SoluMatrix meloxicam in healthy adults. *Clinical rheumatology*, *35*(4), pp.1099-1104.

Imani, M.M. and Safaei, M. (2019). Optimized synthesis of magnesium oxide nanoparticles as bactericidal agents. *Journal of Nanotechnology*, *2019*, p.6063832.

Iqubal, A., Syed, M.A., Ali, J., Najmi, A.K., Haque, M.M. and Haque, S.E. (2020). Nerolidol protects the liver against cyclophosphamide-induced hepatic inflammation, apoptosis, and fibrosis via modulation of Nrf2, NF-κB p65, and caspase-3 signaling molecules in Swiss albino mice. *BioFactors*, *46*(6), pp.963-973.

Irvine, J. (2018). Afrose A. Islam N. *Drug Dev. Ind. Pharm*, *44*, pp.173-183.

Issa, B., Qadri, S., Obaidat, I.M., Bowtell, R.W. and Haik, Y. (2011). PEG coating reduces NMR relaxivity of Mn0. 5Zn0. 5Gd0. 02Fe1. 98O4 hyperthermia nanoparticles. *Journal of Magnetic Resonance Imaging*, *34*(5), pp.1192-1198.

Jackson, C.M., Esnouf, M.P., Winzor, D.J. and Duewer, D.L. (2007). Defining and measuring biological activity: applying the principles of metrology. *Accreditation and quality assurance*, *12*(6), pp.283-294.

Jahangiri, L., Kesmati, M. and Najafzadeh, H. (2013). Evaluation of analgesic and anti-inflammatory effect of nanoparticles of magnesium oxide in mice with and without ketamine. *European Review for Medical and Pharmacological Sciences*, *17*(20), pp.2706-10.

Jahangiri, L., Kesmati, M. and Najafzadeh, H. (2014). Evaluation of anticonvulsive effect of magnesium oxide nanoparticles in comparison with conventional MgO in diabetic and non-diabetic male mice. *Basic and clinical neuroscience*, *5*(2), p.156-161.

Jahnen-Dechent, W. and Ketteler, M. (2012). Magnesium basics. *Clinical kidney journal*, *5*(1), pp.i3-i14.

Jacobson, G.B., Shinde, R. Contag, C.H., and Zare, R.N. (2008). Sustained release of drugs dispersed in polymer nanoparticles. *Angewandte Chemie*, *47*(41), 7880-2.

Jamkhande, P.G., Ghule, N.W., Bamer, A.H. and Kalaskar, M.G. (2019). Metal nanoparticles synthesis: An overview on methods of preparation, advantages and disadvantages, and applications. *Journal of drug delivery science and technology*, *53*, p.101174.

Janhavi, P., Divyashree, S., Sanjailal, K.P. and Muthukumar, S.P. (2022). DoseCal: a virtual calculator for dosage conversion between human and different animal species. *Archives of Physiology and Biochemistry*, *128*(2), pp.426-430.

Janjua, M.R.S.A. (2019). Synthesis of Co3O4 nano aggregates by Co-precipitation method and its catalytic and fuel additive applications. *Open Chemistry*, *17*(1), pp.865-873.

Jeevanandam, J., San Chan, Y. and Danquah, M.K. (2017). Biosynthesis and characterization of MgO nanoparticles from plant extracts via induced molecular nucleation. *New Journal of Chemistry*, *41*(7), pp.2800-2814.

Jianxian, C., Saleem, K., Ijaz, M., Ur-Rehman, M., Murtaza, G. and Asim, M.H. (2020). Development and in vitro evaluation of gastro-protective aceclofenac-

loaded self-emulsifying drug delivery system. *International journal of nanomedicine*, *15*, p.5217-5226.

Jog, R. and Burgess, D.J. (2017). Pharmaceutical amorphous nanoparticles. *Journal of pharmaceutical sciences*, *106*(1), pp.39-65.

Kalepu, S. and Nekkanti, V. (2016). Improved delivery of poorly soluble compounds using nanoparticle technology: a review. *Drug delivery and translational research*, *6*(3), pp.319-332.

Kandpal, N.D., Sah, N., Loshali, R., Joshi, R. and Prasad, J. (2014). Co-precipitation method of synthesis and characterization of iron oxide nanoparticles.

Kang, K.S. (2013). Abnormality on liver function test. *Pediatric gastroenterology, hepatology & nutrition*, *16*(4), pp.225-232.

Kapoor, B., Singh, S.K., Gulati, M., Gupta, R. and Vaidya, Y. (2014). Application of liposomes in treatment of rheumatoid arthritis: quo vadis. *The scientific world Journal*, *2014*, 978351.

Karabulut, G. and Barlas, N. (2018). Genotoxic, histologic, immunohistochemical, morphometric and hormonal effects of di-(2-ethylhexyl)-phthalate (DEHP) on reproductive systems in pre-pubertal male rats. *Toxicology Research*, *7*(5), pp.859-873.

Karimiyan, A., Najafzadeh, H., Ghorbanpour, M. and Hekmati-Moghaddam, S.H. (2015). Antifungal effect of magnesium oxide, zinc oxide, silicon oxide and copper oxide nanoparticles against Candida albicans. *Zahedan Journal of Research in Medical Sciences*, *17*(10).

Kawada, N., Moriyama, T., Kitamura, H., Yamamoto, R., Furumatsu, Y., Matsui, I., Takabatake, Y., Nagasawa, Y., Imai, E., Wilcox, C.S. and Rakugi, H. (2012). Towards developing new strategies to reduce the adverse side-effects of nonsteroidal anti-inflammatory drugs. *Clinical and experimental nephrology*, *16*(1), pp.25-29.

Kawazoe, H., Yano, A., Ishida, Y., Takechi, K., Katayama, H., Ito, R., Yakushijin, Y., Moriguchi, T., Tanaka, M., Tanaka, A. and Araki, H. (2017). Non-steroidal anti-inflammatory drugs induce severe hematologic toxicities in lung cancer patients receiving pemetrexed plus carboplatin: A retrospective cohort study. *PLoS One*, *12*(2), p.e0171066.

Kayal, S. and Ramanujan, R.V. (2010). Doxorubicin loaded PVA coated iron oxide nanoparticles for targeted drug delivery. *Materials Science and Engineering: C*, *30*(3), pp.484-490.

Kermanizadeh, A., Powell, L.G., Stone, V. and Møller, P. (2018). Nanodelivery systems and stabilized solid-drug nanoparticles for orally administered medicine: current landscape. *International journal of nanomedicine*, *13*, p.7575.

Kim, B.Y.S., Rutka, J.T. and Chan, W.C.W. (2010). Effect of Coumarate 3-zhydroxylase Down regulation on lignin structure. *Nanomedicine New England Journal of Medicine*, *363*, pp.2434-2443.

Kim, G., Piao, C., Oh, J. and Lee, M. (2018). Self-assembled polymeric micelles for combined delivery of anti-inflammatory gene and drug to the lungs by inhalation. *Nanoscale*, *10*(18), pp.8503-8514.

Kimmey, M.B. (1992). NSAID, ulcers, and prostaglandins. *The Journal of rheumatology. Supplement*, *36*, pp.68-73.

Kiranmayi, G.V.N. (2018). Preliminary phytochemical screening and in vitro evaluation of anti-inflammatory, antiarthritic, and thrombolytic activities of ethanolic leaf extract of Bauhinia purpurea. *International Journal of Green Pharmacy (IJGP)*, *12*(01).

Kishida, T., Onozato, T., Kanazawa, T., Tanaka, S. and Kuroda, J. (2012). Increase in covalent binding of 5-hydroxydiclofenac to hepatic tissues in rats co-treated with lipopolysaccharide and diclofenac: involvement in the onset of diclofenac-induced idiosyncratic hepatotoxicity. *The Journal of toxicological sciences*, *37*(6), pp.1143-1156.

Kokura, S., Wolf, R.E., Yoshikawa, T., Granger, D.N. and Aw, T.Y. (2000). T-Lymphocyte–Derived Tumor Necrosis Factor Exacerbates Anoxia-Reoxygenation–Induced Neutrophil–Endothelial Cell Adhesion. *Circulation research*, *86*(2), pp.205-213.

Kolbe, H. (1860). Ueber Synthese der Salicylsäure. *Justus Liebigs Annalen der Chemie*, *113*, 125-127.

Kopeckova, K., Eckschlager, T., Sirc, J., Hobzova, R., Plch, J., Hrabeta, J. and

Michalek, J. (2019). Nanodrugs used in cancer therapy. *Biomedical Papers of the Medical Faculty of Palacky University in Olomouc*, *163*(2),122-131.

Kumal, R.R., Karam, T.E. and Haber, L.H. (2015). Determination of the surface charge density of colloidal gold nanoparticles using second harmonic generation. *The Journal of Physical Chemistry C*, *119*(28), pp.16200-16207.

Kumari, A., Singla, R., Guliani, A. and Yadav, S.K. (2014). Nanoencapsulation for drug delivery. *EXCLI journal*, *13*, p.265-286.

Kwon, J., Kim, S., Yoo, H. and Lee, E. (2019). Nimesulide-induced hepatotoxicity: A systematic review and meta-analysis. *PloS one*, *14*(1), p.e0209264.

Laine, L. (2002), December. The gastrointestinal effects of nonselective NSAIDs and COX-2–selective inhibitors. In *Seminars in arthritis and rheumatism* **32**(3) pp. 25-32.

Lee, J.H. and Yeo, Y. (2015a). Controlled drug release from pharmaceutical nanocarriers. *Chemical engineering science*, *125*, pp.75-84.

Lee, J.H. and Yeo, Y. (2015b). Controlled drug release from pharmaceutical nanocarriers. *Chemical engineering science*, *125*, pp.75-84.

Levy, M.Y. and Benita, S. (1990). Drug release from submicronized o/w emulsion: a new in vitro kinetic evaluation model. *International journal of pharmaceutics*, *66*(1-3), pp.29-37.

Lewis, D.A. (1970). The actions of some non-steroidal drugs on lysosomes. *Journal of Pharmacy and Pharmacology*, *22*(12), pp.909-912.

Li, H. and Lykotrafitis, G. (2014). Erythrocyte membrane model with explicit description of the lipid bilayer and the spectrin network. *Biophysical journal*, *107*(3), pp.642-653.

Lichtenberger, L.M. (2001). Where is the evidence that cyclooxygenase inhibition is the primary cause of nonsteroidal anti-inflammatory drug (NSAID)-induced gastrointestinal injury?: Topical injury revisited. *Biochemical pharmacology*, *61*(6), pp.631-637.

Lima, T., Bernfur, K., Vilanova, M. and Cedervall, T. (2020). Understanding the lipid and protein corona formation on different sized polymeric

nanoparticles. *Scientific reports*, *10*(1), pp.1-9.

Lin, P.C., Lin, S., Wang, P.C. and Sridhar, R. (2014). Techniques for physicochemical characterization of nanomaterials. *Biotechnology advances*, *32*(4), pp.711-726.

Liu, T., Li, L., Teng, X., Huang, X., Liu, H., Chen, D., Ren, J., He, J. and Tang, F. (2011). Single and repeated dose toxicity of mesoporous hollow silica nanoparticles in intravenously exposed mice. *Biomaterials*, *32*(6), pp.1657-1668.

Liu, X., Zheng, L., Zhang, R., Liu, G., Xiao, S., Qiao, X., Wu, Y. and Gong, Z. (2016). Toxicological evaluation of advanced glycation end product Nε-(carboxymethyl) lysine: Acute and subacute oral toxicity studies. *Regulatory Toxicology and Pharmacology*, *77*, pp.65-74.

Liu, Y., Yang, G., Jin, S., Xu, L. and Zhao, C.X. (2020). Development of high-drug-loading nanoparticles. *ChemPlusChem*, *85*(9), pp.2143-2157.

Loganathan, S., Valapa, R. B., Mishra, R. K., Pugazhenthi, G., and Thomas, S. (2017). Chapter 4 - Thermogravimetric Analysis for Characterization of Nanomaterials. In S. Thomas, R. Thomas, A. K. Zachariah, & R. K. Mishra (Eds.), *Thermal and Rheological Measurement Techniques for Nanomaterials Characterization* (pp. 67-108): Elsevier.

Lordan, R., Tsoupras, A., and Zabetakis, I. (2019). Chapter 2 - Inflammation. In I. Zabetakis, R. Lordan, & A. Tsoupras (Eds.), *The Impact of Nutrition and Statins on Cardiovascular Diseases* (pp. 23-51): Academic Press.

Loureiro, J.A. and Pereira, M.C. (2020). PLGA based drug carrier and pharmaceutical applications: the most recent advances. *Pharmaceutics*, *12*(9), p.903.

Lu, Y.Y., Gao, J.H., Zhao, C., Wen, S.L., Tang, C.W. and Wang, Y.F. (2018). Cyclooxygenase-2 up-regulates hepatic somatostatin receptor 2 expression. *Scientific Reports*, *8*(1), pp.1-11.

Lucas, G.N.C., Leitão, A.C.C., Alencar, R.L., Xavier, R.M.F., Daher, E.D.F. and Silva, G.B.D. (2018). Pathophysiological aspects of nephropathy caused by non-steroidal anti-inflammatory drugs. *Brazilian Journal of Nephrology*, *41*, pp.124-130.

Lucas, G.N.C., Leitão, A.C.C., Alencar, R.L., Xavier, R.M.F., Daher, E.D.F. and Silva, G.B.D. (2018). Pathophysiological aspects of nephropathy caused by non-steroidal anti-inflammatory drugs. *Brazilian Journal of Nephrology*, *41(1)*, pp.124-130.

Ma, J. and Chen, X. (2021). Anti-inflammatory therapy for coronary atherosclerotic heart disease: unanswered questions behind existing successes. *Frontiers in Cardiovascular Medicine*, *7*, p.631398.

Maehly, A. C. (2006). The Assay of Catalases and Peroxidases. In (Vol. **1**, pp. 357-424).

Malik, P., Gupta, R., Malik, V. and Ameta, R.K. (2021). Emerging nanomaterials for improved biosensing. *Measurement: sensors*, *16*, p.100050.

Maniar, K.H., Jones, I.A., Gopalakrishna, R. and Vangsness Jr, C.T. (2018). Lowering side effects of NSAID usage in osteoarthritis: recent attempts at minimizing dosage. *Expert opinion on pharmacotherapy*, *19*(2), pp.93-102.

Manov, I., Motanis, H., Frumin, I. and Iancu, T.C. (2006). Hepatotoxicity of anti-inflammatory and analgesic drugs: ultrastructural aspects. *Acta Pharmacologica Sinica*, *27*(3), pp.259-272.

Mansouri, M.T., Hemmati, A.A., Naghizadeh, B., Mard, S.A., Rezaie, A. and Ghorbanzadeh, B. (2015). A study of the mechanisms underlying the anti-inflammatory effect of ellagic acid in carrageenan-induced paw edema in rats. *Indian Journal of Pharmacology*, *47*(3), p.292.

Marjoribanks, J., Ayeleke, R.O., Farquhar, C. and Proctor, M. (2015). Nonsteroidal anti-inflammatory drugs for dysmenorrhoea. *Cochrane database of systematic reviews*, (7).

Martinho, N., Damgé, C. and Reis, C.P. (2011). Recent advances in drug delivery systems. *Journal of biomaterials and nanobiotechnology*, *2*(05), p.510.

Matsui, H., Shimokawa, O., Kaneko, T., Nagano, Y., Rai, K. and Hyodo, I. (2011). The pathophysiology of non-steroidal anti-inflammatory drug (NSAID)-induced mucosal injuries in stomach and small intestine. *Journal of clinical biochemistry and nutrition*, *48*(2), pp.107-111.

Mazaleuskaya, L.L., Muzykantov, V.R. and FitzGerald, G.A. (2021).

Nanotherapeutic-directed approaches to analgesia. *Trends in Pharmacological Sciences*, *42*(7), pp.527-550.

Mazayen, Z.M., Ghoneim, A.M., Elbatanony, R.S., Basalious, E.B. and Bendas, E.R. (2022). Pharmaceutical nanotechnology: from the bench to the market. *Future Journal of Pharmaceutical Sciences*, *8*(1), pp.1-11.

McCormack, P. L. (2011). Celecoxib: a review of its use for symptomatic relief in the treatment of osteoarthritis, rheumatoid arthritis and ankylosing spondylitis. *Drugs, 71*(18), 2457-2489.

McDonald, B.F., Coulter, I.S. and Marison, I.W. (2015). Microbeads: A novel multiparticulate drug delivery technology for increasing the solubility and dissolution of celecoxib. *Pharmaceutical Development and Technology*, *20*(2), pp.211-218.

McEvoy, L., Carr, D.F. and Pirmohamed, M. (2021). Pharmacogenomics of NSAID-induced upper gastrointestinal toxicity. *Frontiers in pharmacology*, p.1302.

McNamara, K. and Tofail, S.A. (2017). Nanoparticles in biomedical applications. *Advances in Physics: X*, *2*(1), pp.54-88.

Mello, V.A.D. and Ricci-Júnior, E. (2011). Encapsulation of naproxen in nanostructured system: structural characterization and in vitro release studies. *Química Nova*, *34*, pp.933-939.

Mendenhall, C.L. and Mortiaux, A. (1962). Alterations in serum triglyceride levels in liver disease. *Gastroenterology*, *42*(6), pp.684-685.

Menkes, C.J. (1989). Renal and hepatic effects of NSAIDs in the elderly. *Scandinavian Journal of Rheumatology*, *18*(83), pp.11-13.

Mennini, N., Furlanetto, S., Bragagni, M., Ghelardini, C., Di Cesare Mannelli, L. and Mura, P. (2014). Development of a chitosan-derivative micellar formulation to improve celecoxib solubility and bioavailability. *Drug Development and Industrial Pharmacy*, *40*(11), pp.1494-1502.

Mitra, J. (2022). Exploring the potential of metal oxides for biomedical applications. In K. Mondal (Ed.), *Metal Oxides for Biomedical and Biosensor Applications* (pp. 183-203): Elsevier.

Mizushima, T. (2010). Molecular Mechanism for Various Pharmacological Activities of NSAIDS. *Pharmaceuticals (Basel), 3*(5), 1614-1636.

Monastero, R.N. and Pentyala, S. (2017). Cytokines as biomarkers and their respective clinical cutoff levels. *International journal of inflammation*, *2017*.

Moore, K.W., de Waal Malefyt, R., Coffman, R.L. and O'Garra, A. (2001). Interleukin-10 and the interleukin-10 receptor. *Annual review of immunology*, *19*, p.683.

MoreAmol, N. and ShahTejas, K. (2017). Oroxylum indicum (Linn.) whole stem extract regulates expression of TNFα, IL6, NFkB, P38 MAPK and oxidative status in antitubercular therapy induced hepatotoxicity in Wistar rats. *Matters*, *3*(9).

Moros, J. and Laserna, J. (2019). Laser-induced breakdown spectroscopy (LIBS) of organic compounds: A review. *Applied Spectroscopy*, *73*(9), pp.963-1011.

Morris, C.J. (2003). Carrageenan-induced paw edema in the rat and mouse. *Inflammation protocols*, pp.115-121.

Moura, M.D.G., Lopes, L.C., Silva, M.T., Barberato-Filho, S., Motta, R.H.L. and de Cássia Bergamaschi, C. (2018). Use of steroid and nonsteroidal anti-inflammatories in the treatment of rheumatoid arthritis: systematic review protocol. *Medicine*, *97*(41), pp.e12658-e12658.

Mourdikoudis, S., Pallares, R.M. and Thanh, N.T. (2018). Characterization techniques for nanoparticles: comparison and complementarity upon studying nanoparticle properties. *Nanoscale*, *10*(27), pp.12871-12934.

MSD, M. Nonsteroidal Anti-inflammatory Drug (NSAID) Treatment of Rheumatoid Arthritis. Retrieved fromhttps://www.msdmanuals.com/professional/multimedia/table/nonsteroidal-anti-inflammatory-drug-nsaid-treatment-of-rheumatoid-arthritis

Murthy, S., Effiong, P. and Fei, C.C. (2020). Metal oxide nanoparticles in biomedical applications. In *Metal Oxide Powder Technologies* (pp. 233-251). Elsevier.

Musumba, C., Pritchard, D.M. and Pirmohamed, M. (2009). cellular and molecular mechanisms of NSAID-induced peptic ulcers. *Alimentary pharmacology & therapeutics*, *30*(6), pp.517-531.

Nagai, N. and Ito, Y. (2014). Effect of solid nanoparticle of indomethacin on therapy for rheumatoid arthritis in adjuvant-induced arthritis rat. *Biological and Pharmaceutical Bulletin*, *37*(7), pp.1109-1118.

Nagano, Y., Matsui, H., Muramatsu, M., Shimokawa, O., Shibahara, T., Yanaka, A., Nakahara, A., Matsuzaki, Y., Tanaka, N. and Nakamura, Y. (2005). Rebamipide significantly inhibits indomethacin-induced mitochondrial damage, lipid peroxidation, and apoptosis in gastric epithelial RGM-1 cells. *Digestive diseases and sciences*, *50*(1), pp.S76-S83.

Nagarajan, R. and Hatton, T.A. eds. (2008). *Nanoparticles: synthesis, stabilization, passivation, and functionalization*. American Chemical Society, **996**, pp. 2-14.

Nair, A.B. and Jacob, S. (2016). A simple practice guide for dose conversion between animals and human. *Journal of basic and clinical pharmacy*, *7*(2), p.27.

Nantel, F., Denis, D., Gordon, R., Northey, A., Cirino, M., Metters, K.M. and Chan, C.C., 1999. Distribution and regulation of cyclooxygenase-2 in carrageenan-induced inflammation. *British journal of pharmacology*, *128*(4), pp.853-859.

Narayanan, D., Geena, M.G., Lakshmi, H., Koyakutty, M., Nair, S. and Menon, D. (2013). Poly-(ethylene glycol) modified gelatin nanoparticles for sustained delivery of the anti-inflammatory drug ibuprofen-sodium: an in vitro and in vivo analysis. *Nanomedicine: Nanotechnology, Biology and Medicine*, *9*(6), pp.818-828.

Narayanan, D., Pillai, G. J., Nair, S. V., and Menon, D. (2019). Effect of formulation parameters on pharmacokinetics, pharmacodynamics, and safety of diclofenac nanomedicine. *Drug Delivery and Translational Research, 9*(5), 867-878.

Nelsonjoseph, L., Vishnupriya, B., Amsaveni, R., Bharathi, D., Thangabalu, S. and Rehna, P. (2022). Synthesis and characterization of silver nanoparticles using Acremonium borodinense and their anti-bacterial and hemolytic activity. *Biocatalysis and Agricultural Biotechnology*, *39*, p.102222.

Neupane, B.P., Chaudhary, D., Paudel, S., Timsina, S., Chapagain, B., Jamarkattel, N. and Tiwari, B.R. (2019). Himalayan honey loaded iron oxide nanoparticles: Synthesis, characterization and study of antioxidant and antimicrobial activities. *International journal of nanomedicine*, *14*, p.3533.

Nguyen, N.Y.T., Grelling, N., Wetteland, C.L., Rosario, R. and Liu, H. (2018). Antimicrobial activities and mechanisms of magnesium oxide nanoparticles (nMgO) against pathogenic bacteria, yeasts, and biofilms. *Scientific reports*, *8*(1), pp.1-23.

Nguyen, T.D. and Do, T.O. (2011). Size-and shape-controlled synthesis of monodisperse metal oxide and mixed oxide nanocrystals. *Nanocrystal*, *66*, pp.55-84.

Nies, A.S. (1988). Renal effects of nonsteroidal anti-inflammatory drugs. *Agents and actions. Supplements*, *24*, pp.95-106.

Nikolić, V., Ilić-Stojanović, S., Petrović, S., Tačić, A. and Nikolić, L. (2019). Administration routes for nano drugs and characterization of nano drug loading. In *Characterization and biology of nanomaterials for drug delivery* pp. 587-625.

Nikolova, M.P. and Chavali, M.S. (2020). Metal oxide nanoparticles as biomedical materials. *Biomimetics*, *5*(2), p.27.

Nokhodchi, A. and Maghsoodi, M.J.A.P. (2008). Preparation of spherical crystal agglomerates of naproxen containing disintegrant for direct tablet making by spherical crystallization technique. *Aaps Pharmscitech*, *9*(1), pp.54-59.

Noori, A.J. and Kareem, F.A. (2019). The effect of magnesium oxide nanoparticles on the antibacterial and antibiofilm properties of glass-ionomer cement. *Heliyon*, *5*(10), p.e02568.

Noreen, S., Pervaiz, F., Ashames, A., Buabeid, M., Fahelelbom, K., Shoukat, H., Maqbool, I. and Murtaza, G. (2021). Optimization of novel naproxen-loaded chitosan/carrageenan nanocarrier-based gel for topical delivery: ex vivo, histopathological, and in vivo evaluation. *Pharmaceuticals*, *14*(6), p.557.

O'connor, N., Dargan, P.I. and Jones, A.L. (2003). Hepatocellular damage from non-steroidal anti-inflammatory drugs. *Qjm*, *96*(11), pp.787-791.

Ogidi, O.I., Ogoun, T.R., Njoku, C.O., Charles, E.E., Amgbare, E.B. and Omotehinse, E.T. (2020). Toxicity Studies on the Effects of Non-Steroidal Anti-Inflammatory Drugs in Wistar Albino Rats. *Elixir Pharmacy*, *149*, pp.55010-14.

Olliges, A., Wimmer, S. and Nüsing, R.M. (2011). Defects in mouse nephrogenesis induced by selective and non-selective cyclooxygenase-2 inhibitors. *British journal of pharmacology*, *163*(5), pp.927-936.

Olszewska-Słonina, D.M., Mątewski, D., Czajkowski, R., Olszewski, K.J., WoŸniak, A., Odrowąż-Sypniewska, G., Lis, K., Musiałkiewicz, D. and Kowaliszyn, B. (2011). The concentration of thiobarbituric acid reactive substances (TBARS) and paraoxonase activity in blood of patients with osteoarthrosis after endoprosthesis implantation. *Medical Science Monitor: International Medical Journal of Experimental and Clinical Research*, *17*(9), p.CR498.

Orhan, H. and Şahin, G. (2001). In vitro effects of NSAIDS and paracetamolon oxidative stress-related parameters of human erythrocytes. *Experimental and Toxicologic Pathology*, *53*(2-3), pp.133-140.

Orinya, O.A., Adenkola, A.Y. and Ogbe, R.J. (2016). Haematological and biochemical studies on the effect of diclofenac sodium on Wistar Rattus norvegicus. *International Journal of Biological and Chemical Sciences*, *10*(5), pp.2231-2242.

Orlando, R.C. (2010). The integrity of the esophageal mucosa. Balance between offensive and defensive mechanisms. *Best practice & research Clinical gastroenterology*, *24*(6), pp.873-882.

Pagar, R.R., Musale, S.R., Pawar, G., Kulkarni, D. and Giram, P.S. (2022). Comprehensive Review on the Degradation Chemistry and Toxicity Studies of Functional Materials. *ACS Biomaterials Science & Engineering*.

Pahwa, R., Goyal, A., Bansal, P. and Jialal, I. (2021). Chronic Inflammation.[Updated 2020 Nov 20]. *StatPearls [Internet]. Treasure Island (FL): StatPearls Publishing*.

Pandey, G. and Jain, P. (2020). Assessing the nanotechnology on the grounds of costs, benefits, and risks. *Beni-Suef University Journal of Basic and Applied Sciences*, *9*(1), pp.1-10.

Paolisso, G., Scheen, A., d'Onofrio, F. and Lefebvre, P. (1990). Magnesium and glucose homeostasis. *Diabetologia*, *33*(9), pp.511-514.

Parasuraman, S. (2011). Toxicological screening. *Journal of pharmacology & pharmacotherapeutics*, *2*(2), p.74.

Parekh, V.J., Desai, N.D., Shaikh, M.S. and Shinde, U.A. (2017). Self nanoemulsifying granules (SNEGs) of meloxicam: preparation, characterization, molecular modeling and evaluation of in vivo anti-inflammatory activity. *Drug development and industrial pharmacy*, *43*(4), pp.600-610.

Park, J.A., Cho, K.Y., Han, C.H., Nam, A., Kim, J.H., Lee, S.H. and Choi, J.W. (2019). Quaternized amphiphilic block copolymers/graphene oxide and a poly (vinyl alcohol) coating layer on graphene oxide/poly (vinylidene fluoride) electrospun nanofibers for superhydrophilic and antibacterial properties. *Scientific reports*, *9*(1), pp.1-13.

Park, K. and Bavry, A.A. (2014). Risk of stroke associated with nonsteroidal anti-inflammatory drugs. *Vascular health and risk management*, *10*, p.25-32.

Parveen, S., Misra, R. and Sahoo, S.K. (2012). Nanomedicine: Nanotech. *Biol., Med*, *8*, p.147-166.

Passos, M. L. C., Sarraguça, M. C., Saraiva, M. L. M. F. S., Prasada Rao, T., and Biju, V. M. (2019). Spectrophotometry. In P. Worsfold, C. Poole, A. Townshend, & M. Miró (Eds.), *Encyclopedia of Analytical Science (Third Edition)* (pp. 236-243). Oxford: Academic Press.

Pathan, R. A., Singh, B. K., Pillai, K. K., and Dubey, K. (2010). Naproxen aggravates doxorubicin-induced cardiomyopathy in rats. *Indian journal of pharmacology, 42*(1), 44-49.

Patil, K.R., Mahajan, U.B., Unger, B.S., Goyal, S.N., Belemkar, S., Surana, S.J., Ojha, S. and Patil, C.R. (2019). Animal models of inflammation for screening of anti-inflammatory drugs: Implications for the discovery and development of phytopharmaceuticals. *International journal of molecular sciences*, *20*(18), p.4367.

Peng, W., Cheng, S., Bao, Z., Wang, Y., Zhou, W., Wang, J., Yang, Q., Chen, C. and Wang, W. (2021). Advances in the research of nanodrug delivery system for targeted treatment of liver fibrosis. *Biomedicine & Pharmacotherapy*, *137*,

p.111342.

Pereverzeva, E., Treschalin, I., Treschalin, M., Arantseva, D., Ermolenko, Y., Kumskova, N., Maksimenko, O., Balabanyan, V., Kreuter, J. and Gelperina, S. (2019). Toxicological study of doxorubicin-loaded PLGA nanoparticles for the treatment of glioblastoma. *International journal of pharmaceutics*, *554*, pp.161-178.

Persson, L., Karlsson-Vinkhuyzen, S., Lai, A., Persson, Å. and Fick, S. (2017). The globally harmonized system of classification and labelling of chemicals—explaining the legal implementation gap. *Sustainability*, *9*(12), p.2176.

Petterino, C. and Argentino-Storino, A. (2006). Clinical chemistry and haematology historical data in control Sprague-Dawley rats from pre-clinical toxicity studies. *Experimental and Toxicologic Pathology*, *57*(3), pp.213-219.

Phukan, K., Devi, R. and Chowdhury, D. (2021). Green synthesis of gold nano-bioconjugates from onion peel extract and evaluation of their antioxidant, anti-inflammatory, and cytotoxic studies. *American Chemical Society omega*, *6*(28), pp.17811-17823.

Piotrowski, J., Slomiany, A. and Slomiany, B.L. (1999). Activation of apoptotic caspase-3 and nitric oxide synthase-2 in gastric mucosal injury induced by indomethacin. *Scandinavian journal of gastroenterology*, *34*(2), pp.129-134.

Pirlamarla, P. and Bond, R.M. (2016). FDA labeling of NSAIDs: Review of nonsteroidal anti-inflammatory drugs in cardiovascular disease. *Trends in cardiovascular medicine*, *26*(8), pp.675-680.

Poljsak, B., Šuput, D., and Milisav, I. (2013). Achieving the balance between ROS and antioxidants: when to use the synthetic antioxidants. *Oxidative Medicine and Celluler Longevity*, *2013*, p.11

Prasad, L. K., O'Mary, H., and Cui, Z. (2015). Nanomedicine delivers promising treatments for rheumatoid arthritis. *Nanomedicine (London, England)*, *10*(13), 2063-2074.

Press, A.T., Butans, M.J., Haider, T.P., Weber, C., Neugebauer, S., Kiehntopf, M., Schubert, U.S., Clemens, M.G., Bauer, M. and Kortgen, A. (2017). Fast simultaneous assessment of renal and liver function using polymethine dyes in

animal models of chronic and acute organ injury. *Scientific reports*, *7*(1), pp.1-11.

Ptaschinski, C., and Lukacs, N. W. (2020). Acute and chronic inflammation induces disease pathogenesis. In W. B. Coleman & G. J. Tsongalis (Eds.), *Essential Concepts in Molecular Pathology (Second Edition)* (pp. 19-31): Academic Press.

Pudovkin, M.S., Zelenikhin, P.V., Shtyreva, V., Morozov, O.A., Koryakovtseva, D.A., Pavlov, V.V., Osin, Y.N., Evtugyn, V.G., Akhmadeev, A.A., Nizamutdinov, A.S. and Semashko, V.V. (2018). Coprecipitation method of synthesis, characterization, and cytotoxicity of Pr3+: LaF3 (CPr= 3, 7, 12, 20, 30%) nanoparticles. *Journal of nanotechnology*, *2018*.

Puglia, C., Trombetta, D., Venuti, V., Saija, A. and Bonina, F. (2004). Evaluation of in-vivo topical anti-inflammatory activity of indometacin from liposomal vesicles. *Journal of pharmacy and pharmacology*, *56*(10), pp.1225-1232.

Qi, R., Majoros, I., Misra, A.C., Koch, A.E., Campbell, P., Marotte, H., Bergin, I.L., Cao, Z., Goonewardena, S., Morry, J. and Zhang, S. (2015). Folate receptor-targeted dendrimer-methotrexate conjugate for inflammatory arthritis. *Journal of biomedical nanotechnology*, *11*(8), pp.1431-1441.

Qiao, L., Yang, H., Gao, S., Li, L., Fu, X. and Wei, Q. (2022). Research progress on self-assembled nanodrug delivery systems. *Journal of Materials Chemistry, 10* (12), 1908-1922.

Quarta, A., Curcio, A., Kakwere, H. and Pellegrino, T. (2012). Polymer coated inorganic nanoparticles: tailoring the nanocrystal surface for designing nanoprobes with biological implications. *Nanoscale*, *4*(11), pp.3319-3334.

Rachmawati, H., Safitri, D., Pradana, A.T. and Adnyana, I.K. (2016). TPGS-stabilized curcumin nanoparticles exhibit superior effect on carrageenan-induced inflammation in wistar rat. *Pharmaceutics*, *8*(3), p.24.

Rafiei, S., Rezatofighi, S.E., Ardakani, M.R. and Madadgar, O. (2015). In vitro anti-foot-and-mouth disease virus activity of magnesium oxide nanoparticles. *Iet Nanobiotechnology*, *9*(5), pp.247-251.

Rainsford, K.D. (2007). Anti-inflammatory drugs in the 21st century. *Inflammation in*

the pathogenesis of chronic diseases, pp.3-27.

Raj, V. and Prabha, G. (2016). Synthesis, characterization and in vitro drug release of cisplatin loaded Cassava starch acetate–PEG/gelatin nanocomposites. *Journal of the Association of Arab Universities for Basic and Applied Sciences*, *21*, pp.10-16.

Rajisha, K.R., Deepa, B., Pothan, L.A. and Thomas, S. (2011). Thermomechanical and spectroscopic characterization of natural fibre composites. *Interface Engineering of Natural Fibre Composites for Maximum Performance*, pp.241-274.

Ramanathan, S., Gopinath, S.C., Arshad, M.M., Poopalan, P. and Perumal, V. (2021). Nanoparticle synthetic methods: strength and limitations. In *Nanoparticles in Analytical and Medical Devices* (pp. 31-43). Elsevier.

Ramezanpour, M., Leung, S.S.W., Delgado-Magnero, K.H., Bashe, B.Y.M., Thewalt, J. and Tieleman, D.P. (2016). Computational and experimental approaches for investigating nanoparticle-based drug delivery systems. *Biochimica et Biophysica Acta (BBA)-Biomembranes*, *1858*(7), pp.1688-1709.

Ranathunge, T.A., Karunaratne, D.G.G.P., Rajapakse, R.M.G. and Watkins, D.L. (2019). Doxorubicin loaded magnesium oxide nanoflakes as pH dependent carriers for simultaneous treatment of cancer and hypomagnesemia. *Nanomaterials*, *9*(2), p.208.

Rankin, J.A. (2004). Biological mediators of acute inflammation. *AACN Advanced Critical Care*, *15*(1), pp.3-17.

Rao, K.G., Ashok, C.H., Rao, K.V. and Chakra, C.S. (2014). Structural properties of MgO nanoparticles: synthesized by co-precipitation technique. *International Journal of Science and Research*, *3*(12), pp.43-46.

Rao, P. and Knaus, E.E. (2008). Evolution of nonsteroidal anti-inflammatory drugs (NSAIDs): cyclooxygenase (COX) inhibition and beyond. *Journal of pharmacy & pharmaceutical sciences*, *11*(2), pp.81-110.

Rasmussen, J.W., Martinez, E., Louka, P. and Wingett, D.G. (2010). Zinc oxide nanoparticles for selective destruction of tumor cells and potential for drug

delivery applications. *Expert opinion on drug delivery*, *7*(9), pp.1063-1077.

Ratan, Z.A., Haidere, M.F., Costa, J.J., Runa, N.J., Hosseinzadeh, H. and Cho, J.Y. (2022). Overview of inflammation. In *Recent Advancements in Microbial Diversity* (pp. 29-51). Academic Press.

Rawal, S.U. and Patel, M.M. (2018). Lipid nanoparticulate systems: Modern versatile drug carriers. In *Lipid nanocarriers for drug targeting* (pp. 49-138). William Andrew Publishing.

Reddy, M.N.K., Hussain, M.A., Rao, T.R., Kishna, T.R. and Pavani, V. (2012). Formulation and evaluation of naproxen oral disintegrating tablets. *International Journal of Pharmacy Biological. Science*, *2*, pp.303-316.

Rhen, T. and Cidlowski, J.A. (2005). Antiinflammatory action of glucocorticoids—new mechanisms for old drugs. *New England Journal of Medicine*, *353*(16), pp.1711-1723.

Ribeiro, R.A., Vale, M.L., Thomazzi, S.M., Paschoalato, A.B., Poole, S., Ferreira, S.H. and Cunha, F.Q. (2000). Involvement of resident macrophages and mast cells in the writhing nociceptive response induced by zymosan and acetic acid in mice. *European journal of pharmacology*, *387*(1), pp.111-118.

Ricciotti, E. and FitzGerald, G.A. (2011). Prostaglandins and inflammation. *Arteriosclerosis, thrombosis, and vascular biology*, *31*(5), pp.986-1000.

Ridolfo, R., Tavakoli, S., Junnuthula, V., Williams, D.S., Urtti, A. and van Hest, J.C. (2020). Exploring the impact of morphology on the properties of biodegradable nanoparticles and their diffusion in complex biological medium. *Biomacromolecules*, *22*(1), pp.126-133.

Riva'i, I., Wulandari, I.O., Sulistyarti, H. and Sabarudin, A. (2018). Ex-situ synthesis of polyvinyl alcohol (PVA)-coated Fe3O4 nanoparticles by coprecipitation-ultrasonication method. In *IOP Conference Series: Materials Science and Engineering* **299**(1), p. 012065).

Rizvi, S.A. and Saleh, A.M. (2018). Applications of nanoparticle systems in drug delivery technology. *Saudi pharmaceutical journal*, *26*(1), pp.64-70.

Rizwan, M. and Gwenin, C. (2021). Nanomaterials in renewable energy: UV-Visible

spectroscopy characterization and applications. In *Nano Tools and Devices for Enhanced Renewable Energy* (pp. 103-120). Elsevier.

Robinson, S., Delongeas, J.L., Donald, E., Dreher, D., Festag, M., Kervyn, S., Lampo, A., Nahas, K., Nogues, V., Ockert, D. and Quinn, K. (2008). A European pharmaceutical company initiative challenging the regulatory requirement for acute toxicity studies in pharmaceutical drug development. *Regulatory Toxicology and Pharmacology*, *50*(3), pp.345-352.

Rodriguez-Stanley, S., Redinger, N. and Miner Jr, P.B. (2006). Effect of naproxen on gastric acid secretion and gastric pH. *Alimentary pharmacology and therapeutics*, *23*(12), pp.1719-1724.

Rodwell, V. W., and Murray, R. K. (2018). Porphyrins & Bile Pigments. In V. W. Rodwell, D. A. Bender, K. M. Botham, P. J. Kennelly, & P. A. Weil (Eds.), *Harper's Illustrated Biochemistry, 31e*. New York, NY: McGraw-Hill Education.

Rosado balmayor, E., Azevedo, H., and Reis, R. L. (2011). Controlled Delivery Systems: From Pharmaceuticals to Cells and Genes. *Pharmaceutical research, 28*, 1241-1258.

Ryan, M.F. (1991). The role of magnesium in clinical biochemistry: an overview. *Annals of clinical biochemistry*, *28*(1), pp.19-26.

Saad, J. and Mathew, D. (2022). Nonsteroidal Anti-Inflammatory Drugs Toxicity In: Stat Pearls . Stat Pearls Publishing.

Saag, K.G., Koehnke, R., Caldwell, J.R., Brasington, R., Burmeister, L.F., Zimmerman, B., Kohler, J.A. and Furst, D.E. (1994). Low dose long-term corticosteroid therapy in rheumatoid arthritis: an analysis of serious adverse events. *The American journal of medicine*, *96*(2), pp.115-123.

Sainz, V., Conniot, J., Matos, A.I., Peres, C., Zupanŏiŏ, E., Moura, L., Silva, L.C., Florindo, H.F. and Gaspar, R.S. (2015). Regulatory aspects on nanomedicines. *Biochemical and biophysical research communications*, *468*(3), pp.504-510.

Salah, S., Mahmoud, A.A. and Kamel, A.O. (2017). Etodolac transdermal cubosomes for the treatment of rheumatoid arthritis: ex vivo permeation and in vivo

pharmacokinetic studies. *Drug delivery*, *24*(1), pp.846-856.

Salbitani, G., Bottone, C. and Carfagna, S. (2017). Determination of reduced and total glutathione content in extremophilic microalga Galdieria phlegrea. *Bio-protocol*, *7*(13), pp.e2372-e2372.

Saleem, U., Amin, S., Ahmad, B., Azeem, H., Anwar, F. and Mary, S. (2017). Acute oral toxicity evaluation of aqueous ethanolic extract of Saccharum munja Roxb. roots in albino mice as per OECD 425 TG. *Toxicology reports*, *4*, pp.580-585.

Saleh, T. A. (2021). Surface and morphological characterization of hybrid materials. In T. A. Saleh (Ed.), *Polymer Hybrid Materials and Nanocomposites* (pp. 241-283): William Andrew Publishing.

Salminen, H., and Weiss, J. (2021). Solid lipid nanoparticles and nanostructured lipid carriers. In P. J. García-Moreno, C. Jacobsen, A.-D. Moltke Sørensen, & B. Yesiltas (Eds.), *Omega-3 Delivery Systems* (pp. 371-391): Academic Press.

Salvatella, M., Rossi, I., Del Valle, J.C., Gutiérrez, Y., Pereda, C., Samper, B. and Felíu, J.E. (2004). Inhibition of acid secretion by the nonsteroidal anti-inflammatory drugs diclofenac and piroxicam in isolated gastric glands: analysis of a multifocal mechanism. *American Journal of Physiology-Gastrointestinal and Liver Physiology*, *286*(5), pp.G711-G721.

Sandoval-Acuña, C., Lopez-Alarcón, C., Aliaga, M.E. and Speisky, H. (2012). Inhibition of mitochondrial complex I by various non-steroidal anti-inflammatory drugs and its protection by quercetin via a coenzyme Q-like action. *Chemico-biological interactions*, *199*(1), pp.18-28.

Sarfraz, R.M., Akram, M.R., Ali, M.R., Mahmood, A., Khan, M.U., Ahmad, H. and Qaisar, M.N. (2019). Development and in-vitro evaluation of pH responsive polymeric nano hydrogel carrier system for gastro-protective delivery of naproxen sodium. *Advances in Polymer Technology*, *2019*.

Sarfraz, R.M., Khan, M.U., Mahmood, A., Akram, M.R., Minhas, M.U., Qaisar, M.N., Ali, M.R., Ahmad, H. and Zaman, M. (2020). Synthesis of co-polymeric network of carbopol-g-methacrylic acid nanogels drug carrier system for gastro-protective delivery of ketoprofen and its evaluation. *Polymer-Plastics Technology and Materials*, *59*(10), pp.1109-1123.

Saso, L., Valentini, G., Casini, M.L., Grippa, E., Gatto, M.T., Leone, M.G. and Silvestrini, B. (2001). Inhibition of heat-induced denaturation of albumin by nonsteroidal antiinflammatory drugs (NSAIDs): Pharmacological implications. *Archives of Pharmacal Research*, *24*(2), pp.150-158.

Schäcke, H., Döcke, W.D. and Asadullah, K. (2002). Mechanisms involved in the side effects of glucocorticoids. *Pharmacology & therapeutics*, *96*(1), pp.23-43.

Schjerning, A.M., McGettigan, P. and Gislason, G. (2020). Cardiovascular effects and safety of (non-aspirin) NSAIDs. *Nature Reviews Cardiology*, *17*(9), pp.574-584.

Schmid, F.X. (2001). Biological macromolecules: UV-visible spectrophotometry. *e LS*.

Schultz, T.A. (2011). Nonsteroidal Anti-Inflammatory Drugs (NSAIDs). In *Essence of Anesthesia Practice* (p. 623). WB Saunders.

Schultze, A.E., Ennulat, D. and Aulbach, A.D. (2022). Clinical Pathology in Nonclinical Toxicity Testing. In *Haschek and Rousseaux's Handbook of Toxicologic Pathology* (pp. 295-334). Academic Press.

Sellers, R. S., Morton, D., Michael, B., Roome, N., Johnson, J. K., Yano, B. L.,Schafer, K. (2007). Society of Toxicologic Pathology position paper: organ weight recommendations for toxicology studies. *Toxicologic Pathology, 35*(5), 751-755.

Shahid, S., Ejaz, A., Javed, M., Mansoor, S., Iqbal, S., Elkaeed, E.B., Alzhrani, R.M., Alsaab, H.O., Awwad, N.S., Ibrahium, H.A. and Fatima, U. (2022). The Anti-Inflammatory and Free Radical Scavenging Activities of Bio-Inspired Nano Magnesium Oxide. *Frontiers in Materials*, *9*, p.875163.

Shao, X.R., Wei, X.Q., Song, X., Hao, L.Y., Cai, X.X., Zhang, Z.R., Peng, Q. and Lin, Y.F. (2015). Independent effect of polymeric nanoparticle zeta potential/surface charge, on their cytotoxicity and affinity to cells. *Cell proliferation*, *48*(4), pp.465-474.

Sharma, J.N. and Jawad, N.M. (2005). Adverse effects of COX-2 inhibitors. *The Scientific World JOURNAL*, *5*, pp.629-645.

Shehata, Y.M., Mansour, M.F., Shadad, S. and Arisha, A.H. (2020). Effect of curcumin-magnesium oxide nanoparticles conjugate in type-II diabetic

rats. *Advances in Animal Veterinary Science*, *8*(s1), pp.26-33.

Shen, J. and Burgess, D.J. (2013). In vitro dissolution testing strategies for nanoparticulate drug delivery systems: recent developments and challenges. *Drug delivery and translational research*, *3*(5), pp.409-415.

Shen, S., Wu, Y., Liu, Y. and Wu, D. (2017). High drug-loading nanomedicines: progress, current status, and prospects. *International journal of nanomedicine*, *12***,** p.4085-4109.

Sherwood, E.R. and Toliver-Kinsky, T. (2004). Mechanisms of the inflammatory response. *Best Practice & Research Clinical Anaesthesiology*, *18*(3), pp.385-405.

Shimizu, S., Yamada, Y., Okuno, M., Ohnishi, H., Osawa, Y., Seishima, M. and Moriwaki, H. (2005). Liver injury induced by lipopolysaccharide is mediated by TNFR-1 but not by TNFR-2 or Fas in mice. *Hepatology research*, *31*(3), pp.136-142.

Shnoudeh, A.J., Hamad, I., Abdo, R.W., Qadumii, L., Jaber, A.Y., Surchi, H.S. and Alkelany, S.Z. (2019). Synthesis, characterization, and applications of metal nanoparticles. In *Biomaterials and bionanotechnology* (pp. 527-612). Academic Press.

Shojaee, P., Niroomand-Oscuii, H., Sefidgar, M. and Alinezhad, L. (2020). Effect of nanoparticle size, magnetic intensity, and tumor distance on the distribution of the magnetic nanoparticles in a heterogeneous tumor microenvironment. *Journal of Magnetism and Magnetic Materials*, *498*, p.166089.

Shrivastava, R., Raza, S., Yadav, A., Kushwaha, P. and Flora, S.J. (2014). Effects of sub-acute exposure to TiO2, ZnO and Al2O3 nanoparticles on oxidative stress and histological changes in mouse liver and brain. *Drug and chemical toxicology*, *37*(3), pp.336-347.

Simmons, D.L., Wagner, D. and Westover, K. (2000). Nonsteroidal anti-inflammatory drugs, acetaminophen, cyclooxygenase 2, and fever. *Clinical infectious diseases*, *31,* pp.S211-S218.

Simon, L.S. (1999). Role and regulation of cyclooxygenase-2 during inflammation. *The*

American journal of medicine, *106*(5), pp.37S-42S.

Singh, G. (2000). Gastrointestinal complications of prescription and over-the-counter nonsteroidal anti-inflammatory drugs: a view from the ARAMIS database. Arthritis, Rheumatism, and Aging Medical Information System. *American journal of therapeutics*, *7*(2), pp.115-121.

Singh, M. K., and Singh, A. (2022). Chapter 13 - Fourier transform infrared (FTIR) analysis. In M. K. Singh & A. Singh (Eds.), *Characterization of Polymers and Fibres* (pp. 295-320): Woodhead Publishing.

Singh, P., Ahn, S., Kang, J.P., Veronika, S., Huo, Y., Singh, H., Chokkaligam, M., El-Agamy Farh, M., Aceituno, V.C., Kim, Y.J. and Yang, D.C. (2018). In vitro anti-inflammatory activity of spherical silver nanoparticles and monodisperse hexagonal gold nanoparticles by fruit extract of Prunus serrulata: a green synthetic approach. *Artificial cells, nanomedicine, and biotechnology*, *46*(8), pp.2022-2032.

Smolinske, S.C., Hall, A.H., Vandenberg, S.A., Spoerke, D.G. and McBride, P.V. (1990). Toxic effects of nonsteroidal anti-inflammatory drugs in overdose. *Drug Safety*, *5*(4), pp.252-274.

Soares, S., Sousa, J., Pais, A. and Vitorino, C. (2018). Nanomedicine: principles, properties, and regulatory issues. *Frontier in Chemistry* **6**: 360.

Soddu, L., Trinh, D.N., Dunne, E., Kenny, D., Bernardini, G., Kokalari, I., Marucco, A., Monopoli, M.P. and Fenoglio, I. (2020). Identification of physicochemical properties that modulate nanoparticle aggregation in blood. *Beilstein journal of nanotechnology*, *11*(1), pp.550-567.

Soehngen, E.C., Godin-Ostro, E., Fielder, F.G., Ginsberg, R.S., Slusher, M.A. and Weiner, A.L. (1988). Encapsulation of indomethacin in liposomes provides protection against both gastric and intestinal ulceration when orally administered to rats. *Arthritis & Rheumatism: Official Journal of the American College of Rheumatology*, *31*(3), pp.414-422.

Somanathan, T., Krishna, V.M., Saravanan, V., Kumar, R. and Kumar, R. (2016). MgO nanoparticles for effective uptake and release of doxorubicin drug: pH sensitive controlled drug release. *Journal of Nanoscience and*

Nanotechnology, *16*(9), pp.9421-9431.

Somasundaram, S., Hayllar, H., Rafi, S., Wrigglesworth, J.M., Macpherson, A.J.S. and Bjarnason, I. (1995). The biochemical basis of non-steroidal anti-inflammatory drug-induced damage to the gastrointestinal tract: a review and a hypothesis. *Scandinavian journal of gastroenterology*, *30*(4), pp.289-299.

Somasundaram, S., Rafi, S., Hayllar, J., Sigthorsson, G., Jacob, M., Price, A.B., Macpherson, A., Mahmod, T., Scott, D., Wrigglesworth, J.M. and Bjarnason, I. (1997). Mitochondrial damage: a possible mechanism of the "topical" phase of NSAID induced injury to the rat intestine. *Gut*, *41*(3), pp.344-353.

Sreeharsha, N., Chitrapriya, N., Jang, Y.J. and Kenchappa, V. (2021). Evaluation of nanoparticle drug-delivery systems used in preclinical studies. *Therapeutic Delivery*, *12*(4), pp.325-336.

Sriuttha, P., Sirichanchuen, B. and Permsuwan, U. (2018). Hepatotoxicity of nonsteroidal anti-inflammatory drugs: a systematic review of randomized controlled trials. *International journal of hepatology*, *2018*.

Stanbury, R.M. and Graham, E.M. (1998). Systemic corticosteroid therapy—side effects and their management. *British Journal of Ophthalmology*, *82*(6), pp.704-708.

Stankic, S., Suman, S., Haque, F. and Vidic, J. (2016). Pure and multi metal oxide nanoparticles: synthesis, antibacterial and cytotoxic properties. *Journal of nanobiotechnology*, *14*(1), pp.1-20.

Stark, C. and Steger-Hartmann, T. (2015). Nonclinical safety and toxicology. *New Approaches to Drug Discovery*, *232*, pp.261-283,

Streicher, J. M., and Wang, Y. (2008). The role of COX-2 in heart pathology. *Cardiovasculer and Hematologicaal Agents in Medicine Chemistry, 6*(1), 69-79.

Subramanian, N., Ray, S., Ghosal, S.K., Bhadra, R. and Moulik, S.P. (2004). Formulation design of self-microemulsifying drug delivery systems for improved oral bioavailability of celecoxib. *Biological and Pharmaceutical Bulletin*, *27*(12), pp.1993-1999.

Sukhanova, A., Bozrova, S., Sokolov, P., Berestovoy, M., Karaulov, A. and Nabiev, I. (2018). Dependence of nanoparticle toxicity on their physical and chemical properties. *Nanoscale research letters*, *13*(1), pp.1-21.

Sun, H., Meng, F., Dias, A.A., Hendriks, M., Feijen, J. and Zhong, Z. (2011). α-Amino acid containing degradable polymers as functional biomaterials: rational design, synthetic pathway, and biomedical applications. *Biomacromolecules*, *12*(6), pp.1937-1955.

Sun, S.B., Liu, P., Shao, F.M. and Miao, Q.L. (2015). Formulation and evaluation of PLGA nanoparticles loaded capecitabine for prostate cancer. *International journal of clinical and experimental medicine*, *8*(10), p.19670.

Sutapa, I.W., Wahab, A.W., Taba, P. and La Nafie, N. (2018). Synthesis and structural profile analysis of the MgO nanoparticles produced through the sol-gel method followed by annealing process. *Oriental Journal of Chemistry*, *34*(2), p.1016.

Syed, A. and Devi, V.K. (2019). Potential of targeted drug delivery systems in treatment of rheumatoid arthritis. *Journal of Drug Delivery Science and Technology*, *53*, p.101217.

Tanaka, T., Narazaki, M. and Kishimoto, T. (2014). IL-6 in inflammation, immunity, and disease. *Cold Spring Harbor perspectives in biology*, *6*(10), p.a016295.

Tang, S.Y., Sivakumar, M., Ng, A.M.H. and Shridharan, P. (2012). Anti-inflammatory and analgesic activity of novel oral aspirin-loaded nanoemulsion and nano multiple emulsion formulations generated using ultrasound cavitation. *International journal of pharmaceutics*, *430*(1-2), pp.299-306.

Thapaliya, S., Wree, A., Povero, D., Inzaugarat, M.E., Berk, M., Dixon, L., Papouchado, B.G. and Feldstein, A.E. (2014). Caspase 3 inactivation protects against hepatic cell death and ameliorates fibrogenesis in a diet-induced NASH model. *Digestive diseases and sciences*, *59*(6), pp.1197-1206.

Thilagam, R. and Gnanamani, A. (2020). Preparation, characterization and stability assessment of keratin   and albumin functionalized gold nanoparticles for biomedical applications. *Applied Nanoscience*, *10*(6), pp.1879-1892.

Timbadiya, M.J., Nishteswar, K., Acharya, R. and Nariya, M.B. (2015).

Experimental evaluation of antipyretic and analgesic activities of Amalakyadi Gana: An Ayurvedic formulation. *Ayurveda*, *36*(2), p.220.

Tinoco, M., Yeste, M.P. and Sendra, M. (2022). Advanced analytical techniques for physico-chemical characterization of nano-materials. In *Nano-enabled Agrochemicals in Agriculture* (pp. 79-104). Academic Press.

Tirichen, H., Yaigoub, H., Xu, W., Wu, C., Li, R. and Li, Y. (2021). Mitochondrial reactive oxygen species and their contribution in chronic kidney disease progression through oxidative stress. *Frontiers in physiology*, p.398.

Titus, D., Samuel, E.J.J. and Roopan, S.M. (2019). Nanoparticle characterization techniques. In *Green synthesis, characterization and applications of nanoparticles* (pp. 303-319). Elsevier.

Tiwari, G., Tiwari, R., Sriwastawa, B., Bhati, L., Pandey, S., Pandey, P. and Bannerjee, S.K. (2012). Drug delivery systems: An updated review. *International journal of pharmaceutical investigation*, *2*(1), p.2Tomé, I., Francisco, V., Fernandes, H., and Ferreira, L. (2021). High-throughput screening of nanoparticles in drug delivery. *APL bioengineering, 5*(3), pp.031511-031511.

Tomé, I., Francisco, V., Fernandes, H., and Ferreira, L. (2021). High-throughput screening of nanoparticles in drug delivery. *APL bioengineering, 5*(3),pp. 031511-031511.

Tomić, M., Micov, A., Pecikoza, U. and Stepanović-Petrović, R. (2017). Clinical uses of nonsteroidal anti-inflammatory drugs (NSAIDs) and potential benefits of NSAIDs modified-release preparations. In *Microsized and nanosized carriers for nonsteroidal anti-inflammatory drugs* (pp. 1-29). Academic Press.

Toxicity–Up, A.O. (2001). OECD guideline for testing of chemicals.

Tran, T.T.D., Tran, P.H.L., Lim, J., Park, J.B., Choi, S.K. and Lee, B.J. (2010). Physicochemical principles of controlled release solid dispersion containing a poorly water-soluble drug. *Therapeutic delivery*, *1*(1), pp.51-62.

Trucillo, P. (2021). Drug carriers: Classification, administration, release profiles, and industrial approach. *Processes*, *9*(3), p.470.

Truong, D.H., Nguyen, D.H., Ta, N.T.A., Bui, A.V., Do, T.H. and Nguyen, H.C.

(2019). Evaluation of the use of different solvents for phytochemical constituents, antioxidants, and in vitro anti-inflammatory activities of Severinia buxifolia. *Journal of food quality*, *2019*.

Tsume, Y., Mudie, D.M., Langguth, P., Amidon, G.E. and Amidon, G.L. (2014). The Biopharmaceutics Classification System: subclasses for in vivo predictive dissolution (IPD) methodology and IVIVC. *European Journal of Pharmaceutical Sciences*, *57*, pp.152-163.

Ud Din, F., Aman, W., Ullah, I., Qureshi, O.S., Mustapha, O., Shafique, S. and Zeb, A. (2017). Effective use of nanocarriers as drug delivery systems for the treatment of selected tumors. *International journal of nanomedicine*, *12*, pp.7291-7309.

Ulinski, T., Guigonis, V., Dunan, O. and Bensman, A. (2004). Acute renal failure after treatment with non-steroidal anti-inflammatory drugs. *European journal of pediatrics*, *163*(3), pp.148-150.

Ur Rehman, F., Mazhar, K., Malik, A., Naz, S.S., Shah, K.U., Khan, A., Khan, S., Ahmed, R. and Qaisar, S. (2021). Surface modified multifaceted nanocarriers for oral non-conventional cancer therapy, synthesis and evaluation. *Materials Science and Engineering: C*, *123*, p.111940.

Uzun, B., Atli, O., Perk, B.O., Burukoglu, D.İ.L.E.K. and Ilgin, S. (2015). Evaluation of the reproductive toxicity of naproxen sodium and meloxicam in male rats. *Human & experimental toxicology*, *34*(4), pp.415-429.

Van Eerdenbrugh, B., Vermant, J., Martens, J.A., Froyen, L., Humbeeck, J.V., Van den Mooter, G. and Augustijns, P. (2010). Solubility increases associated with crystalline drug nanoparticles: methodologies and significance. *Molecular pharmaceutics*, *7*(5), pp.1858-1870.

Van Eerdenbrugh, B., Vermant, J., Martens, J.A., Froyen, L., Humbeeck, J.V., Van den Mooter, G. and Augustijns, P. (2010) Solubility increases associated with crystalline drug nanoparticles: methodologies and significance. *Molecular pharmaceutics*, *7*(5), pp.1858-1870.

Van Ngo, H., Nguyen, P.K., Van Vo, T., Duan, W., Tran, V.T., Tran, P.H.L. and Tran, T.T.D. (2016). Hydrophilic-hydrophobic polymer blend for modulation

of crystalline changes and molecular interactions in solid dispersion. *International journal of pharmaceutics*, *513*(1-2), pp.148-152.

Van Rensburg, R. and Reuter, H. (2019). An overview of analgesics: NSAIDs, paracetamol, and topical analgesics Part 1. *South African Family Practice*, *61*(sup1), 4-10.

Varela, M.L., Mogildea, M., Moreno, I. and Lopes, A. (2018). Acute inflammation and metabolism. *Inflammation*, *41*(4), pp.1115-1127.

Varga, Z., rafay ali Sabzwari, S. and Vargova, V. (2017). Cardiovascular risk of nonsteroidal anti-inflammatory drugs: an under-recognized public health issue. *Cureus*, *9*(4), e1144-e1144.

Vega-Vásquez, P., Mosier, N.S. and Irudayaraj, J. (2020). Nanoscale drug delivery systems: From medicine to agriculture. *Frontiers in Bioengineering and Biotechnology*, *8*, p.79.

Ventola, C.L. (2017). Progress in nanomedicine: approved and investigational nanodrugs. *Pharmacy and Therapeutics*, *42*(12), pp.742-755.

Vigato, A.A., Machado, I.P., Franco, M.K.D., Yokaichiya, F., de Sairre, M.I. and de Araujo, D.R. (2022). Chemical and structural characterization of hybrid delivery systems studied by FTIR, NMR, and SAS techniques. In *Hybrid Nanomaterials for Drug Delivery* (pp. 27-51). Woodhead Publishing.

Vincent, C., Kiran, M.D., Jayan, J.S. and Saritha, A. (2020). Determination of drug loading efficiency of nano capsules formed by the O/W emulsification of block copolymer. *Materials Today: Proceedings*, *26*, pp.720-723.

Vinegar, R., Schreiber, W. and Hugo, R. (1969). Biphasic development of carrageenin edema in rats. *Journal of pharmacology and experimental therapeutics*, *166*(1), pp.96-103.

Vogel, H.G. (2002). Drug discovery and evaluation: pharmacological assays.(Ed.) Springer Science & Business Media.

Vollath, D. (2008). Nanomaterials an introduction to synthesis, properties and application. *Environmental Engineering and Management Journal*, *7*(6), pp.865-870.

Vonkeman, H.E. and van de Laar, M.A. (2010), February. Nonsteroidal anti-inflammatory drugs: adverse effects and their prevention. In *Seminars in arthritis and rheumatism* **39**(4), pp. 294-312. WB Saunders.

Walker, J.S. (1995). Australasian Society of Clinical and Experimental Pharmacologists and Toxicologists, 1994: NSAID: An Update on Their Analgesic Effects. *Clinical and Experimental Pharmacology and Physiology*, *22*(11), pp.855-860.

Wallace, J.L. (2000). How do NSAIDs cause ulcer disease? *Best Practice & Research Clinical Gastroenterology*, *14*(1), pp.147-159.

Wallace, J.L. (2012). NSAID gastropathy and enteropathy: distinct pathogenesis likely necessitates distinct prevention strategies. *British journal of pharmacology*, *165*(1), pp.67-74.

Walter, E.J., Hanna-Jumma, S., Carraretto, M. and Forni, L. (2016). The pathophysiological basis and consequences of fever. *Critical Care*, *20*(1), pp.1-10.

Wang, F., Gómez-Sintes, R. and Boya, P. (2018). Lysosomal membrane permeabilization and cell death. *Traffic*, *19*(12), pp.918-931.

Wang, H., Wang, K., Tian, B., Revia, R., Mu, Q., Jeon, M., Chang, F.C. and Zhang, M. (2016). Preloading of Hydrophobic Anticancer Drug into Multifunctional Nanocarrier for Multimodal Imaging, NIR-Responsive Drug Release, and Synergistic Therapy. *Small*, *12*(46), pp.6388-6397.

Wang, Q. (2014). Nanoparticles for applications in drug delivery. In (pp. 159-196).

Wang, R.Y., Tung, Y.T., Chen, S.Y., Lee, Y.L. and Yen, G.C. (2019). Protective effects of camellia oil (Camellia brevistyla) against indomethacin-induced gastrointestinal mucosal damage in vitro and in vivo. *Journal of Functional Foods*, *62*, p.103539.

Wang, X., Michaelis, E.K., Foster, T.C. and Foster, T.C. (2010). Selective neuronal vulnerability to oxidative stress in the brain, *Frontier in Aging Neuroscience.* **2** (2010) 1–13.

Wang, Y. and Xia, Y. (2004). Bottom-up and top-down approaches to the synthesis of monodispersed spherical colloids of low melting-point metals. *Nano*

letters, *4*(10), pp.2047-2050.

Wang, Y., Dave, R. and Pfeffer, R. (2004). Nanoparticle encapsulation with heterogeneous nucleation in a supercritical antisolvent process. *Journal of Supercritical Fluids*, *28*, pp.85-99.

Wani, T.U., Raza, S.N. and Khan, N.A. (2020). Nanoparticle opsonization: Forces involved and protection by long chain polymers. *Polymer Bulletin*, *77*(7), pp.3865-3889.

Washington, I.M. and Van Hoosier, G. (2012). Clinical biochemistry and hematology. In *The laboratory rabbit, guinea pig, hamster, and other rodents* (pp. 57-116). Academic Press.

Watanabe, T., Higuchi, K., Hamaguchi, M., Shiba, M., Tominaga, K., Fujiwara, Y., Matsumoto, T. and Arakawa, T. (2004). Monocyte chemotactic protein-1 regulates leukocyte recruitment during gastric ulcer recurrence induced by tumor necrosis factor-α. *American Journal of Physiology-Gastrointestinal and Liver Physiology*, *287*(4), pp.G919-G928.

Weissig, V., Pettinger, T.K. and Murdock, N. (2014). Nanopharmaceuticals (part 1): products on the market. *International journal of nanomedicine*, *9*, p.4357.

Whittle, B.J. (2003). Gastrointestinal effects of nonsteroidal anti-inflammatory drugs. *Fundamental & clinical pharmacology*, *17*(3), pp.301-313.

Wicki, A., Witzigmann, D., Balasubramanian, V. and Huwyler, J. (2015). Nanomedicine in cancer therapy: challenges, opportunities, and clinical applications. *Journal of controlled release*, *200*, pp.138-157.

Williams, B.D., O'Sullivan, M.M., Saggu, G.S., Williams, K.E., Williams, L.A. and Morgan, J.R. (1987). Synovial accumulation of technetium labelled liposomes in rheumatoid arthritis. *Annals of the rheumatic diseases*, *46*(4), pp.314-318.

Wiśniewska, M., Bogatyrov, V., Ostolska, I., Szewczuk-Karpisz, K., Terpiłowski, K. and Nosal-Wiercińska, A. (2016). Impact of poly (vinyl alcohol) adsorption on the surface characteristics of mixed oxide Mn x O y– SiO2. *Adsorption*, *22*(4), pp.417-423.

Wolf, J.C. and Maack, G. (2017). Evaluating the credibility of histopathology data in environmental endocrine toxicity studies. *Environmental toxicology and*

chemistry, *36*(3), pp.601-611.

Wong, D. M., Bol'shakov, A. A., and Russo, R. E. (2010). Laser Induced Breakdown Spectroscopy. In J. C. Lindon (Ed.), *Encyclopedia of Spectroscopy and Spectrometry (Second Edition)* (pp. 1281-1287). Oxford: Academic Press.

Wong, R.S. (2019). Disease-modifying effects of long-term and continuous use of nonsteroidal anti-inflammatory drugs (NSAIDs) in spondylo-arthritis. *Advances in Pharmacological Sciences*, *201*,pp 5324170.

Wong, R.S. (2019). Role of nonsteroidal anti-inflammatory drugs (NSAIDs) in cancer prevention and cancer promotion. *Advances in pharmacological sciences*, *2019*, pp.3418975-3418975.

Wongrakpanich, S., Wongrakpanich, A., Melhado, K. and Rangaswami, J. (2017). A comprehensive review of non-steroidal anti-inflammatory drug use in the elderly. Aging and Disease. **9** pp.143-150.

Woolbright, B.L. and Jaeschke, H. (2018). Mechanisms of inflammatory liver injury and drug-induced hepatotoxicity. *Current pharmacology reports*, *4*(5), pp.346-357.

Wu, Z., Ma, Y., Zhao, L., Cai, S. and Cheng, G. (2018). Acute and subchronic toxicities of the ethanol and hot-water extracts from Chinese sumac (Rhus chinensis Mill.) fruits by oral administration in rats. *Food and Chemical Toxicology*, *119*, pp.14-23.

Xiong, S., George, S., Yu, H., Damoiseaux, R., France, B., Ng, K.W. and Loo, J.S.C. (2013). Size influences the cytotoxicity of poly (lactic-co-glycolic acid)(PLGA) and titanium dioxide (TiO2) nanoparticles. *Archives of toxicology*, *87*(6), pp.1075-1086.

Yang, H., Xuefeng, Y., Shandong, W. and Jianhua, X. (2020). COX-2 in liver fibrosis. *Clinica Chimica Acta*, *506*, pp.196-203.

Yaqoob, A.A., Ahmad, H., Parveen, T., Ahmad, A. and Oves, M. (2020). Recent advances in metal decorated nano materials and their various biological applications: a review, Front. A Review. *8.*

Yih, T.C. and Al-Fandi, M. (2006). Engineered nanoparticles as precise drug delivery systems. *Journal of cellular biochemistry*, *97*(6), pp.1184-1190.

Yoshitomi, T., Sha, S., Vong, L.B., Chonpathompikunlert, P., Matsui, H. and Nagasaki, Y. (2014). Indomethacin-loaded redox nanoparticles improve oral bioavailability of indomethacin and suppress its small intestinal inflammation. *Therapeutic delivery*, *5*(1), pp.29-38.

Yu, X., Xieripu, A., Xu, Q., Zulipikaer, A., Song, Y., Cai, L. and Chen, J. (2020). GSH-responsive curcumin/doxorubicin encapsulated Bactrian camel serum albumin nanocomposites with synergistic effect against lung cancer cells. *Journal of Biomedical Research*, *34*(1), pp.54-66.

Zamora, R., Vodovotz, Y. and Billiar, T.R. (2000). Inducible nitric oxide synthase and inflammatory diseases. *Molecular medicine*, *6*(5), pp.347-373.

Zarghi, A. and Arfaei, S. (2011). Selective COX-2 inhibitors: a review of their structure-activity relationships. *Iranian journal of pharmaceutical research: IJPR*, *10*(4), pp.655-683.

Zhang, J., Tang, H., Liu, Z. and Chen, B. (2017). Effects of major parameters of nanoparticles on their physical and chemical properties and recent application of nanodrug delivery system in targeted chemotherapy. *International journal of nanomedicine*, *12*, pp.8483-8493.

Zhang, T.T., Xue, R., Zhu, L., Li, J., Fan, Q.Y., Zhong, B.H., Li, Y.F., Ye, C.Y. and Zhang, Y.Z. (2016). Evaluation of the analgesic effects of ammoxetine, a novel potent serotonin and norepinephrine reuptake inhibitor. *Acta Pharmacologica Sinica*, *37*(9), pp.1154-1165.

Zhang, X., Donnan, P.T., Bell, S. and Guthrie, B. (2017). Non-steroidal anti-inflammatory drug induced acute kidney injury in the community dwelling general population and people with chronic kidney disease: systematic review and meta-analysis. *BMC nephrology*, *18*(1), pp.1-12.

Zhang, X.F. (2016). Zhi-Guo liu, Wei shen, Sangiliyandi Gurunathan. SilverNanoparticles: Synthesis, Characterization, Properties, Applications, and Therapeutic Approaches. *International Journal of Molecular Sciences*, *17*, p.1534.

Zhao, Y., Lin, L.N., Lu, Y., Chen, S.F., Dong, L. and Yu, S.H. (2010). Templating synthesis of preloaded doxorubicin in hollow mesoporous silica nanospheres

for biomedical applications. *Advanced Materials*, *22*(46), pp.5255-5259.

Zou, X.H., Guo, L.B., Shen, M., Li, X.Y., Hao, Z.Q., Zeng, Q.D., Lu, Y.F., Wang, Z.M. and Zeng, X.Y. (2014). Accuracy improvement of quantitative analysis in laser-induced breakdown spectroscopy using modified wavelet transform. *Optics express*, *22*(9), pp.10233-10238.